UNIVERSITY OF ALBERTA

Characterization of the mismatch repair-dependent DNA damage response induced by ultraviolet B radiation

by

Kelly Ann Devika Narine ©

A thesis submitted to the Faculty of Graduate Studies and Research
in partial fulfillment of the requirements for the degree of

Doctor of Philosophy

Medical Sciences- Medical Genetics

Edmonton, Alberta
Fall 2008

Library and
Archives Canada

Published Heritage
Branch

395 Wellington Street
Ottawa ON K1A 0N4
Canada

Bibliothèque et
Archives Canada

Direction du
Patrimoine de l'édition

395, rue Wellington
Ottawa ON K1A 0N4
Canada

Your file Votre référence
ISBN: 978-0-494-46395-6
Our file Notre référence
ISBN: 978-0-494-46395-6

NOTICE:
The author has granted a non-exclusive license allowing Library and Archives Canada to reproduce, publish, archive, preserve, conserve, communicate to the public by telecommunication or on the Internet, loan, distribute and sell theses worldwide, for commercial or non-commercial purposes, in microform, paper, electronic and/or any other formats.

The author retains copyright ownership and moral rights in this thesis. Neither the thesis nor substantial extracts from it may be printed or otherwise reproduced without the author's permission.

AVIS:
L'auteur a accordé une licence non exclusive permettant à la Bibliothèque et Archives Canada de reproduire, publier, archiver, sauvegarder, conserver, transmettre au public par télécommunication ou par l'Internet, prêter, distribuer et vendre des thèses partout dans le monde, à des fins commerciales ou autres, sur support microforme, papier, électronique et/ou autres formats.

L'auteur conserve la propriété du droit d'auteur et des droits moraux qui protège cette thèse. Ni la thèse ni des extraits substantiels de celle-ci ne doivent être imprimés ou autrement reproduits sans son autorisation.

In compliance with the Canadian Privacy Act some supporting forms may have been removed from this thesis.

While these forms may be included in the document page count, their removal does not represent any loss of content from the thesis.

Conformément à la loi canadienne sur la protection de la vie privée, quelques formulaires secondaires ont été enlevés de cette thèse.

Bien que ces formulaires aient inclus dans la pagination, il n'y aura aucun contenu manquant.

Canada

ABSTRACT

Many studies have shown that DNA mismatch repair (MMR) has a role outside of repair in response to several types of DNA damage, including ultraviolet radiation (UV). I have studied the role of the MMR proteins Msh2/MSH2 and Msh6 in the UVB-induced DNA damage response, specifically in cell cycle regulation and apoptosis.

My work showed that G2/M cell cycle arrest is diminished in *Msh6*-deficient MEFs and *MSH2*-deficient human cells after UVB irradiation. Furthermore, levels of key cell cycle proteins, such as CHK1 phosphorylated at Serine 345 and CDC25C phosphorylated at Serine 216 are reduced after UVB in the absence of *MSH2*.

My work also demonstrated that Msh6-dependent UVB-induced apoptosis occurs through the mitochondria via mitochondrial membrane depolarization. Compared to their wildtype counterparts, mouse embryonic fibroblasts (MEFs) deficient in *Msh6* had reduced levels of mitochondrial membrane depolarization, misregulated release of cytochrome c into the cytosol and reduced levels of caspase 9 after UVB irradiation. I showed that *Msh6*-deficient MEFs have misregulated translocation of Bax after UVB irradiation that is associated with the abnormal apoptotic response in the absence of Msh6. By examining apoptosis levels and levels of cleaved caspase 3 after peptide inhibition of caspase 8, my studies indicated that there is a possibility that Msh6-dependent apoptosis involves feedback loop-dependent activation of caspase 8 via cleaved caspase 3. Furthermore, I have illustrated that this Msh6-dependent apoptosis after UVB radiation is p53-independent.

I have shown for the first time that caspase 2, an initiator caspase, localizes to the centrosomes in MEFs, irrespective of MMR status and UVB treatment.

This thesis demonstrates that in response to UVB-induced DNA damage, MMR is important in maintaining proper cellular responses, such as cell cycle arrest and apoptosis, which act to maintain genomic integrity. The data presented in this dissertation help elucidate for the first time some of the mechanisms underlying the MMR-dependent UVB-induced DNA damage response and highlight the importance of MMR in the avoidance of UVB-induced tumorigenesis. This research is important in enhancing our understanding of the mechanisms that prevent non-melanoma skin cancer, a prevalent cancer in Canada.

ACKNOWLEDGEMENTS

There are many people whom I have to thank for their generous support and input over the course of my graduate studies career.

First and foremost is my graduate supervisor, Dr. Susan Andrew. Susan, you have been an exemplary mentor and role model to me and I could not have asked for anyone better. I have learned so much from you, more than I can ever say. Thank you for always being my champion and for everything that you do (which is far too much to list).

To my co-supervisor, Dr. Victor Tron, your endless enthusiasm and intellectual contributions have meant so much to me. You have also been a wonderful role model and I thank you for your innovative ideas that make science fun.

To Dr. Michael Walter, my acting supervisor, you have been a great help to me during my graduate studies. Thank you for your always insightful suggestions and the continuous support that you have shown right from the very beginning until the very end. I will always be an unofficial member of your lab.

To Dr. Gordon Chan, one of the most knowledgeable and supportive committee members any student could ask for. Thank you very much for all of your input and guidance over the years.

Thank you to Honey Chan for all your technical assistance with confocal microscopy and to Dorothy Rutkowski, for all your technical assistance with flow cytometry.

To the past and present members of the Andrew and Tron labs: we had some great times that made this experience a really fun one! Thanks to Cindy for all your outstanding work over the last few months. Particularly I would like to thank Katie, a great friend and peer. You are one of the most supportive people I know and I am so glad that we took this journey together. Also, to Dr. Leah Young, I have to say that I would have never made it to this point without you. Your vast knowledge never ceases to amaze me. I know I could not have gotten through the thesis-writing without you. Thank you for all your help in editing, making figures, statistics, etc. (too many things to write down). Your scientific and non-scientific input throughout the years has certainly made me a better scientist and a more knowledgeable person. Thank you for being a great role-model, in and out of the lab.

To my wonderful family: Mom, Dad, Tam, Raj and Shivani. I really could not have made it this far in life without you all. Mom and Dad, you have supported me in so many ways. Thank you sincerely for everything you have done and everything you are. You make me believe that all things are possible. To my fabulous and immensely talented sister, Tammy, thank you for all the support through good times and the bad. You are the best role model I could have in life (well, you and Mom).

To my dear friends Anjali, Kim and Daisy, thanks for all the great times and I look forward to many more! I really relied on you both throughout this degree and throughout my time in Edmonton. Thank you for all the encouragement, listening, advising and the laughter along the way.

Finally, to Rajen, words cannot even say just how much your love, encouragement and support have meant to me over the years. You have always been there for me, especially in difficult times. Thank you from the bottom of my heart for everything.

TABLE OF CONTENTS

Chapter 1~ Literature Review 1
Introduction 2
Genomic instability..3
DNA mismatch repair 6
Mammalian DNA mismatch repair 6
DNA mismatch repair and interacting proteins 9
Mutations in DNA mismatch repair and hereditary non-polyposis colorectal cancer 10
Mismatch repair deficient individuals 12
Micorsatellite instability in sporadic cancer 13
Mouse models of DNA mismatch repair 14
MutSα signal transduction 15
Eukaryotic strand discrimination 17
Multifunctionality of DNA mismatch repair 18
Cellular response to DNA damage 19
Mismatch repair and the DNA damage response 21
UV radiation 25
Non-melanoma skin cancer 28
DNA mismatch repair and skin cancer 28
DNA mismatch repair and the response to UV-induced DNA damage 29
Hypothesis and summary of studies 31
References 34

Chapter 2~ Materials and Methods 56
Cell cycle- human 57
Cell Cycle- mouse 59
Apoptosis 61
References 66

Chapter 3~ Characterization of the cell cycle response to UVB-induced DNA damage in mismatch repair-proficient and –deficient cells 67
Introduction 68
Results 73
Cell cycle analysis of Msh6$^{+/+}$ and Msh6$^{-/-}$ murine embryonic fibroblasts following UVB radiation 73
Cell cycle analysis of JMG (MSH2$^{+/+}$) and KM (MSH2$^{-/-}$) cells following UVB radiation 75
Cell cycle protein analysis in JMG (MSH2$^{+/+}$) and KM (MSH2$^{-/-}$) following UVB radiation 77
Discussion 82
References 86

Chapter 4~ Characterization of the mitochondrial/intrinsic apoptotic response to UVB-induced DNA damage in mismatch repair-proficient and -deficient murine embryonic fibroblasts 93
Introduction 94
Results 99
p53 levels in $Msh6^{+/+}$ and $Msh6^{-/-}$ murine embryonic fibroblasts 99
Apoptosis levels in $Msh6^{+/+}$, $Msh6^{-/-}$, $Msh6^{-/-}$ $p53^{+/-}$, $Msh6^{-/-}$ $p53^{-/-}$, $p53^{-/-}$ murine embryonic fibroblasts 101
Mitochondrial membrane potential in $Msh6^{+/+}$ and $Msh6^{-/-}$ murine embryonic fibroblasts 102
Pro-apoptotic protein levels in $Msh6^{+/+}$ and $Msh6^{-/-}$ murine embryonic fibroblasts 106
Apoptosis levels in $Msh6^{+/+}$ and $Msh6^{-/-}$ murine embryonic fibroblasts after caspase inhibitors 113
Cleaved caspase 3 levels in $Msh6^{+/+}$ and $Msh6^{-/-}$ murine embryonic fibroblasts after caspase 9 inhibitor 116
Discussion 117
References 127

Chapter 5~ Characterization of the role of caspase 2 after UVB-induced DNA damage in mismatch repair-proficient and -deficient murine embryonic fibroblasts 137
Introduction 138
Results 143
Caspase 2 levels in $Msh6^{+/+}$ and $Msh6^{-/-}$ murine embryonic fibroblasts 143
Caspase 2 sub-cellular localization in murine embryonic fibroblasts 146
Caspase 2 levels in centrosomal fractions of $Msh6^{+/+}$ and $Msh6^{-/-}$ murine embryonic fibroblasts 164
Caspase 2 levels in cytosolic, nuclear and particulate fractions of $Msh6^{+/+}$ and $Msh6^{-/-}$ murine embryonic fibroblasts 168
Apoptosis levels in $Msh6^{+/+}$ and $Msh6^{-/-}$ murine embryonic fibroblasts after caspase 2 inhibitor 170
Cleaved caspase 3 levels in $Msh6^{+/+}$ and $Msh6^{-/-}$ murine embryonic fibroblasts after caspase 2 inhibitor 172
Discussion 174
References 182

Chapter 6~ Characterization of the extrinsic apoptotic response to UVB-induced DNA damage in mismatch repair-proficient and -deficient murine embryonic fibroblasts 189
Introduction 190
Results 196
Intrinsic apoptotic protein levels in $Msh6^{+/+}$ and $Msh6^{-/-}$ murine embryonic fibroblasts 196

Apoptosis levels in Msh6^+/+^ and Msh6^-/-^ murine embryonic fibroblasts after caspase 8 inhibitor 206
Cleaved caspase 3 levels in Msh6^+/+^ and Msh6^-/-^ murine embryonic fibroblasts after caspase 8 inhibitor..............................208
Discussion 210
References 217

Chapter 7~ General discussion and conclusions 225
Characterization of the cell cycle response to UVB-induced DNA damage in mismatch repair-proficient and –deficient cells 227
Future directions 229
Characterization of the mitochondrial/intrinsic apoptotic response to UVB-induced DNA damage in mismatch repair -proficient and -deficient murine embryonic fibroblasts 229
Future directions 233
Characterization of the role of caspase 2 after UVB-induced DNA damage in mismatch repair-proficient and -deficient murine embryonic fibroblasts 234
Future directions 236
Characterization of the death receptor/extrinsic apoptotic response to UVB-induced DNA damage in mismatch repair-proficient and -deficient murine embryonic fibroblasts 236
Future directions 240
Conclusions 240
References 242

LIST OF FIGURES

Figure 1-1: DNA mismatch repair system in mammals..............................8
Figure 1-2: DNA damage response pathways 20
Figure 1-3: UV light spectrum 26
Figure 1-4: UV-induced DNA adducts 27

Figure 3-1: Schematic of cell cycle progression with checkpoints 69
Figure 3-2: G2/M cell cycle checkpoint pathway 70
Figure 3-3: Cell cycle distribution in *Msh6*$^{+/+}$ and *Msh6*$^{-/-}$ murine embryonic fibroblasts following UVB radiation 74
Figure 3-4: G2/M phase in *Msh6*$^{+/+}$ and *Msh6*$^{-/-}$ murine embryonic fibroblasts following UVB radiation 75
Figure 3-5: G2/M phase in JMG (*MSH2*$^{+/+}$) and KM (*MSH2*$^{-/-}$) cells following UVB radiation 76
Figure 3-6: CHK1 levels in JMG (*MSH2*$^{+/+}$) and KM (*MSH2*$^{-/-}$) cells following UVB radiation 78
Figure 3-7: CDC25C levels in JMG (*MSH2*$^{+/+}$) and KM (*MSH2*$^{-/-}$) cells following UVB radiation 79
Figure 3-8: CDC2 levels in JMG (*MSH2*$^{+/+}$) and KM (*MSH2*$^{-/-}$) cells following UVB radiation 80
Figure 3-9: WEE1 levels in JMG (*MSH2*$^{+/+}$) and KM (*MSH2*$^{-/-}$) cells following UVB radiation 81

Figure 4-1: Mitochondrial apoptotic pathway 96
Figure 4-2: p53 levels in *Msh6*$^{+/+}$ and *Msh6*$^{-/-}$ murine embryonic fibroblasts ...100
Figure 4-3: Apoptosis levels in *Msh6*$^{+/+}$, *Msh6*$^{-/-}$, *Msh6*$^{-/-}$ *p53*$^{+/-}$, *Msh6*$^{-/-}$ *p53*$^{-/-}$, *p53*$^{-/-}$ murine embryonic fibroblasts 102
Figure 4-4: Mitochondrial membrane potential in *Msh6*$^{+/+}$ and *Msh6*$^{-/-}$ murine embryonic fibroblasts 104
Figure 4-5: Cellular fractionation of *Msh6*$^{+/+}$ and *Msh6*$^{-/-}$ murine embryonic fibroblasts 105

Figure 4-6: Bax levels in *Msh6*$^{+/+}$ and *Msh6*$^{-/-}$ murine embryonic fibroblast fractions 107

Figure 4-7: Bid levels in *Msh6*$^{+/+}$ and *Msh6*$^{-/-}$ murine embryonic fibroblast fractions 108

Figure 4-8: Cytochrome c release in *Msh6*$^{+/+}$ and *Msh6*$^{-/-}$ murine embryonic fibroblast fractions 109

Figure 4-9: Smac/DIABLO levels in *Msh6*$^{+/+}$ and *Msh6*$^{-/-}$ murine embryonic fibroblasts 110

Figure 4-10: Caspase 9 levels in *Msh6*$^{+/+}$ and *Msh6*$^{-/-}$ murine embryonic fibroblasts 111

Figure 4-11: Cleaved caspase 3 levels in *Msh6*$^{+/+}$ and *Msh6*$^{-/-}$ murine embryonic fibroblasts 112

Figure 4-12: Apoptosis levels (via Annexin V/PI assay) after pan-caspase inhibitor in *Msh6*$^{+/+}$ and *Msh6*$^{-/-}$ murine embryonic fibroblasts 114

Figure 4-13: Apoptosis levels (via Annexin V/PI assay) after caspase 9 inhibitor in *Msh6*$^{+/+}$ and *Msh6*$^{-/-}$ murine embryonic fibroblasts 115

Figure 4-14: Cleaved caspase 3 levels after caspase 9 inhibitor in *Msh6*$^{+/+}$ and *Msh6*$^{-/-}$ murine embryonic fibroblasts 116

Figure 5-1: Caspase 2 apoptotic pathway 139

Figure 5-2: Pro-caspase 2 levels in *Msh6*$^{+/+}$ and *Msh6*$^{-/-}$ murine embryonic fibroblasts 144

Figure 5-3: Pro- and cleaved caspase 2 levels in *Msh6*$^{+/+}$ and *Msh6*$^{-/-}$ murine embryonic fibroblasts 145

Figure 5-4: Caspase 2 localization in *Msh6*$^{+/+}$ and *Msh6*$^{-/-}$ murine embryonic fibroblasts 148

Figure 5-5: Caspase 2 localization in *Msh2*$^{+/+}$ and *Msh2*$^{-/-}$ murine embryonic fibroblasts 150

Figure 5-6: Caspase 2 does not localize to the Golgi in *Msh6*$^{+/+}$ and *Msh6*$^{-/-}$ murine embryonic fibroblasts 152

Figure 5-7: Caspase 2 does not localize to the Golgi in *Msh2*$^{+/+}$ and *Msh2*$^{-/-}$ murine embryonic fibroblasts 153

Figure 5-8: Caspase 2 does not localize to the ER in *Msh6*$^{+/+}$ and *Msh6*$^{-/-}$ murine embryonic fibroblasts 155

Figure 5-9: Caspase 2 does not localize to the ER in *Msh2*$^{+/+}$ and *Msh2*$^{-/-}$ murine embryonic fibroblasts 156

Figure 5-10: Caspase 2 may localize to the mitochondria in *Msh6*$^{+/+}$ and *Msh6*$^{-/-}$ murine embryonic fibroblasts 158

Figure 5-11: Caspase 2 may localize to the mitochondria in *Msh2*$^{+/+}$ and *Msh2*$^{-/-}$ murine embryonic fibroblasts 159

Figure 5-12: Caspase 2 localizes to the centrosomes in *Msh6*$^{+/+}$ and *Msh6*$^{-/-}$ murine embryonic fibroblasts 161

Figure 5-13: Caspase 2 localizes to the centrosomes in *Msh2*$^{+/+}$ and *Msh2*$^{-/-}$ murine embryonic fibroblasts 163

Figure 5-14: Caspase 2 levels in centrosomal fractions of *Msh6*$^{+/+}$ and *Msh6*$^{-/-}$ murine embryonic fibroblasts 165

Figure 5-15: Caspase 2 does not localize to the PML bodies in *Msh6*$^{+/+}$ and *Msh6*$^{-/-}$ murine embryonic fibroblasts 166

Figure 5-16: Caspase 2 does not localize to the PML bodies in *Msh2*$^{+/+}$ and *Msh2*$^{-/-}$ murine embryonic fibroblasts 167

Figure 5-17: Caspase 2 levels in cytosolic, nuclear and membrane/particulate fractions of *Msh6*$^{+/+}$ and *Msh6*$^{-/-}$ murine embryonic fibroblasts 170

Figure 5-18: Apoptosis levels (via Annexin V/PI assay) after caspase 2 inhibitor in *Msh6*$^{+/+}$ and *Msh6*$^{-/-}$ murine embryonic fibroblasts 171

Figure 5-19: Caspase 3 levels after caspase 2 inhibitor in *Msh6*$^{+/+}$ and *Msh6*$^{-/-}$ murine embryonic fibroblasts 173

Figure 6-1 A: TNFα-TNFR1 apoptotic pathway 192

Figure 6-1 B: FasL-Fas apoptotic pathway 193

Figure 6-2: TNFα levels in *Msh6*$^{+/+}$ and *Msh6*$^{-/-}$ murine embryonic fibroblasts 197

Figure 6-3: TNFR1 levels in *Msh6*$^{+/+}$ and *Msh6*$^{-/-}$ murine embryonic fibroblasts 198
Figure 6-4: TRADD levels in *Msh6*$^{+/+}$ and *Msh6*$^{-/-}$ murine embryonic fibroblasts 199
Figure 6-5: RIP levels in *Msh6*$^{+/+}$ and *Msh6*$^{-/-}$ murine embryonic fibroblasts 200
Figure 6-6: Fas levels in *Msh6*$^{+/+}$ and *Msh6*$^{-/-}$ murine embryonic fibroblasts 201
Figure 6-7: FADD-pSer191 levels in *Msh6*$^{+/+}$ and *Msh6*$^{-/-}$ murine embryonic fibroblasts 202
Figure 6-8: Caspase 10 levels in *Msh6*$^{+/+}$ and *Msh6*$^{-/-}$ murine embryonic fibroblasts 204
Figure 6-9: Caspase 8 levels in *Msh6*$^{+/+}$ and *Msh6*$^{-/-}$ murine embryonic fibroblasts 206
Figure 6-10: Apoptosis levels (via Annexin V/PI assay) after caspase 8 inhibitor in *Msh6*$^{+/+}$ and *Msh6*$^{-/-}$ murine embryonic fibroblasts 207
Figure 6-11: Caspase 3 levels after caspase 8 inhibitor in *M*[illegible]$^{+/+}$ and *Msh6*$^{-/-}$ murine embryonic fibroblasts 209

Figure 7-1: Model of Msh6-dependent apoptosis after UVB-induced DNA damage 239

LIST OF ABBREVIATIONS, SYMBOLS AND NOMENCLATURE

6-4PP	6-4 photoproduct
6-TG	6-Thioguanine
ADP	Adenosine diphosphate
ATP	Adenosine triphosphate
ATR	Ataxia telangiectasia related protein
BASC	BRCA1-associated genome surveillance complex
BLM	Bloom's syndrome protein
CDC2	Cell division cycle 2 protein
CDC25C	Cell division cycle 25 C
CHK1	Checkpoint kinase 1 protein
CIN	Chromosomal instability
COX IV	Cytochrome oxidase subunit IV
CPD	Cyclobutane pyrimidine dimmer
DD	Death domain
DED	Death effector domain
DISC	Death-inducing signaling complex
DNA	Deoxyribonucleic Acid
ER	Endoplasmic reticulum
FADD	Fas-associated death domain protein
HNPCC	Hereditary non-polyposis colorectal cancer
IAP	Inhibitor of apoptosis
IR	Ionizing radiation
kDa	Kilo Dalton(s)
MBD4	Methyl-CpG binding domain protein
MEFs	Mouse embryonic fibroblasts
MGMT	Methylguanine DNA methyltransferase
MMR	DNA mismatch repair
MNNG	*N*-methyl-*N'*-nitroso-*N*-nitrosoguanidine
MNU	methylnitrosourea
MOMP	Mitochondrial outer membrane permeabilization
MSI	Microsatellite instability
NER	Nucleotide excision repair
NF1	Neurofibromatosis type 1
O^6-MG	O^6-Methylguanine
PARP	Poly (ADP-ribose) polymerase
PCC	Pearson's correlation coefficient
PCNA	Proliferating cell nuclear antigen
PIDD	p53-inducible protein with death domain
PML	Promyelocytic leukemia nuclear bodies

p/s	Penicillin/streptomycin
RAIDD	RIP-associated ICH-1/CED-3 homologous protein with death domain
RIP	Receptor interacting protein
Smac/DIABLO	Second mitochondria-derived activator of caspases/Direct IAP binding protein with low PI
TCR	Transcription coupled repair
TMZ	Temozolomide
TNFa	Tumor necrosis factor alpha
TNFR1	TNF receptor
TRADD	TNFR1-associated protein with death domain
TRAF2	TNF receptor-associated factor 2
TRAIL	TNF-related apoptosis inducing ligand
UV	Ultraviolet radiation

~ Chapter 1 ~

Literature Review

Introduction

The pathway to tumorigenesis is complex. Understanding of the cellular response underlying the development of tumorigenesis is important because of the implicit relationship to the treatment and prevention of cancer. There are several ways in which the cell maintains genomic stability: through cell cycle checkpoints, DNA repair and programmed cell death. The cell cycle checkpoint allows the cell time to repair damaged DNA, while apoptosis proceeds if there is too much damage to the DNA. There exist multiple pathways of repair in the cell, including the DNA mismatch repair (MMR) pathway. Cells that lack MMR are predisposed to tumorigenesis through multiple pathways including increased mutagenesis, or the mutator phenotype, decreased apoptosis and decreased ability to undergo cell cycle arrest in response to DNA damage. How a cell determines which pathway will proceed is dependent on the type of DNA damage that occurs, the specific DNA damage sensors involved and the mechanism that transduces the signal to the downstream pathway. There is little known about the mechanisms and pathways that mediate MMR-dependent processes outside the realm of repair. The involvement of the MMR proteins in DNA damage recognition and repair, cell cycle arrest and apoptosis make studying these proteins a valuable way to gain insight into the DNA damage response. The role of MMR in the cellular response to DNA damage and in tumorigenesis is therefore one of significant importance to the field of cancer research.

Genomic Instability

Cancer results from the accumulation of genetic alterations. Indeed, nearly all tumors and leukemias display genomic instability. The hypothesis that cancer cells are genomically unstable was first made in 1929, when Theodor Boveri observed aneuploidy in tumor cells. Since this initial hypothesis, the concept of genomic instability has greatly expanded. There are innumerable different genetic alterations that have been observed in human cancers. These genetic alterations are divided in to two general categories: simple sequence alterations and large scale genomic alterations.

Simple sequence alterations are changes in a small number of base pairs and include base substitutions or point mutations and insertions/deletions on the nucleotide level. DNA mutations can lead to changes in the amino acid sequence that may be pathogenic, or can result in no changes to the amino acid sequence, thus are silent mutations. If mutations occur in the coding regions of genes, they may interfere with gene function, leading to changes in protein structure and/or function. If a mutation is within a splice site, additional exons or skipped exons may result, producing a protein with altered function or a non-functional protein. A mutation can also lead to the formation of a truncated protein, if a premature stop codon is created by altering the amino acid sequence. Insertion/deletion loops can also form in the absence of MMR and are caused by microsatellite (mono- and dinucleotide repeats) slippage during DNA replication. Microsatellite instability (MSI) is the measure of instability on the DNA level and results when microsatellite slippage is left unrepaired. In order to maintain DNA fidelity, the intrinsic proofreading ability of DNA polymerases acts as the first line of defence during

DNA replication. Additionally, a repair system, DNA mismatch repair (MMR) is a post-replicative repair system that ensures replication fidelity by repairing small insertion-deletion loops and single base mismatches involving normal or damaged bases that have not been repaired by DNA polymerase proofreading. The process of DNA replication produces one error in approximately 1×10^7 cells (Boland 1997). When MMR genes are inactivated the rate of spontaneous mutation increases 50 to1000-fold (Modrich and Lahue 1996; Jiricny 1998; Buermeyer et al. 1999; Kolodner and Marsischky 1999; Schofield and Hsieh 2003). This "mutator phenotype" is readily observed by assessing microsatellite instability that occurs at repetitive tracts of DNA, such as at mono- and dinucleotide repeats [reviewed in (Andrew and Peters 2001)]. MMR proteins can also recognize and repair mismatches containing altered bases resulting from DNA damage or errors in repair of damaged bases. MMR works in concert with other repair mechanisms, such as base excision repair, nucleotide excision repair, non-homologous end-joining and homologous recombination repair that exist in order to ensure the repair of DNA damage by endogenous or exogenous factors. All of these repair pathways exist in order to ensure stability of the genome.

Early in the progession towards tumorigenesis, if mutations occur in genes that function in the maintenance of genomic stability, such as MMR, this promotes increased genomic mutation rates. The increase in genomic mutation rate can account for the discrepancy between the low levels of mutations in normal cells and the large number of mutations that typify a wide variety of human malignancies (Loeb 1991). The overall rate of spontaneous mutations in somatic human cells has been approximated at 1.4×10^{-10}

nucleotides/cell/division or 2.0 x 10^{-7} mutations/gene/cell division (DeMars and Held 1972). This is far too low to account for the thousands of DNA alterations observed in human cancer cells.

Large scale genomic alterations, or chromosomal instability (CIN), includes variations in chromosome number (aneuploidy) and chromosome structure (chromosomal translocations, inversions, deletions and duplications). CIN is characteristic of many human solid tumors [reviewed in (Coleman and Tsongalis 1999)]. Structural chromosomal instability is caused by defects in DNA damage response, cell cycle checkpoints or telomere dysfunction [reviewed in (Gollin 2005)], while aneuploidy results from defects in chromosome segregation. One of the most characterized chromosomal variations is the Philadelphia chromosome [trans(9;22) (q34;q11)] that is associated with chronic myelogenous leukemia. It was the first non-random, recurring chromosomal alteration associated with the development and pathogenesis of a disease (Nowell 1974). Centrosomes have also been shown to be important in maintenance of chromosomal stability. These organelles are integral in ensuring proper chromosomal segregation during mitosis. Anomalous centrosome number has been found in various types of cancers including breast, prostate, colon and brain (Doxsey 1998).

The doctrine states that MSI and CIN are mechanistically distinct. For example, a recent study analyzing the relationship between CIN, MSI and epigenetic instability in colorectal cancer concluded that CIN and MSI in colorectal cancers can be considered as two alternative mechanisms (Derks et al. 2008). However, recent evidence suggests considerable overlap between these two pathways in particular cancers, including a possible role for MMR.

DNA Mismatch Repair

Mammalian DNA Mismatch Repair

The repair of mismatches by MMR is initiated by a MutS heterodimer. This consists of MSH2 bound to MSH6 (MutSα), or MSH2 bound to MSH3 (MutSβ) (Fig. 1-1). The MutSα heterodimer preferentially binds to single base mismatches, while MutSβ preferentially binds to small insertion/deletion loops, although there is some extent of functional overlap between the two [reviewed in (Jiricny 1998; Buermeyer et al. 1999; Jiricny 2006). MutSα is found in greater abundance than MutSβ and is the primary mismatch recognition heterodimer (Drummond et al. 1997). In the absence of MutSβ, MutSα has the ability to compensate for MutSβ in the repair of insertion/deletion loops, however, this compensation is not reciprocal. Thus, the loss of MSH2 or MSH6 has a greater impact on the frequency of mutations and consequently on tumorigenesis than does loss of MSH3 (Genschel et al. 1998). After initial binding by either MutSα or MutSβ, the MutL heterodimer is recruited to the site of the mismatch (Fig. 1-1). Several MutL heterodimers exist: MutLα, which consists of MLH1 bound to PMS2, is the MutL heterodimer primarily involved in mismatch correction (Prolla et al. 1994; Li and Modrich 1995; Flores-Rozas and Kolodner 1998). The MutLβ heterodimers consist of MLH1/MLH3 or MLH1/PMS1 and play a minor role in MMR. After recruitment of the MutS and MutL heterodimers to the DNA mismatch, additional proteins are recruited to the site of the mismatch including those involved in the excision of the mismatch and resynthesis and ligation of the corrected strand. Exonuclease 1 (EXO1) performs 5'-3' excision from the MutLα incision site to beyond the mismatch (Kadyrov et al. 2006). Replication protein A (RPA) seems to be involved in many stages of MMR, including binding to nicked heteroduplex DNA prior to MutSα or MutSβ, protecting the single strand DNA region gapped by excision, as well as facilitating DNA resynthesis (Ramilo et al. 2002; Dzantiev et al. 2004; Zhang et al. 2005; Guo et al. 2006). Finally, DNA polymerase δ (pol δ) resynthesizes the DNA strand [reviewed in (Li 2008)]. Proliferating cell nuclear antigen (PCNA) has been shown to interact with MSH2, MSH3, MSH6 and MLH1 and is hypothesized to play roles in the initiation and resynthesis steps of MMR (Umar et al. 1996; Gu et al. 1998; Clark et al. 2000; Flores-Rozas et al. 2000; Kleczkowska et al. 2001). PCNA also may help localize MutSα and MutSβ to mispairs in newly replicated DNA (Lau and Kolodner 2003; Shell et al. 2007).

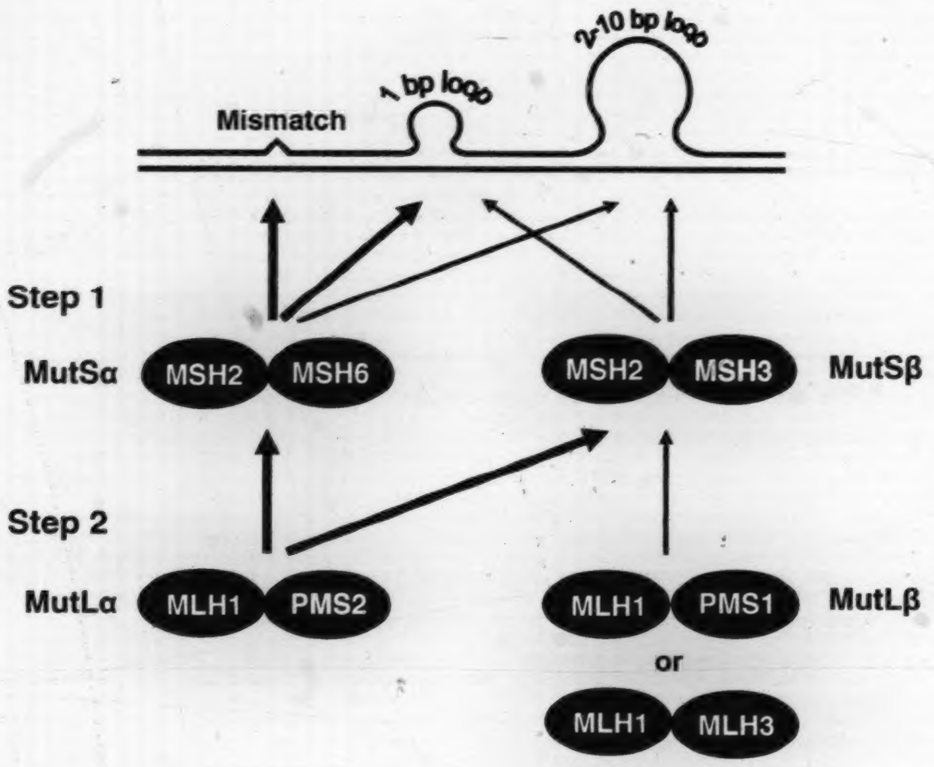
2-10 bp loop
1 bp loop
Mismatch
Step 1
MutSα
MSH2
MSH6
MSH2
MSH3
MutSβ
Step 2
MutLα
MLH1
PMS2
MLH1
PMS1
MutLβ
or
MLH1
MLH3

Figure1-1: Mammalian DNA mismatch repair

Step 1: MutSα (MSH2/MSH6) heterodimer binds to DNA mismatches or 1nucleotide small loops. MutSβ (MSH2/MSH3) heterodimer binds to DNA loops up to 10 nucleotides. Step 2: MutL heterodimer binds and the DNA adduct is processed. The MutLα heterodimer, MLH1/PMS2 is the predominant MutL complex and binds both MutS dimers. The MutLβ heterodimers, MLH1/PMS1 or MLH1/MLH3 are only minor partners in the DNA mismatch repair process and only bind to MutSβ heterodimer.

MSH2 and MSH6 have been shown to be phosphorylated *in vivo*, as well as *in vitro* by protein kinase C and casein kinase II (Christmann et al. 2002). Evidence strongly suggests that phosphorylation of MutSα increases the mismatch-binding capacity of this heterodimer and may have an impact on its nuclear translocation. Experiments have suggested that the MutSα complex is preformed in the cytosol and translocated to the nucleus dependent upon protein phosphorylation and alkylation damage. Phosphorylated MSH2 and co-immunoprecipitated phosphorylated MSH6 are present in the cytoplasm and predominantly in the nucleus. Phosphorylation *in vivo* and *in vitro* was found to be more efficient for MSH6, which contains more potential phosphorylation sites than MSH2. Since MSH6, not MSH2, contains a potential nuclear localization signal, MSH6 seems to be required for translocation of MSH2 into the nucleus (Christmann and Kaina 2000; Christmann et al. 2002).

DNA Mismatch Repair and Interacting Proteins

MMR interactions with other proteins are only beginning to be elucidated. There are many studies suggesting functional overlap between MMR and other repair pathways, as well as cell cycle and apoptosis pathways. MMR proteins interact with proteins involved in the cell cycle checkpoint pathway. Studies have shown that both Chk1 and Chk2/CHK2 interact with MSH2 (Brown et al. 2003; Adamson et al. 2005). Wang and Qin (2003) demonstrated that MSH2 interacts with the ATR kinase constitutively to form a signaling module that regulates the phosphorylation of downstream effectors including Chk1. They also found that MSH2 and ATR function upstream to regulate the response pathway to DNA damage caused by MNNG (Wang and Qin 2003). PCNA has been shown to interact MSH2, MSH3, MSH6 and MLH1, suggesting that it plays a role in multiple steps of MMR (Umar et al. 1996; Gu et al. 1998; Clark et al. 2000; Flores-Rozas et al. 2000; Kleczkowska et al. 2001). Additionally, MSH2, MSH6 and MLH1 have been shown to be components of BASC (BRCA1-associated genome surveillance complex) (Wang et al. 2000). BASC is a large protein complex of tumor suppressors, DNA damage repair proteins and signal transducing proteins, such as ATM and the MRN complex, that function in DNA repair and DNA damage surveillance. The proteins in this complex may work in monitoring DNA and promoting DNA damage responses such as cell cycle checkpoints, DNA repair or apoptosis.

Mutations in DNA Mismatch Repair Genes and Hereditary Non-polyposis Colorectal Cancer

The MMR genes rose in importance in the field of cancer genetics when mutations in these genes became associated with the hereditary colon cancer syndrome, hereditary non-polyposis colorectal cancer (HNPCC). HNPCC is an autosomal dominant cancer syndrome that accounts for approximately 5-10% of all human sporadic colorectal cancers. HNPCC presents with an early age of onset, between 40 and 45 years of age, and high penetrance. The incidence of this disease is approximately 1/1000 in the general population (Umar et al. 2004). Persons with HNPCC have a highly increased life-time risk of developing cancers of the colon and endometrium [reviewed in (Vasen 2007)]. In addition to these primary cancers, patients with HNPCC also may have an increased risk of developing cancers of the stomach, ovary, pancreas and gastrointestinal tract (Baglioni and Genuardi 2004).

HNPCC is characterized by a germline heterozygous mutation in one of the MMR genes. Subsequently, a second mutation, or 'hit', causes silencing of the second allele. This follows Knudson's two-hit hypothesis of cancer development. In Knudson's two-hit model, cancer is developed through the loss of function of both copies of a tumor suppressor gene (Knudson 1971). In the case of HNPCC, the first 'hit' is the inherited germline mutation of one of the MMR genes in the cells of an affected individual and the second 'hit' occurs when the MMR gene is inactivated in a specific tissue, such as colon, endometrium, or ovary. Inactivation of MMR genes may occur via point mutations, large deletions, or hypermethylation of the promoter of *MLH1* or another MMR gene (Herman et al. 1998; Pinto et al. 2008). Inactivation of the MMR gene leads to the mutator phenotype (discussed earlier); that is, increased mutation frequency (Parsons et al. 1993) and acquisition of subsequent mutations in other tumor suppressor genes which lead to tumorigenesis.

Microsatellites are tandemly repeated mono-, di-, tri-, quatra-, or pentanucleotide sequences distributed throughout the genome. Microsatellites are commonly found in non-coding regions of the human genome, although they are also found within the coding regions of certain genes as *BAX*, *PTEN* and *TGFβRII*. In the absence of functional MMR, insertion/deletion loops caused by strand slippage during DNA replication are left unrepaired and leads to propagation of the expanded/contracted repeat in the daughter DNA strand. Microsatellite instability is a hallmark of HNPCC tumors. Over 85% of HNPCC tumors display high MSI, while 17% of sporadic colorectal tumors display high MSI (Pedroni et al. 1999; Woerner et al. 2005). Mutations occurring within non-random repetitive DNA tracts in the absence of MMR have been identified in HNPCC tumors, helping to map key pathways involved in tissue specific tumorigenesis [reviewed in (Peltomaki 2001)].

Mutations in *MSH2* and *MLH1* are the most prevalent in HNPCC, accounting for approximately 90% of identified HNPCC mutations. Of the remaining 10% of identified mutations, *MSH6* is primarily mutated, followed by *PMS2* and *PMS1*, which are rarely mutated [reviewed in (Peltomaki 2001)]. *MSH3* has not been reported to be involved in HNPCC (Korhonen et al. 2007). Although germline mutations in *MSH2, MLH1, MSH6, PMS2* and *PMS1* have been associated with the development of HNPCC, only approximately 50% of HNPCC patients have any mutations in the known MMR genes. This indicates that there are mutations in other genes involved in the development of HNPCC that have yet to be identified (Abdel-Rahman et al. 2005).

DNA Mismatch Repair-deficient Individuals

There are rare individuals with inherited homozygous mutations in a MMR gene [reviewed in (Felton et al. 2007)]. In the earliest reports, 4 siblings with inherited mutations in both alleles of *MLH1* developed lymphoma or leukemia before the age of six. Three of the four children developed café au lait spots, and two of these three children concurrently developed neurofibromas consistent with Neurofibromatosis type I (NF1), despite no family history of this disease (Ricciardone et al. 1999; Wang et al. 1999). Since then, homozygous mutations in *MLH1, MSH2, MSH6* and *PMS2* have been described in individuals/families. Individuals with no MMR function present with childhood onset of hematological and brain malignancies. Those with residual MMR function can also present with gastrointestinal cancers and an age of onset in the second to fourth decade. Individuals with biallelic MMR mutations often present with café-au-lait spots, regardless of the level of MMR function remaining. Our laboratory has described a novel homozygous mutation in the *MSH2* gene in a 24 month-old individual. This child presented with acute lymphocytic leukemia (T-cell) and numerous café-au-lait spots consistent with NF1 (Whiteside et al. 2002). Constitutive loss of MMR results in genome-wide instability, but tumorigenesis occurs in specific tissues. In contrast, HNPCC patients that inherit a heterozygous mutation in one of the MMR genes rarely develop hematological cancers, although they have been shown to occur (Hirano et al. 2002). It is the different mode of inheritance (homozygous versus heterozygous) of mutations in MMR genes that leads to different phenotypes.

Microsatellite Instability in Sporadic Cancer

A variable but significant number of sporadic cancers demonstrate varying levels of MSI and/or defects in MMR in specific tissues, including cancers of the skin, colon, endometrium, ovary, cervix, prostate, stomach, lung and brain (Risinger et al. 1993; Boyer et al. 1995; Egawa et al. 1995; Chen et al. 1996; dos Santos et al. 1996; Claij and te Riele 1999; Alvino et al. 2002; Leahy et al. 2002; Castiglia et al. 2003). For example, 17% of sporadic colorectal tumors display high MSI (Pedroni et al. 1999; Woerner et al. 2005).To date the list of sporadic cancers with MSI has grown to include studies on a wide variety of cancers. Therefore, loss of /defects in MMR are important steps towards sporadic cancer, underscoring the significance of understanding how misregulated MMR leads to tumorigenesis.

Mouse Models of DNA Mismatch Repair

Mice with homozygous deficiencies for each of the MMR genes *Msh2, Msh3, Msh4, Msh5, Msh6, Mlh1, Pms1, Pms2* and *Mlh3* have been created using homologous recombination in order to aid in the elucidation of mammalian MMR function. In contrast to humans, mice heterozygous for one of the MMR genes are not cancer prone. The most prevalent cancers that mice homozygous deficient for any one of the MMR genes develop are early onset thymic lymphomas. Other tumors types such as ovarian and gastrointestinal also develop, but at lower frequencies (Baker et al. 1995; de Wind et al. 1995; Reitmair et al. 1995; Edelmann et al. 1996; Edelmann et al. 1997; Narayanan et al. 1997; Prolla et al. 1998; de Wind et al. 1999; Edelmann et al. 1999; Edelmann et al. 2000; Kneitz et al. 2000). Rare individuals with biallelic MMR mutations also develop hemotological malignancies, suggesting that the mouse may be a suitable model for cancer development in the absence of MMR, despite differences in loss of heterozygosity between mouse and humans. I utilized $Msh2^{-/-}$ *and* $Msh6^{-/-}$ mice and their isogenic wildtype counterparts to obtain mouse embryonic fibroblasts (MEFs) for my studies. Mice with null mutations in *Msh2* and *Msh6* have a reduced life span; $Msh2^{-/-}$ mice develop T-cell thymic lymphomas at an early age (approximately 2 months) (de Wind et al. 1995; Reitmair et al. 1995), while $Msh6^{-/-}$ mice develop a broader spectrum of tumors. Published data reports that the most predominant types of tumors were gastrointestinal tumors and B- and T-cell lymphomas (Edelmann et al. 1997). Our colony of the identical mice develops predominantly B- and T-cell lymphomas.

MutSα Signal Transduction

Although my thesis focuses on the roles of MMR other than repair, an understanding of what is known regarding the mechanism behind MMR activity in DNA repair is helpful. A brief overview of models of MMR action follows.

During DNA repair, the binding of MutS heterodimers to DNA mismatches initiate the MMR machinery. Three models have been proposed to describe how eukaryotic MMR recognizes mismatched bases in DNA and transduces the signal to engage other MMR machinery: 1) the molecular switch/sliding clamp model, 2) the ATP-dependent translocation model, and 3) the induced fit model.

In the molecular switch/sliding clamp model, MutSα is hypothesized to act as a molecular switch that is regulated by ATP hydrolysis and ADP/ATP binding. The MSH2-MSH6-ADP complex can bind with high affinity to the mismatch. Upon binding, ADP is exchanged for ATP, which promotes a conformational change in MSH2-MSH6 into a clamp with a diminished affinity for the mismatch and thus can diffuse freely along the DNA, recruiting other components of the MMR machinery (Fishel 1998; Bellacosa 2001).

The ATP-dependent translocation model is based initially upon electron microscopic examination of MutS in *E. coli* bound to heteroduplex DNA [reviewed in (Bellacosa 2001)]. MutS generates an ATP hydrolysis-dependent DNA loop structure with the mismatch within the loop. Recognition of the DNA mismatch is not dependent on ADP binding, although the presence of ADP increases mismatch binding specificity. The binding of ATP promotes the dissociation of MutSα from the mismatch and diffusion along the DNA, signaling to other MMR proteins (Blackwell et al. 1998; Bellacosa 2001).

The induced fit model is based on the crystal structure of bacterial MutS bound to DNA mismatches. Based upon the distortion of mismatch DNA and the conformational changes that MutS undergoes upon DNA binding, this model proposes that MutS proteins do not leave the mismatch but promotes subsequent repair steps via protein-protein interaction with other MMR proteins like MutL and MutH (Lamers et al. 2000; Obmolova et al. 2000; Bellacosa 2001). In the induced fit model, ATP is necessary for 'proofreading' to confirm mismatch recognition by MutS and for enabling downstream repair events [reviewed in (Bellacosa 2001)].

Eukaryotic Strand Discrimination

DNA strand discrimination by MMR in *E. coli* is well established and based on recognition of different methylation patterns between the template and daughter DNA strands by the *E. coli* MMR protein MutH to target repair of the newly synthesized DNA strand. In eukaryotes, the lack of MutH orthologs indicates that there are other protein(s) or other mechanisms to perform strand discrimination. There are currently two main mechanisms proposed in the literature as a means of strand discrimination in eukaryotes.

The first involves recognition of single strand breaks, such as Okazaki fragments, in the DNA created during DNA synthesis. Experiments *in vitro* have shown that mammalian MMR preferentially repairs DNA with single strand breaks (Holmes et al. 1990; Thomas et al. 1991). Other work has demonstrated that MutSα and MutSβ heterodimers in *S. cerevisiae* predominantly repair the lagging strand (Pavlov et al. 2003). These data have led to the hypothesis that MutSα and MutSβ recognize mispaired DNA and that irregularities in the DNA, such as Okazaki fragments present during DNA replication in the lagging strand, direct MMR machinery to the daughter strand (Pavlov et al. 2003; Wang and Hays 2004).

The second mechanism suggests that MMR protein interactions with PCNA and orientation of the replication enzymes may be a possible mechanism of strand discrimination (Hsieh 2001). MMR is localized to DNA replication foci and is bound to the replication machinery via PCNA (Kleczkowska et al. 2001). PCNA interacts with MSH2, MSH3, MSH6 and MLH1 and is hypothesized to play roles in the initiation and resynthesis steps of MMR (Umar et al. 1996; Gu et al. 1998; Clark et al. 2000; Flores-Rozas et al. 2000; Kleczkowska et al. 2001). Moreover, PCNA enhances MSH2/MSH6 mispair binding specificity (Lau and Kolodner 2003).

The Multifunctionality of DNA Mismatch Repair

The established function of MMR is the maintenance of genomic stability through correction of single base mismatches and insertion-deletion loops that occur during DNA replication. In addition to its primary role in DNA repair, MMR is also involved in a variety of other cellular processes, such as the DNA damage response (to be discussed in subsequent sections of this literature review), double strand break repair and meiotic recombination.

Double strand breaks (DSB) in DNA are caused by a variety of elements including ionizing radiation and DNA replication. Mammalian cells possess two mechanisms for repairing DSB: non-homologous end joining and homologous recombination repair [reviewed in (Helleday et al. 2007)]. Non-homologous end joining is an error-prone repair mechanism, while homologous recombination repair is more precise. It has been shown in *S. cerevisiae* that MutSα binds to Holliday junctions that form during homologous recombination repair with a high affinity, perhaps even higher affinity than it binds to mismatched bases (Marsischky et al. 1999). Also in *S. cerevisiae*, MSH2 interacts with recombination proteins to regulate the length of heteroduplexes (Alani et al. 1994). It was shown that human MLH1 interacts with the Bloom's syndrome protein

(BLM). This is a helicase that promotes branch migration of Holliday junctions by unwinding duplexed DNA (Langland et al. 2001).

Studies in mice have shown that MMR plays a role in eukaryotic meiosis. *Mlh1*$^{-/-}$ and *Mlh3*$^{-/-}$ mice exhibit male and female sterility (Baker et al. 1996; de Vries et al. 1999; Kneitz et al. 2000; Lipkin et al. 2002). It has been shown that Mlh3 is necessary for Mlh1 binding to meiotic chromosomes, thus the cause of sterility in *Mlh1*$^{-/-}$ and *Mlh3*$^{-/-}$ mice may be caused by similar mechanisms (Lipkin et al. 2002). *Pms2*$^{-/-}$ male mice show sterility that is caused by abnormal chromosomal synapsis/pairing and recombination during meiosis. In contrast, *Pms2*$^{-/-}$ female mice are fertile (Baker et al. 1995). The effects of MMR mutations in meiosis in humans remains unclear, however, the findings outlined above show the importance of MMR in meiosis in mice.

Cellular Response to DNA Damage

Cells have several response pathways to process DNA damage and restore genetic stability dependent on the type and extent of the DNA damage. DNA damage or replication stress is detected by sensor proteins. The damage signal is passed to "transducers" of the signal which transmit it to the "effector" proteins that ultimately decide the fate of the cell (Zhou and Elledge 2000). Cell cycle checkpoints control mechanisms to temporarily delay cell cycle progression, allowing time for DNA repair to occur before the damage/mutation is propagated through mitosis. Alternatively, apoptotic machinery promotes programmed cell death when the damage is excessive or not reparable (Fig. 1-2).

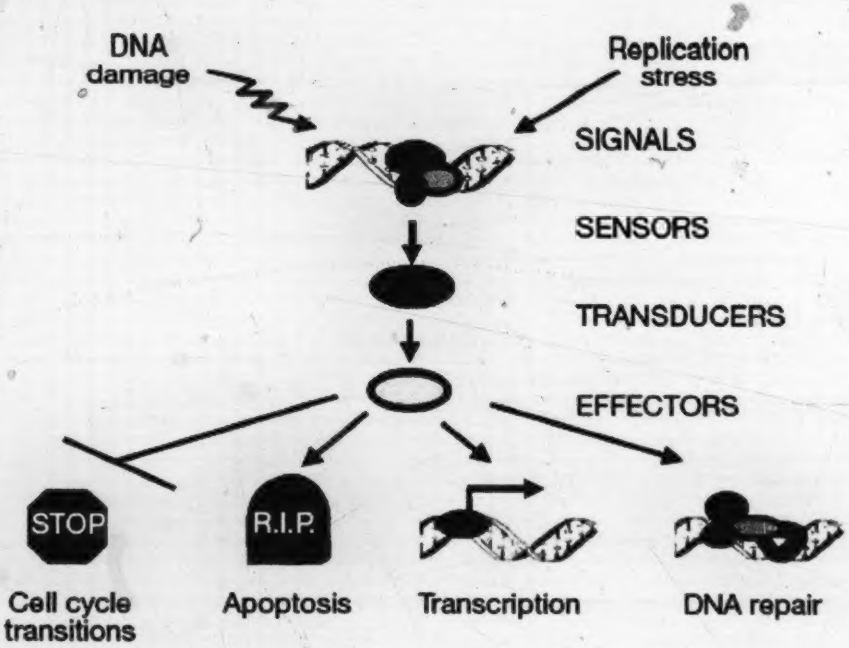
DNA
damage
Replication
stress
SIGNALS
SENSORS
TRANSDUCERS
EFFECTORS
STOP
R.I.P.
Cell cycle
transitions
Apoptosis
Transcription
DNA repair

Figure 1-2: DNA damage response

Signaling cascade from DNA damage or replication stress, through the sensing of the DNA lesions, the transduction of the signal, resulting in cellular changes such as changes in transcription, apoptosis, cell cycle arrest and DNA repair (Zhou and Elledge 2000).

Repair of endogenous or exogenous DNA damage occurs through multiple DNA repair pathways. Nucleotide excision repair (NER) removes bulky DNA lesions with the potential to block DNA replication, such as lesions imparted by ultraviolet (UV) radiation. These lesions are primarily the cyclobutane pyrimidine dimers (CPDs) and the (6-4) photoproducts (6-4PPs). Base excision repair repairs non-bulky lesions, such as bases with alkylation or oxidation damage, or single strand breaks. The non-homologous end joining and homologous recombination repair mechanisms repair double strand breaks. DNA mismatch repair (MMR) primarily repairs mismatched DNA that occurs during replication (discussed previously) and also repairs DNA adducts imparted by such things as alkylating agents [reviewed in (Lieberman 2008)]. Many of the proteins involved in the DNA damage response are involved in multiple pathways. For example, BRCA1 is involved in homologous recombination, cell cycle checkpoint regulation and apoptosis (Powell and Kachnic 2003).

Mismatch Repair and the DNA Damage Response

Recent studies have shown that the MMR proteins are multi-functional, with roles in the regulation of cell cycle, apoptosis, homeologous recombination, as well as DNA repair [reviewed in (Iyer et al. 2006)]. Increasing evidence suggests that MMR proteins have a role in recognizing DNA damage and contributing to DNA damage responses independent of repair. This comes from studies with genetic mutants that have allowed for the separation of function. MMR mutants defective in apoptosis are still functional in repair and vice versa (Drotschmann et al. 2004; Lin et al. 2004; Yang et al. 2004). A mouse model with a homozygous point mutation for G647A in *Msh2* was created by Lin et al. (2004). The *Msh2*$^{G647A/G647A}$ mouse displayed delayed onset of tumorigenesis compared to *Msh2*$^{-/-}$ mice. However, *Msh2*$^{G647A/G647A}$ MEFs had repair defects similar to *Msh2*$^{-/-}$ mice. Interestingly, *Msh2*$^{G647A/G647A}$ MEFs were sensitive to treatment with cisplatin, similar to *Msh2*$^{+/+}$ MEFs. Thus, the *Msh2*$^{G647A/G647A}$ mouse was able to initiate apoptosis after treatment with cisplatin, despite having a defect in repair (Lin et al. 2004). In the same year, Yang et al. (2004) developed another mouse model with uncoupled DNA mismatch repair and apoptosis, this time with a dominant missense mutation in *Msh6* that led to increased mutation rates associated with the loss of DNA repair.

Msh6$^{TD/TD}$ MEFs displayed sensitivity to cisplatin, similar to *Msh6*$^{+/+}$ MEFs (Yang et al. 2004).

In an elegant experiment, Cejka et al. (2004) described how the level of MLH1 protein is important in the normal cell death and G2/M checkpoint response to *N*-methyl-*N'*-nitro-*N*-nitrosoguanidine (MNNG). Using a cellular system in which MLH1 levels can be controlled, this group found that low levels of MLH1 expression (10% of normal) was sufficient for repair activity but not for cell cycle arrest and apoptosis following exposure to MNNG (Cejka et al. 2003). This study illustrates the importance of the proper level of MMR proteins in the cellular response to DNA damage.

Mismatch Repair and Alkylating Agents

The response of MMR to treatment with alkylating agents is one of the most characterized in the literature. Such S_N1 alkylating agents as MNNG, methylnitrosourea (MNU), and temozolomide (TMZ) are used in chemotherapy and cause methylation of nucleotide bases. 0^6-methylguanine (0^6-meG) is a common adduct formed after treatment with MNNG and is highly mutagenic because it mispairs with thymine instead of cytosine during DNA replication. 0^6-meG adducts are primarily repaired by methylguanine methyltransferase (MGMT). Lack of MMR confers a resistance to alkylating agents in eukaryotes and allows for accumulation of a greater number of DNA mutations prior to cell death (Aquilina and Bignami 2001). In cells deficient for any of the MMR proteins MSH2, MSH6 or MLH1, there is a decrease in apoptosis and G2/M checkpoint levels after treatment with MNNG, compared to MMR-proficient controls (Toft et al. 1999; Cejka et al. 2003; Lutzen et al. 2004; Stojic et al. 2004; Yang et al. 2004; Adamson et al. 2005). The restoration of MMR function restores sensitivity to the alkylating agent (Aquilina and Bignami 2001).

The precise mechanism by which MutSα recognition of 0^6-meG in the genome signals apoptosis remains to be determined. Two models exist; one is the 'futile repair' model in which the 0^6-meG adduct on the template strand results in a base mispair (most commonly to a T) and the induction of post-replicative MMR. The removal of the mispaired T on the daughter strand, rather than the removal of the 0^6-meG on the template strand, leads to the re-insertion of the mispaired T by DNA polymerase, which re-initiates mispair recognition and removal of the mispaired T by MMR. This leads to 'futile' cycles of repair with excision and resynthesis that result in the persistence of the DNA lesion and DNA strand breaks. Cell cycle arrest or apoptosis is promoted via other DNA damage sensors that recognize the single or double strand breaks (Kaina 1998; Karran 2001; Kaina 2003).

Experimental evidence supports the second hypothesis that MMR is involved in the 'signaling' of apoptosis in response to DNA damaging agents, such as alkylating agents. Hickman and Samson (1999) showed that, for DNA base damage by alkylation, the first step in the programmed cell death 'signaling' pathway requires MutSα and that such MutSα-dependent signaling of apoptosis is largely p53-independent (Hickman and Samson 1999).

Mismatch Repair and Cisplatin

Cisplatin [(cis-diamminedichloroplatinum (II)] is a widely used chemotherapeutic drug. It induces DNA-protein cross-links, DNA interstrand and intrastrand cross-links and DNA monoadducts. Cisplatin adducts are primarily repaired by NER, although Mutsα has been shown to bind to the 1,2-intrastrand d(GpG) crosslink induced by cisplatin (Duckett et al. 1996). Experiments performed in primary MEFs deficient for *Msh2* show decreased early G2/M arrest after exposure to cisplatin, compared to *Msh2* wildtype MEFs (Marquez et al. 2003). MEFs deficient for *Msh6* display increased survival and decreased apoptosis versus wildtype MEFs after treatment with cisplatin (Yang et al. 2004). Similarly, tumor cell lines with MMR deficiency are more resistant to the cytotoxic effects of cisplatin compared to the same cell lines with functional MMR (Aebi et al. 1996; Fink et al. 1997).

Mismatch Repair and Ionizing Radiation

Ionizing radiation (IR) is used as a treatment for solid tumors. IR induces single and double strand breaks in DNA, as well as single nucleotide modifications and DNA-protein cross-links [reviewed in (Meyers et al. 2004)]. There is conflicting data in the literature about the response of MMR to IR. It has been shown that MEFs deficient in the MMR proteins Msh2, Mlh1 or Pms2 display increased survival post-IR (Fritzell et al. 1997; Zeng et al. 2000). However, studies by other groups have shown that MMR-deficient cells display decreased survival post-IR. Using *Msh2*$^{-/-}$ MEFs, Franchitto et al. (2003) demonstrated decreased cell survival and G2/M arrest as well as increased chromosomal damage post-IR compared to *Msh2*$^{+/+}$ MEFs (Franchitto et al. 2003). In tumor cells deficient in MLH1, there was decreased cell survival and G2/M arrest compared to the control cell line in which chromosome 3 had been re-introduced to restore MLH1 function (Davis et al. 1998).

Mismatch Repair and 6-thioguanine

6-thioguanine (6-TG) is an antimetabolite used to treat leukemia. 6-TG incorporates into RNA and DNA, where it becomes methylated to become 6-methylthioguanine which mispairs with thymine during DNA replication. Cells deficient in one of the MMR proteins MSH2, MSH6 or MLH1 have been shown to be resistant to treatment with 6-TG. Furthermore, MMR is important in the regulation of G2/M arrest through the ATR-Chk1 pathway after cellular exposure to 6-TG (Hawn et al. 1995; Glaab et al. 1998; Berry et al. 2000; Yan et al. 2003; Yamane et al. 2004; Yan et al. 2004).

UV Radiation

Ultraviolet (UV) radiation is divided into three categories according to wavelength (Fig. 1-3). UVC radiation (200-250nm) has the highest amount of energy, however, it is not biologically relevant as this radiation does not reach the surface of the Earth because of absorption by the ozone layer. UVB radiation (290-320nm) is considered to be the most biologically relevant form of UV in the development of skin carcinogenesis, as it reaches the Earth's surface and possesses enough energy to cause DNA damage. UVA radiation (320-400nm) generates reactive oxygen species, but is minimally involved in UV-induced DNA damage. It is 1000 times less effective than UVB in causing apoptotic keratinocytes, known as sunburn cells. UVB radiation is readily absorbed by DNA, inducing the formation of the DNA lesions cyclobutane pyrimidine dimers (CPDs) and 6-4 photoproducts (6-4PPs) (Fig. 1-4).

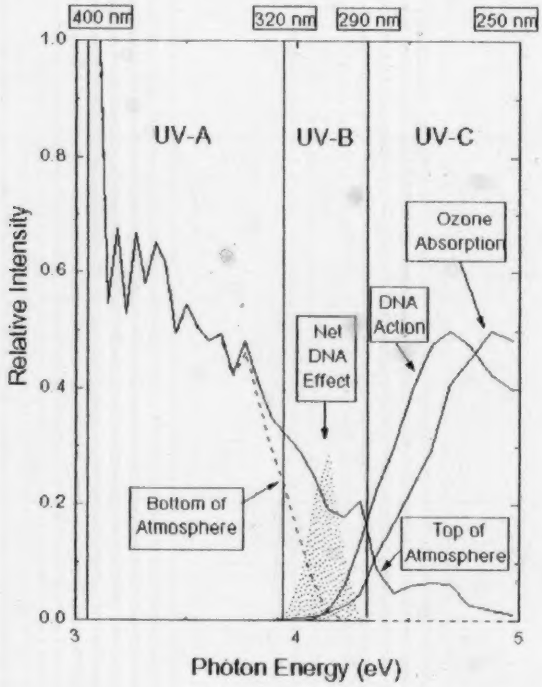

Figure 1-3: Ultraviolet light spectrum

UVC (200-250nm) has the highest energy but does not reach the earth's surface due to the ozone layer. UVB (290-320nm) is important in skin tumorigenesis and is 1000 times more efficient than UVA (320-400nm) in causing skin erythema (www.phys.ksu.edu/gene/e3f3.html).

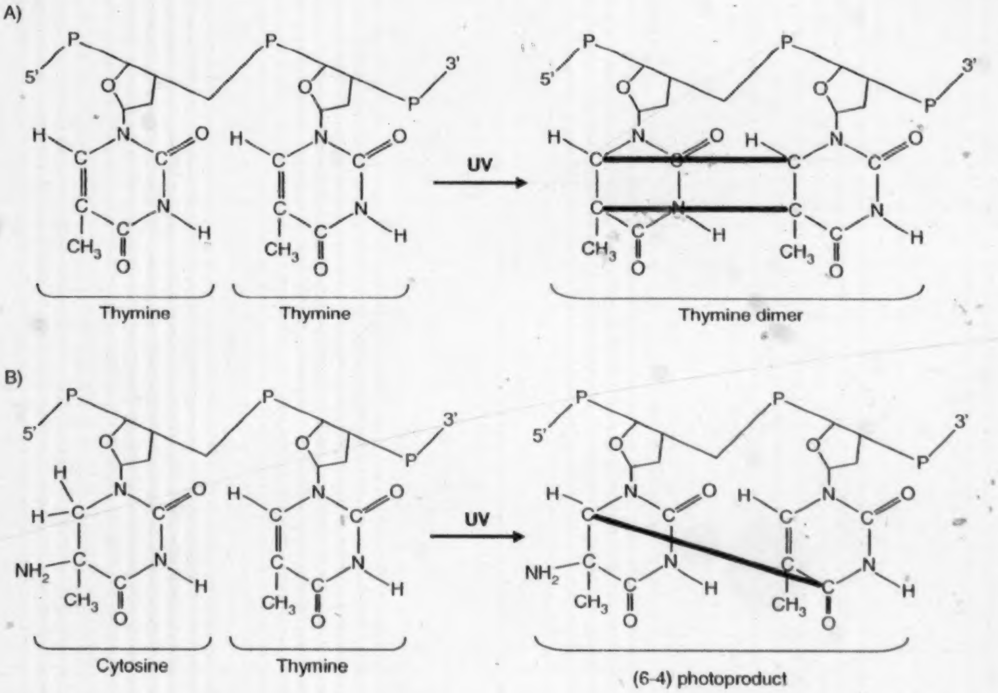
A)
5'
P
O
N
H
C
O
CH$_3$
H
3'
UV
Thymine
Thymine
Thymine dimer
B)
NH$_2$
Cytosine
Thymine
(6-4) photoproduct

Figure 1-4: UV-induced DNA adducts

A) Formation of a cyclobutane pyrmidine dimer after UV radiation (thymine dimer illustrated). Double bond forms between C-4 and C-5 carbons of two adjacent pyrimidines TT or CC and becomes saturated to produce a four-membered ring
B) Formation of a (6-4) photoproduct after UV radiation. Single bond forms between C-4 and C-6 position of two adjacent pyrimidines, either CT or CC residues. [Adapted from (Matsumura and Ananthaswamy 2002)].

Non-melanoma Skin Cancer

The incidence of skin cancer in Canada is high. Non-melanoma skin cancer (NMSC) is a common form of human skin cancer that causes a significant public health burden. According to the Canadian Cancer Society that there will be an estimated 73,000 new cases of NMSC in Canada in 2008 (Canadian Cancer society website). This high incidence of NMSC reflects the fact that Canadians are exposed to increasing amounts of UVB radiation from the sun due in part to ozone depletion, which normally shields the earth from solar radiation (Moseley and Mackie 1997; de Gruijl 1999). As stated above, UVB radiation is a powerful environmental carcinogen that plays a significant role in the development of skin cancer through generation of mutagenic DNA lesions. If left un-repaired, UVB-induced DNA lesions can cause genomic instability and/or mutations that lead to cellular dysfunction and/or unscheduled proliferation (de Gruijl et al. 2001). Understanding of the mechanisms that underlie the cellular response to UVB-induced DNA damage, including apoptosis, will further our understanding of the pathogenesis of skin cancer and aid in the prevention of this disease.

DNA Mismatch Repair and Skin Cancer

A recently published comprehensive study by our laboratory measured the MMR proteins MSH2, MSH3, MSH6, MLH1 and PMS2 in over 200 non-melanoma skin cancer (NMSC) biopsies. By comparing relative nuclear and cytoplasmic staining, this investigation demonstrated that subcellular localization of MMR proteins was misregulated in human NMSC. Moreover, MMR protein levels were increased in both squamous cell carcinomas (SCC) and basal cell carcinomas (BCC) compared to normal skin. In terms of MMR protein levels, BCC was more similar to normal skin than SCC, which is an interesting observation as SCC is more aggressive than BCC. MMR protein levels were consistently predictive of histology (Young et al. 2007). The findings in this study are consistent with other studies that report increased levels of MSH2 in SCC (Liang et al. 2001) and BCC (Rass et al. 2000). Another recent study has shown increased levels of MSH2 mRNA in malignant melanoma, metastases of melanoma, and a melanoma cell line as compared with melanocytic nevi or primary cultured benign melanocytes. Furthermore, treatment of melanoma cells with UVB led to increased levels of MSH2 RNA after 30 minutes (Seifert et al. 2008). Conversely, an earlier study showed that biallelic inactivation of MLH1 occurred in primary melanoma and suggests that disruption/loss of MMR might have had a role in the development of melanoma (Castiglia et al. 2003). These studies show a role for MMR in both NMSC and melanoma.

DNA Mismatch Repair and the Response to UV-induced DNA Damage

CPDs and 6-4PPs are primarily removed by nucleotide excision repair (NER). The role of MMR in post-UV repair remains controversial in part due to the diversity of model organisms, UV dosage employed and recently retracted data [reviewed in (Young et al. 2003)]. In mammalian cells, it has been shown that the MutS heterodimer binds to UVB-induced mismatch/photoproduct compound lesions (Mu et al. 1997; Wang et al. 1999). Evidence exists both for and against a role for MMR in the transcription coupled repair (TCR) of CPDs [reviewed in (Young et al. 2003)]. In mammalian cells MSH2 has been demonstrated to bind to the endonuclease ERCC1 (Lan et al. 2004). Using several MMR-deficient human cancer cell lines, Mellon et al. (1996) showed that there was a decrease in the TCR of UV-induced CPDs (Mellon and Champe 1996). In a later study also using human cell lines, it was shown that defects in *MSH2* or *MLH1* resulted in reduced TCR of UV damage. Introduction of chromosomes carrying either *hMSH2* or *hMLH1* into these cell lines restored their ability to carry out TCR (Leadon and Avrutskaya 1997). This manuscript was later retracted due to methodologic errors in assays of transcription-coupled DNA repair. The majority of work has shown that MMR does not affect NER in mammalian cells post UV (Sweder et al. 1996; Sonneveld et al. 2001; Meira et al. 2002; Rochette et al. 2002; Yoshino et al. 2002; Kobayashi et al. 2004). MMR does not participate in the excision and/or repair of photoproducts, but may still be required to counteract the acquisition of mismatches due to error-prone translesion synthesis through these photoproducts, and therefore is important for the suppression of UV-induced mutagenesis and subsequent tumorigenesis.

The use of different wavelengths of UV radiation in MMR studies has caused some confusion in the literature. Most of the research examining the role of MMR to UV-induced DNA damage utilizes UVC radiation, however MMR is not involved in the cell survival and repair of UVC-induced DNA adducts (Rochette et al. 2002; Lutzen et al. 2004; Shin-Darlak et al. 2005). Furthermore, UVB radiation is more relevant in the development of skin tumors.

Evidence supports a role for MMR in the cellular response to UVB radiation. The MutSα heterodimer has been shown to bind to UV-induced DNA adducts, but not to participate in their repair (Wang et al. 1999). Moreover, *Msh2* is transcriptionally upregulated following UVB (Scherer et al. 2000). Experiments *in vivo* performed in our laboratory and by other groups have shown that mice deficient in either *Msh2* or *Msh6* develop skin tumors at a lower cumulative dose of UVB radiation compared to MMR proficient mice (Meira et al. 2001; Meira et al. 2002; Yoshino et al. 2002; Young et al. 2004). Previous studies in our laboratory and by other groups have demonstrated that *MSH2/Msh2* is important in the normal cell cycle response to UVB-induced DNA damage (van Oosten et al. 2005; Narine et al. 2007). Studies on apoptosis in our laboratory and others have shown that MEFs deficient in *Msh2* or *Msh6* have a decreased levels of apoptosis compared to their wildtype counterparts after irradiation with UVB (Peters et al. 2003; Young et al. 2003; Seifert et al. 2008). Substantiating these *in vitro* studies are *in vivo* experiments that show decreased apoptosis in *Msh2*$^{-/-}$ and *Msh6*$^{-/-}$ mouse epidermis compared to wildtype mice following irradiation with UVB (Young et al. 2004).

Hypothesis and Summary of Studies

Previous work in our laboratory has identified a role for MMR in the UVB-induced cellular response, specifically in apoptosis (Peters et al. 2003; Young et al. 2003). Apoptosis was identified as an important cellular response in the DNA damage-induced pathway to tumorigenesis, as mice lacking functional MMR develop skin tumors at a lower cumulative dose of UVB compared to wildtype mice (Young et al. 2004). This has also been found by other groups (Meira et al. 2001; Meira et al. 2002; Yoshino et al. 2002). The mechanism underlying the MMR-associated DNA damage response is currently unknown but is integral to our understanding of DNA damage recognition and the cell's ability to determine whether DNA repair or apoptosis will be initiated. I hypothesized that MMR plays a role in facilitating cell cycle arrest and apoptosis after DNA damage induced by UVB. To further the understanding of the mechanism of MMR-dependent apoptosis in response to DNA damage, I utilized human and mouse cell lines deficient in MMR proteins MSH2, or Msh2 and Msh6, respectively, to examine the MMR-dependent cellular response to UVB-induced DNA damage.

I examined the role of MMR in the cell cycle response following UVB by assessing the cell cycle distribution and the levels of G2/M cell cycle proteins. I also examined the mechanism of *Msh6* in the apoptotic response to UVB by assaying depolarization of the mitochondrial membrane, the translocation and levels of various mitochondrial apoptotic proteins and the levels of death receptor apoptotic proteins. The experiments I undertook shed light on the mechanism by which MMR-dependent apoptosis and cell cycle regulation occur. This research is important to the enhancement of our understanding of mechanisms that prevent non-melanoma skin cancer, a prevalent cancer in Canada. Furthermore, apoptosis is the key means by which chemotherapy and radiation kill tumor cells. As a high percentage of sporadic tumors demonstrate a loss of MMR, determining the mechanism by which MMR influences apoptosis will be important in chemotherapeutic approaches to cancer treatment.

References

Abdel-Rahman, W. M., M. Ollikainen, R. Kariola, H. J. Jarvinen, J. P. Mecklin, M. Nystrom-Lahti, S. Knuutila and P. Peltomaki (2005). "Comprehensive characterization of HNPCC-related colorectal cancers reveals striking molecular features in families with no germline mismatch repair gene mutations." Oncogene **24**(9): 1542-51.

Adamson, A. W., D. I. Beardsley, W. J. Kim, Y. Gao, R. Baskaran and K. D. Brown (2005). "Methylator-induced, mismatch repair-dependent G2 arrest is activated through Chk1 and Chk2." Mol Biol Cell **16**(3): 1513-26.

Aebi, S., B. Kurdi-Haidar, R. Gordon, B. Cenni, H. Zheng, D. Fink, R. D. Christen, C. R. Boland, M. Koi, R. Fishel and S. B. Howell (1996). "Loss of DNA mismatch repair in acquired resistance to cisplatin." Cancer Res **56**(13): 3087-90.

Alani, E., R. A. Reenan and R. D. Kolodner (1994). "Interaction between mismatch repair and genetic recombination in Saccharomyces cerevisiae." Genetics **137**(1): 19-39.

Alvino, E., G. Marra, E. Pagani, S. Falcinelli, R. Pepponi, C. Perrera, R. Haider, D. Castiglia, G. Ferranti, E. Bonmassar, J. Jiricny, G. Zambruno and S. D'Atri (2002). "High-frequency microsatellite instability is associated with defective DNA mismatch repair in human melanoma." J Invest Dermatol **118**(1): 79-86.

Andrew, S. E. and A. C. Peters (2001). "DNA instability and human disease." Am J Pharmacogenomics **1**(1): 21-8.

Aquilina, G. and M. Bignami (2001). "Mismatch repair in correction of replication errors and processing of DNA damage." J Cell Physiol **187**(2): 145-54.

Baglioni, S. and M. Genuardi (2004). "Simple and complex genetics of colorectal cancer susceptibility." Am J Med Genet C Semin Med Genet **129**(1): 35-43.

Baker, S. M., C. E. Bronner, L. Zhang, A. W. Plug, M. Robatzek, G. Warren, E. A. Elliott, J. Yu, T. Ashley, N. Arnheim and et al. (1995). "Male mice defective in the DNA mismatch repair gene PMS2 exhibit abnormal chromosome synapsis in meiosis." Cell **82**(2): 309-19.

Baker, S. M., C. E. Bronner, L. Zhang, A. W. Plug, M. Robatzek, G. Warren, E. A. Elliott, J. Yu, T. Ashley, N. Arnheim, R. A. Flavell and R. M. Liskay (1995). "Male mice defective in the DNA mismatch repair gene PMS2 exhibit abnormal chromosome synapsis in meiosis." Cell **82**(2): 309-19.

Baker, S. M., A. W. Plug, T. A. Prolla, C. E. Bronner, A. C. Harris, X. Yao, D. M. Christie, C. Monell, N. Arnheim, A. Bradley, T. Ashley and R. M. Liskay (1996). "Involvement of mouse Mlh1 in DNA mismatch repair and meiotic crossing over." Nat Genet **13**(3): 336-42.

Bellacosa, A. (2001). "Functional interactions and signaling properties of mammalian DNA mismatch repair proteins." Cell Death Differ **8**(11): 1076-92.

Berry, S. E., T. W. Davis, J. E. Schupp, H. S. Hwang, N. de Wind and T. J. Kinsella (2000). "Selective radiosensitization of drug-resistant MutS homologue-2 (MSH2) mismatch repair-deficient cells by halogenated thymidine (dThd) analogues: Msh2 mediates dThd analogue DNA levels and the differential cytotoxicity and cell cycle effects of the dThd analogues and 6-thioguanine." Cancer Res **60**(20): 5773-80.

Blackwell, L. J., D. Martik, K. P. Bjornson, E. S. Bjornson and P. Modrich (1998). "Nucleotide-promoted release of hMutSalpha from heteroduplex DNA is consistent with an ATP-dependent translocation mechanism." J Biol Chem **273**(48): 32055-62.

Boland, C. R. (1997). "Genetic pathways to colorectal cancer." Hosp Pract (Minneap) **32**(11): 79-84, 87-96.

Boyer, J. C., A. Umar, J. I. Risinger, J. R. Lipford, M. Kane, S. Yin, J. C. Barrett, R. D. Kolodner and T. A. Kunkel (1995). "Microsatellite instability, mismatch repair deficiency, and genetic defects in human cancer cell lines." Cancer Res **55**(24): 6063-70.

Brown, K. D., A. Rathi, R. Kamath, D. I. Beardsley, Q. Zhan, J. L. Mannino and R. Baskaran (2003). "The mismatch repair system is required for S-phase checkpoint activation." Nat Genet **33**(1): 80-4.

Buermeyer, A. B., S. M. Deschenes, S. M. Baker and R. M. Liskay (1999). "Mammalian DNA mismatch repair." Annu Rev Genet **33**: 533-64.

Castiglia, D., E. Pagani, E. Alvino, P. Vernole, G. Marra, E. Cannavo, J. Jiricny, G. Zambruno and S. D'Atri (2003). "Biallelic somatic inactivation of the mismatch repair gene MLH1 in a primary skin melanoma." Genes Chromosomes Cancer **37**(2): 165-75.

Cejka, P., L. Stojic, N. Mojas, A. M. Russell, K. Heinimann, E. Cannavo, M. di Pietro, G. Marra and J. Jiricny (2003). "Methylation-induced G(2)/M arrest requires a full complement of the mismatch repair protein hMLH1." Embo J **22**(9): 2245-54.

Chen, X. Q., M. Stroun, J. L. Magnenat, L. P. Nicod, A. M. Kurt, J. Lyautey, C. Lederrey and P. Anker (1996). "Microsatellite alterations in plasma DNA of small cell lung cancer patients." Nat Med **2**(9): 1033-5.

Christmann, M. and B. Kaina (2000). "Nuclear translocation of mismatch repair proteins MSH2 and MSH6 as a response of cells to alkylating agents." J Biol Chem **275**(46): 36256-62.

Christmann, M., M. T. Tomicic and B. Kaina (2002). "Phosphorylation of mismatch repair proteins MSH2 and MSH6 affecting MutSalpha mismatch-binding activity." Nucleic Acids Res **30**(9): 1959-66.

Claij, N. and H. te Riele (1999). "Microsatellite instability in human cancer: a prognostic marker for chemotherapy?" Exp Cell Res **246**(1): 1-10.

Clark, A. B., F. Valle, K. Drotschmann, R. K. Gary and T. A. Kunkel (2000). "Functional interaction of proliferating cell nuclear antigen with MSH2-MSH6 and MSH2-MSH3 complexes." J Biol Chem **275**(47): 36498-501.

Coleman, W. B. and G. J. Tsongalis (1999). "The role of genomic instability in human carcinogenesis." Anticancer Res **19**(6A): 4645-64.

Davis, T. W., C. Wilson-Van Patten, M. Meyers, K. A. Kunugi, S. Cuthill, C. Reznikoff, C. Garces, C. R. Boland, T. J. Kinsella, R. Fishel and D. A. Boothman (1998). "Defective expression of the DNA mismatch repair protein, MLH1, alters G2-M cell cycle checkpoint arrest following ionizing radiation." Cancer Res **58**(4): 767-78.

de Gruijl, F. R. (1999). "Skin cancer and solar UV radiation." Eur J Cancer **35**(14): 2003-9.

de Gruijl, F. R., H. J. van Kranen and L. H. Mullenders (2001). "UV-induced DNA damage, repair, mutations and oncogenic pathways in skin cancer." J Photochem Photobiol B **63**(1-3): 19-27.

de Vries, S. S., E. B. Baart, M. Dekker, A. Siezen, D. G. de Rooij, P. de Boer and H. te Riele (1999). "Mouse MutS-like protein Msh5 is required for proper chromosome synapsis in male and female meiosis." Genes Dev **13**(5): 523-31.

de Wind, N., M. Dekker, A. Berns, M. Radman and H. te Riele (1995). "Inactivation of the mouse Msh2 gene results in mismatch repair deficiency, methylation tolerance, hyperrecombination, and predisposition to cancer." Cell **82**(2): 321-30.

de Wind, N., M. Dekker, N. Claij, L. Jansen, Y. van Klink, M. Radman, G. Riggins, M. van der Valk, K. van't Wout and H. te Riele (1999). "HNPCC-like cancer predisposition in mice through simultaneous loss of Msh3 and Msh6 mismatch-repair protein functions." Nat Genet **23**(3): 359-62.

DeMars, R. and K. R. Held (1972). "The spontaneous azaguanine-resistant mutants of diploid human fibroblasts." Humangenetik **16**(1): 87-110.

Derks, S., C. Postma, B. Carvalho, S. M. van den Bosch, P. T. Moerkerk, J. G. Herman, M. P. Weijenberg, A. P. de Bruine, G. A. Meijer and M. van Engeland (2008). "Integrated analysis of chromosomal, microsatellite and epigenetic instability in colorectal cancer identifies specific associations between promoter methylation of pivotal tumour suppressor and DNA repair genes and specific chromosomal alterations." Carcinogenesis **29**(2): 434-9.

dos Santos, N. R., R. Seruca, M. Constancia, M. Seixas and M. Sobrinho-Simoes (1996). "Microsatellite instability at multiple loci in gastric carcinoma: clinicopathologic implications and prognosis." Gastroenterology **110**(1): 38-44.

Doxsey, S. (1998). "The centrosome--a tiny organelle with big potential." Nat Genet **20**(2): 104-6.

Drotschmann, K., R. P. Topping, J. E. Clodfelter and F. R. Salsbury (2004). "Mutations in the nucleotide-binding domain of MutS homologs uncouple cell death from cell survival." DNA Repair (Amst) **3**(7): 729-42.

Drummond, J. T., J. Genschel, E. Wolf and P. Modrich (1997). "DHFR/MSH3 amplification in methotrexate-resistant cells alters the hMutSalpha/hMutSbeta ratio and reduces the efficiency of base-base mismatch repair." Proc Natl Acad Sci U S A **94**(19): 10144-9.

Duckett, D. R., J. T. Drummond, A. I. Murchie, J. T. Reardon, A. Sancar, D. M. Lilley and P. Modrich (1996). "Human MutSalpha recognizes damaged DNA base pairs containing O6-methylguanine, O4-methylthymine, or the cisplatin-d(GpG) adduct." Proc Natl Acad Sci U S A **93**(13): 6443-7.

Dzantiev, L., N. Constantin, J. Genschel, R. R. Iyer, P. M. Burgers and P. Modrich (2004). "A defined human system that supports bidirectional mismatch-provoked excision." Mol Cell **15**(1): 31-41.

Edelmann, W., P. E. Cohen, M. Kane, K. Lau, B. Morrow, S. Bennett, A. Umar, T. Kunkel, G. Cattoretti, R. Chaganti, J. W. Pollard, R. D. Kolodner and R. Kucherlapati (1996). "Meiotic pachytene arrest in MLH1-deficient mice." Cell **85**(7): 1125-34.

Edelmann, W., P. E. Cohen, B. Kneitz, N. Winand, M. Lia, J. Heyer, R. Kolodner, J. W. Pollard and R. Kucherlapati (1999). "Mammalian MutS homologue 5 is required for chromosome pairing in meiosis." Nat Genet **21**(1): 123-7.

Edelmann, W., A. Umar, K. Yang, J. Heyer, M. Kucherlapati, M. Lia, B. Kneitz, E. Avdievich, K. Fan, E. Wong, G. Crouse, T. Kunkel, M. Lipkin, R. D. Kolodner and R. Kucherlapati (2000). "The DNA mismatch repair genes Msh3 and Msh6 cooperate in intestinal tumor suppression." Cancer Res **60**(4): 803-7.

Edelmann, W., K. Yang, A. Umar, J. Heyer, K. Lau, K. Fan, W. Liedtke, P. E. Cohen, M. F. Kane, J. R. Lipford, N. Yu, G. F. Crouse, J. W. Pollard, T. Kunkel, M. Lipkin, R. Kolodner and R. Kucherlapati (1997). "Mutation in the mismatch repair gene Msh6 causes cancer susceptibility." Cell **91**(4): 467-77.

Egawa, S., T. Uchida, K. Suyama, C. Wang, M. Ohori, S. Irie, M. Iwamura and K. Koshiba (1995). "Genomic instability of microsatellite repeats in prostate cancer: relationship to clinicopathological variables." Cancer Res **55**(11): 2418-21.

Felton, K. E., D. M. Gilchrist and S. E. Andrew (2007). "Constitutive deficiency in DNA mismatch repair." Clin Genet **71**(6): 483-98.

Fink, D., H. Zheng, S. Nebel, P. S. Norris, S. Aebi, T. P. Lin, A. Nehme, R. D. Christen, M. Haas, C. L. MacLeod and S. B. Howell (1997). "In vitro and in vivo resistance to cisplatin in cells that have lost DNA mismatch repair." Cancer Res **57**(10): 1841-5.

Fishel, R. (1998). "Mismatch repair, molecular switches, and signal transduction." Genes Dev **12**(14): 2096-101.

Flores-Rozas, H., D. Clark and R. D. Kolodner (2000). "Proliferating cell nuclear antigen and Msh2p-Msh6p interact to form an active mispair recognition complex." Nat Genet **26**(3): 375-8.

Flores-Rozas, H. and R. D. Kolodner (1998). "The Saccharomyces cerevisiae MLH3 gene functions in MSH3-dependent suppression of frameshift mutations." Proc Natl Acad Sci U S A **95**(21): 12404-9.

Franchitto, A., P. Pichierri, R. Piergentili, M. Crescenzi, M. Bignami and F. Palitti (2003). "The mammalian mismatch repair protein MSH2 is required for correct MRE11 and RAD51 relocalization and for efficient cell cycle arrest induced by ionizing radiation in G2 phase." Oncogene **22**(14): 2110-20.

Fritzell, J. A., L. Narayanan, S. M. Baker, C. E. Bronner, S. E. Andrew, T. A. Prolla, A. Bradley, F. R. Jirik, R. M. Liskay and P. M. Glazer (1997). "Role of DNA mismatch repair in the cytotoxicity of ionizing radiation." Cancer Res **57**(22): 5143-7.

Genschel, J., S. J. Littman, J. T. Drummond and P. Modrich (1998). "Isolation of MutSbeta from human cells and comparison of the mismatch repair specificities of MutSbeta and MutSalpha." J Biol Chem **273**(31): 19895-901.

Glaab, W. E., J. I. Risinger, A. Umar, J. C. Barrett, T. A. Kunkel and K. R. Tindall (1998). "Resistance to 6-thioguanine in mismatch repair-deficient human cancer cell lines correlates with an increase in induced mutations at the HPRT locus." Carcinogenesis **19**(11): 1931-7.

Gollin, S. M. (2005). "Mechanisms leading to chromosomal instability." Semin Cancer Biol **15**(1): 33-42.

Gu, L., Y. Hong, S. McCulloch, H. Watanabe and G. M. Li (1998). "ATP-dependent interaction of human mismatch repair proteins and dual role of PCNA in mismatch repair." Nucleic Acids Res **26**(5): 1173-8.

Guo, S., Y. Zhang, F. Yuan, Y. Gao, L. Gu, I. Wong and G. M. Li (2006). "Regulation of replication protein A functions in DNA mismatch repair by phosphorylation." J Biol Chem **281**(31): 21607-16.

Hawn, M. T., A. Umar, J. M. Carethers, G. Marra, T. A. Kunkel, C. R. Boland and M. Koi (1995). "Evidence for a connection between the mismatch repair system and the G2 cell cycle checkpoint." Cancer Res **55**(17): 3721-5.

Helleday, T., J. Lo, D. C. van Gent and B. P. Engelward (2007). "DNA double-strand break repair: from mechanistic understanding to cancer treatment." DNA Repair (Amst) **6**(7): 923-35.

Herman, J. G., A. Umar, K. Polyak, J. R. Graff, N. Ahuja, J. P. Issa, S. Markowitz, J. K. Willson, S. R. Hamilton, K. W. Kinzler, M. F. Kane, R. D. Kolodner, B. Vogelstein, T. A. Kunkel and S. B. Baylin (1998). "Incidence and functional consequences of hMLH1 promoter hypermethylation in colorectal carcinoma." Proc Natl Acad Sci U S A **95**(12): 6870-5.

Hickman, M. J. and L. D. Samson (1999). "Role of DNA mismatch repair and p53 in signaling induction of apoptosis by alkylating agents." Proc Natl Acad Sci U S A **96**(19): 10764-9.

Hirano, K., K. Yamashita, N. Yamashita, Y. Nakatsumi, H. Esumi, A. Kawashima, T. Ohta, M. Mai and T. Minamoto (2002). "Non-Hodgkin's lymphoma in a patient with probable hereditary nonpolyposis colon cancer: report of a case and review of the literature." Dis Colon Rectum **45**(2): 273-9.

Holmes, J., Jr., S. Clark and P. Modrich (1990). "Strand-specific mismatch correction in nuclear extracts of human and Drosophila melanogaster cell lines." Proc Natl Acad Sci U S A **87**(15): 5837-41.

Hsieh, P. (2001). "Molecular mechanisms of DNA mismatch repair." Mutat Res **486**(2): 71-87.

Iyer, R. R., A. Pluciennik, V. Burdett and P. L. Modrich (2006). "DNA mismatch repair: functions and mechanisms." Chem Rev **106**(2): 302-23.

Jiricny, J. (1998). "Replication errors: cha(lle)nging the genome." Embo J **17**(22): 6427-36.

Jiricny, J. (2006). "The multifaceted mismatch-repair system." Nat Rev Mol Cell Biol **7**(5): 335-46.

Kadyrov, F. A., L. Dzantiev, N. Constantin and P. Modrich (2006). "Endonucleolytic function of MutLalpha in human mismatch repair." Cell **126**(2): 297-308.

Kaina, B. (1998). "Critical steps in alkylation-induced aberration formation." Mutat Res **404**(1-2): 119-24.

Kaina, B. (2003). "DNA damage-triggered apoptosis: critical role of DNA repair, double-strand breaks, cell proliferation and signaling." Biochem Pharmacol **66**(8): 1547-54.

Karran, P. (2001). "Mechanisms of tolerance to DNA damaging therapeutic drugs." Carcinogenesis **22**(12): 1931-7.

Kleczkowska, H. E., G. Marra, T. Lettieri and J. Jiricny (2001). "hMSH3 and hMSH6 interact with PCNA and colocalize with it to replication foci." Genes Dev **15**(6): 724-36.

Kneitz, B., P. E. Cohen, E. Avdievich, L. Zhu, M. F. Kane, H. Hou, Jr., R. D. Kolodner, R. Kucherlapati, J. W. Pollard and W. Edelmann (2000). "MutS homolog 4 localization to meiotic chromosomes is required for chromosome pairing during meiosis in male and female mice." Genes Dev **14**(9): 1085-97.

Knudson, A. G., Jr. (1971). "Mutation and cancer: statistical study of retinoblastoma." Proc Natl Acad Sci U S A **68**(4): 820-3.

Kobayashi, K., M. O'Driscoll, P. Macpherson, L. Mullenders, M. Vreeswijk and P. Karran (2004). "XPC lymphoblastoid cells defective in the hMutSalpha DNA mismatch repair complex exhibit normal sensitivity to UVC radiation and normal transcription-coupled excision repair of DNA cyclobutane pyrimidine dimers." DNA Repair (Amst) **3**(6): 649-57.

Kolodner, R. D. and G. T. Marsischky (1999). "Eukaryotic DNA mismatch repair." Curr Opin Genet Dev **9**(1): 89-96.

Korhonen, M. K., T. E. Raevaara, H. Lohi and M. Nystrom (2007). "Conditional nuclear localization of hMLH3 suggests a minor activity in mismatch repair and supports its role as a low-risk gene in HNPCC." Oncol Rep **17**(2): 351-4.

Lamers, M. H., A. Perrakis, J. H. Enzlin, H. H. Winterwerp, N. de Wind and T. K. Sixma (2000). "The crystal structure of DNA mismatch repair protein MutS binding to a G x T mismatch." Nature **407**(6805): 711-7.

Lan, L., T. Hayashi, R. M. Rabeya, S. Nakajima, S. Kanno, M. Takao, T. Matsunaga, M. Yoshino, M. Ichikawa, H. Riele, S. Tsuchiya, K. Tanaka and A. Yasui (2004). "Functional and physical interactions between ERCC1 and MSH2 complexes for resistance to cis-diamminedichloroplatinum(II) in mammalian cells." DNA Repair (Amst) **3**(2): 135-43.

Langland, G., J. Kordich, J. Creaney, K. H. Goss, K. Lillard-Wetherell, K. Bebenek, T. A. Kunkel and J. Groden (2001). "The Bloom's syndrome protein (BLM) interacts with MLH1 but is not required for DNA mismatch repair." J Biol Chem **276**(32): 30031-5.

Lau, P. J. and R. D. Kolodner (2003). "Transfer of the MSH2.MSH6 complex from proliferating cell nuclear antigen to mispaired bases in DNA." J Biol Chem **278**(1): 14-7.

Leadon, S. A. and A. V. Avrutskaya (1997). "Differential involvement of the human mismatch repair proteins, hMLH1 and hMSH2, in transcription-coupled repair." Cancer Res **57**(17): 3784-91.

Leahy, K. M., R. L. Ornberg, Y. Wang, B. S. Zweifel, A. T. Koki and J. L. Masferrer (2002). "Cyclooxygenase-2 inhibition by celecoxib reduces proliferation and induces apoptosis in angiogenic endothelial cells in vivo." Cancer Res **62**(3): 625-31.

Li, G. M. (2008). "Mechanisms and functions of DNA mismatch repair." Cell Res **18**(1): 85-98.

Li, G. M. and P. Modrich (1995). "Restoration of mismatch repair to nuclear extracts of H6 colorectal tumor cells by a heterodimer of human MutL homologs." Proc Natl Acad Sci U S A **92**(6): 1950-4.

Liang, S. B., M. Furihata, T. Takeuchi, H. Sonobe and Y. Ohtsuki (2001). "Reduced human mismatch repair protein expression in the development of precancerous skin lesions to squamous cell carcinoma." Virchows Arch **439**(5): 622-7.

Lieberman, H. B. (2008). "DNA damage repair and response proteins as targets for cancer therapy." Curr Med Chem **15**(4): 360-7.

Lin, D. P., Y. Wang, S. J. Scherer, A. B. Clark, K. Yang, E. Avdievich, B. Jin, U. Werling, T. Parris, N. Kurihara, A. Umar, R. Kucherlapati, M. Lipkin, T. A. Kunkel and W. Edelmann (2004). "An Msh2 point mutation uncouples DNA mismatch repair and apoptosis." Cancer Res **64**(2): 517-22.

Lipkin, S. M., P. B. Moens, V. Wang, M. Lenzi, D. Shanmugarajah, A. Gilgeous, J. Thomas, J. Cheng, J. W. Touchman, E. D. Green, P. Schwartzberg, F. S. Collins and P. E. Cohen (2002). "Meiotic arrest and aneuploidy in MLH3-deficient mice." Nat Genet **31**(4): 385-90.

Loeb, L. A. (1991). "Mutator phenotype may be required for multistage carcinogenesis." Cancer Res **51**(12): 3075-9.

Lutzen, A., H. C. Bisgaard and L. J. Rasmussen (2004). "Cyclin D1 expression and cell cycle response in DNA mismatch repair-deficient cells upon methylation and UV-C damage." Exp Cell Res **292**(1): 123-34.

Marquez, N., S. C. Chappell, O. J. Sansom, A. R. Clarke, J. Court, R. J. Errington and P. J. Smith (2003). "Single cell tracking reveals that Msh2 is a key component of an early-acting DNA damage-activated G2 checkpoint." Oncogene **22**(48): 7642-8.

Marsischky, G. T., S. Lee, J. Griffith and R. D. Kolodner (1999). "'Saccharomyces cerevisiae MSH2/6 complex interacts with Holliday junctions and facilitates their cleavage by phage resolution enzymes." J Biol Chem **274**(11): 7200-6.

Matsumura, Y. and H. N. Ananthaswamy (2002). "Short-term and long-term cellular and molecular events following UV irradiation of skin: implications for molecular medicine." Expert Rev Mol Med **2002**: 1-22.

Meira, L. B., D. L. Cheo, A. M. Reis, N. Claij, D. K. Burns, H. te Riele and E. C. Friedberg (2002). "Mice defective in the mismatch repair gene Msh2 show increased predisposition to UVB radiation-induced skin cancer." DNA Repair (Amst) **1**(11): 929-34.

Meira, L. B., A. M. Reis, D. L. Cheo, D. Nahari, D. K. Burns and E. C. Friedberg (2001). "Cancer predisposition in mutant mice defective in multiple genetic pathways: uncovering important genetic interactions." Mutat Res **477**(1-2): 51-8.

Mellon, I. and G. N. Champe (1996). "Products of DNA mismatch repair genes mutS and mutL are required for transcription-coupled nucleotide-excision repair of the lactose operon in Escherichia coli." Proc Natl Acad Sci U S A **93**(3): 1292-7.

Meyers, M., A. Hwang, M. W. Wagner and D. A. Boothman (2004). "Role of DNA mismatch repair in apoptotic responses to therapeutic agents." Environ Mol Mutagen **44**(4): 249-64.

Modrich, P. and R. Lahue (1996). "Mismatch repair in replication fidelity, genetic recombination, and cancer biology." Annu Rev Biochem **65**: 101-33.

Moseley, H. and R. M. Mackie (1997). "Ultraviolet B radiation was increased at ground level in scotland during a period of ozone depletion." Br J Dermatol **137**(1): 101-2.

Mu, D., M. Tursun, D. R. Duckett, J. T. Drummond, P. Modrich and A. Sancar (1997). "Recognition and repair of compound DNA lesions (base damage and mismatch) by human mismatch repair and excision repair systems." Mol Cell Biol **17**(2): 760-9.

Narayanan, L., J. A. Fritzell, S. M. Baker, R. M. Liskay and P. M. Glazer (1997). "Elevated levels of mutation in multiple tissues of mice deficient in the DNA mismatch repair gene Pms2." Proc Natl Acad Sci U S A **94**(7): 3122-7.

Narine, K. A., K. E. Felton, A. A. Parker, V. A. Tron and S. E. Andrew (2007). "Non-tumor cells from an MSH2-null individual show altered cell cycle effects post-UVB." Oncol Rep **18**(6): 1403-11.

Nowell, P. C. (1974). "Diagnostic and prognostic value of chromosome studies in cancer." Ann Clin Lab Sci **4**(4): 234-40.

Obmolova, G., C. Ban, P. Hsieh and W. Yang (2000). "Crystal structures of mismatch repair protein MutS and its complex with a substrate DNA." Nature **407**(6805): 703-10.

Parsons, R., G. M. Li, M. J. Longley, W. H. Fang, N. Papadopoulos, J. Jen, A. de la Chapelle, K. W. Kinzler, B. Vogelstein and P. Modrich (1993). "Hypermutability and mismatch repair deficiency in RER+ tumor cells." Cell **75**(6): 1227-36.

Pavlov, Y. I., I. M. Mian and T. A. Kunkel (2003). "Evidence for preferential mismatch repair of lagging strand DNA replication errors in yeast." Curr Biol **13**(9): 744-8.

Pedroni, M., M. G. Tamassia, A. Percesepe, L. Roncucci, P. Benatti, G. Lanza, Jr., R. Gafa, C. Di Gregorio, R. Fante, L. Losi, L. Gallinari, F. Scorcioni, F. Vaccina, G. Rossi, A. M. Cesinaro and M. Ponz de Leon (1999). "Microsatellite instability in multiple colorectal tumors." Int J Cancer **81**(1): 1-5.

Peltomaki, P. (2001). "Deficient DNA mismatch repair: a common etiologic factor for colon cancer." Hum Mol Genet **10**(7): 735-40.

Peters, A. C., L. C. Young, T. Maeda, V. A. Tron and S. E. Andrew (2003). "Mammalian DNA mismatch repair protects cells from UVB-induced DNA damage by facilitating apoptosis and p53 activation." DNA Repair (Amst) **2**(4): 427-35.

Pinto, M., Y. Wu, R. G. Mensink, L. Cirnes, R. Seruca and R. M. Hofstra (2008). "Somatic mutations in mismatch repair genes in sporadic gastric carcinomas are not a cause but a consequence of the mutator phenotype." Cancer Genet Cytogenet **180**(2): 110-4.

Powell, S. N. and L. A. Kachnic (2003). "Roles of BRCA1 and BRCA2 in homologous recombination, DNA replication fidelity and the cellular response to ionizing radiation." Oncogene **22**(37): 5784-91.

Prolla, T. A., S. M. Baker, A. C. Harris, J. L. Tsao, X. Yao, C. E. Bronner, B. Zheng, M. Gordon, J. Reneker, N. Arnheim, D. Shibata, A. Bradley and R. M. Liskay (1998). "Tumour susceptibility and spontaneous mutation in mice deficient in Mlh1, Pms1 and Pms2 DNA mismatch repair." Nat Genet **18**(3): 276-9.

Prolla, T. A., D. M. Christie and R. M. Liskay (1994). "Dual requirement in yeast DNA mismatch repair for MLH1 and PMS1, two homologs of the bacterial mutL gene." Mol Cell Biol **14**(1): 407-15.

Ramilo, C., L. Gu, S. Guo, X. Zhang, S. M. Patrick, J. J. Turchi and G. M. Li (2002). "Partial reconstitution of human DNA mismatch repair in vitro: characterization of the role of human replication protein A." Mol Cell Biol **22**(7): 2037-46.

Rass, K., P. Gutwein, S. M. Muller, M. Friedrich, V. Meineke, C. Welter, W. Tilgen and J. Reichrath (2000). "Immunohistochemical analysis of DNA mismatch repair enzyme hMSH-2 in normal human skin and basal cell carcinomas." Histochem J **32**(2): 93-7.

Reitmair, A. H., R. Schmits, A. Ewel, B. Bapat, M. Redston, A. Mitri, P. Waterhouse, H. W. Mittrucker, A. Wakeham, B. Liu and et al. (1995). "MSH2 deficient mice are viable and susceptible to lymphoid tumours." Nat Genet **11**(1): 64-70.

Ricciardone, M. D., T. Ozcelik, B. Cevher, H. Ozdag, M. Tuncer, A. Gurgey, O. Uzunalimoglu, H. Cetinkaya, A. Tanyeli, E. Erken and M. Ozturk (1999). "Human MLH1 deficiency predisposes to hematological malignancy and neurofibromatosis type 1." Cancer Res **59**(2): 290-3.

Risinger, J. I., A. Berchuck, M. F. Kohler, P. Watson, H. T. Lynch and J. Boyd (1993). "Genetic instability of microsatellites in endometrial carcinoma." Cancer Res **53**(21): 5100-3.

Rochette, P. J., N. Bastien, B. C. McKay, J. P. Therrien, E. A. Drobetsky and R. Drouin (2002). "Human cells bearing homozygous mutations in the DNA mismatch repair genes hMLH1 or hMSH2 are fully proficient in transcription-coupled nucleotide excision repair." Oncogene **21**(37): 5743-52.

Scherer, S. J., S. M. Maier, M. Seifert, R. G. Hanselmann, K. D. Zang, H. K. Muller-Hermelink, P. Angel, C. Welter and M. Schartl (2000). "p53 and c-Jun functionally synergize in the regulation of the DNA repair gene hMSH2 in response to UV." J Biol Chem **275**(48): 37469-73.

Schofield, M. J. and P. Hsieh (2003). "DNA mismatch repair: molecular mechanisms and biological function." Annu Rev Microbiol **57**: 579-608.

Seifert, M., S. J. Scherer, W. Edelmann, M. Bohm, V. Meineke, M. Lobrich, W. Tilgen and J. Reichrath (2008). "The DNA-mismatch repair enzyme hMSH2 modulates UV-B-induced cell cycle arrest and apoptosis in melanoma cells." J Invest Dermatol **128**(1): 203-13.

Shell, S. S., C. D. Putnam and R. D. Kolodner (2007). "The N terminus of Saccharomyces cerevisiae Msh6 is an unstructured tether to PCNA." Mol Cell **26**(4): 565-78.

Shin-Darlak, C. Y., A. M. Skinner and M. S. Turker (2005). "A role for Pms2 in the prevention of tandem CC --> TT substitutions induced by ultraviolet radiation and oxidative stress." DNA Repair (Amst) **4**(1): 51-7.

Sonneveld, E., H. Vrieling, L. H. Mullenders and A. van Hoffen (2001). "Mouse mismatch repair gene Msh2 is not essential for transcription-coupled repair of UV-induced cyclobutane pyrimidine dimers." Oncogene **20**(4): 538-41.

Stojic, L., N. Mojas, P. Cejka, M. Di Pietro, S. Ferrari, G. Marra and J. Jiricny (2004). "Mismatch repair-dependent G2 checkpoint induced by low doses of SN1 type methylating agents requires the ATR kinase." Genes Dev **18**(11): 1331-44.

Sweder, K. S., R. A. Verhage, D. J. Crowley, G. F. Crouse, J. Brouwer and P. C. Hanawalt (1996). "Mismatch repair mutants in yeast are not defective in transcription-coupled DNA repair of UV-induced DNA damage." Genetics **143**(3): 1127-35.

Thomas, D. C., J. D. Roberts and T. A. Kunkel (1991). "Heteroduplex repair in extracts of human HeLa cells." J Biol Chem **266**(6): 3744-51.

Toft, N. J., D. J. Winton, J. Kelly, L. A. Howard, M. Dekker, H. te Riele, M. J. Arends, A. H. Wyllie, G. P. Margison and A. R. Clarke (1999). "Msh2 status modulates both apoptosis and mutation frequency in the murine small intestine." Proc Natl Acad Sci U S A **96**(7): 3911-5.

Umar, A., A. B. Buermeyer, J. A. Simon, D. C. Thomas, A. B. Clark, R. M. Liskay and T. A. Kunkel (1996). "Requirement for PCNA in DNA mismatch repair at a step preceding DNA resynthesis." Cell **87**(1): 65-73.

Umar, A., J. I. Risinger, E. T. Hawk and J. C. Barrett (2004). "Testing guidelines for hereditary non-polyposis colorectal cancer." Nat Rev Cancer **4**(2): 153-8.

van Oosten, M., G. J. Stout, C. Backendorf, H. Rebel, N. de Wind, F. Darroudi, H. J. van Kranen, F. R. de Gruijl and L. H. Mullenders (2005). "Mismatch repair protein Msh2 contributes to UVB-induced cell cycle arrest in epidermal and cultured mouse keratinocytes." DNA Repair (Amst) **4**(1): 81-9.

Vasen, H. F. (2007). "Review article: The Lynch syndrome (hereditary nonpolyposis colorectal cancer)." Aliment Pharmacol Ther **26 Suppl 2**: 113-26.

Wang, H. and J. B. Hays (2004). "Signaling from DNA mispairs to mismatch-repair excision sites despite intervening blockades." Embo J **23**(10): 2126-33.

Wang, H., C. W. Lawrence, G. M. Li and J. B. Hays (1999). "Specific binding of human MSH2.MSH6 mismatch-repair protein heterodimers to DNA incorporating thymine- or uracil-containing UV light photoproducts opposite mismatched bases." J Biol Chem **274**(24): 16894-900.

Wang, Q., C. Lasset, F. Desseigne, D. Frappaz, C. Bergeron, C. Navarro, E. Ruano and A. Puisieux (1999). "Neurofibromatosis and early onset of cancers in hMLH1-deficient children." Cancer Res **59**(2): 294-7.

Wang, Y., D. Cortez, P. Yazdi, N. Neff, S. J. Elledge and J. Qin (2000). "BASC, a super complex of BRCA1-associated proteins involved in the recognition and repair of aberrant DNA structures." Genes Dev **14**(8): 927-39.

Wang, Y. and J. Qin (2003). "MSH2 and ATR form a signaling module and regulate two branches of the damage response to DNA methylation." Proc Natl Acad Sci U S A **100**(26): 15387-92.

Whiteside, D., R. McLeod, G. Graham, J. L. Steckley, K. Booth, M. J. Somerville and S. E. Andrew (2002). "A homozygous germ-line mutation in the human MSH2 gene predisposes to hematological malignancy and multiple cafe-au-lait spots." Cancer Res **62**(2): 359-62.

Woerner, S. M., M. Kloor, A. Mueller, J. Rueschoff, N. Friedrichs, R. Buettner, M. Buzello, P. Kienle, H. P. Knaebel, E. Kunstmann, C. Pagenstecher, H. K.

Schackert, G. Moslein, H. Vogelsang, M. von Knebel Doeberitz and J. F. Gebert (2005). "Microsatellite instability of selective target genes in HNPCC-associated colon adenomas." Oncogene.

Yamane, K., K. Taylor and T. J. Kinsella (2004). "Mismatch repair-mediated G2/M arrest by 6-thioguanine involves the ATR-Chk1 pathway." Biochem Biophys Res Commun **318**(1): 297-302.

Yan, T., S. E. Berry, A. B. Desai and T. J. Kinsella (2003). "DNA Mismatch Repair (MMR) Mediates 6-Thioguanine Genotoxicity by Introducing Single-strand Breaks to Signal a G(2)-M Arrest in MMR-proficient RKO Cells." Clin Cancer Res **9**(6): 2327-34.

Yan, T., A. B. Desai, J. W. Jacobberger, R. M. Sramkoski, T. Loh and T. J. Kinsella (2004). "CHK1 and CHK2 are differentially involved in mismatch repair-mediated 6-thioguanine-induced cell cycle checkpoint responses." Mol Cancer Ther **3**(9): 1147-57.

Yang, G., S. J. Scherer, S. S. Shell, K. Yang, M. Kim, M. Lipkin, R. Kucherlapati, R. D. Kolodner and W. Edelmann (2004). "Dominant effects of an Msh6 missense mutation on DNA repair and cancer susceptibility." Cancer Cell **6**(2): 139-50.

Yoshino, M., Y. Nakatsu, H. te Riele, S. Hirota, Y. Kitamura and K. Tanaka (2002). "Additive roles of XPA and MSH2 genes in UVB-induced skin tumorigenesis in mice." DNA Repair (Amst) **1**(11): 935-40.

Young, L. C., J. B. Hays, V. A. Tron and S. E. Andrew (2003). "DNA mismatch repair proteins: potential guardians against genomic instability and tumorigenesis induced by ultraviolet photoproducts." J Invest Dermatol **121**(3): 435-40.

Young, L. C., J. Listgarten, M. J. Trotter, S. E. Andrew and V. A. Tron (2007). "Evidence that dysregulated DNA mismatch repair characterizes human nonmelanoma skin cancer." Br J Dermatol.

Young, L. C., A. C. Peters, T. Maeda, W. Edelmann, R. Kucherlapati, S. E. Andrew and V. A. Tron (2003). "DNA mismatch repair protein Msh6 is required for optimal levels of ultraviolet-B-induced apoptosis in primary mouse fibroblasts." J Invest Dermatol **121**(4): 876-80.

Young, L. C., K. J. Thulien, M. R. Campbell, V. A. Tron and S. E. Andrew (2004). "DNA mismatch repair proteins promote apoptosis and suppress tumorigenesis in response to UVB irradiation: an in vivo study." Carcinogenesis **25**(10): 1821-7.

Zeng, M., L. Narayanan, X. S. Xu, T. A. Prolla, R. M. Liskay and P. M. Glazer (2000). "Ionizing radiation-induced apoptosis via separate Pms2- and p53-dependent pathways." Cancer Res **60**(17): 4889-93.

Zhang, Y., F. Yuan, S. R. Presnell, K. Tian, Y. Gao, A. E. Tomkinson, L. Gu and G. M. Li (2005). "Reconstitution of 5'-directed human mismatch repair in a purified system." Cell **122**(5): 693-705.

Zhou, B. B. and S. J. Elledge (2000). "The DNA damage response: putting checkpoints in perspective." Nature **408**(6811): 433-9.

~ Chapter 2 ~

Materials and Methods

Cell Cycle (human)

Cell culture: Normal human lymphoblastoid cell lines MM (*MSH2*$^{+/+}$), MR (*MSH2*$^{+/+}$) and JMG (*MSH2*$^{+/+}$), and MSH2-null human lymphoblastoid cell line KM (*MSH2*$^{-/-}$) (Whiteside et al. 2002) were cultured with RPMI 1640 plus 10% fetal bovine serum (FBS; Gibco/Invitrogen, Burlington, ON, Canada). The human lymphoblastoid cell lines MM (*MSH2*$^{+/+}$), MR (*MSH2*$^{+/+}$), JMG (*MSH2*$^{+/+}$) and KM (*MSH2*$^{-/-}$) were immortalized by EBV. All cell lines were grown in 5% CO_2 at 37°C.

UVB irradiation: MM (*MSH2*$^{+/+}$), MR (*MSH2*$^{+/+}$), JMG (*MSH2*$^{+/+}$) and KM (*MSH2*$^{-/-}$) cells were suspended in RPMI 1640 with no FBS and exposed to UVB light (290-320nm) from a bank of six unfiltered UVB bulbs (FS20T12/UVB-BP, Light Sources Inc., Orange CT), with the lid on to filter out UVC. The intensity of the UVB source was measured using IL1700 radiometer with a SED 240/UVB-1/W detector (International Light, Newburyport, MA). Following UVB irradiation, RPMI with FBS was added to reach a final concentration of 10% FBS.

Flow cytometry: MM (*MSH2*$^{+/+}$), MR (*MSH2*$^{+/+}$), JMG (*MSH2*$^{+/+}$) and KM (*MSH2*$^{-/-}$) cells were pelleted and washed with RPMI 1640 without FBS and resuspended in 250-500μL Vindelov propidium iodide stain (10mM Tris pH 8.0, 10mM NaCl, 700U RNase A, 0.075mM PI, 1mM NP40). Flow cytometry was performed using Becton Dickenson FACScan (Becton Dickenson, San Jose, CA), and the data was analyzed using ModFit LT, version 2.0 (Verity Software House, Topsham, ME). Mean levels of cells in G2/M phase were compared using the student's t-test.

Immunoblot analysis: JMG (*MSH2*$^{+/+}$) and KM (*MSH2*$^{-/-}$) cells were harvested and lysed (50mM Tris pH 7.5, 10mM $MgCl_2$, 1% SDS) and sonicated in the presence of protease inhibitors (Complete protease inhibitor cocktail tablets, Roche Diagnostics, Laval, PQ, Canada). Lysates were diluted with protein loading buffer [2.5% (wt/vol) SDS, 5% (vol/vol) β-mercaptoethanol], separated by discontinuous SDS polyacrylamide gel electrophoresis and electro-transferred onto 0.45uM Immobilon-P PVDF membrane (Fisher Scientific, Pittsburgh, PA) in Tris/glycine SDS transfer buffer. Immunoblots were blocked in 5% (wt/vol) dry milk/TBST. Primary antibodies used were as follows: CDC2, p53 (#610037, #15791A, BD Biosciences, Mississauga, ON, Canada), CDC2phos (Tyr15), CDC25Cphos (Ser216), CHK1phos (Ser345), p53phos (Ser15) (#9111, #9526, #2341, #9284, Cell Signaling Technology, Beverly MA), CDC25C, WEE1 (#05-507, #06-972, Upstate, Charlottesville, VA) and CHK1 (#KAM-CC111, Stressgen Bioreagents, Victoria, BC, Canada). Antibody binding was visualized using the appropriate horseradish-peroxidase conjugated secondary antibody and ECL (Amersham Bioscience, Picataway, NJ) or ECL Plus (Amersham Bioscience, Picataway, NJ) on Fuji SuperRX film (Fujifilm, Stamford, CT). The Quantity One densitometry program (Biorad Laboratories, Hercules, CA) was utilized to account for loading variations. The densitometry values for the proteins of interest were normalized either to actin or to total protein levels as determined by amido black stain. Immunoblots were replicated 3 times and a representative figure is shown.

Cell Cycle (mouse)

Cell Culture: *Msh6*$^{+/+}$ and *Msh6*$^{-/-}$ primary mouse embryonic fibroblasts (MEFs) were generated from day 13 mouse embryos. Individual embryos were disaggregated in trypsin, large cellular debris was removed, and the remaining cells were plated in 5-100mm^2 plates in Dulbecco's modified Eagle's medium (DMEM) plus 20% fetal bovine serum (FBS) and 1% penicillin/streptomycin (p/s)(Gibco/Invitrogen, Burlington, ON, Canada). Cellular debris was used to genotype the embryos. Cells were maintained in DMEM plus 20% FBS (Gibco/Invitrogen) and expanded for 2 to 3 days before splitting 1:4. Cells were cryopreserved upon reaching 75% confluency. Once retrieved from liquid nitrogen storage, cells were expanded for 2 to 3 days before plating for UVB experiments. Before plating for UVB irradiation, the MEFs were not split more than once (1:4) as MMR-deficient cells have a mutator phenotype and may acquire additional genetic aberrations during replication. During this time, the MEFs were monitored closely and were not grown beyond 7 days after initial plating. All cell lines were grown in 5% CO2 at 37°C. Adapted from (Young et al. 2003).

UVB irradiation: *Msh6*$^{+/+}$ and *Msh6*$^{-/-}$ primary mouse embryonic fibroblasts (MEFs) were washed with PBS and then PBS was removed. Cell lines were exposed to UVB (290-320nm) from a bank of six unfiltered UVB bulbs (FS20T12/UVB-BP, Light Sources Inc., Orange CT), with the lid on to filter out UVC. The intensity of the UVB source was measured using IL1700 radiometer with a SED 240/UVB-1/W detector (International Light, Newburyport, MA). Following UVB irradiation, DMEM plus 20% FBS and p/s was replaced on the MEFs.

Flow cytometry: Untreated and UVB-treated *Msh6*$^{+/+}$ and *Msh6*$^{-/-}$ primary MEFs and medium were harvested by trypsinization and centrifuged. After rinsing in PBS and centrifuging, cell pellets were resuspended in 500μL Vindelov propidium iodide stain (10mM Tris pH 8.0, 10mM NaCl, 700U RNase A, 0.075mM PI, 1mM NP40). Flow cytometry was performed using Becton Dickenson FACScalibur (Becton Dickenson, San Jose, CA), and the data was analyzed using ModFit LT, version 2.0 (Verity Software House, Topsham, ME). Mean levels of cells in G2/M phase were compared using the student's t-test.

Apoptosis

Cell Culture: *Msh6*$^{+/+}$, *Msh6*$^{-/-}$, *Msh2*$^{+/+}$ and *Msh2*$^{-/-}$ primary mouse embryonic fibroblasts (MEFs) were generated and cultured as described above in Dulbecco's modified Eagle's medium (DMEM) plus 20% fetal bovine serum (FBS) and 1% penicillin/streptomycin (p/s) in 5% CO2 at 37°C.

UVB irradiation: *Msh6*$^{+/+}$, *Msh6*$^{-/-}$, *Msh2*$^{+/+}$ and *Msh2*$^{-/-}$ primary mouse embryonic fibroblasts (MEFs) were washed with PBS and then PBS was removed. Cell lines were exposed to UVB (290-320nm) from a bank of six unfiltered UVB bulbs (FS20T12/UVB-BP, Light Sources Inc., Orange CT), with the lid on to filter out UVC. The intensity of the UVB source was measured using IL1700 radiometer with a SED 240/UVB-1/W detector (International Light, Newburyport, MA). Following UVB irradiation, DMEM plus 20% FBS and p/s was replaced on the MEFs.

Mitochondrial membrane sensor assay: Untreated and UVB-treated *Msh6*$^{+/+}$ and *Msh6*$^{-/-}$ primary MEFs and medium were harvested by trypsinization and centrifuged. Cells were stained with MitoSensor reagent using the ApoAlert™ Mitochondrial Membrane Sensor Kit (Clontech Laboratories, Inc., Mountain View, CA) according to manufacturer instructions and analyzed by flow cytometry using Becton Dickenson FACScalibur and BD CellQuest™ program (Becton Dickenson, San Jose, CA). Mean levels of mitochondrial membrane depolarization were compared using the student's t-test.

Cytochrome c release assay: Untreated and UVB-treated *Msh6*$^{+/+}$ and *Msh6*$^{-/-}$ primary MEFs and medium were harvested by cell scraping. Mitochondrial and cytosolic fractions were obtained by using the ApoAlert™ Cell Fractionation Kit (Clontech Laboratories, Inc., Mountain View, CA) according to manufacturer instructions.

Immunoblot analysis: *Msh6*$^{+/+}$ and *Msh6*$^{-/-}$ MEFs were harvested and cell pellets were resuspended in loading buffer (100mM Tris pH 6.8, 16% glycerol, 3.2% SDS) and sonicated. Eight % 2-mercaptoethanol with bromophenol blue was added and boiled at 100 °C for 10 minutes. Protein was separated by discontinuous SDS polyacrylamide gel electorphoresis and electro-transferred onto 0.45uM Immobilon-P PVDF membrane (Fisher Scientific, Pittsburgh, PA) in Tris/glycine SDS transfer buffer. Blots were blocked in 5% (wt/vol) dry milk/TBST. Primary antibodies used were as follows: Caspase 2 (#MAB3501, Chemicon, Temecula, CA), Caspase 2 (#611023, BD Transduction, Mississauga, ON, Canada), Caspase 2, Caspase 8, Caspase 10 #3027-100, #3259-100, #3410-100, Biovision, Mountain View, CA), BAX (#556467, BD Pharmingen, San Diego CA), Fas (#341289, Calbiochem, San Diego, CA), COX4, Cytochrome c (#S2207, #S2050, BD Biosciences/Clontech, Mountain View, CA), TNFR1 (#ab7365, Abcam Inc., Cambridge MA), Caspase 3, Caspase 8, Caspase 9, Caspase 10, Bid, FADD-pSer191, TNFα, TRADD, RIP (#9664, #4927, #9504, #9505, #9752, #9664, #2003, #2785, #3707, #3694, #4926, Cell Signaling Technology, Beverly MA). Antibody binding was visualized using the appropriate horseradish-peroxidase conjugated secondary antibody and ECL (Amersham Bioscience, Picataway, NJ) on Fuji SuperRX film (Fujifilm, Stamford, CT). The Quantity One densitometry program (Biorad

Laboratories, Hercules, CA) was utilized to account for loading variations. The densitometry values for the proteins of interest were normalized either to gamma tubulin or to total protein levels as determined by amido black stain. Immunoblots were replicated 2 to 3 times and a representative is shown.

Immunofluorescence: *Msh6*$^{+/+}$, *Msh6*$^{-/-}$, *Msh2*$^{+/+}$ and *Msh2*$^{-/-}$ primary MEFs were split onto coverslips coated with poly-L-lysine (0.1mg/mL; Sigma, Saint Louis, MO). Cells were untreated or treated with 300J/m^2 UVB and fixed with methanol at various timepoints after treatment. Cells on coverslips were blocked in 1% BSA (Sigma, Saint Louis, MO) in PBS for 1 hour at room temperature. Primary and secondary antibodies were diluted in blocking buffer and incubated for 1 hour at room temperature and all washes were performed in PBS (3x5 min). Cells were incubated with primary antibody: Caspase 2 (#MAB3501, Chemicon, Temecula, CA; #611023, BD Transduction, Mississauga, ON, Canada; #3027-100, Biovision, Mountain View, CA), Msh2, Msh6 (#610361, #610919, BD Transduction, Mississauga, ON, Canada), gamma tubulin (#T6557, Sigma, Saint Louis, MO), PML (#MAB3738, Chemicon, Temecula, CA). After washing, cells were incubated with fluorescent secondary antibodies (Molecular Probes, Invitrogen, Eugene, OR): Alexa Fluor 488 donkey anti-rat IgG (#21208), Alexa Fluor 568 goat anti-mouse IgG1 (#21124), Alexa Fluor 594 goat anti-mouse IgG1 (#21125), Alexa Fluor 488 donkey anti-rabbit IgG (#21206), Alexa Fluor 488 goat anti-mouse IgG1 (#21121), Alexa Fluor 594 goat anti-mouse IgG2b (#21145), Alexa Fluor 594 donkey anti-rat IgG (#21209). Cells were washed and stained with organelle stains (Molecular Probes, Invitrogen, Eugene, OR) diluted in PBS for 20 min. at room temperature:

endoplasmic reticulum- concanavalin A, Alexa Fluor 488 (#C11252); Golgi- wheat germ agglutinin, Alexa Fluor 488 (#W11261); mitochondria-Mitotracker red (#M-7512). After final washing, coverslips were mounted on slides with mounting medium containing DAPI (#H-1200, Vector Laboratories, Inc., Burlingame, CA). Slides were analysed by confocal microscopy. Photomicrographs obtained were analysed by Image-Pro Plus version. 5.1 to obtain Pearson's correlation coefficients.

Centrosome isolation from primary MEFs: Primary *Msh6*$^{+/+}$ and *Msh6*$^{-/-}$ MEFs were generated and cultured as above. MEFs were incubated with DMEM containing 1 μg of cytochalasine D/ml and 0.2 μM nocodazole for 1 h at 37°C to depolymerize the actin and microtubule filaments. MEFs were harvested by trypsinization and centrosomes were isolated as described in (Kanai et al. 2003).

Cellular fractionation: Untreated and UVB-treated *Msh6*$^{+/+}$ and *Msh6*$^{-/-}$ primary MEFs and medium were harvested by cell scraping. Cytosolic, nuclear, membrane/particulate, and cytoskeletal fractions were obtained by using the FractionPREP™ Cell Fractionation System (Biovision Research Products, Mountain View, CA) according to manufacturer instructions.

Apoptosis assay of primary MEFs: Primary *Msh6*$^{+/+}$ and *Msh6*$^{-/-}$ MEFs were generated, cultured and UVB-irradiated for experiments as described above. Adherent and suspension MEFs were collected 24 or 48 hrs following UVB irradiation. Cells were stained using an Annexin-FITC Apoptosis Kit (BD Pharmingen, San Diego CA). The percentage of apoptotic cells was determined by flow cytometry using Becton Dickenson FACScalibur and BD CellQuest™ program (Becton Dickenson, San Jose, CA).

Caspase inhibitor treatment of primary MEFs: Primary *Msh6*$^{+/+}$ and *Msh6*$^{-/-}$ MEFs were generated and cultured as above. Medium was removed and cells were rinsed with PBS. Caspase inhibitor: Z-VAD-FMK, Z-VDVAD-FMK, Z-LEHD-FMK or Z-IETD-FMK was added to fresh medium to a concentration of 100uM and incubated at 37°C for 2 hours. Medium was removed and cells were rinsed with PBS and then UVB-irradiated as described above. Medium with caspase inhibitor was replaced and cells were incubated at 37°C for 24 hours and then adherent and suspension MEFs were collected. As the caspase inhibitors were resuspended in DMSO, MEFs were mock treated, as above, with the corresponding volume of DMSO alone.

Statistical Analysis: In figure 4-3: Apoptosis levels in MEFs 24 hours after irradiation with UVB, mean apoptosis levels were compared using ANOVA and Bonferroni's correction for multiple comparisons. In figures 4-12, 4-13, 5-18 and 6-10: Apoptosis levels in *Msh6*$^{+/+}$ and *Msh6*$^{-/-}$ MEFs after treatment with caspase inhibitor, mean apoptosis levels were compared using a one-tailed student's t-test.

References

Kanai, M., W. M. Tong, E. Sugihara, Z. Q. Wang, K. Fukasawa and M. Miwa (2003). "Involvement of poly(ADP-Ribose) polymerase 1 and poly(ADP-Ribosyl)ation in regulation of centrosome function." Mol Cell Biol **23**(7): 2451-62.

Whiteside, D., R. McLeod, G. Graham, J. L. Steckley, K. Booth, M. J. Somerville and S. E. Andrew (2002). "A homozygous germ-line mutation in the human MSH2 gene predisposes to hematological malignancy and multiple cafe-au-lait spots." Cancer Res **62**(2): 359-62.

Young, L. C., A. C. Peters, T. Maeda, W. Edelmann, R. Kucherlapati, S. E. Andrew and V. A. Tron (2003). "DNA mismatch repair protein Msh6 is required for optimal levels of ultraviolet-B-induced apoptosis in primary mouse fibroblasts." J Invest Dermatol **121**(4): 876-80.

~ Chapter 3 ~

Characterization of the cell cycle response to UVB-induced DNA damage in mismatch repair-proficient and –deficient cells

The data presented in this chapter have been published.

Kelly A. Narine, Kathleen E. Felton, Arabesque A. Parker, Victor A. Tron and Susan E. Andrew. (2007) Non-tumor cells from an MSH2-null individual show altered cell cycle effects post-UVB. Oncology Reports 18(6):1403-11.

All experimental design and data analysis were performed by Kelly Narine. Kathleen Felton contributed to the western blots in Figures 2-4 to 2-8. All other experimentation was performed by Kelly Narine.

Introduction

Cell cycle arrest is an important event, triggered by DNA damage, allowing for full repair of the damage prior to DNA replication (Fig. 3-1). In this way, it is a key event towards the maintenance of genomic integrity. Although NER is the predominant pathway of repair of UV-induced DNA adducts, observations in yeast indicate that recognition of UV-induced DNA adducts by sensor proteins, independent of NER, may be the first step in initiating UV-induced cell cycle arrest (Zhang et al. 2003). Initiation of cell cycle checkpoint occurs rapidly after DNA damage and activation of ATM and ATR. Once active, ATM and ATR activate CHK1 and CHK2 which phosphorylate CDC25C, leading to its inhibition. CDC2 is then phosphorylated by MYT1 and WEE1 to induce G2/M arrest. The removal of these inhibitory phosphates on CDC2 is prevented by CDC25C being inactive, thus inhibiting cell cycle progression into mitosis [Fig. 3-2; reviewed in (Taylor and Stark 2001; Sancar et al. 2004)].

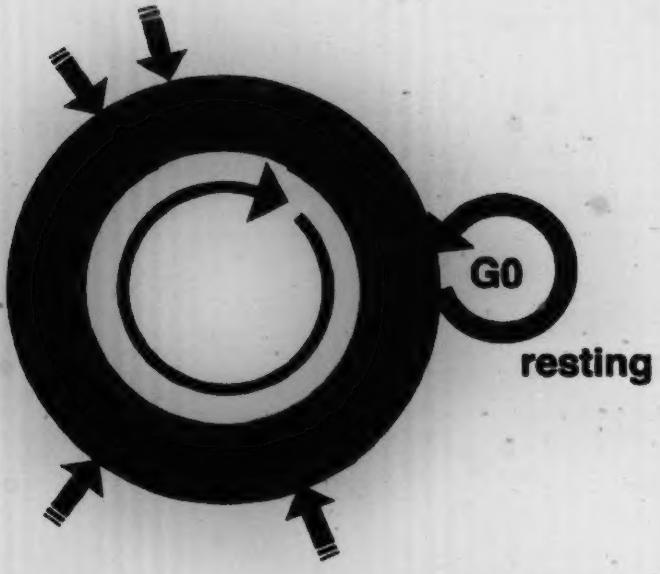

Figure 3-1: Schematic of cell cycle progression with checkpoints.

Cell cycle progression with checkpoints shown with red arrows. Our studies focus on the checkpoint that occurs between G2 and M (mitosis) phases of the cell cycle (homepage.mac.com/enognog/checkpoint.htm).

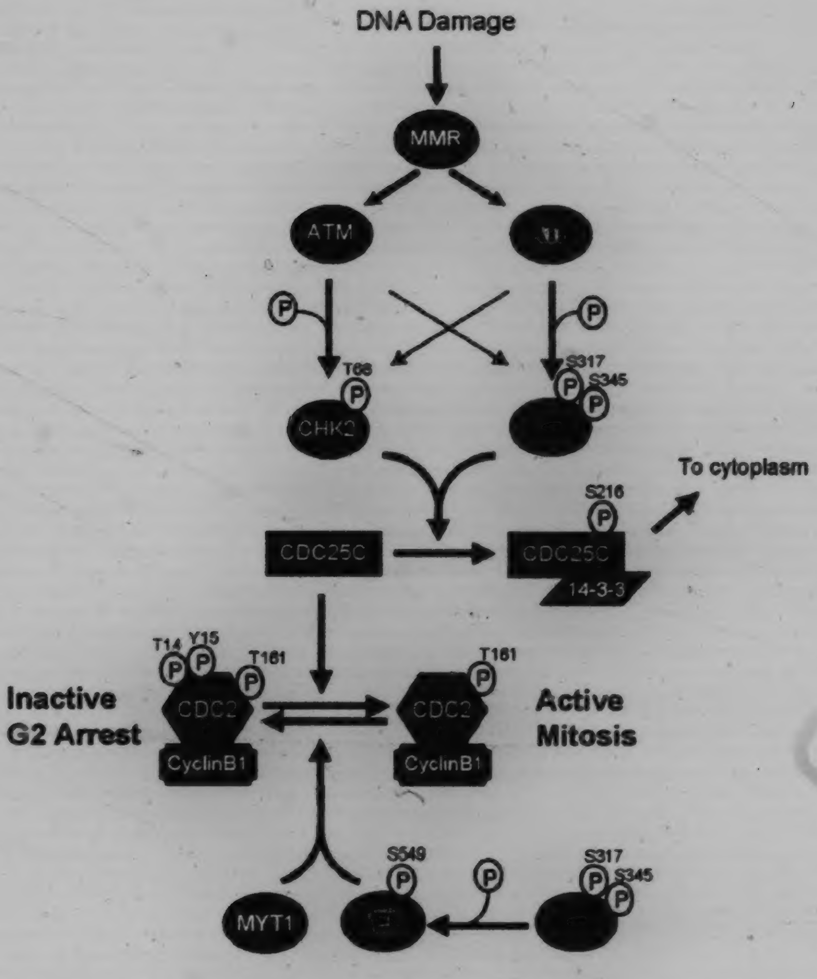
DNA Damage
MMR
ATM
P
P
T68
P
CHK2
S317
P
S345
P
To cytoplasm
S216
P
CDC25C
CDC25C
14-3-3
T14
Y15
P
P
T161
P
Inactive
G2 Arrest
CDC2
CyclinB1
T161
P
CDC2
CyclinB1
Active
Mitosis
S549
P
P
S317
P
S345
P
MYT1

Figure 3-2: Schematic of G2/M cell cycle regulation with potential position of mismatch repair

In response to DNA damage, ATM and ATR are activated. Once active, ATM and ATR phosphorylate and activate CHK1 and CHK2. CHK1/2 phosphorylate and inhibit CDC25C, promoting interaction with 14-3-3 and movement of CDC25C to the cytoplasm. Inhibiting CDC25C prevents the removal of inhibitory phosphates on CDC2 and prevents cell cycle progression into mitosis. CDC2 is phosphorylated at T14 and Y15 by MYT1 and WEE1 to induce G2/M arrest, but activated by phosphorylation at T161. Adapted from (Pietenpol and Stewart 2002).

Increasing evidence suggests that MMR proteins have a role in recognizing DNA damage and contributing to DNA damage responses independent of repair. It has been shown that MMR is a player in DNA damage-induced cell cycle arrest. Studies have demonstrated that deficiency in Msh2 leads to a lower percentage of cells arrested in S-phase after UVB exposure as compared to wildtype cells, both *in vivo* and *in vitro* (van Oosten et al. 2005; Seifert et al. 2008). There is diminished G2/M arrest in the absence of MMR proteins MSH2, MLH1 or PMS2 in response to treatment by DNA damaging agents such as IR (Davis et al. 1998; Yan et al. 2001; Franchitto et al. 2003), cisplatin (Duckett et al. 1996; Reitmair et al. 1997) and 6-TG (Hawn et al. 1995; Meyers et al. 2001; Yan et al. 2003). One of the most characterized responses of MMR-deficient cells occurs following DNA damage induced by alkylating agents. Cells defective in MSH2 or MLH1 show no G2 arrest and are resistant to cytotoxicity induced by MNNG (Koi et al. 1994; Umar et al. 1997). In addition, MMR proteins interact with proteins involved in the G2/M checkpoint pathway. Studies have shown that both Chk1 and Chk2/CHK2 interact with MSH2 (Brown et al. 2003; Adamson et al. 2005) and this interaction is enhanced after MNNG exposure (Adamson et al. 2005). Using normal HeLa nuclear extracts, Wang and Qin (2003) demonstrated that MSH2 co-immunoprecipitates with ATR and ATRIP, both of which regulate the downstream phosphorylation of CHK1 (Wang and Qin 2003).

Studies using mouse models or cell lines deficient in MMR have suggested a role outside of repair for MMR in the UV-induced DNA damage response (Meira et al. 2001; Meira et al. 2002; Yoshino et al. 2002; Peters et al. 2003; Young et al. 2004). When my studies were initiated, there were no published reports on the MMR-dependent UVB-induced effects on the cell cycle. I hypothesized that loss of MMR would result in reduced G2/M arrest that could contribute in part to UVB-induced tumorigenesis. Many studies examining the roles of mammalian MMR use HNPCC tumor cell lines as a MMR-deficient model. These cancer cell lines have a mutator phenotype and may have acquired additional genetic alterations affecting their behavior (Bhattacharyya et al. 1994; Branch et al. 1995; Malkhosyan et al. 1996; Richards et al. 1997). I have used primary *Msh6*$^{+/+}$ and *Msh6*$^{-/-}$ MEFs to study cell cycle response after UVB of MMR-deficient cells in isogenic, non-tumor cells. However, due to the difficulty in obtaining results using available reagents for studying the cell cycle response on the protein level in primary mouse cells, I have included cell cycle data from human non-tumor MSH2-proficient and –deficient cells in order to fully elucidate the role of MMR in the post-UVB cell cycle response. We have generated an EBV-immortalized lymphoblastoid cell line derived from normal blood obtained from an individual with bi-allelic *MSH2* mutations resulting in a *MSH2*-null cell line (Whiteside et al. 2002). Despite identification of other MMR-null patients, this cell line is unique as a *MSH2*$^{-/-}$, non-tumor human cell line. By comparing the cell cycle responses of non-tumor cells deficient for Msh6 and for MSH2 to MMR-proficient cells, our studies show that MMR plays a role in facilitating G2/M arrest after UVB-induced DNA damage, prior to a neoplastic state. These data provide support that the MMR proteins Msh6 and MSH2 are involved in the normal cell cycle response of cells post-UVB.

Results

G2/M cell cycle arrest in *Msh6*$^{+/+}$ and *Msh6*$^{-/-}$ murine embryonic fibroblasts following UVB radiation

The cell cycle phase distribution was studied by flow cytometry in unsynchronized untreated *Msh6*$^{+/+}$ and *Msh6*$^{-/-}$ MEFs before and after irradiation with 300J/m^2 UVB (Fig. 3-3). Cell cycle analysis shows that there was a significant reduction in the fold induction of *Msh6*$^{-/-}$ cells with 4N DNA content (G2/M) 24 hours after UVB, compared to *Msh6*$^{+/+}$ cells ($p<0.05$). 48 hours after irradiation with UVB, both *Msh6*$^{+/+}$ and *Msh6*$^{-/-}$ MEFs showed an increased number of cells in G2/M phase compared to 24 hours, although the difference between *Msh6*$^{-/-}$ MEFs and *Msh6*$^{-/-}$ MEFs was not significant (Fig. 3-4). This shows that Msh6 plays a role in G2/M cell cycle arrest after UVB radiation.

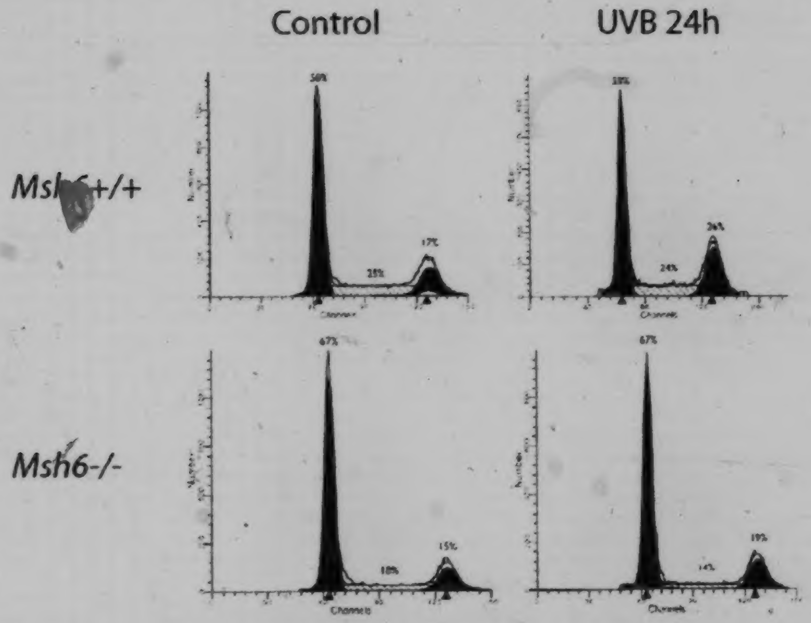

Figure 3-3: Cell cycle histograms of *Msh6*$^{+/+}$ and *Msh6*$^{-/-}$ MEFs.

Flow cytometry histograms of a representative trial showing the G1, S, and G2/M phases of the cell cycle in untreated and 300J/m^2 UVB-irradiated *Msh6*$^{+/+}$ and *Msh6*$^{-/-}$ MEFs 24 hours after treatment.

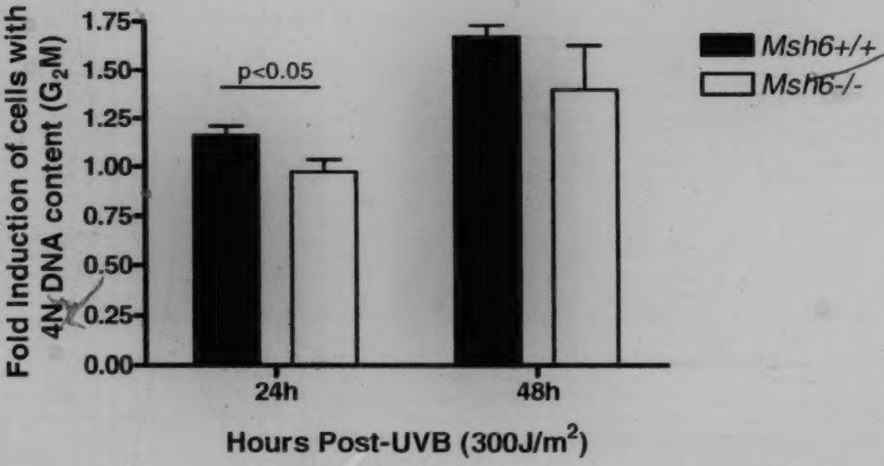

Figure 3-4: Induction of G2/M Phase in *Msh6*$^{+/+}$ and *Msh6*$^{-/-}$ MEFs after 300J/m^2 UVB

Msh6$^{+/+}$ and *Msh6*$^{-/-}$ MEFs were treated with 300J/m^2 UVB and analyzed by flow cytometry after PI staining. Values were normalized to values for untreated controls for each genotype to obtain the fold induction of G2/M. The difference in values between *Msh6*$^{+/+}$ and *Msh6*$^{-/-}$ MEFs at 24 hours was significant ($p<0.05$, n=3) and was not significant at 48 hours (n=3).

G2/M cell cycle arrest in JMG (*MSH2*$^{+/+}$) and KM (*MSH2*$^{-/-}$) lymphoblastoid cell lines following UVB radiation

Complementation of the KM (*MSH2*$^{-/-}$) cell line with wildtype *MSH2* cDNA was unsuccessful. Thus, we compared the cell cycle response of KM (*MSH2*$^{-/-}$) to 3 wildtype cell lines: MM, MR and JMG (*MSH2*$^{+/+}$); results from JMG are shown as a representative MMR-proficient cell line. The cell cycle phase distribution was studied by flow cytometry in unsynchronized untreated JMG (*MSH2*$^{+/+}$) and KM (*MSH2*$^{-/-}$) cells and after irradiation with 250J/m^2 UVB. Cell cycle analysis shows that there was a significant reduction in G2/M phase of untreated KM (*MSH2*$^{-/-}$) cells compared to untreated JMG

($MSH2^{+/+}$) ($p<0.05$). There was also a significant reduction in the G2/M phase of KM ($MSH2^{-/-}$) cells compared to JMG ($MSH2^{+/+}$) cells at 48 and 72 hours post-UVB ($p<0.05$, $p<0.01$, respectively; Fig. 3-5 A). Furthermore, the fold induction of KM ($MSH2^{-/-}$) cells in G2/M phase was significantly reduced at 72 hours post-UVB compared to JMG ($MSH2^{+/+}$) cells ($p<0.05$; Fig. 3-5 B). This shows that that the MMR protein MSH2 plays a role in G2/M cell cycle arrest after UVB-induced DNA damage.

A

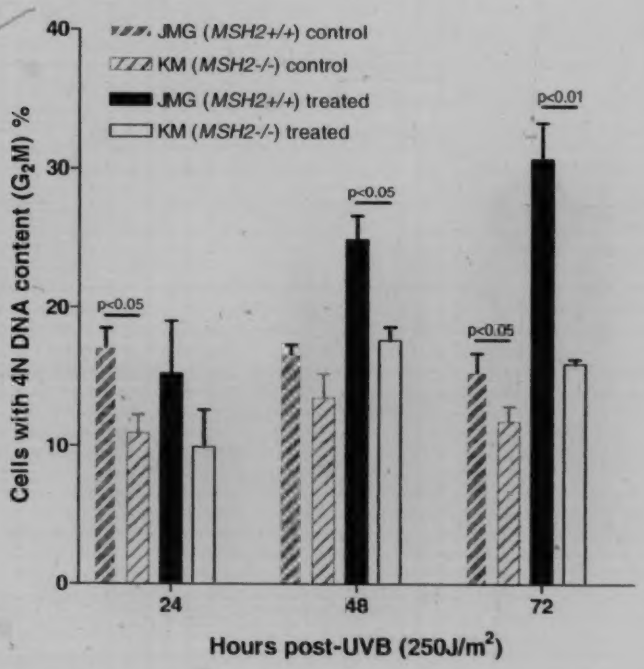

Figure 3-5 A: G2/M phase in untreated JMG (*MSH2*$^{+/+}$) and KM (*MSH2*$^{-/-}$) cells and after 250J/m^2 UVB

Control JMG ($MSH2^{+/+}$) and KM ($MSH2^{-/-}$) cells and those treated with 250J/m^2 UVB were analyzed by flow cytometry after PI staining (n=3). The differences in values between untreated JMG ($MSH2^{+/+}$) and untreated KM ($MSH2^{-/-}$) cells at 24 and 72 hours were significant ($p<0.05$) and between treated JMG ($MSH2^{+/+}$) and treated KM ($MSH2^{-/-}$) cells at 48 and 72 hours were significant ($p<0.05$ and $p<0.01$, respectively). The difference in values between treated JMG ($MSH2^{+/+}$) and treated KM ($MSH2^{-/-}$) cells at 24 hours was not significant, nor was the difference in values between untreated JMG ($MSH2^{+/+}$) and untreated KM ($MSH2^{-/-}$) cells at 48 hours.

B

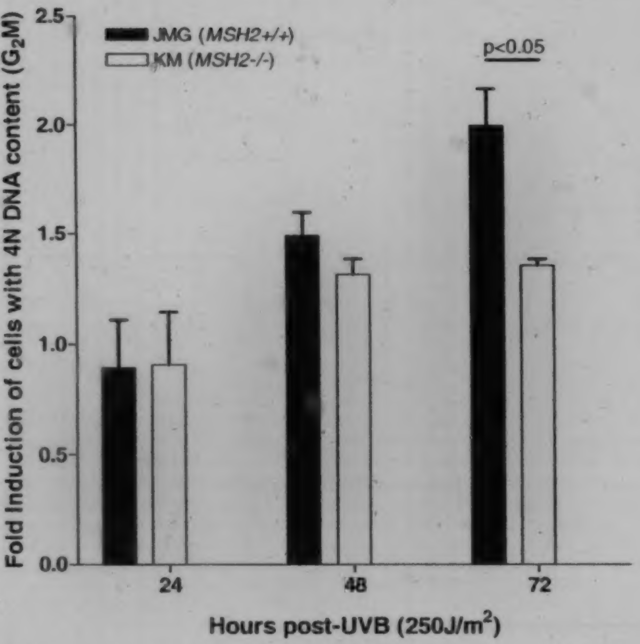

Figure 3-5 B: Induction of G2/M phase in JMG (*MSH2*$^{+/+}$) and KM (*MSH2*$^{-/-}$) cells after 250J/m^2 UVB

JMG (*MSH2*$^{+/+}$) and KM (*MSH2*$^{-/-}$) cells were treated with 250J/m^2 UVB and analyzed by flow cytometry after PI staining (n=3). Values were normalized to values for untreated controls for each cell line to obtain the fold induction of G2/M. The difference in values between JMG (*MSH2*$^{+/+}$) and KM (*MSH2*$^{-/-}$) cells at 72 hours was significant ($p<0.05$). The differences in values between JMG (*MSH2*$^{+/+}$) and KM (*MSH2*$^{-/-}$) cells at 24 and 48 hours were not significant.

Deficiency in MSH2 leads to decreased induction of the cell cycle proteins CHK1-pSer345 and CDC25C-pSer216

Levels of proteins involved in the G2/M pathway were studied after UVB exposure and compared to untreated controls. The levels of total CHK1 were lower in untreated KM (*MSH2*$^{-/-}$) cell line compared to the untreated JMG (*MSH2*$^{+/+}$) control cell line. Following

UVB radiation the levels of total CHK1 were modestly reduced in each of JMG (*MSH2*$^{+/+}$) and KM (*MSH2*$^{-/-}$) cell lines compared to their respective untreated controls (Fig. 3-6 A). CHK1 is activated through phosphorylation by ATM and ATR at residue serine 345 (Ser345). KM (*MSH2*$^{-/-}$) cells showed a decreased level of CHK1 phosphorylated at Ser345 in untreated cells compared to JMG (*MSH2*$^{+/+}$) untreated cells. Following UVB radiation the levels of CHK1-pSer345 were not as high in KM (*MSH2*$^{-/-}$) cells as JMG (*MSH2*$^{+/+}$) cells from 4 to 48 hours. KM (*MSH2*$^{-/-}$) cells had sustained levels of CHK1-pSer345 from 4 to 24 hours after UVB irradiation and returned to basal levels at 48 hours (Fig. 3-6 B).

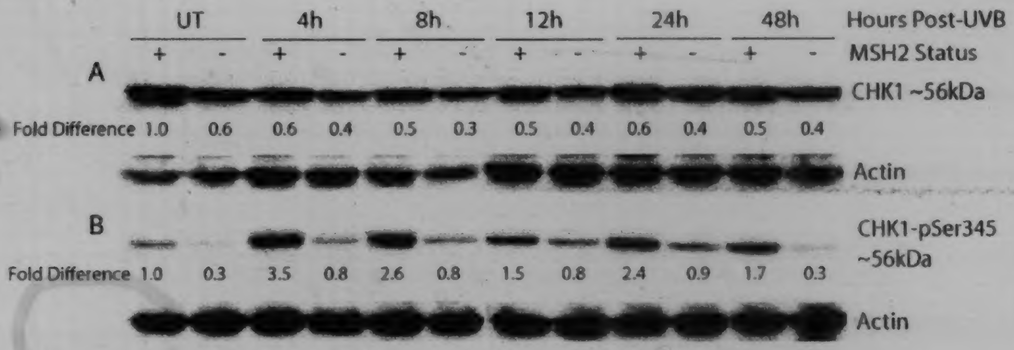

Figure 3-6: A) CHK1 and B) CHK1-pSer345 protein levels after UVB radiation

Protein extracts from JMG (*MSH2*$^{+/+}$) and KM (*MSH2*$^{-/-}$) cells irradiated with 250J/m^2 UVB were analyzed by western blot. Actin was used as a loading control. Densitometry was used to quantify the protein levels which were normalized to the loading control and then to the JMG (*MSH2*$^{+/+}$) untreated protein level to obtain the fold difference in protein levels for each lane.

The integral driver of the transition between G2 phase and mitosis is the CDC2-cyclin B1 complex. Inhibitory phosphates on CDC2 are removed by CDC25C. Untreated KM (*MSH2*$^{-/-}$) cells had approximately half the amount of CDC25C as untreated JMG (*MSH2*$^{+/+}$) cells. Following UVB radiation there was no substantial difference in the change of levels of CDC25C between the JMG (*MSH2*$^{+/+}$) and KM (*MSH2*$^{-/-}$) cell lines (Fig. 3-7 A). During G2/M arrest, CDC25C is inhibited by phosphorylation at serine 216 (Ser216). Although both JMG (*MSH2*$^{+/+}$) and KM (*MSH2*$^{-/-}$) cells had approximately equal levels of CDC25C-pSer216 when untreated and 4 hours after UVB treatment, KM (*MSH2*$^{-/-}$) cells had decreased levels of CDC25C-pSer216 at 8, 12 and 24 hours after UVB radiation compared to JMG (*MSH2*$^{+/+}$) cells (Fig. 3-7 B).

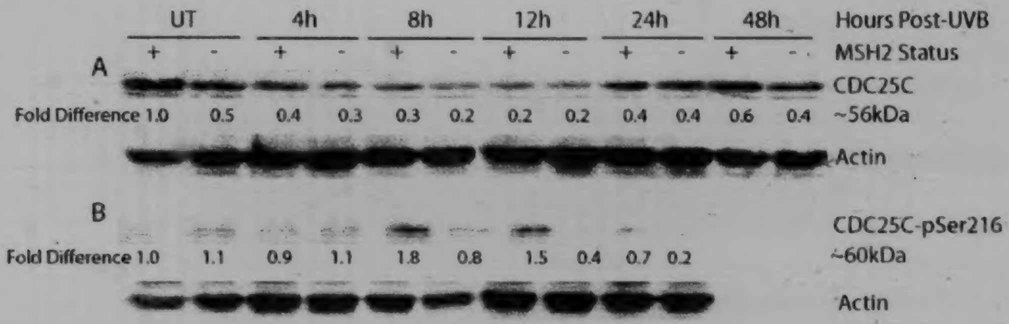
UT
4h
8h
12h
24h
48h
Hours Post-UVB
+ - + - + - + - + - + -
MSH2 Status
A
CDC25C
Fold Difference 1.0 0.5 0.4 0.3 0.3 0.2 0.2 0.2 0.4 0.4 0.6 0.4
~56kDa
Actin
B
CDC25C-pSer216
Fold Difference 1.0 1.1 0.9 1.1 1.8 0.8 1.5 0.4 0.7 0.2
~60kDa
Actin

Figure 3-7: A) CDC25C and B) CDC25C-pSer216 protein levels after UVB radiation

Protein extracts from JMG (*MSH2*$^{+/+}$) and KM (*MSH2*$^{-/-}$) cells irradiated with 250J/m^2 UVB were analyzed by western blot. Actin was used as a loading control. Densitometry was used to quantify the protein levels which were normalized to the loading control and then to the JMG (*MSH2*$^{+/+}$) untreated protein level to obtain the fold difference in protein levels for each lane.

Total CDC2 protein levels were analyzed. Untreated KM (*MSH2*$^{-/-}$) cells had approximately half the amount as untreated JMG (*MSH2*$^{+/+}$). CDC2 levels decreased following UVB radiation in the JMG (*MSH2*$^{+/+}$) cell line and this decrease was maintained over 48 hours. Post-UVB exposure the level of CDC2 in the KM (*MSH2*$^{-/-}$) cell line remained unchanged from untreated levels (Fig. 3-8 A). There was no appreciable difference in the levels of CDC2-pTyr15, Thr14 levels in untreated KM (*MSH2*$^{-/-}$) cells compared to untreated JMG (*MSH2*$^{+/+}$) cells, or after UVB treatment. Levels of CDC2-pTyr15, Thr14 increased in both JMG (*MSH2*$^{+/+}$) and KM (*MSH2*$^{-/-}$) cells at 12 hours post-UVB and by 48 hours the levels of CDC2-pTyr15, Thr14 returned to untreated levels in both cell lines (Fig. 3-8 B).

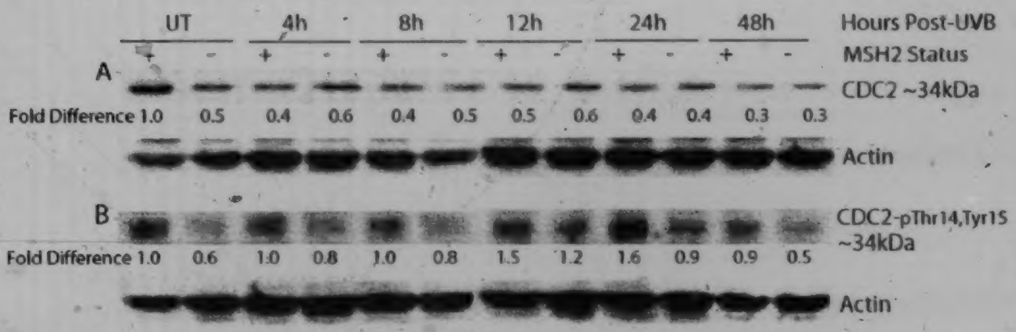
UT
4h
8h
12h
24h
48h
Hours Post-UVB
+ - + - + - + - + - + -
MSH2 Status
A
CDC2 ~34kDa
Fold Difference 1.0 0.5 0.4 0.6 0.4 0.5 0.5 0.6 0.4 0.4 0.3 0.3
Actin
B
CDC2-pThr14,Tyr15 ~34kDa
Fold Difference 1.0 0.6 1.0 0.8 1.0 0.8 1.5 1.2 1.6 0.9 0.9 0.5
Actin

Figure 3-8: A) CDC2 and B) CDC2-pThr14, Tyr15 protein levels after UVB radiation

Protein extracts from JMG (*MSH2*$^{+/+}$) and KM (*MSH2*$^{-/-}$) cells irradiated with 250J/m^2 UVB were analyzed by western blot. Actin was used as a loading control. Densitometry was used to quantify the protein levels which were normalized to the loading control and then to the JMG (*MSH2*$^{+/+}$) untreated protein level to obtain the fold difference in protein levels for each lane.

One of the kinases that maintains inhibitory phosphates on CDC2 is WEE1. WEE1 levels were analyzed in JMG ($MSH2^{+/+}$) and KM ($MSH2^{-/-}$) cells following UVB radiation. There were no substantial differences in the levels of WEE1 between JMG ($MSH2^{+/+}$) and KM ($MSH2^{-/-}$) cells, both untreated and after UVB (Fig. 3-9).

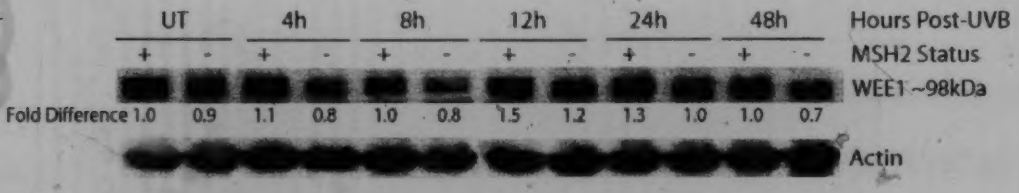
UT
4h
8h
12h
24h
48h
Hours Post-UVB
+ - + - + - + - + - + -
MSH2 Status
WEE1 ~98kDa
Fold Difference 1.0 0.9 1.1 0.8 1.0 0.8 1.5 1.2 1.3 1.0 1.0 0.7
Actin

Figure 3-9: WEE1 protein levels after UVB radiation

Protein extracts from JMG ($MSH2^{+/+}$) and KM ($MSH2^{-/-}$) cells irradiated with 250J/m^2 UVB were analyzed by western blot. Actin was used as a loading control. Densitometry was used to quantify the protein levels which were normalized to the loading control and then to the JMG ($MSH2^{+/+}$) untreated protein level to obtain the fold difference in protein levels for each lane.

Discussion

Many studies have indicated the importance of a functional MMR system for the appropriate activation of cell cycle checkpoints in response to several types of DNA damage (Kaina et al. 1997; Modrich 1997; D'Atri et al. 1998; Duckett et al. 1999; Hickman and Samson 1999; Brown et al. 2003; Hirose et al. 2003; Wang and Qin 2003; van Oosten et al. 2005; Seifert et al. 2008). I assessed the influence of the MMR protein Msh6 by comparing the cell cycle response of *Msh6*$^{+/+}$ and *Msh6*$^{-/-}$ MEFs after UVB-induced DNA damage. We also studied the role of MSH2 in the cell cycle in a non-tumor cell line generated from an individual with bi-allelic *MSH2* mutations resulting in a MMR-null phenotype (Whiteside et al. 2002).

We have previously shown that MMR is important in the prevention of UVB-induced skin cancer via its role in triggering UVB-induced apoptosis (Young et al. 2004). By demonstrating that the lack of Msh6 and MSH2 leads to abrogated G2/M cell cycle arrest as well as altered levels and decreased induction of several integral cell cycle proteins, MMR is shown to be an important component in the cell cycle response of normal, non-tumor cells to UVB-induced DNA damage.

Cell cycle analysis shows that there was a significant reduction in the fold induction of *Msh6*$^{-/-}$ MEFs with 4N DNA content (G2/M) 24 hours after UVB, compared to *Msh6*$^{+/+}$ MEFs($p<0.05$; Fig. 3-4). In the MSH2-deficient non-tumorigenic human cell line, there is also a significant reduction in the percentage of untreated cells in G2/M phase ($p<0.05$) and a partial reduction in G2/M arrest 48 ($p<0.05$) and 72 hours ($p<0.01$) following UVB radiation compared to MSH2-proficient cells (Fig. 3-5 A). Moreover, the fold-induction of cells into G2/M arrest is significantly reduced in KM (*MSH2*$^{-/-}$) cells compared to JMG (*MSH2*$^{+/+}$) cells at 72 hours post-UVB (1.2-fold induction versus 2-fold induction respectively; $p<0.05$; Fig. 3-5 B). These findings are in agreement with previous studies using 6-TG and IR to induce DNA damage (Buermeyer et al. 1999; Yan et al. 2001). This partial reduction in G2/M arrest is predicted to contribute, along with reduced apoptosis and repair, to the development of neoplasia in the absence of MMR by reducing the amount of time the cell has to repair DNA damage prior to entering mitosis [reviewed in (Young et al. 2003; O'Brien and Brown 2006; Seifert and Reichrath 2006)]. The differences seen in the time to G2/M arrest in *Msh6*-proficient MEFs versus *MSH2*-proficient human cells are most likely due to the inherent differences between primary mouse fibroblasts and transformed human lymphoblastoid cells.

Our data is consistent with the model that suggests a mechanism by which MMR acts upstream in G2/M arrest and apoptosis following DNA damage. In response to UVB radiation the MMR protein MSH2 binds to DNA lesions and may recruit cell cycle proteins, thus affecting the initiation of the G2/M cell cycle arrest cascade. Studies by Hays *et al*. (2005) show that human MutSα and *E. coli* MutS bind to DNA that contains "matched" photoproducts (T[CPD]T/AA, T[6-4PP]T/AA) as efficiently as it does to homoduplex DNA (Hays et al. 2005). In certain contexts these MMR complexes bind selectively to "mismatched" photoproducts (T[CPD]**T/AG**, T[6-4PP]**T/AG**), but with no excision of the damage. Hays et al. suggest that this formation of "dead-end intermediates" may be a mechanism for the initiation of 'signaling' by the MMR system.

Western blot analysis was attempted to study the levels of the key cell cycle proteins listed below in mouse. However, due to the lack of success obtaining results with the majority of the antibodies in mouse, the data obtained from western blot analysis in human is presented to elucidate the role of MMR in the cell cycle following UVB radiation.

The spontaneous levels of the key cell cycle regulators CHK1, CHK1-pSer345, CDC25C, CDC2, and CDC2-pTyr15, Thr14 were reduced by approximately 2-fold in untreated KM (*MSH2*$^{-/-}$) cells compared to JMG (*MSH2*$^{+/+}$) cells. There were also reduced amounts of CHK1-pSer345 and CDC25C-pSer216 after UVB treatment in KM (*MSH2*$^{-/-}$) cells compared to JMG (*MSH2*$^{+/+}$) cells. It was previously demonstrated that MSH2 co-immunoprecipitates with ATR and ATRIP, activating CHK1 following MNNG exposure (Wang and Qin 2003; Adamson et al. 2005). MMR proteins may behave similarly in response to other DNA damaging agents. Therefore, following UVB radiation MSH2 may directly influence ATR and CHK1 activation, contributing to protein complex formation necessary for ATM/ATR activation and induction of G2/M arrest through the CDC2 pathway. Immunoblots to observe total and activated ATR were also investigated in this study, however due to the high amount of background signal and non-specific banding that occurred no conclusions could be made regarding levels of expression of these proteins in the cell lysates. Support for the recruitment of this pathway was demonstrated by reduction in CHK1-pSer345 (Fig. 3-6) and CDC25C-pSer216 (Fig. 3-7) in MMR deficient cells after UVB treatment. However, as MMR deficiency only partially decreases the G2/M cell cycle arrest, ATM/ATR are predicted to be activated by MMR-independent mechanisms as well.

The antibody used to recognize phosphorylated CDC2 (Tyr15) resulted in a reproducible doublet on immunoblots (Fig. 3-8). This doublet is most likely due to a second phosphorylation event at Thr14 also associated with inhibition of CDC2. The lower band reflects Tyr15 phosphorylation, and the upper band reflects both Thr14 and Tyr15 phosphorylation (Borgne and Meijer 1996; Fletcher et al. 2002). A similar pattern was seen with WEE1. The antibody used detects both the unmodified form of WEE1 and the isoform phosphorylated at Ser549 by CHK1. The upper band is associated with phosphorylated WEE1 and the lower band represents the unphosphorylated form of WEE1 (Upstate technical support, personal communication, October 14, 2004) (Fig. 3-9).

In conclusion, MMR proteins Msh6 and MSH2 play a role in G2/M arrest after UVB-induced DNA damage. This is illustrated by diminished G2/M arrest in Msh6-deficient MEFs and MSH2-deficient human cells and decreased induction of several key cell cycle proteins after UVB in MSH2-deficient cells. The mechanism by which the MMR proteins trigger downstream cell cycle protein activation remains to be determined.

References

Adamson, A. W., D. I. Beardsley, W. J. Kim, Y. Gao, R. Baskaran and K. D. Brown (2005). "Methylator-induced, mismatch repair-dependent G2 arrest is activated through Chk1 and Chk2." Mol Biol Cell **16**(3): 1513-26.

Bhattacharyya, N. P., A. Skandalis, A. Ganesh, J. Groden and M. Meuth (1994). "Mutator phenotypes in human colorectal carcinoma cell lines." Proc Natl Acad Sci U S A **91**(14): 6319-23.

Borgne, A. and L. Meijer (1996). "Sequential dephosphorylation of p34(cdc2) on Thr-14 and Tyr-15 at the prophase/metaphase transition." J Biol Chem **271**(44): 27847-54.

Branch, P., R. Hampson and P. Karran (1995). "DNA mismatch binding defects, DNA damage tolerance, and mutator phenotypes in human colorectal carcinoma cell lines." Cancer Res **55**(11): 2304-9.

Brown, K. D., A. Rathi, R. Kamath, D. I. Beardsley, Q. Zhan, J. L. Mannino and R. Baskaran (2003). "The mismatch repair system is required for S-phase checkpoint activation." Nat Genet **33**(1): 80-4.

Buermeyer, A. B., S. M. Deschenes, S. M. Baker and R. M. Liskay (1999). "Mammalian DNA mismatch repair." Annu Rev Genet **33**: 533-64.

D'Atri, S., L. Tentori, P. M. Lacal, G. Graziani, E. Pagani, E. Benincasa, G. Zambruno, E. Bonmassar and J. Jiricny (1998). "Involvement of the mismatch repair system in temozolomide-induced apoptosis." Mol Pharmacol **54**(2): 334-41.

Davis, T. W., C. Wilson-Van Patten, M. Meyers, K. A. Kunugi, S. Cuthill, C. Reznikoff, C. Garces, C. R. Boland, T. J. Kinsella, R. Fishel and D. A. Boothman (1998).

"Defective expression of the DNA mismatch repair protein, MLH1, alters G2-M cell cycle checkpoint arrest following ionizing radiation." Cancer Res **58**(4): 767-78.

Duckett, D. R., S. M. Bronstein, Y. Taya and P. Modrich (1999). "hMutSalpha- and hMutLalpha-dependent phosphorylation of p53 in response to DNA methylator damage." Proc Natl Acad Sci U S A **96**(22): 12384-8.

Duckett, D. R., J. T. Drummond, A. I. Murchie, J. T. Reardon, A. Sancar, D. M. Lilley and P. Modrich (1996). "Human MutSalpha recognizes damaged DNA base pairs containing O6-methylguanine, O4-methylthymine, or the cisplatin-d(GpG) adduct." Proc Natl Acad Sci U S A **93**(13): 6443-7.

Fletcher, L., Y. Cheng and R. J. Muschel (2002). "Abolishment of the Tyr-15 inhibitory phosphorylation site on cdc2 reduces the radiation-induced G(2) delay, revealing a potential checkpoint in early mitosis." Cancer Res **62**(1): 241-50.

Franchitto, A., P. Pichierri, R. Piergentili, M. Crescenzi, M. Bignami and F. Palitti (2003). "The mammalian mismatch repair protein MSH2 is required for correct MRE11 and RAD51 relocalization and for efficient cell cycle arrest induced by ionizing radiation in G2 phase." Oncogene **22**(14): 2110-20.

Hawn, M. T., A. Umar, J. M. Carethers, G. Marra, T. A. Kunkel, C. R. Boland and M. Koi (1995). "Evidence for a connection between the mismatch repair system and the G2 cell cycle checkpoint." Cancer Res **55**(17): 3721-5.

Hays, J. B., P. D. Hoffman and H. Wang (2005). "Discrimination and versatility in mismatch repair." DNA Repair (Amst) **4**(12): 1463-74.

Hickman, M. J. and L. D. Samson (1999). "Role of DNA mismatch repair and p53 in signaling induction of apoptosis by alkylating agents." Proc Natl Acad Sci U S A **96**(19): 10764-9.

Hirose, Y., M. Katayama, D. Stokoe, D. A. Haas-Kogan, M. S. Berger and R. O. Pieper (2003). "The p38 mitogen-activated protein kinase pathway links the DNA mismatch repair system to the G2 checkpoint and to resistance to chemotherapeutic DNA-methylating agents." Mol Cell Biol **23**(22): 8306-15.

Kaina, B., A. Ziouta, K. Ochs and T. Coquerelle (1997). "Chromosomal instability, reproductive cell death and apoptosis induced by O6-methylguanine in Mex-, Mex+ and methylation-tolerant mismatch repair compromised cells: facts and models." Mutat Res **381**(2): 227-41.

Koi, M., A. Umar, D. P. Chauhan, S. P. Cherian, J. M. Carethers, T. A. Kunkel and C. R. Boland (1994). "Human chromosome 3 corrects mismatch repair deficiency and microsatellite instability and reduces N-methyl-N'-nitro-N-nitrosoguanidine tolerance in colon tumor cells with homozygous hMLH1 mutation." Cancer Res **54**(16): 4308-12.

Malkhosyan, S., A. McCarty, H. Sawai and M. Perucho (1996). "Differences in the spectrum of spontaneous mutations in the hprt gene between tumor cells of the microsatellite mutator phenotype." Mutat Res **316**(5-6): 249-59.

Meira, L. B., D. L. Cheo, A. M. Reis, N. Claij, D. K. Burns, H. te Riele and E. C. Friedberg (2002). "Mice defective in the mismatch repair gene Msh2 show increased predisposition to UVB radiation-induced skin cancer." DNA Repair (Amst) **1**(11): 929-34.

Meira, L. B., A. M. Reis, D. L. Cheo, D. Nahari, D. K. Burns and E. C. Friedberg (2001). "Cancer predisposition in mutant mice defective in multiple genetic pathways: uncovering important genetic interactions." Mutat Res **477**(1-2): 51-8.

Meyers, M., M. W. Wagner, H. S. Hwang, T. J. Kinsella and D. A. Boothman (2001). "Role of the hMLH1 DNA mismatch repair protein in fluoropyrimidine-mediated cell death and cell cycle responses." Cancer Res **61**(13): 5193-201.

Modrich, P. (1997). "Strand-specific mismatch repair in mammalian cells." J Biol Chem **272**(40): 24727-30.

O'Brien, V. and R. Brown (2006). "Signalling cell cycle arrest and cell death through the MMR System." Carcinogenesis **27**(4): 682-92.

Peters, A. C., L. C. Young, T. Maeda, V. A. Tron and S. E. Andrew (2003). "Mammalian DNA mismatch repair protects cells from UVB-induced DNA damage by facilitating apoptosis and p53 activation." DNA Repair (Amst) **2**(4): 427-35.

Pietenpol, J. A. and Z. A. Stewart (2002). "Cell cycle checkpoint signaling: cell cycle arrest versus apoptosis." Toxicology **181-182**: 475-81.

Reitmair, A. H., R. Risley, R. G. Bristow, T. Wilson, A. Ganesh, A. Jang, J. Peacock, S. Benchimol, R. P. Hill, T. W. Mak, R. Fishel and M. Meuth (1997). "Mutator phenotype in Msh2-deficient murine embryonic fibroblasts." Cancer Res **57**(17): 3765-71.

Richards, B., H. Zhang, G. Phear and M. Meuth (1997). "Conditional mutator phenotypes in hMSH2-deficient tumor cell lines." Science **277**(5331): 1523-6.

Sancar, A., L. A. Lindsey-Boltz, K. Unsal-Kacmaz and S. Linn (2004). "Molecular mechanisms of mammalian DNA repair and the DNA damage checkpoints." Annu Rev Biochem **73**: 39-85.

Seifert, M. and J. Reichrath (2006). "The role of the human DNA mismatch repair gene hMSH2 in DNA repair, cell cycle control and apoptosis: implications for pathogenesis, progression and therapy of cancer." J Mol Histol **37**(5-7): 301-7.

Seifert, M., S. J. Scherer, W. Edelmann, M. Bohm, V. Meineke, M. Lobrich, W. Tilgen and J. Reichrath (2008). "The DNA-mismatch repair enzyme hMSH2 modulates UV-B-induced cell cycle arrest and apoptosis in melanoma cells." J Invest Dermatol **128**(1): 203-13.

Taylor, W. R. and G. R. Stark (2001). "Regulation of the G2/M transition by p53." Oncogene **20**(15): 1803-15.

Umar, A., M. Koi, J. I. Risinger, W. E. Glaab, K. R. Tindall, R. D. Kolodner, C. R. Boland, J. C. Barrett and T. A. Kunkel (1997). "Correction of hypermutability, N-methyl-N'-nitro-N-nitrosoguanidine resistance, and defective DNA mismatch repair by introducing chromosome 2 into human tumor cells with mutations in MSH2 and MSH6." Cancer Res **57**(18): 3949-55.

van Oosten, M., G. J. Stout, C. Backendorf, H. Rebel, N. de Wind, F. Darroudi, H. J. van Kranen, F. R. de Gruijl and L. H. Mullenders (2005). "Mismatch repair protein Msh2 contributes to UVB-induced cell cycle arrest in epidermal and cultured mouse keratinocytes." DNA Repair (Amst) **4**(1): 81-9.

Wang, Y. and J. Qin (2003). "MSH2 and ATR form a signaling module and regulate two branches of the damage response to DNA methylation." Proc Natl Acad Sci U S A **100**(26): 15387-92.

Whiteside, D., R. McLeod, G. Graham, J. L. Steckley, K. Booth, M. J. Somerville and S. E. Andrew (2002). "A homozygous germ-line mutation in the human MSH2 gene predisposes to hematological malignancy and multiple cafe-au-lait spots." Cancer Res **62**(2): 359-62.

Yan, T., S. E. Berry, A. B. Desai and T. J. Kinsella (2003). "DNA Mismatch Repair (MMR) Mediates 6-Thioguanine Genotoxicity by Introducing Single-strand Breaks to Signal a G(2)-M Arrest in MMR-proficient RKO Cells." Clin Cancer Res **9**(6): 2327-34.

Yan, T., J. E. Schupp, H. S. Hwang, M. W. Wagner, S. E. Berry, S. Strickfaden, M. L. Veigl, W. D. Sedwick, D. A. Boothman and T. J. Kinsella (2001). "Loss of DNA mismatch repair imparts defective cdc2 signaling and G(2) arrest responses without altering survival after ionizing radiation." Cancer Res **61**(22): 8290-7.

Yoshino, M., Y. Nakatsu, H. te Riele, S. Hirota, Y. Kitamura and K. Tanaka (2002). "Additive roles of XPA and MSH2 genes in UVB-induced skin tumorigenesis in mice." DNA Repair (Amst) **1**(11): 935-40.

Young, L. C., J. B. Hays, V. A. Tron and S. E. Andrew (2003). "DNA mismatch repair proteins: potential guardians against genomic instability and tumorigenesis induced by ultraviolet photoproducts." J Invest Dermatol **121**(3): 435-40.

Young, L. C., K. J. Thulien, M. R. Campbell, V. A. Tron and S. E. Andrew (2004). "DNA mismatch repair proteins promote apoptosis and suppress tumorigenesis in response to UVB irradiation: an in vivo study." Carcinogenesis **25**(10): 1821-7.

Zhang, H., J. Taylor and W. Siede (2003). "Checkpoint arrest signaling in response to UV damage is independent of nucleotide excision repair in Saccharomyces cerevisiae." J Biol Chem **278**(11): 9382-7.

~ Chapter 4 ~

Characterization of the mitochondrial/intrinsic apoptotic response to UVB-induced DNA damage in mismatch repair-proficient and -deficient murine embryonic fibroblasts

The data presented in this chapter are being prepared for submission to Carcinogenesis.

All experimental design, data analysis and experimentation were performed by Kelly Narine with the exception of the apoptosis assay in Figure 4-3 which was performed by Leah C. Young, Kyle J. Thulien and Angela M. Keuling.

Introduction

Apoptosis can be triggered via two major pathways: an extrinsic/death receptor pathway initiated when ligands bind to their death receptors (Chapter 6), or an intrinsic/mitochondrial pathway initiated by internal cellular stress such as DNA damage, imparted by such stimuli as UVB radiation.

The ratios and activity of pro- and anti-apoptotic members of the Bcl-2 family of proteins determine subsequent apoptotic events. The anti-apoptotic or pro-survival members of the Bcl-2 family include Bcl-2 itself as well as Bcl-$_{XL}$, Bcl-$_{W}$, A1 and Mcl-1. The pro-apoptotic Bcl-2 family members can be broken into 2 groups: 1) "multidomain" proteins such as Bax, Bak and Bok that share BH1, BH2 and BH3 domains with Bcl-2, and 2) "BH3-only" proteins such as Bid, Bad and Bim that only have the short BH3 interaction domain that is necessary for apoptosis. The activation of BH3-only apoptotic proteins is triggered by various stimuli that induce cellular stress, including nutrient deprivation and DNA damage induced by various agents, including UVB [reviewed in (Danial and Korsmeyer 2004; Jin and El-Deiry 2005; Spierings et al. 2005)].

Pro-apoptotic Bax and Bak are integral in triggering the central step of the intrinsic apoptotic pathway: mitochondrial outer membrane permeabilization (MOMP). MOMP has been shown to be associated with a reduction in mitochondrial membrane potential, which may occur when pores form in the mitochondrial outer membrane (Zhou et al. 2005). As MOMP occurs, proteins housed in the intermembrane space are released into the cytosol, such as cytochrome c and Smac/DIABLO. Cytochrome c binds Apaf1 and subsequently caspase 9 to form the ATP-mediated apoptosome. Binding of caspase 9 causes cleavage and activation of this caspase. Active caspase 9 then cleaves executioner caspases, caspases 3 and 7, which in turn cleave downstream targets like poly (ADP-ribose) polymerase (PARP) and inhibitor of caspase-activated deoxyribonuclease (ICAD). Smac/DIABLO is an antagonist of the inhibitor of apoptosis proteins (IAPs) by acting as a competitive inhibitor (Du et al. 2000; Suzuki et al. 2001; Hegde et al. 2003) (Fig. 4-1).

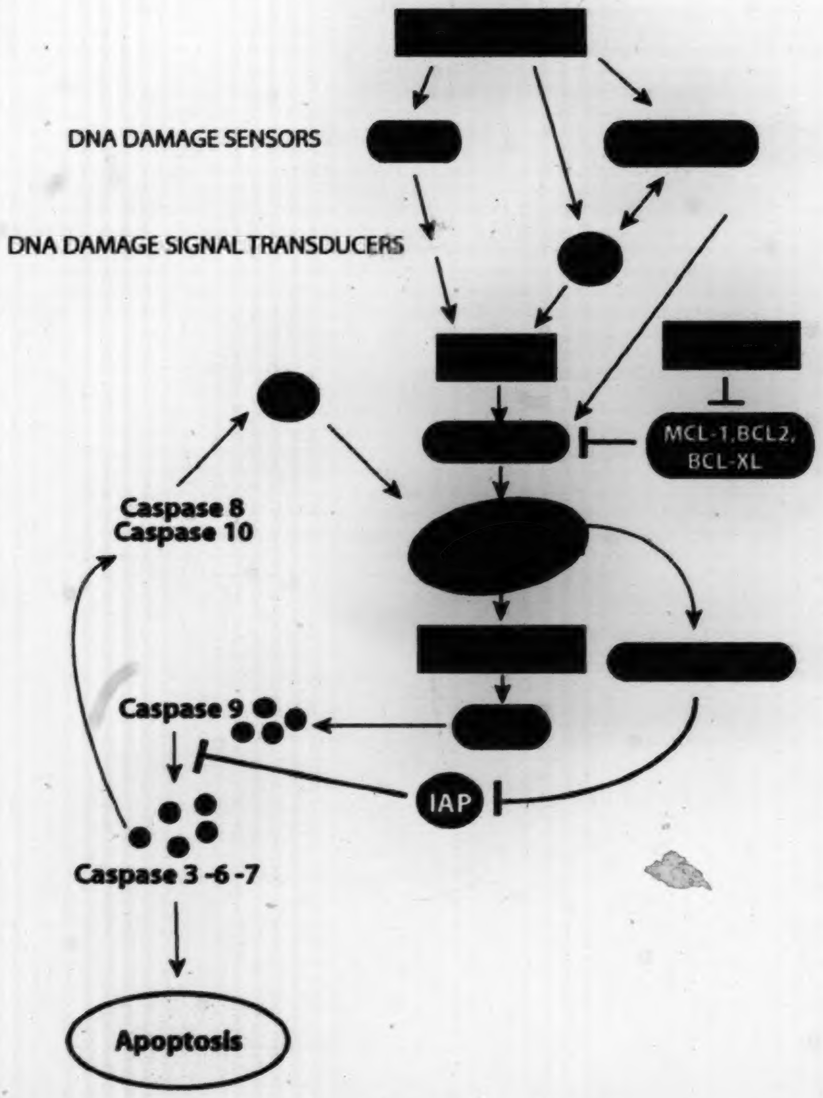
DNA DAMAGE SENSORS
DNA DAMAGE SIGNAL TRANSDUCERS
MCL-1,BCL2,
BCL-XL
Caspase 8
Caspase 10
Caspase 9
IAP
Caspase 3 -6 -7
Apoptosis

Figure 4-1: Schematic of mitochondrial apoptosis with potential position of Msh6

DNA damage can act directly on p53, caspase 2 and potentially Msh6 to initiate downstream apoptosis via the mitochondrial/intrinsic pathway. Bim and Puma activate Bax and Bak translocation to the mitochondria, while Bad and Noxa inhibit the binding and neutralization of Bax and Bak by anti-apoptotic proteins such as Mcl-1, Bcl-2 and Bcl-xl. Mitochondria undergo mitochondrial membrane permeability, associated with a reduction in mitochondrial membrane potential. Cytochrome c and Smac/DIABLO are released from the mitochondria into the cytosol, where Smac/DIABLO binds to and inhibits the inhibitors of apoptosis (IAPs). Cytochrome c forms the apoptosome with Apaf-1 and caspase 9, which activates downstream effector caspases 3, 6 and 7, effecting apoptosis. Caspase 3 can activate caspase 8/10 which in turn cleave Bid. The truncated Bid can translocate to the mitochondria, thus amplifying the apoptotic signal.

Evidence suggests that UV damage-induced apoptosis occurs through the mitochondrial apoptotic pathway. It has been shown that after UVB, cytochrome c release is an early event, occurring before or simultaneously with caspase activation and considerably before reduction in mitochondrial transmembrane potential (Bossy-Wetzel et al. 1998). A later study by a different group showed that cytochrome c and Smac/DIABLO release from the mitochondria are triggered by Bax accumulation in the outer mitochondrial membrane after UV radiation. Both were released early in apoptosis , but contrary to the previously discussed study, cytochrome c and Smac/DIABLO release from the mitochondria coincided with mitochondrial membrane depolarization (Zhou et al. 2005). Bivik et al. (2006) demonstrate that UVA/B induces mitochondrial apoptosis in human melanocytes, dislaying cytochrome c release and caspase 3 activation (Bivik et al. 2006). Likewise, the induction of UV-induced apoptosis is important in human keratinocytes and involves caspase 9 activation and cytochrome c release (Denning et al. 2002; Sitailo et al. 2002).

In addition to the mitochondrial apoptotic pathway, studies have also shown a link between UV exposure and the recruitment of the extrinsic apoptotic pathway. TNFα, TNFR1, Fas and FasL are upregulated after exposure to UV, which is associated with the induction of apoptosis (Kock et al. 1990; Leverkus et al. 1997; Zhuang et al. 1999). This pathway of apoptosis will be explored further in Chapter 6. Published reports have shown that both the mitochondrial and death receptor pathways of apoptosis are recruited after UV (Takasawa and Tanuma 2003) and that there may be overlap of these 2 apoptotic pathways via caspase 3 activation of caspase 8, which will be discussed in Chapter 6 (Sitailo et al. 2002).

Studies have demonstrated a role for MMR in the cellular response to UV-induced DNA damage (Meira et al. 2002; Yoshino et al. 2002; Peters et al. 2003; Young et al. 2003; Young et al. 2004; van Oosten et al. 2005; Narine et al. 2007). Our previous studies have shown that MEFs and *in vivo* keratinocytes deficient in either Msh2 or Msh6 have increased survival after UVB treatment and reduced levels of UVB-induced apoptosis compared to wildtype cellular controls (Peters et al. 2003; Young et al. 2003).

MMR has been shown to be involved in the cellular apoptotic response [reviewed in (Iyer et al. 2006)]. The role of MMR in the DNA damage response after UV radiation [reviewed in (Young et al. 2003)] and the evidence that UVB-induced apoptosis occurs through the mitochondrial apoptotic pathway (see above) has led me to test the hypothesis that MMR plays a role in UVB-induced apoptosis through the mitochondria. I investigated several proteins known to play a role in promoting mitochondrial membrane depolarization to elucidate the potential mechanism by which Msh6 can be influencing apoptotic events post-UVB.

Results

No appreciable dffference in p53 levels between *Msh6*$^{+/+}$ and *Msh6*$^{-/-}$ murine embryonic fibroblasts

p53 is a key tumor suppressor protein involved in DNA repair, cell cycle progression and apoptosis after many types of DNA damage, including UV. Evidence suggests that MMR acts both upstream (Duckett et al. 1999; Hickman and Samson 1999; Lin et al. 2001; Peters et al. 2003) and downstream (Scherer et al. 1996; Scherer et al. 2000; Warnick et al. 2001) of p53 after DNA damage. I investigated whether MMR affects p53 protein levels in *Msh6*$^{+/+}$or *Msh6*$^{-/-}$ MEFs after UVB. **Note: densitometry was performed and the values obtained were normalized to the loading control only.** Western blot analysis shows that total p53 was not detectable in untreated *Msh6*$^{+/+}$and *Msh6*$^{-/-}$ MEFs. In *Msh6*$^{+/+}$ MEFs levels of total p53 increased steadily from1 hour until 12 hours after UVB treatment, when it remained stable until 48 hours post-UVB. At this timepoint total p53 protein levels decreased to barely detectable levels seen at 1 hour post-UVB. In *Msh6*$^{-/-}$ MEFs levels of total p53 protein also increased steadily from1 hour until 12 hours after UVB treatment. From 24 to 48 hours post-UVB the levels of total p53 decreased and at the last timepoint, returned to barely detectable levels seen at 1 hour post-UVB. Overall, there was no appreciable difference in the levels of total p53 protein between *Msh6*$^{+/+}$ and *Msh6*$^{-/-}$ MEFs over time, indicating that Msh6 does not affect total p53 levels after UVB irradiation (Fig. 4-2 A).

p53 is phosphorylated in response to cellular stress. Examination of protein levels of p53 phosphorylated at serine15 in *Msh6*$^{+/+}$ and *Msh6*$^{-/-}$ MEFs illustrated the same pattern as seen with p53 total protein levels. p53-pSer15 was not detectable in either *Msh6*$^{+/+}$ or *Msh6*$^{-/-}$ untreated MEFs but increased over time after UVB until 48 hours, when p53-pSer15 levels had decreased to levels observed at 1 hour post-UVB. There was no appreciable difference in the levels of p53-pSer15 protein between *Msh6*$^{+/+}$ and *Msh6*$^{-/-}$ MEFs over time, indicating that Msh6 does not affect p53-pSer15 levels after UVB irradiation (Fig. 4-2 B).

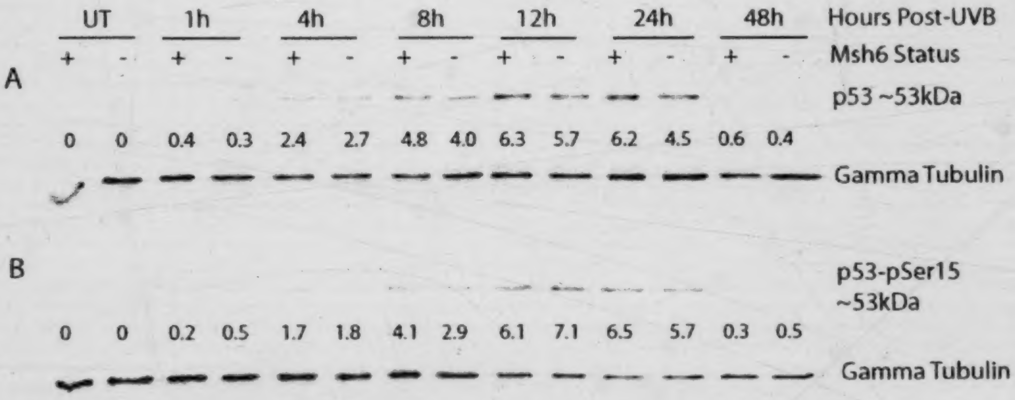
UT
1h
4h
8h
12h
24h
48h
Hours Post-UVB
+ - + - + - + - + - + - + -
Msh6 Status
A
p53 ~53kDa
0 0 0.4 0.3 2.4 2.7 4.8 4.0 6.3 5.7 6.2 4.5 0.6 0.4
Gamma Tubulin
B
p53-pSer15 ~53kDa
0 0 0.2 0.5 1.7 1.8 4.1 2.9 6.1 7.1 6.5 5.7 0.3 0.5
Gamma Tubulin

Figure 4-2: A) p53 and B) p53-Serine15 protein levels after UVB radiation

Protein extracts from *Msh6*$^{+/+}$ and *Msh6*$^{-/-}$ MEFs irradiated with 300J/m^2 UVB were analyzed by western blot. Gamma tubulin was used as a loading control. Densitometry was used to quantify the protein levels which were normalized to the loading control to obtain the protein levels for each lane.

Apoptosis levels in *Msh6*$^{+/+}$, *Msh6*$^{-/-}$, *Msh6*$^{-/-}$ *p53*$^{+/-}$, *Msh6*$^{-/-}$ *p53*$^{-/-}$, *p53*$^{-/-}$ murine embryonic fibroblasts

We have previously found that loss of Msh6 results in reduced UVB-induced apoptosis *in vitro* (Young et al. 2003). As stated previously, there is evidence that MMR can act both upstream and downstream of p53 after DNA damage. Although we found no evidence of Msh6-dependent changes in p53 protein levels after UVB (Fig. 4-2), there are reports that suggest that the MMR- and the p53- DNA damage response pathways may be partially interconnected (Cranston et al. 1997; Cranston and Fishel 1999; Scherer et al. 2000; Toft et al. 2002). We wanted to study the effect of loss of p53 in addition to Msh6 deficiency on levels of apoptosis in MEFs. Levels of UVB-induced apoptosis were measured in *Msh6*$^{-/-}$; *p53*$^{+/-}$ MEFs and compared in MEFs of related genotypes (Fig. 4-3) to determine if Msh6-associated apoptosis was p53-dependent or -independent. There were no significant differences between the levels of apoptosis for the *Msh6*$^{-/-}$; *p53*$^{+/-}$ MEFs and *Msh6*$^{-/-}$ MEFs. However, complete loss of p53 in addition to Msh6 deficiency resulted in significant decreases in apoptosis greater than observed for p53 deficiency or Msh6 deficiency alone (Fig. 4-3). This suggests that there are non-overlapping pathways between Msh6-dependent and p53-dependent apoptosis in these cell lines.

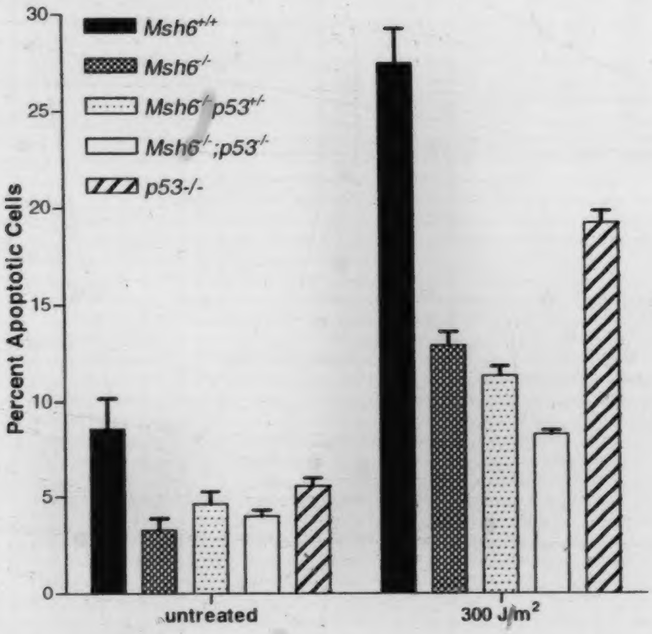

Figure 4-3: Apoptosis levels in MEFs 24 hours after irradiation with UVB

Error bars denote standard error of the mean. Mean apopotosis levels were compared using ANOVA and Bonferroni's correction for multiple comparisons. The percentage of apoptotic cells for each genotype was compared to all other genotypes. All comparisons were significant ($p<0.001$, n=3) with the exception of *Msh6*$^{-/-}$;*p53*$^{+/-}$ vs. *Msh6*$^{-/-}$ ($p>0.05$, n=3).

Alterations in mitochondrial membrane potential are reduced in *Msh6*$^{-/-}$ murine embryonic fibroblasts

Reductions in mitochondrial membrane potential have been shown to associate with permeability change in the mitochondrial membrane that allows the flux of proteins, such as cytochrome c and Smac/DIABLO, out of the mitochondria and into the cytoplasm. Cytochrome c forms part of the apoptosome, which drives apoptosis, and Smac/DIABLO enhances the apoptotic event by restricting the inhibitor of apoptosis proteins (IAPs). Flow cytometry was utilized to assess the number of cells with reduction in mitochondrial membrane potential, thus indicating that apoptosis is occurring through mitochondria. *Msh6*$^{+/+}$ and *Msh6*$^{-/-}$ MEFs were fluorescently stained 24 hours after DNA damage was induced by 250 or 300J/m^2 UVB exposure. Two doses of UVB were used in order to determine if there was a dose-dependent response to UVB with respect to alterations in mitochondrial membrane potential. Analysis showed that cells that were undergoing apoptosis exhibited green fluorescence, while those that were intact fluoresced red. After 250J/m^2 UVB there was a significantly lower proportion of *Msh6*$^{-/-}$ MEFs with alterations in mitochondrial membrane potential versus *Msh6*$^{+/+}$ MEFs (17% in *Msh6*$^{-/-}$ MEFs versus 26% in *Msh6*$^{+/+}$ MEFs; $p<0.05$). Also, after 300J/m^2 UVB 22% of *Msh6*$^{-/-}$ MEFs versus 31% of *Msh6*$^{+/+}$ MEFs showed altered mitochondrial membrane potential ($p<0.05$; Fig. 4-4 A). Furthermore, the induction of *Msh6*$^{-/-}$ MEFs with altered mitochondrial membrane potential was significantly reduced compared to *Msh6*$^{+/+}$ MEFs after 250 and 300J/m^2 UVB ($p<0.05$; Fig. 4-4 B). This data shows that UVB-induced, Msh6-dependent apoptosis is occurring through the mitochondria. The reduced number of Msh6-deficient cells undergoing alterations in mitochondrial membrane potential may partially account for the reduced apoptosis levels in MMR-deficient cells compared to MMR-proficient cells that were demonstrated in this work (Fig. 4-3) and previously by others in our laboratory.

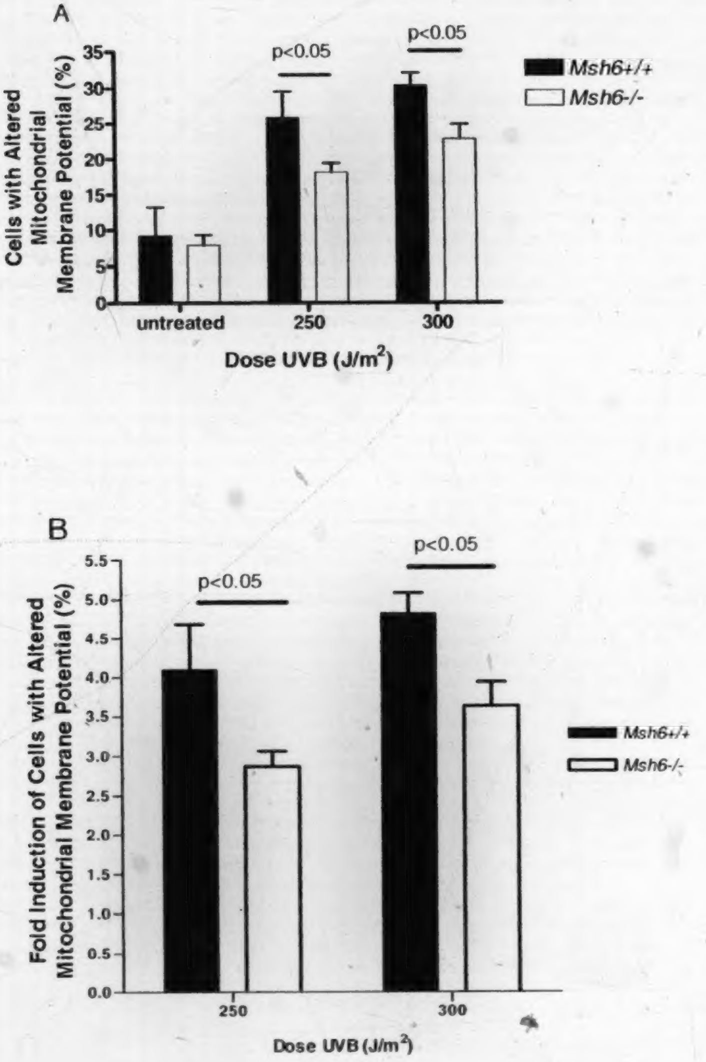

Figure 4-4: Decreased number of *Msh6*$^{-/-}$ MEFs with altered mitochondrial membrane potential 24 hours after treatment with UVB.

A) 24 hours after UVB radiation, there are significantly fewer *Msh6*$^{-/-}$ MEFs with a reduction in mitochondrial membrane potential versus *Msh6*$^{+/+}$ MEFs. The differences in values between *Msh6*$^{+/+}$ and *Msh6*$^{-/-}$ MEFs at both 250 and 300 J/m^2 UVB were significant ($p<0.05$, n=3) and was not significant between untreated *Msh6*$^{+/+}$ and *Msh6*$^{-/-}$ MEFs (n=3).
B) 24 hours after UVB radiation, fold-induction of *Msh6*$^{-/-}$ MEFs is also reduced versus *Msh6*$^{+/+}$ MEFs. The differences in values between *Msh6*$^{+/+}$ and *Msh6*$^{-/-}$ MEFs at 250 and 300 J/m^2 UVB were significant ($p<0.05$, n=3).

Cellular fractionation of *Msh6*$^{+/+}$ and *Msh6*$^{-/-}$ murine embryonic fibroblasts

The activity of apoptotic proteins depends not only upon their levels in the cell, but also upon their localization within the cell. During apoptosis both pro- and anti-apoptotic proteins translocate from the mitochondria to the cytosol and vice versa. *Msh6*$^{+/+}$ and *Msh6*$^{-/-}$ MEFs were fractionated into mitochondrial and cytosolic fractions in order to assess the localization of various apoptotic proteins such as cytochrome c, Bax and Bid in response to UVB. As cytochrome c oxidase/complex IV (COX IV) is only expressed in the mitochondria, the COX IV antibody was used as a control to ensure the integrity of mitochondrial and cytosolic fractions. As seen in Figure 4-5, COX IV protein was present abundantly in the mitochondrial fractions and absent in the cytosolic fractions of both *Msh6*$^{+/+}$ and *Msh6*$^{-/-}$ MEFs, irrespective of treatment, indicating that cytosolic fractions were free of contamination by mitochondrial protein (Fig. 4-5).

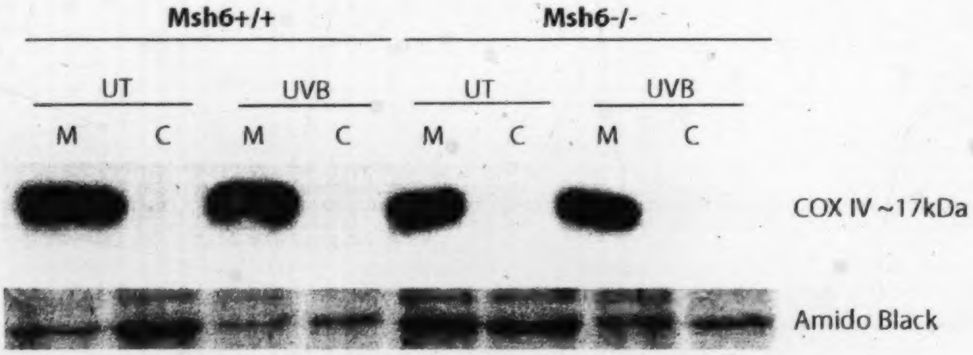

Figure 4-5: Cellular fractionation of *Msh6*$^{+/+}$ and *Msh6*$^{-/-}$ MEFs

Protein extracts from *Msh6*$^{+/+}$ and *Msh6*$^{-/-}$ MEFs irradiated with 300J/m^2 UVB and fractionated into mitochondrial (M) and cytosolic fractions (C) 24 hours post-UVB were analyzed by western blot. Amido black was used as a loading control. COX IV, a mitochondrial protein, was used to show integrity of the fractions.

Bax levels are misregulated in *Msh6*$^{-/-}$ murine embryonic fibroblasts fractions

Bax is a pro-apoptotic member of the Bcl-2 family of proteins. After DNA damage, Bax can have direct or indirect effects on the mitochondria to induce mitochondrial membrane permeability, thus causing the release of mitochondrial proteins. Bax is present in the cytosol of healthy cells. During apoptosis it undergoes a conformational change and translocates to the outer mitochondrial membrane. Western blot analysis shows that there was almost 2-fold more Bax protein in the cytosol of untreated *Msh6*$^{+/+}$ MEFs compared to the mitochondrial levels in untreated *Msh6*$^{+/+}$ MEFs. 24 hours after UVB irradiation there was more than a 2-fold increase in Bax protein levels in the mitochondria of *Msh6*$^{+/+}$ MEFs compared to untreated *Msh6*$^{+/+}$ MEFs and almost no Bax protein in the cytosol of UVB-treated *Msh6*$^{+/+}$ MEFs. In *Msh6*$^{-/-}$ MEFs, there was no appreciable difference in Bax protein levels between untreated mitochondrial and cytosolic fractions. After UVB treatment in *Msh6*$^{-/-}$ MEFs, there was almost 2-fold more Bax protein in the cytosol than in the mitochondria, illustrating a misregulation of Bax translocation after UVB-induced DNA damage in Msh6-deficient MEFs (Fig. 4-6).

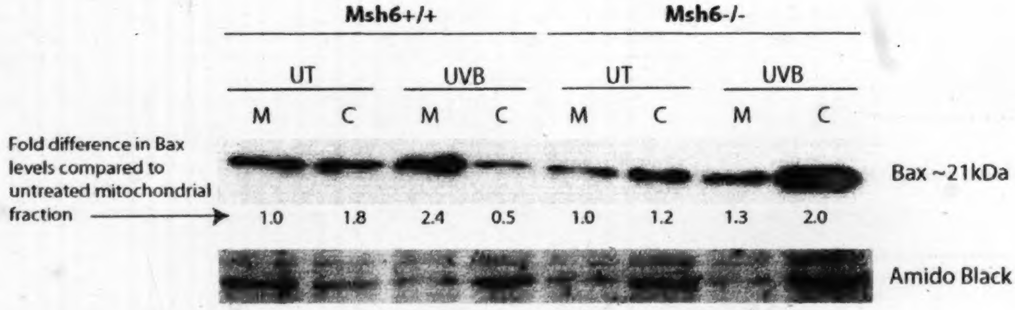

Figure 4-6: Bax levels in *Msh6*$^{+/+}$ and *Msh6*$^{-/-}$ MEF cellular fractions

Protein extracts from *Msh6*$^{+/+}$ and *Msh6*$^{-/-}$ MEFs irradiated with 300J/m^2 UVB and fractionated into mitochondrial (M) and cytosolic fractions (C) 24 hours post-UVB were analyzed by western blot. Amido black was used as a loading control. Densitometry was used to quantify the protein levels which were normalized to the loading control and then to the untreated mitochondria protein level for each corresponding genotype to obtain the fold difference in protein levels.

Full length Bid levels in *Msh6*$^{+/+}$ and *Msh6*$^{-/-}$ murine embryonic fibroblasts fractions

Bid is a pro-apoptotic member of the Bcl-2 family of proteins that is truncated and activated by caspases 8 and 10. Truncated Bid mediates the apoptotic signal to the mitochondria, leading to the release of pro-apoptotic mitochondrial proteins such as cytochrome c and Smac/DIABLO. To test if alterations in Bax above were due to the extrinsic apoptotic stimuli and to test if Bid plays a role in Msh6-dependent apoptosis post-UVB, immunoblot analysis with Bid was undertaken. The antibody used hybridized to full length Bid, but was unsuccessful in hybridizing to the truncated form of Bid. Protein analysis shows that there was much more full length Bid protein in the cytoplasm than in the mitochondria of untreated *Msh6*$^{+/+}$ and *Msh6*$^{-/-}$ MEFs. 24 hours after UVB treatment, Bid protein was upregulated in the cytoplasm with some translocation to the mitochondria, however the majority of signal remained in the cytoplasm of both *Msh6*$^{+/+}$

and *Msh6*$^{-/-}$ MEFs (Fig. 4-7). The levels and localization patterns of full length Bid were similar in *Msh6*$^{+/+}$ and *Msh6*$^{-/-}$ MEFs, indicating that the activity of full length Bid is not dependent on Msh6 and is not involved in Msh6-associated apoptosis.

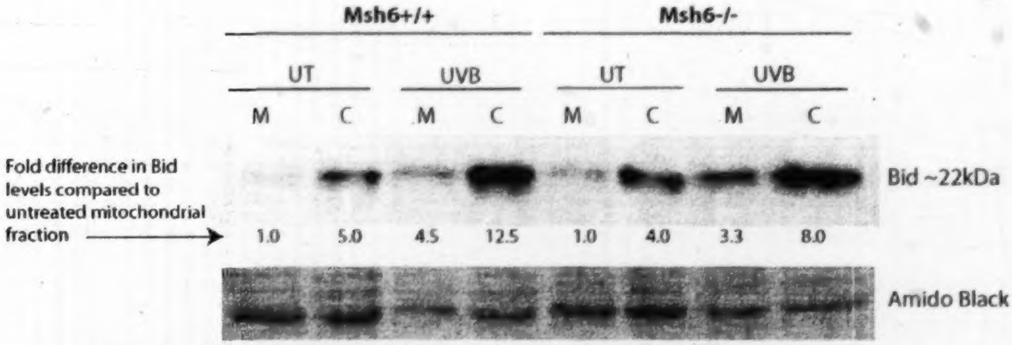

Msh6+/+
Msh6-/-
UT
UVB
UT
UVB
M
C
M
C
M
C
M
C
Fold difference in Bid levels compared to untreated mitochondrial fraction
1.0
5.0
4.5
12.5
1.0
4.0
3.3
8.0
Bid ~22kDa
Amido Black

Figure 4-7: Bid levels in *Msh6*$^{+/+}$ and *Msh6*$^{-/-}$ MEF cellular fractions

Protein extracts from *Msh6*$^{+/+}$ and *Msh6*$^{-/-}$ MEFs irradiated with 300J/m^2 UVB and fractionated into mitochondrial (M) and cytosolic fractions (C) 24 hours post-UVB were analyzed by western blot. Amido black was used as a loading control. Densitometry was used to quantify the protein levels which were normalized to the loading control and then to the untreated mitochondria protein level for each corresponding genotype to obtain the fold difference in protein levels.

Cytochrome c release is misregulated in *Msh6*$^{-/-}$ murine embryonic fibroblasts fractions

Cytochrome c is released from the mitochondria into the cytosol and forms a complex with caspase 9 and Apaf-1, known as the apoptosome. Upon activation of caspase 9, the apoptsome acts as a main driver of apoptosis. Protein analysis shows that there was approximately 2-fold more cytochrome c in the cytosol of untreated *Msh6*$^{+/+}$ and *Msh6*$^{-/-}$ MEFs compared to the mitochondria. 24 hours after UVB irradiation of *Msh6*$^{+/+}$ MEFs, cytochrome c levels increased in the mitochondria and the cytoplasm compared to untreated cells. However, the majority of cytochrome c was in the cytosol than in the mitochondria of *Msh6*$^{+/+}$ MEFs after UVB radiation. In *Msh6*$^{-/-}$ MEFs 24 hours after UVB irradiation, cytochrome c levels increased by 2-fold in the mitochondria and remain unchanged in the cytosol compared to untreated *Msh6*$^{-/-}$ MEFs. There were equal amounts of cytochrome c in the mitochondria as in the cytosol of *Msh6*$^{-/-}$ MEFs 24 hours after treatment with UVB, illustrating a misregulation of cytochrome c release after UVB-induced DNA damage in Msh6-deficient MEFs (Fig. 4-8).

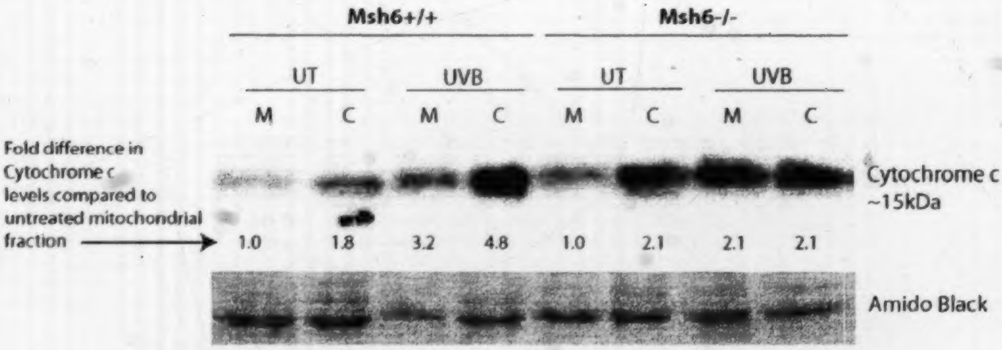
Msh6+/+
Msh6-/-
UT
UVB
UT
UVB
M
C
M
C
M
C
M
C
Fold difference in Cytochrome c levels compared to untreated mitochondrial fraction
1.0
1.8
3.2
4.8
1.0
2.1
2.1
2.1
Cytochrome c ~15kDa
Amido Black

Figure 4-8: Cytochrome c levels in *Msh6*$^{+/+}$ and *Msh6*$^{-/-}$ MEF cellular fractions

Protein extracts from *Msh6*$^{+/+}$ and *Msh6*$^{-/-}$ MEFs irradiated with 300J/m^2 UVB and fractionated into mitochondrial (M) and cytosolic fractions (C) 24 hours post-UVB were analyzed by western blot. Amido black was used as a loading control. Densitometry was used to quantify the protein levels which were normalized to the loading control and then to the untreated mitochondria protein level for each corresponding genotype to obtain the fold difference in protein levels.

Smac/DIABLO has no role in UVB-induced apoptosis in *Msh6*$^{+/+}$ and *Msh6*$^{-/-}$ murine embryonic fibroblasts

Smac/DIABLO is a mitochondrial protein released into the cytoplasm that binds to and neutralizes/inhibits the inhibitors of apoptosis (IAPs), thus contributing to the apoptotic cascade. Protein analysis shows that there were no appreciable differences in Smac/DIABLO protein levels in untreated cells and over time after UVB treatment between *Msh6*$^{+/+}$ and *Msh6*$^{-/-}$ MEFs, suggesting that Smac/DIABLO does not have a role in Msh6-associated apoptosis after UVB-induced DNA damage (Fig. 4-9).

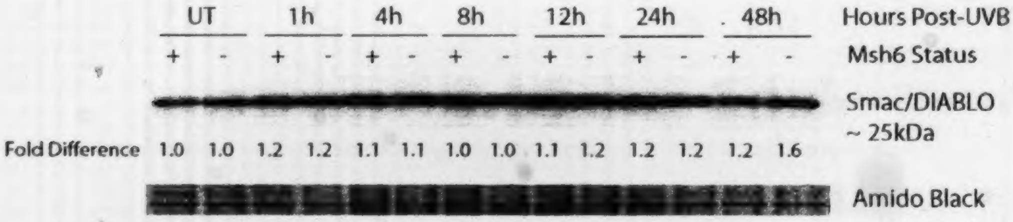

Figure 4-9: Smac/DIABLO protein levels after UVB radiation

Protein extracts from *Msh6*$^{+/+}$ and *Msh6*$^{-/-}$ MEFs irradiated with 300J/m^2 UVB were analyzed by western blot. Amido black was used as a loading control. Densitometry was used to quantify the protein levels which were normalized to the loading control and then to the *Msh6*$^{+/+}$ untreated protein level to obtain the fold difference in protein levels for each lane.

Caspase 9 has a role in UVB-induced apoptosis in *Msh6*$^{+/+}$ and *Msh6*$^{-/-}$ murine embryonic fibroblasts

Caspase 9 is an apical inducer of the intrinsic apoptotic pathway. It forms the apoptosome along with Apaf-1 and cytochrome c and this complex is known as the main driver of apoptosis. Western blot analysis shows that there was no substantial difference in the levels of pro-caspase 9 between untreated *Msh6*$^{+/+}$ and *Msh6*$^{-/-}$ MEFs and over time after 300J/m^2 UVB (Fig. 4-10 A).

The apoptosome catalytically cleaves caspase 9 into active caspase 9, which in turn activates downstream effector caspases 3, 6 and 7. There was no appreciable difference in the levels of cleaved caspase 9 protein between untreated *Msh6*$^{+/+}$ and *Msh6*$^{-/-}$ MEFs. After UVB treatment in *Msh6*$^{+/+}$ MEFs, levels of cleaved caspase 9 protein increased up to 12 hours post-UVB to almost 2-fold greater than control levels. At 24 and 48 hours post-UVB levels of cleaved caspase 9 protein decreased to control levels. In *Msh6*$^{-/-}$ MEFs after UVB treatment, levels of cleaved caspase 9 protein remained stable over time, with no substantial change compared to the control level. Cleaved caspase 9 protein levels were decreased by approximately 2-fold at 4, 8 and 12 hours post-UVB in *Msh6*$^{-/-}$ MEFs compared to *Msh6*$^{+/+}$ MEFs, indicating that cleaved caspase 9 protein has a role in Msh6-dependent apoptosis after UVB radiation (Fig. 4-10 B).

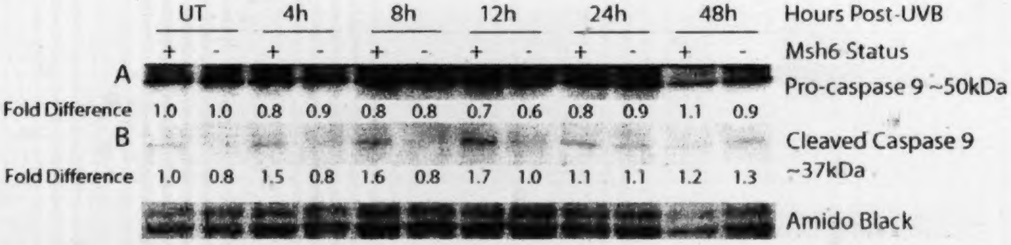
UT
4h
8h
12h
24h
48h
Hours Post-UVB
+ - + - + - + - + - + -
Msh6 Status
A
Pro-caspase 9 ~50kDa
Fold Difference 1.0 1.0 0.8 0.9 0.8 0.8 0.7 0.6 0.8 0.9 1.1 0.9
B
Cleaved Caspase 9 ~37kDa
Fold Difference 1.0 0.8 1.5 0.8 1.6 0.8 1.7 1.0 1.1 1.1 1.2 1.3
Amido Black

Figure 4-10: A) pro-caspase 9 and B) cleaved caspase 9 protein levels after UVB radiation

Protein extracts from *Msh6*$^{+/+}$ and *Msh6*$^{-/-}$ MEFs irradiated with 300J/m^2 UVB were analyzed by western blot. Amido black was used as a loading control. Densitometry was used to quantify the protein levels which were normalized to the loading control and then to the Msh6+/+ untreated protein level to obtain the fold difference in protein levels for each lane.

Cleaved caspase 3 levels in *Msh6*$^{+/+}$ and *Msh6*$^{-/-}$ murine embryonic fibroblasts

Caspase 3 is the quintessential executioner caspase, responsible for the cleavage of many intra-cellular proteins that lead to apoptosis, including PARP. Cleavage of caspase 3 is a hallmark of cell death and was used as a measure of apoptosis on the protein level. **Note: densitometry was performed and the values obtained were normalized to the loading control only.** Western blot analysis shows that there were undetectable levels of cleaved caspase 3 protein in untreated *Msh6*$^{+/+}$ and *Msh6*$^{-/-}$ MEFs and from 1 to 8 hours after UVB in *Msh6*$^{+/+}$ and *Msh6*$^{-/-}$ MEFs. At 12 hours post-UVB, levels of cleaved caspase 3 protein were barely detectable and were equivalent in *Msh6*$^{+/+}$ and *Msh6*$^{-/-}$ MEFs. Levels of cleaved caspase 3 protein peaked at 24 hours post-UVB in both *Msh6*$^{+/+}$ and *Msh6*$^{-/-}$ MEFs and decreased in both at 48 hours post-UVB. Cleaved caspase 3 protein levels were 2-fold lower at 48 hours post-UVB in *Msh6*$^{-/-}$ MEFs compared to *Msh6*$^{+/+}$ MEFs, indicating that cleaved caspase 3 protein levels after UVB radiation are partially dependent on Msh6 (Fig. 4-11).

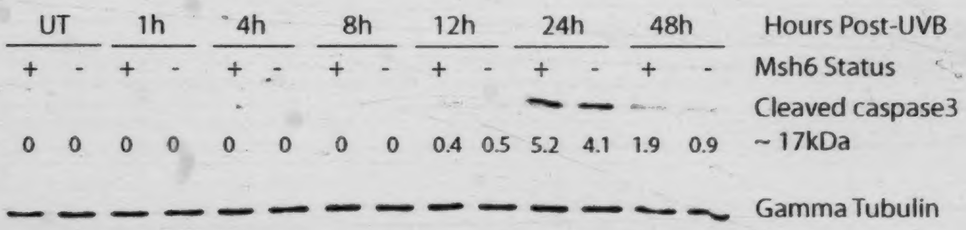

Figure 4-11: Cleaved caspase 3 protein levels after UVB radiation

Protein extracts from *Msh6*$^{+/+}$ and *Msh6*$^{-/-}$ MEFs irradiated with 300J/m^2 UVB were analyzed by western blot. Gamma tubulin was used as a loading control. Densitometry was used to quantify the protein levels which were normalized to the loading control to obtain the protein levels for each lane.

Apoptosis levels after pan-caspase inhibitor in Msh6$^{+/+}$ and *Msh6*$^{-/-}$ murine embryonic fibroblasts

Z-VAD-FMK, a general caspase inhibitor was used to study the effect of inhibition of multiple caspases, including caspases 1, 3, 4 and 7, on levels of apoptosis in *Msh6*$^{+/+}$ and *Msh6*$^{-/-}$ MEFs after UVB treatment in order to determine an appropriate dose for subsequent apoptosis inhibitors (inhibitors of caspases 2, 8 and 9). In Figure 4-12, the relative levels of apoptosis 24 hours after treatment with UVB and Z-VAD-FMK are shown. Apoptosis levels in *Msh6*$^{+/+}$ and *Msh6*$^{-/-}$ MEFs treated with 300J/m^2 UVB alone were set to 100%. Cells treated with UVB and general caspase inhibitor were normalized to their corresponding genotype treated with UVB alone. Figure 4-12 shows that apoptosis in *Msh6*$^{+/+}$ MEFs decreased to an average of approximately 50% and apoptosis in *Msh6*$^{-/-}$ MEFs decreased to an average of 65% after treatment with UVB and Z-VAD-FMK, but the difference was not significant. This illustrates that inhibition of multiple caspases caused reduced levels of apoptosis in both *Msh6*$^{+/+}$ and *Msh6*$^{-/-}$ MEFs after UVB and that a standard dose of 100uM of caspase inhibitor was sufficient to elicit the reduction in apoptosis in these cell lines (Fig. 4-12).

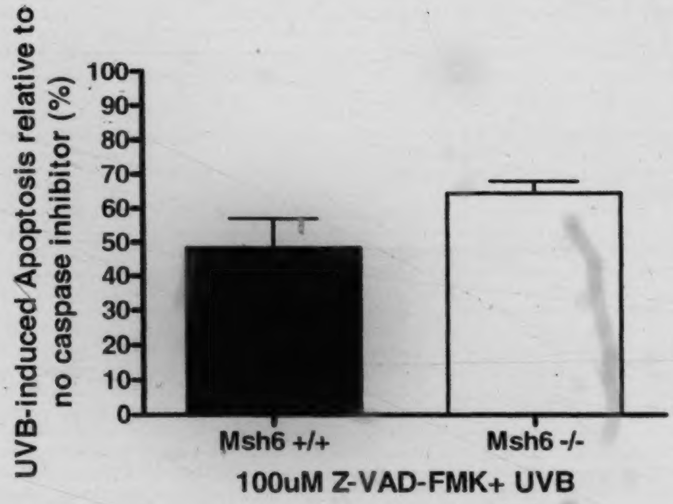

Figure 4-12: Relative decrease in apoptosis levels 24 hours after treatment with Z-VAD-FMK, a general caspase inhibitor

Msh6$^{+/+}$ and *Msh6*$^{-/-}$ MEFs treated with 300J/m^2 UVB alone or in combination with Z-VAD-FMK were analyzed by flow cytometry after Annexin V-PI staining. Apoptosis levels of cells treated with UVB alone are set to 100 and apoptosis levels of cells cells treated with Z-VAD-FMK in combination with UVB are represented as a percentage of this value. The difference between the relative apoptosis of *Msh6*$^{+/+}$ and *Msh6*$^{-/-}$ MEFs was not significant (n=3).

Apoptosis levels after caspase 9 inhibitor in *Msh6*$^{+/+}$ and *Msh6*$^{-/-}$ murine embryonic fibroblasts

In order to confirm the involvement of caspase 9 in Msh6-mediated apoptosis based on the results in figure 4-10, Z-LEHD-FMK, a specific and irreversible inhibitor of caspase 9, was used to study the specific effect of caspase 9 on levels of Msh6-associated apoptosis in *Msh6*$^{+/+}$ and *Msh6*$^{-/-}$ MEFs after UVB treatment. In Figure 4-13, the relative levels of apoptosis 24 hours after treatment with UVB and Z-LEHD-FMK are shown. Apoptosis levels in *Msh6*$^{+/+}$ and *Msh6*$^{-/-}$ MEFs treated with 300J/m^2 UVB alone were set to 100%. Cells treated with UVB and caspase 9 inhibitor were normalized to their corresponding genotype treated with UVB alone. Figure 4-13 shows that apoptosis in *Msh6*$^{+/+}$ MEFs decreased to an average of 70%, while apoptosis in *Msh6*$^{-/-}$ MEFs decreased to an average of just 90% after treatment with UVB and Z-LEHD-FMK ($p<0.05$). This illustrates that inhibition of caspase 9 resulted in significantly less apoptosis in *Msh6*$^{+/+}$ MEFs compared to *Msh6*$^{-/-}$ MEFs after UVB, indicating that *Msh6*-deficient MEFs are less affected by inhibition of caspase 9 after UVB (Fig. 4-13).

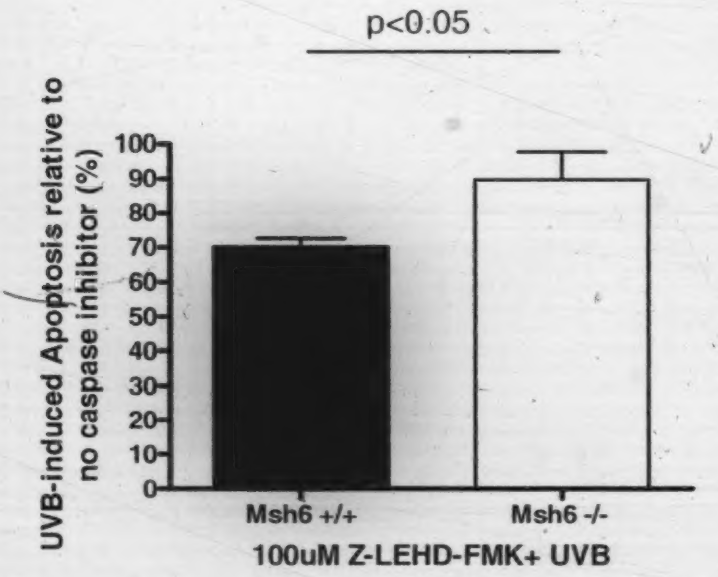

Figure 4-13: Relative decrease in apoptosis levels 24 hours after treatment with Z-LEHD-FMK, a specific inhibitor of caspase 9

Msh6$^{+/+}$ and *Msh6*$^{-/-}$ MEFs treated with 300J/m^2 UVB alone or in combination with Z-LEHD-FMK were analyzed by flow cytometry after Annexin V-PI staining. Apoptosis levels of cells treated with UVB alone are set to 100 and apoptosis levels of cells cells treated with Z-LEHD-FMK in combination with UVB are represented as a percentage of this value. The difference between the relative apoptosis of *Msh6*$^{+/+}$ and *Msh6*$^{-/-}$ MEFs is significant ($p<0.05$, n=3).

Cleaved caspase 3 levels after caspase 9 inhibitor in *Msh6*$^{+/+}$ and *Msh6*$^{-/-}$ murine embryonic fibroblasts

Z-LEHD-FMK, a specific and irreversible inhibitor of caspase 9 was used to study the specific contribution of caspase 9 on Msh6-associated apoptosis in *Msh6*$^{+/+}$ and *Msh6*$^{-/-}$ MEFs after UVB treatment. Cleavage of caspase 3 was used as a measure of cell death on the protein level. In untreated cells there was no cleavage of caspase 3 in either *Msh6*$^{+/+}$ or *Msh6*$^{-/-}$ MEFs. 24 hours after treatment with 300J/m^2 UVB cleaved caspase 3 levels were equal in *Msh6*$^{+/+}$ and *Msh6*$^{-/-}$ MEFs, similar to the findings in figure 4-11 at 24 hours post-UVB. After treatment with UVB and Z-LEHD-FMK, the amount of cleaved caspase 3 protein remained unchanged from UVB control levels in *Msh6*$^{+/+}$ MEFs. In *Msh6*$^{-/-}$ MEFs, after treatment with UVB and Z-LEHD-FMK, the amount of cleaved caspase 3 protein increased by approximately 2-fold compared to UVB control levels (Fig. 4-14). This indicates that inhibition of caspase 9 had a small effect on caspase 3 cleavage in *Msh6*$^{+/+}$ and *Msh6*$^{-/-}$ MEFs after UVB-induced DNA damage.

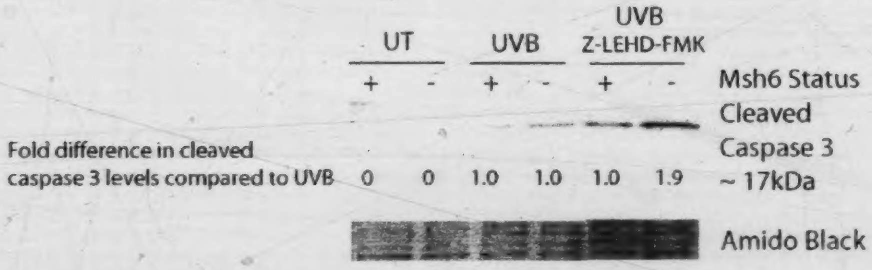
UT
UVB
UVB Z-LEHD-FMK
+ - + - + -
Msh6 Status
Cleaved Caspase 3 ~ 17kDa
Fold difference in cleaved caspase 3 levels compared to UVB
0 0 1.0 1.0 1.0 1.9
Amido Black

Figure 4-14: Cleaved caspase 3 protein levels 24 hours after UVB radiation using Z-LEHD-FMK, a specific inhibitor of caspase 9

Protein extracts from *Msh6*$^{+/+}$ and *Msh6*$^{-/-}$ MEFs treated with 300J/m^2 UVB alone or in combination with Z-LEHD-FMK were analyzed by western blot. Amido black was used as a loading control. Densitometry was used to quantify the protein levels which were normalized to the loading control and then to the UVB control protein level for each corresponding genotype to obtain the fold difference in protein levels for each lane.

Discussion

Published reports by various groups including our own have provided evidence that MMR has a role in the UVB-induced apoptotic response (Peters et al. 2003) (Meira et al. 2002; Yoshino et al. 2002; Young et al. 2003; Young et al. 2004; van Oosten et al. 2005; Gorbunova et al. 2007; Narine et al. 2007). It has been shown that MMR binds to UVB-induced mismatch/photoproduct compound lesions (Mu et al. 1997; Wang et al. 1999), but does not appear to participate in repair of these lesions in mammalian systems [reviewed in (Young et al. 2003)]. Thus, the role for the MMR proteins in the UVB-induced DNA damage response is outside that of repair.

Young et al. (2003) and Peters et al. (2003) showed that *Msh2*$^{-/-}$ and *Msh6*$^{-/-}$ MEFs underwent significantly less apoptosis after UVB radiation compared to their wildtype counterparts (Peters et al. 2003; Young et al. 2003). I hypothesized that Msh6-dependent apoptosis may be occurring through the intrinsic mitochondrial pathway. Specifically, after cellular damage by UVB, Msh6 may play a role in transducing the apoptotic signal through the mitochondria, thus affecting such things as:

1) release of mitochondrial proteins like cytochrome c and Smac/DIABLO,
2) levels of caspase 9 and
3) caspase 3 cleavage.

It is important to identify the proteins involved in MMR-dependent apoptosis in order to determine how loss of MMR contributes to tumorigenesis through reduction in apoptotic response. Little is known as to how DNA damage triggers an apoptotic cascade and which proteins are involved between the DNA damage sensors and the apoptotic proteins. I chose to use *Msh6*$^{-/-}$ MEFs to determine the role of this particular protein in apoptosis.

The p53 tumor suppressor is an important molecule in the response to cellular stress, by mediating cell cycle arrest and apoptosis after DNA damage (Rodier et al. 2007). Reports have shown that a link exists between p53 and MMR in that p53 may act either upstream (Duckett et al. 1999; Hickman and Samson 1999; Lin et al. 2001; Peters et al. 2003) or downstream (Scherer et al. 1996; Scherer et al. 2000; Warnick et al. 2001) of MMR. Levels of total p53 protein and the phosphorylated form of p53 protein, p53-pSer15, were analyzed in untreated and UVB treated *Msh6*$^{+/+}$ and *Msh6*$^{-/-}$ MEFs. Over time after UVB treatment there were no appreciable differences in total p53 or p53-pSer15 protein between *Msh6*$^{+/+}$ and *Msh6*$^{-/-}$ MEFs. This indicates that Msh6 is not upstream of p53 in the DNA damage response pathway after UVB (Fig. 4-2).

Although this finding shows no Msh6-dependent changes in p53 protein levels after UVB, studies have shown a relationship between the MMR pathway and the p53 pathway. Experiments *in vivo* have shown that loss of Msh2 in combination with loss of p53 exacerbates the onset of tumorigenesis in mouse (Cranston et al. 1997; Cranston and Fishel 1999; Scherer et al. 2000; Toft et al. 2002). To determine if the Msh6- and p53-DNA damage response pathways are interconnected, apoptosis levels of several different genotypes of MEFs were analyzed. *Msh6*$^{-/-}$*;p53*$^{-/-}$ MEFs displayed significant decreases in apoptosis, greater than those observed in *Msh6*$^{-/-}$ or *p53*$^{-/-}$ MEFs alone. This indicates that the Msh6 and p53 UVB-induced DNA damage response pathways are unique and non-overlapping (Fig. 4-3). Thus, this data in combination with data from Fig. 4-2 shows that p53 does not have a role in Msh6-dependent apoptosis after UVB radiation.

I hypothesized that if Msh6 is acting as a sensor for DNA damage, it would be acting via the intrinsic apoptotic pathway, through the reduction of mitochondrial membrane potential. Reduction in mitochondrial membrane potential is associated with mitochondrial outer membrane permeability (MOMP). There is controversy in the literature concerning the order in which these events occur. However, most of the reports indicate that MOMP occurs before mitochondrial membrane depolarization. Nevertheless, these events are the 2 integral steps in mitochondrial apoptosis and are the defining characteristics of this apoptotic pathway [(Bossy-Wetzel et al. 1998; Goldstein et al. 2005; Zhou et al. 2005); reviewed in (Jin and El-Deiry 2005; Zoratti et al. 2005; Gogvadze et al. 2006)]. I wanted to determine if Msh6-dependent apoptosis occurs through the mitochondria. Figure 4-4 shows that, 24 hours after treatment with UVB (either 250 or 300J/m^2), there is a significant reduction in the number of *Msh6*$^{-/-}$ MEFs with reduced mitochondrial membrane potential compared to *Msh6*$^{+/+}$ MEFs (Fig. 4-4 A). Also, the induction of *Msh6*$^{-/-}$ MEFs with altered mitochondrial membrane potential was significantly reduced compared to *Msh6*$^{+/+}$ MEFs (Fig. 4-4 B).

Bax and Bak mediate permeabilization of the outer mitochondrial membrane by undergoing conformational changes mediated by BH3-only proteins that lead to Bax and Bak oligomerization in the outer mitochondrial membrane (Li et al. 1998; Gross et al. 1999; Antonsson et al. 2000; Desagher and Martinou 2000; Ruffolo et al. 2000; Wei et al.

2000; Martinou and Green 2001; Wei et al. 2001; Kuwana et al. 2002). This leads to mitochondrial membrane permeability, release of proteins from the intermembrane space, such as cytochrome c and Smac/DIABLO, and subsequent reduction in the mitochondrial membrane potential. These events have been shown to occur after UV irradiation (Bossy-Wetzel et al. 1998; Takasawa and Tanuma 2003; Van Laethem et al. 2004; Takasawa et al. 2005; Zhou et al. 2005). Lack of Msh6 attenuates the depolarization of the mitochondrial membrane, which corresponds to the reduction in apoptosis seen in MMR-deficient cells seen previously in our lab. From this, it can be seen that Msh6-dependent apoptosis after UVB-induced DNA damage is occurring through the mitochondria.

The apoptotic event depends upon the action of many cellular proteins. Further to the levels of these proteins being vital to apoptosis, their cellular localization is also an integral aspect of the regulation of apoptosis. As such, I wanted to study both the levels and localization of apoptotic proteins such as cytochrome c, Bax and Bid after UVB radiation in *Msh6*$^{+/+}$ and *Msh6*$^{-/-}$ MEFs fractionated into mitochondrial and cytosolic cellular fractions. Such analysis can aid in identifying how Msh6 is activating apoptosis post-UVB exposure. Van Laethem et al. (2005) showed that UVB irradiation of human skin led to the formation of sunburn cells (apoptotic keratinocytes) and that this phenomenon was associated with a rapid re-distribution of Bax from the cytosol to the mitochondria (Van Laethem et al. 2004), Bivik et al. (2006) had similar findings in human melanocytes (Bivik et al. 2006), indicating that Bax translocation from the cytosol to the mitochondria is induced by UVB. My results show that, 24 hours after UVB treatment Bax levels decrease greatly in the cytosol and increase greatly in the mitochondria of *Msh6*$^{+/+}$ MEFs compared to untreated cells. Conversely, in *Msh6*$^{-/-}$ MEFs 24 hours after treatment with UVB Bax levels increase greatly in the cytosol and remain stable in the mitochondria compared to untreated cells. Thus, Bax translocation may be regulated by Msh6 and is important in Msh6-dependent apoptosis after UVB radiation (Fig. 4-6). A proportion of human tumors with defective MMR are characterized by mutations in a microsatellite in the coding region of *Bax*, resulting in inactivation of the *Bax* gene (Rampino et al. 1997; Percesepe et al. 1998). This inactivation of *Bax* is thought to contribute to tumorigenesis through disruption of apoptosis (de la Chapelle 2003). In contrast, I observed a Bax misregulation in *Msh6*$^{-/-}$ MEFs compared to *Msh6*$^{+/+}$ MEFs following UVB irradiation. Spontaneous tumors from *Msh6*$^{-/-}$ mice do not display MSI. Furthermore, our *in vivo* studies of UVB-induced tumorigenesis in *Msh2*$^{-/-}$ and *Msh6*$^{-/-}$ mice do not support the idea that MSI contributes to UVB-induced, MMR-dependent apoptosis (Young et al. 2004). The misregulation of Bax in *Msh6*$^{-/-}$ MEFs provides support for the idea that *Bax* inactivation in humans contributes to misregulated apoptosis and contributes to tumorigenesis.

Bid is a pro-apoptotic protein that links the mitochondrial/intrinsic and the death receptor/extrinsic pathways of apoptosis. Bid is truncated (tBid) and activated by caspase 8/10 after death ligands bind (for example TNFα, FasL) bind to their death receptors (for example TNFR1, Fas) and caspase 8 is subsequently activated (see Chapter 6). tBid translocates to the mitochondria and induces release of cytochrome c (Li et al. 1998; Luo et al. 1998; Gross et al. 1999). It has been shown that full length Bid interacts with Bax and directly regulates its activation during TNFα–induced apoptosis (Pei et al. 2007). I examined the levels of full length Bid in Msh6-proficient and –deficient MEFs and found that the levels and localization patterns of this protein were similar in *Msh6*$^{+/+}$ and *Msh6*$^{-/-}$ MEF fractions. This shows that full length Bid does not have a role in Msh6-dependent apoptosis after UVB-induced DNA damage, in keeping with my hypothesis that Msh6-dependent apoptosis is being initiated by nuclear effects of UVB and activation of the intrinsic apoptotic pathway (Fig. 4-7). I was unable to assess tBid due to limitation of reagents available at the time.

As discussed above, Bax and Bid have a direct role in MOMP, allowing release of mitochondrial proteins like cytochrome c. Cytochrome c is released from the mitochondria after UVB radiation (Bossy-Wetzel et al. 1998; Adrain et al. 2001; Takasawa and Tanuma 2003; Van Laethem et al. 2004; Takasawa et al. 2005; Zhou et al. 2005; Bivik et al. 2006), as well as after treatment with other agents like staurosporine and etoposide (Kluck et al. 1997; Yang et al. 1997). I found that untreated *Msh6*$^{+/+}$ and *Msh6*$^{-/-}$ MEFs had similar levels of cytochrome c in the cytosol and the mitochondria (Fig. 4-8). It is somewhat surprising to see cytochrome c in the mitochondria of healthy, unperturbed cells. This may have resulted from the untreated MEFs being too confluent, with low levels of cytochrome c in the mitochondria induced by cellular stress, despite attempts to reduce this. Over-homogenization of cells can result in disruption of the mitochondrial membranes, causing leakage of mitochondrial proteins into the cytosol. However, this is unlikely to have resulted in the untreated MEFs during cellular fractionation because the control western blot showed cytosolic fractions free from contamination from the mitochondrial marker COX IV (Fig. 4-5).

24 hours after treatment with UVB, there is a 2.5-fold increase in the amount of cytochrome c in the cytosol of *Msh6*$^{+/+}$ MEFs compared to untreated *Msh6*$^{+/+}$ MEFs and there is also a 3-fold increase in the amount of cytochrome c in the mitochondria after UVB treatment. In *Msh6*$^{-/-}$ MEFs, there is no increase in the amount of cytochrome c in the cytosol of UVB-treated cells compared to untreated cells, and only a 2-fold increase in the amount of cytochrome c in the mitochondria after UVB treatment (Fig. 4-8). This demonstrates that the release of cytochrome c is important in Msh6-dependent apoptosis after UVB, consistent with alterations in mitochondrial outer membrane permeabilization.

Like cytochrome c, Smac/DIABLO is also released from the mitochondrial intermembrane space during MOMP. Smac/DIABLO functions to neutralize the inhibition of caspases by IAPs (Roy et al. 1997; Deveraux et al. 1998; Du et al. 2000; Verhagen et al. 2000). It is controversial whether Smac/DIABLO is released from the mitochondria at the same time as cytochrome c, or after. Western blot analysis of whole cell protein extracts showed that there were no Msh6-dependent changes in Smac/DIABLO protein levels post-UVB, suggesting that Smac/DIABLO does not have a role in Msh6-associated apoptosis after UVB-induced DNA damage (Fig. 4-9). However, further study in to the levels and translocation of Smac/DIABLO protein after UVB radiation in cytosolic and mitochondrial fractions may be more informative.

Caspase 9 forms the apoptosome along with Apaf-1 and cytochrome c and this complex is known as the main driver of apoptosis. After cleavage and activation by the apoptosome, activated caspase 9 cleaves downstream executioner caspases 3 and 7.

Hakem et al. (1998) demonstrated that the role of caspase 9 in UV-induced apoptosis is cell type-dependent. Thymocytes and splenocytes that are deficient in caspase 9 still undergo caspase cleavage and apoptosis after UV treatment, however, UV-induced apoptosis in embryonic stem cells and fibroblasts is dependent on caspase 9 (Hakem et al. 1998). In Figure 4-10 it can be seen that cleaved caspase 9 levels are regulated in a Msh6-dependent manner. This result is in keeping with reduced levels of cytochrome c seen in *Msh6*-null cells. Thus, caspase 9 is important in Msh6-dependent apoptosis after UVB-induced DNA damage.

Cleavage of caspase 3 is a hallmark of cell death and was used as a measure of apoptosis on the protein level. Cleaved caspase 3 protein was only detected at 24 and 48 hours post-UVB and only at 48 hours after treatment was there a substantial difference in the levels of this protein. There was a 2-fold decrease in cleaved caspase 3 protein in *Msh6*$^{-/-}$ MEFs compared to *Msh6*$^{+/+}$ MEFs at 48 hours post-UVB, indicating that caspase 3 plays a role in Msh6-dependent apoptosis after UVB-induced DNA damage (Fig. 4-11).

The general caspase inhibitor Z-VAD-FMK, which is known to be protective of apoptosis by inhibition of caspases 1, 3, 4 and 7, was used to determine the dosage and apoptotic response to caspase inhibition on *Msh6*$^{+/+}$ and *Msh6*$^{-/-}$ MEFs. Peptide caspase inhibitors bind to the active site(s) on the targeted caspase, thus competitively inhibiting the binding of downstream targets of the inhibited caspase. The dose of 100uM was effective in eliciting a decrease in apoptosis 24 hours after UVB radiation and was used as the standard dose for all subsequent caspase inhibitors. Levels of apoptosis decreased to approximately 50% on average in *Msh6*$^{+/+}$ MEFs and to approximately 65% on average in *Msh6*$^{-/-}$ MEFs, demonstrating that these cells were susceptible to inhibition of multiple caspases via use of Z-VAD-FMK after UVB radiation (Fig. 4-12). There was no significant difference in UVB-induced apoptosis between *Msh6*$^{+/+}$ and *Msh6*$^{-/-}$ MEFs after caspase inhibition by Z-VAD-FMK. *Msh6*$^{-/-}$ MEFs still undergo apoptosis after UVB-induced DNA damage [Fig. 4-3; (Young et al. 2003)] and the inhibition of multiple caspases, including two effector caspases 3 and 7 is sufficient to impede apoptosis after UVB irradiation in these cells. Caspase 3 is known to cleave PARP, however, studies have shown that caspases 3 and 7 are not vital to integral apoptosis-related events such as apoptotic morphology, cell detachment, or proteolytic degradation of PARP, lamin B, Rb, DNA PK_{CS} and others. Caspase 6 may perform a redundant function to that of caspases 3 and 7 in *Msh6*$^{+/+}$ and *Msh6*$^{-/-}$ MEFs (Janicke et al. 1998; Del Bello et al. 2004).

The role of caspase 9 in Msh6-dependent apoptosis was also explored through assays for global apoptosis levels and cleavage of caspase 3 after treatment of cells with UVB and Z-LEHD-FMK, a specific and irreversible inhibitor of caspase 9. As seen in figure 4-13, apoptosis in *Msh6*$^{+/+}$ MEFs decreased to an average of 70%, while apoptosis in *Msh6*$^{-/-}$ MEFs decreased to an average of just 90% after treatment with UVB and Z-LEHD-FMK ($p<0.05$). This demonstrates that inhibition of caspase 9 resulted in significantly less apoptosis in *Msh6*$^{+/+}$ MEFs compared to *Msh6*$^{-/-}$ MEFs after UVB, re-iterating the findings in Fig. 4-10, that caspase 9 plays a role in Msh6-dependent apoptosis after UVB-induced DNA damage.

Further to the above assay on global levels of apoptosis after inhibition of caspase 9, I used the irreversible inhibitor of caspase 9, Z-LEHD-FMK, in order to assess the contribution of caspase 9 on cell death via cleavage of caspase 3 in *Msh6*$^{+/+}$ and *Msh6*$^{-/-}$ MEFs after UVB treatment (Fig. 4-14). 24 hours after treatment with UVB and Z-LEHD-FMK there was a 2-fold increase in cleaved caspase 3 in *Msh6*$^{-/-}$ MEFs compared to M*sh6*$^{+/+}$ MEFs, corroborating the results in figure 4-13 showing increased apoptosis in *Msh6*$^{-/-}$ MEFs compared to M*sh6*$^{+/+}$ MEFs after UVB and Z-LEHD-FMK treatment. This is additional evidence that caspase 9 has a role in Msh6-dependent apoptosis after UVB-induced apoptosis.

Overall, it seems that the mitochondrial pathway of apoptosis is harnessed in a Msh6-associated manner after UVB-induced DNA damage. This is evidenced by the Msh6-dependent differences in mitochondrial membrane potential, the misregulated translocation of cytochrome c in Msh6-deficient cells, the decreased levels of cleaved caspase 9 in Msh6-deficient cells, the diminished global apoptotic response after inhibition of caspase 9 in Msh6-proficient cells and the misregulation of the integral mitochondrial apoptotic protein Bax.

References

Adrain, C., E. M. Creagh and S. J. Martin (2001). "Apoptosis-associated release of Smac/DIABLO from mitochondria requires active caspases and is blocked by Bcl-2." Embo J **20**(23): 6627-36.

Antonsson, B., S. Montessuit, S. Lauper, R. Eskes and J. C. Martinou (2000). "Bax oligomerization is required for channel-forming activity in liposomes and to trigger cytochrome c release from mitochondria." Biochem J **345 Pt 2**: 271-8.

Bivik, C. A., P. K. Larsson, K. M. Kagedal, I. K. Rosdahl and K. M. Ollinger (2006). "UVA/B-induced apoptosis in human melanocytes involves translocation of cathepsins and Bcl-2 family members." J Invest Dermatol **126**(5): 1119-27.

Bossy-Wetzel, E., D. D. Newmeyer and D. R. Green (1998). "Mitochondrial cytochrome c release in apoptosis occurs upstream of DEVD-specific caspase activation and independently of mitochondrial transmembrane depolarization." Embo J **17**(1): 37-49.

Cranston, A., T. Bocker, A. Reitmair, J. Palazzo, T. Wilson, T. Mak and R. Fishel (1997). "Female embryonic lethality in mice nullizygous for both Msh2 and p53." Nat Genet **17**(1): 114-8.

Cranston, A. and R. Fishel (1999). "Female embryonic lethality in Msh2-Trp53 nullizygous mice is strain dependent." Mamm Genome **10**(10): 1020-2.

Danial, N. N. and S. J. Korsmeyer (2004). "Cell death: critical control points." Cell **116**(2): 205-19.

de la Chapelle, A. (2003). "Microsatellite instability." N Engl J Med **349**(3): 209-10.

Del Bello, B., M. A. Valentini, P. Mangiavacchi, M. Comporti and E. Maellaro (2004). "Role of caspases-3 and -7 in Apaf-1 proteolytic cleavage and degradation events during cisplatin-induced apoptosis in melanoma cells." Exp Cell Res **293**(2): 302-10.

Denning, M. F., Y. Wang, S. Tibudan, S. Alkan, B. J. Nickoloff and J. Z. Qin (2002). "Caspase activation and disruption of mitochondrial membrane potential during UV radiation-induced apoptosis of human keratinocytes requires activation of protein kinase C." Cell Death Differ **9**(1): 40-52.

Desagher, S. and J. C. Martinou (2000). "Mitochondria as the central control point of apoptosis." Trends Cell Biol **10**(9): 369-77.

Deveraux, Q. L., N. Roy, H. R. Stennicke, T. Van Arsdale, Q. Zhou, S. M. Srinivasula, E. S. Alnemri, G. S. Salvesen and J. C. Reed (1998). "IAPs block apoptotic events induced by caspase-8 and cytochrome c by direct inhibition of distinct caspases." Embo J **17**(8): 2215-23.

Du, C., M. Fang, Y. Li, L. Li and X. Wang (2000). "Smac, a mitochondrial protein that promotes cytochrome c-dependent caspase activation by eliminating IAP inhibition." Cell **102**(1): 33-42.

Duckett, D. R., S. M. Bronstein, Y. Taya and P. Modrich (1999). "hMutSalpha- and hMutLalpha-dependent phosphorylation of p53 in response to DNA methylator damage." Proc Natl Acad Sci U S A **96**(22): 12384-8.

Gogvadze, V., S. Orrenius and B. Zhivotovsky (2006). "Multiple pathways of cytochrome c release from mitochondria in apoptosis." Biochim Biophys Acta **1757**(5-6): 639-47.

Goldstein, J. C., C. Munoz-Pinedo, J. E. Ricci, S. R. Adams, A. Kelekar, M. Schuler, R. Y. Tsien and D. R. Green (2005). "Cytochrome c is released in a single step during apoptosis." Cell Death Differ **12**(5): 453-62.

Gorbunova, V., A. Seluanov, Z. Mao and C. Hine (2007). "Changes in DNA repair during aging." Nucleic Acids Res.

Gross, A., X. M. Yin, K. Wang, M. C. Wei, J. Jockel, C. Milliman, H. Erdjument-Bromage, P. Tempst and S. J. Korsmeyer (1999). "Caspase cleaved BID targets mitochondria and is required for cytochrome c release, while BCL-XL prevents this release but not tumor necrosis factor-R1/Fas death." J Biol Chem **274**(2): 1156-63.

Hakem, R., A. Hakem, G. S. Duncan, J. T. Henderson, M. Woo, M. S. Soengas, A. Elia, J. L. de la Pompa, D. Kagi, W. Khoo, J. Potter, R. Yoshida, S. A. Kaufman, S. W. Lowe, J. M. Penninger and T. W. Mak (1998). "Differential requirement for caspase 9 in apoptotic pathways in vivo." Cell **94**(3): 339-52.

Hegde, R., S. M. Srinivasula, P. Datta, M. Madesh, R. Wassell, Z. Zhang, N. Cheong, J. Nejmeh, T. Fernandes-Alnemri, S. Hoshino and E. S. Alnemri (2003). "The polypeptide chain-releasing factor GSPT1/eRF3 is proteolytically processed into an IAP-binding protein." J Biol Chem **278**(40): 38699-706.

Hickman, M. J. and L. D. Samson (1999). "Role of DNA mismatch repair and p53 in signaling induction of apoptosis by alkylating agents." Proc Natl Acad Sci U S A **96**(19): 10764-9.

Iyer, R. R., A. Pluciennik, V. Burdett and P. L. Modrich (2006). "DNA mismatch repair: functions and mechanisms." Chem Rev **106**(2): 302-23.

Janicke, R. U., P. Ng, M. L. Sprengart and A. G. Porter (1998). "Caspase-3 is required for alpha-fodrin cleavage but dispensable for cleavage of other death substrates in apoptosis." J Biol Chem **273**(25): 15540-5.

Jin, Z. and W. S. El-Deiry (2005). "Overview of cell death signaling pathways." Cancer Biol Ther **4**(2): 139-63.

Kluck, R. M., E. Bossy-Wetzel, D. R. Green and D. D. Newmeyer (1997). "The release of cytochrome c from mitochondria: a primary site for Bcl-2 regulation of apoptosis." Science **275**(5303): 1132-6.

Kock, A., T. Schwarz, R. Kirnbauer, A. Urbanski, P. Perry, J. C. Ansel and T. A. Luger (1990). "Human keratinocytes are a source for tumor necrosis factor alpha: evidence for synthesis and release upon stimulation with endotoxin or ultraviolet light." J Exp Med **172**(6): 1609-14.

Kuwana, T., M. R. Mackey, G. Perkins, M. H. Ellisman, M. Latterich, R. Schneiter, D. R. Green and D. D. Newmeyer (2002). "Bid, Bax, and lipids cooperate to form supramolecular openings in the outer mitochondrial membrane." Cell **111**(3): 331-42.

Leverkus, M., M. Yaar and B. A. Gilchrest (1997). "Fas/Fas ligand interaction contributes to UV-induced apoptosis in human keratinocytes." Exp Cell Res **232**(2): 255-62.

Li, H., H. Zhu, C. J. Xu and J. Yuan (1998). "Cleavage of BID by caspase 8 mediates the mitochondrial damage in the Fas pathway of apoptosis." Cell **94**(4): 491-501.

Lin, X., K. Ramamurthi, M. Mishima, A. Kondo, R. D. Christen and S. B. Howell (2001). "P53 modulates the effect of loss of DNA mismatch repair on the sensitivity of human colon cancer cells to the cytotoxic and mutagenic effects of cisplatin." Cancer Res **61**(4): 1508-16.

Luo, X., I. Budihardjo, H. Zou, C. Slaughter and X. Wang (1998). "Bid, a Bcl2 interacting protein, mediates cytochrome c release from mitochondria in response to activation of cell surface death receptors." Cell **94**(4): 481-90.

Martinou, J. C. and D. R. Green (2001). "Breaking the mitochondrial barrier." Nat Rev Mol Cell Biol **2**(1): 63-7.

Meira, L. B., D. L. Cheo, A. M. Reis, N. Claij, D. K. Burns, H. te Riele and E. C. Friedberg (2002). "Mice defective in the mismatch repair gene Msh2 show increased predisposition to UVB radiation-induced skin cancer." DNA Repair (Amst) **1**(11): 929-34.

Mu, D., M. Tursun, D. R. Duckett, J. T. Drummond, P. Modrich and A. Sancar (1997). "Recognition and repair of compound DNA lesions (base damage and mismatch) by human mismatch repair and excision repair systems." Mol Cell Biol **17**(2): 760-9.

Narine, K. A., K. E. Felton, A. A. Parker, V. A. Tron and S. E. Andrew (2007). "Non-tumor cells from an MSH2-null individual show altered cell cycle effects post-UVB." Oncol Rep **18**(6): 1403-11.

Pei, Y., D. Xing, X. Gao, L. Liu and T. Chen (2007). "Real-time monitoring full length bid interacting with Bax during TNF-alpha-induced apoptosis." Apoptosis **12**(9): 1681-90.

Percesepe, A., P. Kristo, L. A. Aaltonen, M. Ponz de Leon, A. de la Chapelle and P. Peltomaki (1998). "Mismatch repair genes and mononucleotide tracts as mutation targets in colorectal tumors with different degrees of microsatellite instability." Oncogene **17**(2): 157-63.

Peters, A. C., L. C. Young, T. Maeda, V. A. Tron and S. E. Andrew (2003). "Mammalian DNA mismatch repair protects cells from UVB-induced DNA damage by facilitating apoptosis and p53 activation." DNA Repair (Amst) **2**(4): 427-35.

Rampino, N., H. Yamamoto, Y. Ionov, Y. Li, H. Sawai, J. C. Reed and M. Perucho (1997). "Somatic frameshift mutations in the BAX gene in colon cancers of the microsatellite mutator phenotype." Science **275**(5302): 967-9.

Rodier, F., J. Campisi and D. Bhaumik (2007). "Two faces of p53: aging and tumor suppression." Nucleic Acids Res **35**(22): 7475-84.

Roy, N., Q. L. Deveraux, R. Takahashi, G. S. Salvesen and J. C. Reed (1997). "The c-IAP-1 and c-IAP-2 proteins are direct inhibitors of specific caspases." Embo J **16**(23): 6914-25.

Ruffolo, S. C., D. G. Breckenridge, M. Nguyen, I. S. Goping, A. Gross, S. J. Korsmeyer, H. Li, J. Yuan and G. C. Shore (2000). "BID-dependent and BID-independent pathways for BAX insertion into mitochondria." Cell Death Differ **7**(11): 1101-8.

Scherer, S. J., S. M. Maier, M. Seifert, R. G. Hanselmann, K. D. Zang, H. K. Muller-Hermelink, P. Angel, C. Welter and M. Schartl (2000). "p53 and c-Jun functionally synergize in the regulation of the DNA repair gene hMSH2 in response to UV." J Biol Chem **275**(48): 37469-73.

Scherer, S. J., C. Welter, K. D. Zang and S. Dooley (1996). "Specific in vitro binding of p53 to the promoter region of the human mismatch repair gene hMSH2." Biochem Biophys Res Commun **221**(3): 722-8.

Sitailo, L. A., S. S. Tibudan and M. F. Denning (2002). "Activation of caspase-9 is required for UV-induced apoptosis of human keratinocytes." J Biol Chem **277**(22): 19346-52.

Spierings, D., G. McStay, M. Saleh, C. Bender, J. Chipuk, U. Maurer and D. R. Green (2005). "Connected to death: the (unexpurgated) mitochondrial pathway of apoptosis." Science **310**(5745): 66-7.

Suzuki, Y., Y. Imai, H. Nakayama, K. Takahashi, K. Takio and R. Takahashi (2001). "A serine protease, HtrA2, is released from the mitochondria and interacts with XIAP, inducing cell death." Mol Cell **8**(3): 613-21.

Takasawa, R., H. Nakamura, T. Mori and S. Tanuma (2005). "Differential apoptotic pathways in human keratinocyte HaCaT cells exposed to UVB and UVC." Apoptosis **10**(5): 1121-30.

Takasawa, R. and S. Tanuma (2003). "Sustained release of Smac/DIABLO from mitochondria commits to undergo UVB-induced apoptosis." Apoptosis **8**(3): 291-9.

Toft, N. J., L. J. Curtis, O. J. Sansom, A. L. Leitch, A. H. Wyllie, H. te Riele, M. J. Arends and A. R. Clarke (2002). "Heterozygosity for p53 promotes microsatellite instability and tumorigenesis on a Msh2 deficient background." Oncogene **21**(41): 6299-306.

Van Laethem, A., S. Van Kelst, S. Lippens, W. Declercq, P. Vandenabeele, S. Janssens, J. R. Vandenheede, M. Garmyn and P. Agostinis (2004). "Activation of p38 MAPK is required for Bax translocation to mitochondria, cytochrome c release and apoptosis induced by UVB irradiation in human keratinocytes." Faseb J **18**(15): 1946-8.

van Oosten, M., G. J. Stout, C. Backendorf, H. Rebel, N. de Wind, F. Darroudi, H. J. van Kranen, F. R. de Gruijl and L. H. Mullenders (2005). "Mismatch repair protein Msh2 contributes to UVB-induced cell cycle arrest in epidermal and cultured mouse keratinocytes." DNA Repair (Amst) **4**(1): 81-9.

Verhagen, A. M., P. G. Ekert, M. Pakusch, J. Silke, L. M. Connolly, G. E. Reid, R. L. Moritz, R. J. Simpson and D. L. Vaux (2000). "Identification of DIABLO, a mammalian protein that promotes apoptosis by binding to and antagonizing IAP proteins." Cell **102**(1): 43-53.

Wang, H., C. W. Lawrence, G. M. Li and J. B. Hays (1999). "Specific binding of human MSH2.MSH6 mismatch-repair protein heterodimers to DNA incorporating thymine- or uracil-containing UV light photoproducts opposite mismatched bases." J Biol Chem **274**(24): 16894-900.

Warnick, C. T., B. Dabbas, C. D. Ford and K. A. Strait (2001). "Identification of a p53 response element in the promoter region of the hMSH2 gene required for expression in A2780 ovarian cancer cells." J Biol Chem **276**(29): 27363-70.

Wei, M. C., T. Lindsten, V. K. Mootha, S. Weiler, A. Gross, M. Ashiya, C. B. Thompson and S. J. Korsmeyer (2000). "tBID, a membrane-targeted death ligand, oligomerizes BAK to release cytochrome c." Genes Dev **14**(16): 2060-71.

Wei, M. C., W. X. Zong, E. H. Cheng, T. Lindsten, V. Panoutsakopoulou, A. J. Ross, K. A. Roth, G. R. MacGregor, C. B. Thompson and S. J. Korsmeyer (2001).

"Proapoptotic BAX and BAK: a requisite gateway to mitochondrial dysfunction and death." Science **292**(5517): 727-30.

Yang, J., X. Liu, K. Bhalla, C. N. Kim, A. M. Ibrado, J. Cai, T. I. Peng, D. P. Jones and X. Wang (1997). "Prevention of apoptosis by Bcl-2: release of cytochrome c from mitochondria blocked." Science **275**(5303): 1129-32.

Yoshino, M., Y. Nakatsu, H. te Riele, S. Hirota, Y. Kitamura and K. Tanaka (2002). "Additive roles of XPA and MSH2 genes in UVB-induced skin tumorigenesis in mice." DNA Repair (Amst) **1**(11): 935-40.

Young, L. C., J. B. Hays, V. A. Tron and S. E. Andrew (2003). "DNA mismatch repair proteins: potential guardians against genomic instability and tumorigenesis induced by ultraviolet photoproducts." J Invest Dermatol **121**(3): 435-40.

Young, L. C., A. C. Peters, T. Maeda, W. Edelmann, R. Kucherlapati, S. E. Andrew and V. A. Tron (2003). "DNA mismatch repair protein Msh6 is required for optimal levels of ultraviolet-B-induced apoptosis in primary mouse fibroblasts." J Invest Dermatol **121**(4): 876-80.

Young, L. C., K. J. Thulien, M. R. Campbell, V. A. Tron and S. E. Andrew (2004). "DNA mismatch repair proteins promote apoptosis and suppress tumorigenesis in response to UVB irradiation: an in vivo study." Carcinogenesis **25**(10): 1821-7.

Zhou, L. L., L. Y. Zhou, K. Q. Luo and D. C. Chang (2005). "Smac/DIABLO and cytochrome c are released from mitochondria through a similar mechanism during UV-induced apoptosis." Apoptosis **10**(2): 289-99.

Zhuang, L., B. Wang, G. A. Shinder, G. M. Shivji, T. W. Mak and D. N. Sauder (1999). "TNF receptor p55 plays a pivotal role in murine keratinocyte apoptosis induced by ultraviolet B irradiation." J Immunol **162**(3): 1440-7.

Zoratti, M., I. Szabo and U. De Marchi (2005). "Mitochondrial permeability transitions: how many doors to the house?" Biochim Biophys Acta **1706**(1-2): 40-52.

~ Chapter 5 ~
Characterization of the role of caspase 2 after UVB-induced DNA damage in mismatch repair-proficient and -deficient murine embryonic fibroblasts

The data presented in this chapter are being prepared for submission to Carcinogenesis.

All experimental design, data analysis and experimentation were performed by Kelly Narine with the exception of the centrosome isolation used in Figure 5-14 which was performed by Randi Gombos.

Introduction

Caspase 2 belongs to the group of initiator caspases, along with caspases 8, 9 and 10. Several studies have identified caspase 2 as an important molecule in both mitochondrial/intrinsic (Fig. 5-1) and death receptor/extrinsic apoptosis (Paroni et al. 2001; Guo et al. 2002; Lassus et al. 2002; Paroni et al. 2002; Robertson et al. 2002; Enoksson et al. 2004; He et al. 2004; Lin et al. 2004; Robertson et al. 2004; Tinel and Tschopp 2004; Wagner et al. 2004; Shin et al. 2005; Zhivotovsky and Orrenius 2005; Bonzon et al. 2006; Lavrik et al. 2006; Vakifahmetoglu et al. 2006), although there is much controversy in the literature about the precise role of caspase 2 in these pathways of apoptosis. There is evidence that caspase 2 is required for Bax activation and translocation to the mitochondria, has a direct role in mitochondrial outer membrane permeabilization (MOMP) and is important for the release of proapoptotic proteins such as cytochrome c and Smac/DIABLO (Guo et al. 2002; Lassus et al. 2002; Robertson et al. 2002; Enoksson et al. 2004; Robertson et al. 2004; Cao et al. 2008). There is also evidence that caspase 2 activation may occur downstream of Bax/Bak, caspase 9 activation and apoptosome formation (Paroni et al. 2001; O'Reilly et al. 2002; He et al. 2004; Ruiz-Vela et al. 2005; Samraj et al. 2007). It has been reported that caspase 2 is important in triggering the intrinsic apoptotic pathway through cleavage of Bid (Guo et al. 2002; Gao et al. 2005; Bonzon et al. 2006). He *et al.* have suggested that caspase activation, including activation of caspase 2, occurs in a complex set of feedback loops and not as a linear cascade (He et al. 2004). Caspase 2 is activated following several types of DNA damage, including etoposide, cisplatin and UV radiation (Paroni et al. 2001; Lassus et al. 2002; Robertson et al. 2002; He et al. 2004; Lin et al. 2004).

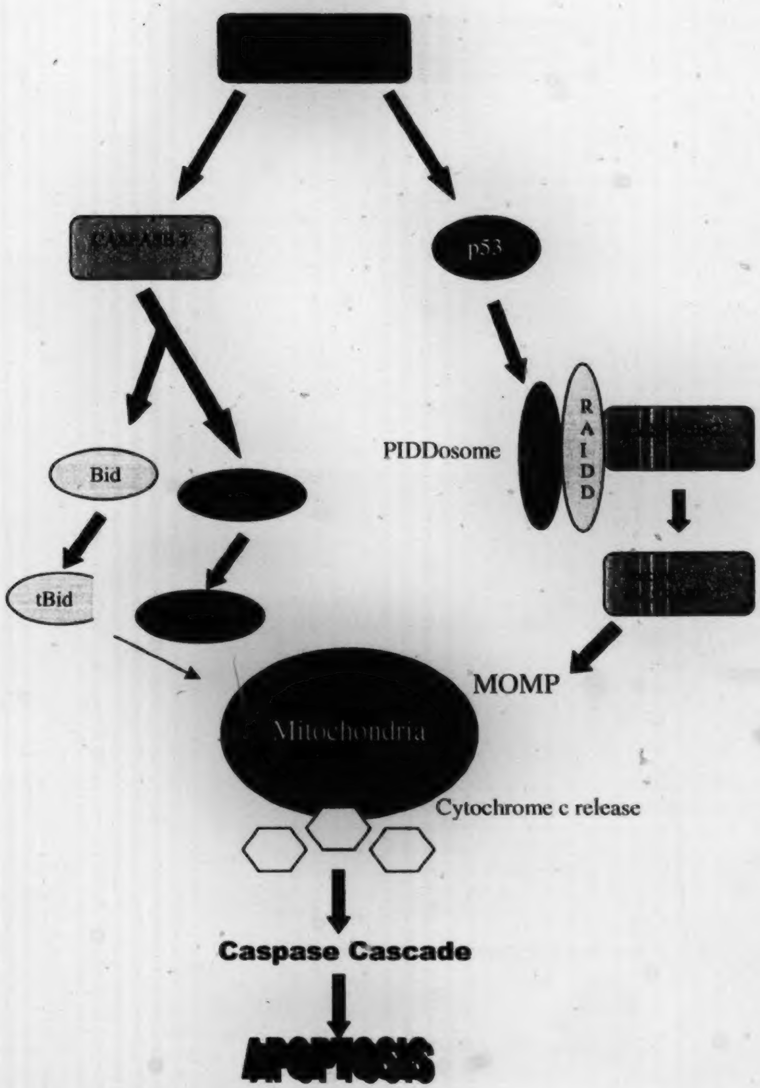
CASPASE 2
p53
Bid
tBid
PIDDosome
R
A
I
D
D
MOMP
Mitochondria
Cytochrome c release
Caspase Cascade
APOPTOSIS

Figure 5-1: Caspase 2 apoptotic pathway

After DNA damage, caspase 2 is important for cytolic Bax integration into the mitochondrial outer membrane. Caspase 2 is has also been shown to cleave Bid, which translocates to the mitochondria. Bax and tBid translocation to the mitochondria leads to cytochrome c release, activating downstream caspases 3, 6 and 7.
Alternatively, PIDD is upregulated by p53 after DNA damage to mediate p53-dependent apoptosis. The PIDDosome, comprised of PIDD, RAIDD and caspase 2 activate caspase 2 which leads to mitochondrial outer membrane permeabilization, cytochrome c release and activation of the downstream caspase cascade.

Caspase 2 was shown to interact with the proteins p53-induced protein with a death domain (PIDD) and receptor interacting protein (RIP)-associated ICH-1/CED-3 homologous protein with a death domain (RAIDD). The caspase 2-PIDD-RAIDD complex is known as the PIDDosome and caspase 2 activation has been shown to involve these 2 proteins (Tinel and Tschopp 2004). However, there are other additional, presently unidentified, factor(s) required for caspase 2 processing/activation (Vakifahmetoglu et al. 2006). The identification of the PIDDosome complex suggests that there may be a link between caspase 2 and p53. Indeed, it has been shown that DNA damage-induced apoptosis mediated by p53 leads to caspase 2 activation which is necessary for downstream apoptotic events such as cytochrome c release, effector caspase activation and apoptosis inducing factor (AIF) translocation (Ren et al. 2005; Seth et al. 2005; Tyagi et al. 2006; Baptiste-Okoh et al. 2008). Studies have also shown that the reciprocal action may be occurring; caspase 2 regulates p53 stabilization and activation for efficient apoptosis induced by genotoxic stress (Tyagi et al. 2006; Vakifahmetoglu et al. 2006).

There is some data that suggests that our understanding of caspase 2 action is incomplete; there are no substantial impairments in apoptosis in caspase 2-deficient mice, indicating that caspase 2 does not have a non-redundant role in apoptosis (Bergeron et al. 1998; O'Reilly et al. 2002). Furthermore, lymphocytes and fibroblasts lacking both caspase 2 and caspase 9 still released cytochrome c from mitochondria, displayed mitochondrial transmembrane depolarization and underwent apoptosis following treatment with various apoptotic stimuli (Marsden et al. 2004).

Caspase 2 is the only known nuclear caspase and has been shown to localize to other areas in the cell including the cytosol, mitochondria, Golgi complex and promyelocytic leukemia protein nuclear bodies (PML nuclear bodies; (Zhivotovsky et al. 1999; Mancini et al. 2000; Yuan et al. 2001; Paroni et al. 2002; Tang et al. 2005). Caspase 2 has been shown to be involved in DNA damage-mediated apoptosis in numerous cell lines [(Baptiste-Okoh et al. 2008); reviewed in (Zhivotovsky and Orrenius 2005)] and caspase 2 interacts with cyclin D3, a regulator of the cell cycle (Mendelsohn et al. 2002), suggesting a connection between cell cycle and cell death.

The multi-functional MMR proteins play a role in cell cycle and apoptosis after DNA damage (Wang and Qin 2003), yet the mechanism and other proteins involved in these DNA damage-induced pathways are only beginning to be elucidated. I hypothesized that caspase 2, being a nuclear protein activated by UV radiation, able to initiate mitochondrial outer membrane permeabilization by affecting Bax translocation and Bid cleavage, may be regulated in a UVB-induced, MMR–dependent manner. Specifically, caspase 2 may be activated in response to UVB-induced DNA damage in an Msh6-dependent manner to induce apoptosis through the mitochondrial apoptotic pathway. Alternatively, caspase 2 may be activated after UVB via death receptor complex formation to induce apoptosis in an Msh6-dependent manner. This pathway will be explored further in chapter 6.

In order to test my hypothesis I examined caspase 2 protein levels in *Msh6*$^{+/+}$ and *Msh6*$^{-/-}$ MEFs and in cellular fractions of these MEFs in order to elucidate the translocation of caspase 2 after UVB-induced DNA damage. As little is known about caspase 2 in MEFs, and likely cell-type specific behavior, I also studied the localization of caspase 2 in *Msh6*$^{+/+}$ and *Msh6*$^{-/-}$ MEFs via immunofluorescence. To confirm and expand the results investigating colocalization of caspase 2 and MMR, *Msh2*$^{-/-}$ MEFs were also used in some experiments outlined in this chapter.

Results

Pro-caspase 2 has no role in UVB-induced apoptosis in *Msh6*$^{+/+}$ and *Msh6*$^{-/-}$ murine embryonic fibroblasts

In order to determine whether caspase 2 is regulated in a Msh6-dependent manner after UVB, western blot analysis was undertaken. Three antibodies were used in this chapter for various experiments, and western blots were performed using two of the antibodies: the Chemicon antibody (Fig. 5-2) and the Biovision antibody (Fig. 5-3). Figure 5-2 shows that there was no appreciable difference in pro-caspase 2 levels between untreated *Msh6*$^{+/+}$ and *Msh6*$^{-/-}$ MEFs or after UVB treatment using the Chemicon antibody. There was also no substantial change in pro-caspase 2 levels in untreated *Msh6*$^{+/+}$ and *Msh6*$^{-/-}$ MEFs or after UVB treatment (Fig. 5-2). This shows that there is no role for pro-caspase 2 protein in Msh6-dependent apoptosis after UVB treatment, however, this protein did not identify cleaved caspase 2. This antibody was used in immunofluorescence studies to determine caspase 2 cellular localization (Fig. 5-10 to 5-13).

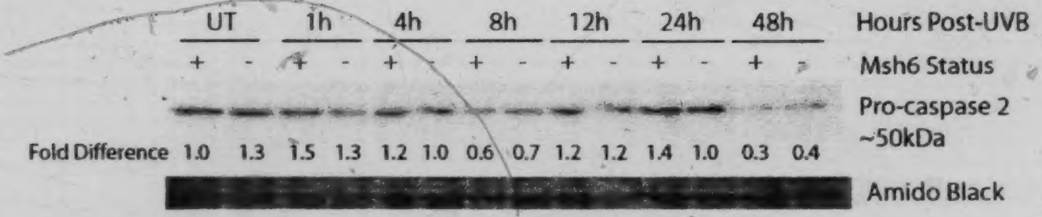

Figure 5-2: Pro-caspase 2 protein levels after UVB radiation

Protein extracts from *Msh6*$^{+/+}$ and *Msh6*$^{-/-}$ MEFs irradiated with 300J/m^2 UVB were analyzed by western blot. Gamma tubulin was used as a loading control. Densitometry was used to quantify the protein levels which were normalized to the loading control and then to the *Msh6*$^{+/+}$ untreated protein level to obtain the fold difference in protein levels for each lane.

Cleaved and pro-caspase 2 have no role in UVB-induced apoptosis in *Msh6*$^{+/+}$ and *Msh6*$^{-/-}$ murine embryonic fibroblasts

Western blot analysis using the Biovision antibody confirms that there was no appreciable difference in pro-caspase 2 levels between untreated *Msh6*$^{+/+}$ and *Msh6*$^{-/-}$ MEFs or after UVB treatment (Fig. 5-3 A).

Caspase 2 is cleaved after DNA damage, including that induced by UV. Levels of cleaved or activated caspase 2 were higher in untreated *Msh6*$^{-/-}$ MEFs than in *Msh6*$^{+/+}$ MEFs. After UVB treatment, levels of cleaved caspase 2 increased in both *Msh6*$^{+/+}$ and *Msh6*$^{-/-}$ MEFs. However, there is no obvious difference in the levels of cleaved caspase 2 between *Msh6*$^{+/+}$ and *Msh6*$^{-/-}$ MEFs. At 1 hour post-UVB, the hybridization of cleaved caspase 2 antibody to *Msh6*$^{-/-}$ MEF protein was not complete, thus densitometry levels could not be measured accurately. However, based on the values seen in all other timepoints, it appears that cleaved caspase 2 is not activated in an Msh6-dependent manner after UVB-induced DNA damage (Fig. 5-3 B). This antibody was used in immunofluorescence studies to determine caspase 2 cellular localization (Fig. 5-4, 5-5, 5-15, 5-16).

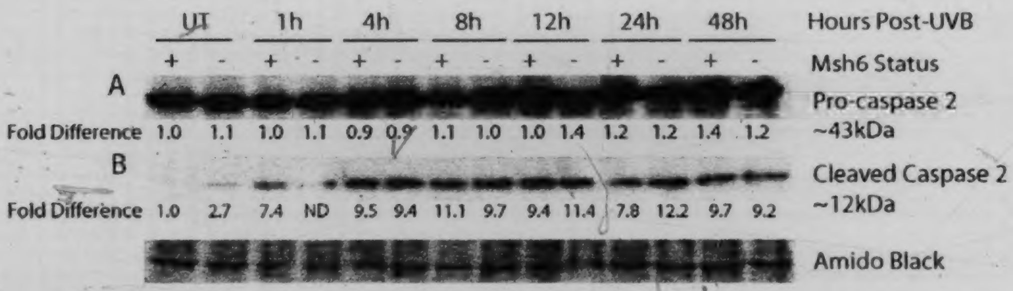
UT
1h
4h
8h
12h
24h
48h
Hours Post-UVB
+ - + - + - + - + - + - + -
Msh6 Status
A
Pro-caspase 2
~43kDa
Fold Difference 1.0 1.1 1.0 1.1 0.9 0.9 1.1 1.0 1.0 1.4 1.2 1.2 1.4 1.2
B
Cleaved Caspase 2
~12kDa
Fold Difference 1.0 2.7 7.4 ND 9.5 9.4 11.1 9.7 9.4 11.4 7.8 12.2 9.7 9.2
Amido Black

Figure 5-3: A) pro-caspase 2 and B) cleaved caspase 2 protein levels after UVB radiation

Protein extracts from *Msh6*$^{+/+}$ and *Msh6*$^{-/-}$ MEFs irradiated with 300J/m^2 UVB were analyzed by western blot. Gamma tubulin was used as a loading control. Densitometry was used to quantify the protein levels which were normalized to the loading control and then to the *Msh6*$^{+/+}$ untreated protein level to obtain the fold difference in protein levels for each lane. ND = densitometry not done.

For the following immunofluorescence experiments Pearson's correlation coefficient was generated to assess the degree of signal overlap, or colocalization, between 2 proteins using Image-Pro Plus analysis software. Pearson's correlation coefficient (herein referred to as PCC) is one of the standard measures of pattern recognition (Bolte and Cordelieres 2006). It is used for describing the correlation of the intensity distribution between channels and takes into consideration only the similarity between shapes, not the intensities of the signal. PCC values can range from -1.0 to +1.0, with -1.0 being no overlap whatsoever between signals and +1.0 being a perfect correlation. In the following experiments only PCC values of 0.5 or greater are considered to have some degree of overlap between signals, as values from -0.5 to +0.5 are difficult to interpret (Bolte and Cordelieres 2006). In addition, PCC values were obtained for control slides, where only secondary antibody was used to determine the background signal. The control PCC values were compared to the sample PCC values to determine if there was signal overlap beyond that of the background. This allowed for visualization of signal intensity across all different fluorescence channels at specific points in the cell. The images and PCC values in the following immunofluorescence experiments are representative of large scale analysis.

Caspase 2 localization in *Msh6*$^{+/+}$ and *Msh6*$^{-/-}$ murine embryonic fibroblasts

Confocal microscopy was used to study the localization of caspase 2 using the Biovision antibody. Untreated and UVB-treated *Msh6*$^{+/+}$ and *Msh6*$^{-/-}$ MEFs were probed for caspase 2 and Msh6 to determine if there was colocalization between the 2 proteins. PCC values ranged from 0.29 (very low) to 0.61 (low) in untreated and UVB-treated *Msh6*$^{+/+}$ and *Msh6*$^{-/-}$ MEFs. Furthermore, the PCC values of the secondary antibody alone control slides were 0.33 for *Msh6*$^{+/+}$ MEFs and 0.48 for *Msh6*$^{-/-}$ MEFs. Because the PCCs for the control slides were similar to the PCCs for the sample slides, it can be seen that the fluorescence in the cytoplasm of these cells is mostly background and non-specific, especially in untreated cells. 24 hours after treatment with UVB, there was bright and distinctive nuclear staining of *Msh6*$^{+/+}$ MEFs but not in *Msh6*$^{-/-}$ MEFs, corresponding to Msh6 protein. In fact, of 200 MEFs counted for each of untreated *Msh6*$^{+/+}$ MEFs, UVB-treated *Msh6*$^{+/+}$ MEFs, untreated *Msh6*$^{-/-}$ MEFs, and UVB-treated *Msh6*$^{-/-}$ MEFs, 12% of untreated *Msh6*$^{+/+}$ MEFs had bright nuclear fluorescence, while 97% of UVB-treated

Msh6$^{+/+}$ MEFs had bright nuclear fluorescence. There were no untreated *Msh6*$^{-/-}$ MEFs with nuclear fluorescence and a mere 1% of UVB-treated *Msh6*$^{-/-}$ MEFs showed 1-3 discrete fluorescent foci in the nucleus, not the all-over nuclear staining seen in *Msh6*$^{+/+}$ MEFs. Overall, it can be seen that there is no appreciable difference in caspase 2 protein localization between *Msh6*$^{+/+}$ and *Msh6*$^{-/-}$ MEFs, either untreated or 24 hours after UVB treatment, indicating that Msh6 does not influence caspase 2 localization (Fig. 5-4).

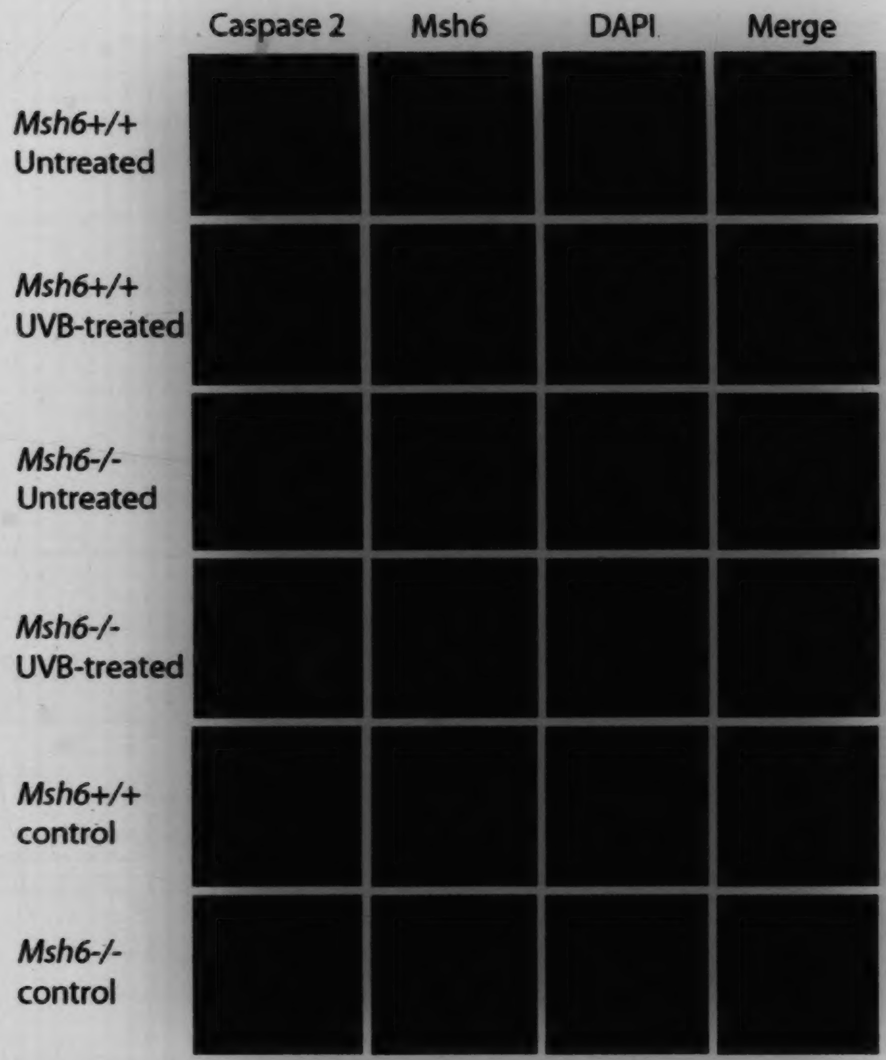
Caspase 2
Msh6
DAPI
Merge
Msh6+/+ Untreated
Msh6+/+ UVB-treated
Msh6-/- Untreated
Msh6-/- UVB-treated
Msh6+/+ control
Msh6-/- control

Figure 5-4: Caspase 2 and Msh6 localization in $Msh6^{+/+}$ and $Msh6^{-/-}$ MEFs

Untreated and UVB-treated $Msh6^{+/+}$ and $Msh6^{-/-}$ MEFs were analysed by confocal microscopy to examine the localization of caspase 2 and Msh6. Control slides were stained with fluorescent secondary antibodies and DAPI. Bar = 10uM.

Caspase 2 localization in *Msh2*$^{+/+}$ and *Msh2*$^{-/-}$ murine embryonic fibroblasts

Immunofluorescence was visualized by confocal microscopy. As Msh6 and Msh2 have distinct roles, untreated and UVB-treated *Msh2*$^{+/+}$ and *Msh2*$^{-/-}$ MEFs were also probed for caspase 2, using the Biovision antibody, and Msh2 to determine if there was colocalization between the 2 proteins. PCC values ranged from 0.44 to 0.59 in untreated and UVB-treated *Msh2*$^{+/+}$ and *Msh2*$^{-/-}$ MEFs, which are relatively low values. Furthermore, the PCC values of the secondary alone control slides were 0.46 for *Msh2*$^{+/+}$ MEFs and 0.44 for *Msh2*$^{-/-}$ MEFs. Because the PCC values for the control slides were similar to the PCC values for the sample slides, it can be seen that the fluorescence in the cytoplasm of these cells is mostly background and non-specific. However, 24 hours after treatment with UVB, distinct punctate staining was seen in the nuclei of *Msh2*$^{+/+}$ and *Msh2*$^{-/-}$ MEFs probed for caspase 2. As well, 24 hours after treatment with UVB, there was aggregation of signal in the nuclei of *Msh2*$^{+/+}$ MEFs but not in *Msh2*$^{-/-}$ MEFs, corresponding to Msh2 protein. Overall, it can be seen that there was no appreciable difference in caspase 2 protein localization between *Msh2*$^{+/+}$ and *Msh2*$^{-/-}$ MEFs, either untreated or 24 hours after UVB treatment, suggesting that Msh2 does not influence caspase 2 localization (Fig. 5-5).

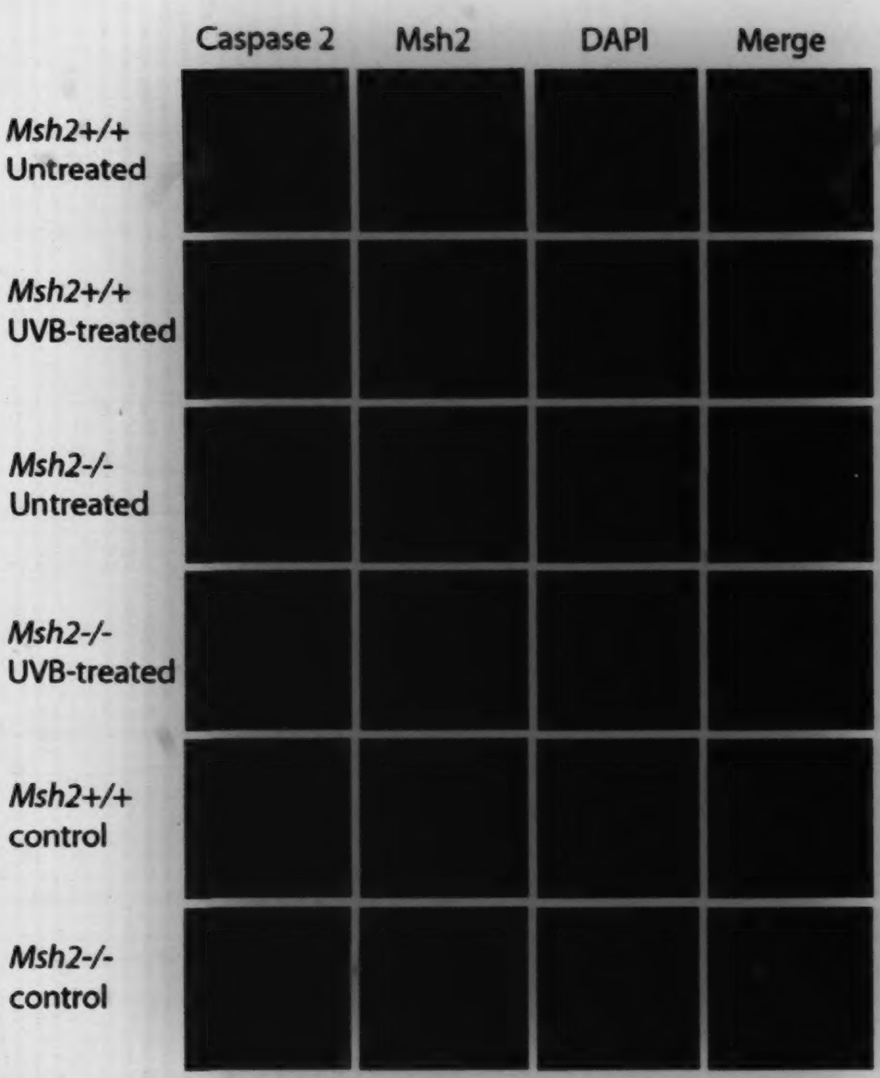
Caspase 2
Msh2
DAPI
Merge
Msh2+/+ Untreated
Msh2+/+ UVB-treated
Msh2-/- Untreated
Msh2-/- UVB-treated
Msh2+/+ control
Msh2-/- control

Figure 5-5: Caspase 2 and Msh2 localization in *Msh2*$^{+/+}$ and *Msh2*$^{-/-}$ MEFs

Untreated and UVB-treated *Msh2*$^{+/+}$ and *Msh2*$^{-/-}$ MEFs were analysed by confocal microscopy to examine the localization of caspase 2 and Msh2. Control slides were stained with fluorescent secondary antibodies and DAPI. Bar = 10uM.

Caspase 2 does not localize to the Golgi complex in *Msh6*$^{+/+}$ and *Msh6*$^{-/-}$ or *Msh2*$^{+/+}$ and *Msh2*$^{-/-}$ murine embryonic fibroblasts

Untreated and UVB-treated *Msh6*$^{+/+}$ and *Msh6*$^{-/-}$ MEFs and *Msh2*$^{+/+}$ and *Msh2*$^{-/-}$ MEFs were probed for caspase 2 using a BD Transduction antibody not used in western blot analysis and a specific dye for the Golgi complex was used to determine if caspase 2 localizes to the Golgi in these MEFs. It can be seen that caspase 2 did not localize to the Golgi complex in *Msh6*$^{+/+}$ and *Msh6*$^{-/-}$ MEFs (Fig. 5-6) nor in *Msh2*$^{+/+}$ and *Msh2*$^{-/-}$ MEFs (Fig. 5-7) and MMR status did not affect the localization pattern of caspase 2, in untreated cells or 24 hours after UVB.

Caspase 2
Golgi Stain
DAPI
Merge
Msh6+/+ Untreated
Msh6+/+ UVB-treated
Msh6-/- Untreated
Msh6-/- UVB-treated
Msh6+/+ Caspase 2 control
Msh6-/- Caspase 2 control

Figure 5-6: Caspase 2 does not localize to the Golgi complex in *Msh6*$^{+/+}$ and *Msh6*$^{-/-}$ MEFs

Untreated and UVB-treated *Msh6*$^{+/+}$ and *Msh6*$^{-/-}$ MEFs were analysed by confocal microscopy to examine potential caspase 2 localization to the Golgi complex. Control slides were stained with fluorescent secondary antibody, Golgi stain and DAPI. Bar = 10uM.

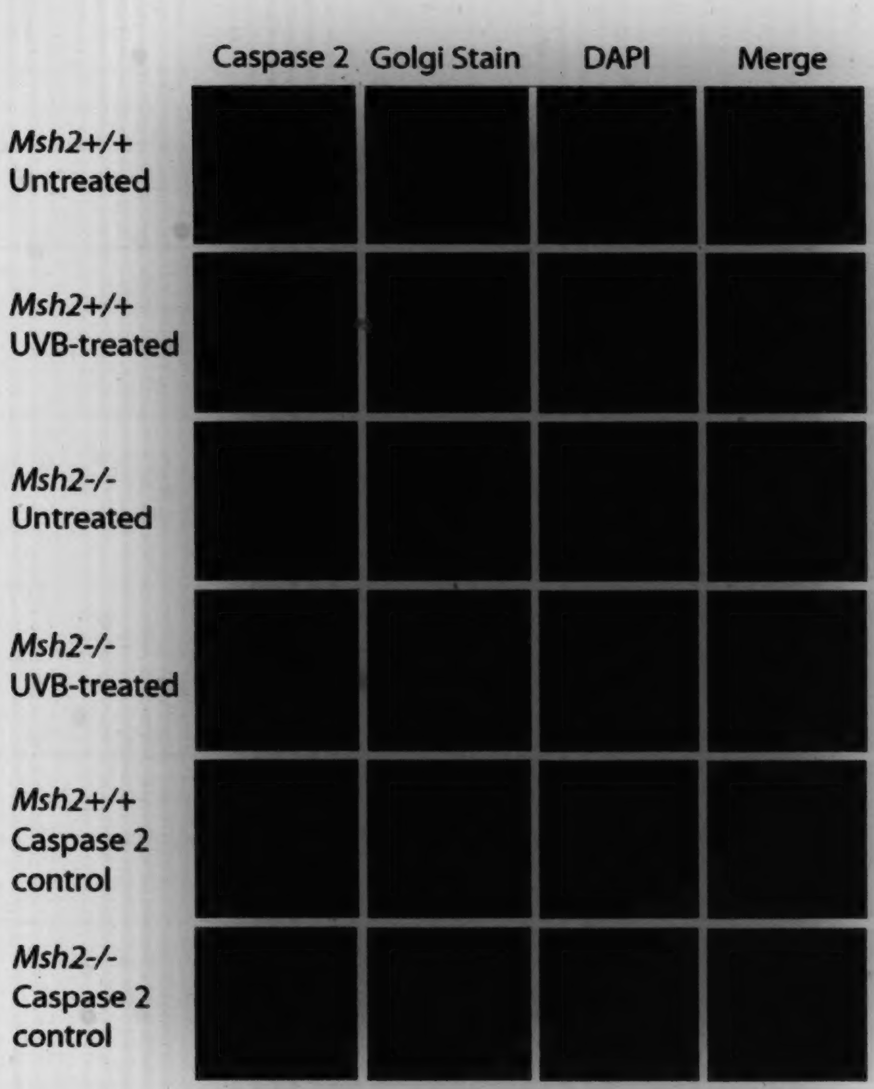
Caspase 2
Golgi Stain
DAPI
Merge
Msh2+/+ Untreated
Msh2+/+ UVB-treated
Msh2-/- Untreated
Msh2-/- UVB-treated
Msh2+/+ Caspase 2 control
Msh2-/- Caspase 2 control

Figure 5-7: Caspase 2 does not localize to the Golgi complex in *Msh2*$^{+/+}$ and *Msh2*$^{-/-}$ MEFs

Untreated and UVB-treated *Msh2*$^{+/+}$ and *Msh2*$^{-/-}$ MEFs were analysed by confocal microscopy to examine potential caspase 2 localization to the Golgi complex. Control slides were stained with fluorescent secondary antibody, Golgi stain and DAPI. Bar = 10uM.

Caspase 2 does not localize to the Endoplasmic Reticulum in *Msh6*$^{+/+}$ and *Msh6*$^{-/-}$ and M*sh2*$^{+/+}$ and *Msh2*$^{-/-}$ murine embryonic fibroblasts

Untreated and UVB-treated *Msh6*$^{+/+}$ and *Msh6*$^{-/-}$ MEFs were probed for caspase 2 using a BD Transduction antibody not used in western blot analysis and a specific dye for the endoplasmic reticulum (ER) was used to determine if caspase 2 localizes to the ER. It was seen that caspase 2 did not localize to the ER in *Msh6*$^{+/+}$ and *Msh6*$^{-/-}$ MEFs (Fig. 5-8) nor in *Msh2*$^{+/+}$ and *Msh2*$^{-/-}$ MEFs (Fig. 5-9) and MMR status did not affect the localization pattern of caspase 2, in untreated cells or 24 hours after UVB.

Caspase 2
ER Stain
DAPI
Merge
Msh6+/+ Untreated
Msh6+/+ UVB-treated
Msh6-/- Untreated
Msh6-/- UVB-treated
Msh6+/+ Caspase 2 control
Msh6-/- Caspase 2 control

Figure 5-8: Caspase 2 does not localize to the endoplasmic reticulum (ER) in *Msh6*$^{+/+}$ and *Msh6*$^{-/-}$ MEFs

Untreated and UVB-treated *Msh6*$^{+/+}$ and *Msh6*$^{-/-}$ MEFs were analysed by confocal microscopy to examine potential caspase 2 localization to the ER. Control slides were stained with fluorescent secondary antibody, ER stain and DAPI. Bar = 10uM.

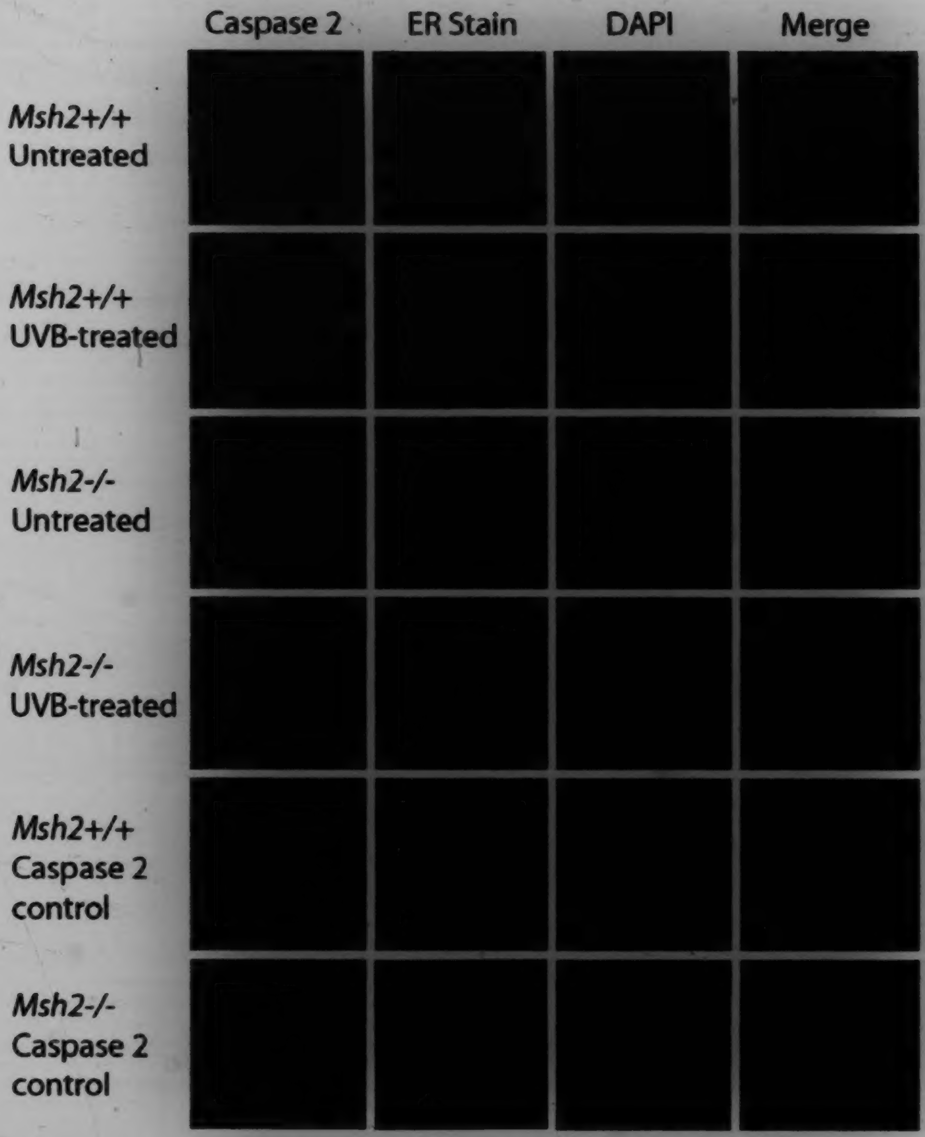
Caspase 2
ER Stain
DAPI
Merge
Msh2+/+ Untreated
Msh2+/+ UVB-treated
Msh2-/- Untreated
Msh2-/- UVB-treated
Msh2+/+ Caspase 2 control
Msh2-/- Caspase 2 control

Figure 5-9: Caspase 2 does not localize to the endoplasmic reticulum (ER) in *Msh2*$^{+/+}$ and *Msh2*$^{-/-}$ MEFs

Untreated and UVB-treated *Msh2*$^{+/+}$ and *Msh2*$^{-/-}$ MEFs were analysed by confocal microscopy to examine potential caspase 2 localization to the ER. Control slides were stained with fluorescent secondary antibody, ER stain and DAPI. Bar = 10uM.

Caspase 2 may localize to the mitochondria in *Msh6*$^{+/+}$ and *Msh6*$^{-/-}$ and *Msh2*$^{+/+}$ and *Msh2*$^{-/-}$ murine embryonic fibroblasts

Untreated and UVB-treated *Msh6*$^{+/+}$ and *Msh6*$^{-/-}$ MEFs were probed for caspase 2 using the Chemicon antibody and Mitotracker red was used to determine if caspase 2 localizes to the mitochondria in *Msh6*$^{+/+}$ and *Msh6*$^{-/-}$ MEFs and in *Msh2*$^{+/+}$ and *Msh2*$^{-/-}$ MEFs. PCC values were approximately 0.70 in untreated *Msh6*$^{+/+}$ MEFs, 0.84 in untreated *Msh6*$^{-/-}$ MEFs, 0.66 in UVB-treated *Msh6*$^{+/+}$ MEFs and 0.71 in UVB-treated *Msh6*$^{-/-}$ MEFs. PCC values were approximately 0.70 in untreated *Msh2*$^{+/+}$ and *Msh2*$^{-/-}$ MEFs and approximately 0.80 in UVB-treated *Msh2*$^{+/+}$ and *Msh2*$^{-/-}$ MEFs. From these values, it can be concluded that caspase 2 localizes to the mitochondria in *Msh6*$^{+/+}$ and *Msh6*$^{-/-}$ MEFs and in *Msh2*$^{+/+}$ and *Msh2*$^{-/-}$ MEFs, both untreated and 24 hours after UVB radiation. However, even though there were very low levels of secondary antibody present in the control slides, the PCC values were high for both the wildtype and knockout controls: 0.77 for *Msh6*$^{-/-}$ MEFs and 0.68 for *Msh6*$^{+/+}$ MEFs. Similar PCC values were obtained for *Msh2*$^{+/+}$ and *Msh2*$^{-/-}$ MEF controls, respectively. From this data, it is inconclusive whether caspase 2 localizes to the mitochondria in *Msh6*$^{+/+}$ and *Msh6*$^{-/-}$ MEFs (Fig. 5-10) or in *Msh2*$^{+/+}$ and *Msh2*$^{-/-}$ MEFs (Fig. 5-11).

Caspase 2
Mitotracker
DAPI
Merge
Msh6+/+ Untreated
Msh6+/+ UVB-treated
Msh6-/- Untreated
Msh6-/- UVB-treated
Msh6+/+ Caspase 2 control
Msh6-/- Caspase 2 control

Figure 5-10: Caspase 2 may localize to the mitochondria in *Msh6*$^{+/+}$ and *Msh6*$^{-/-}$ MEFs

Untreated and UVB-treated *Msh6*$^{+/+}$ and *Msh6*$^{-/-}$ MEFs were analysed by confocal microscopy to examine potential caspase 2 localization to the mitochondria. Control slides were stained with fluorescent secondary antibody, Mitotracker red and DAPI. Bar = 10uM.

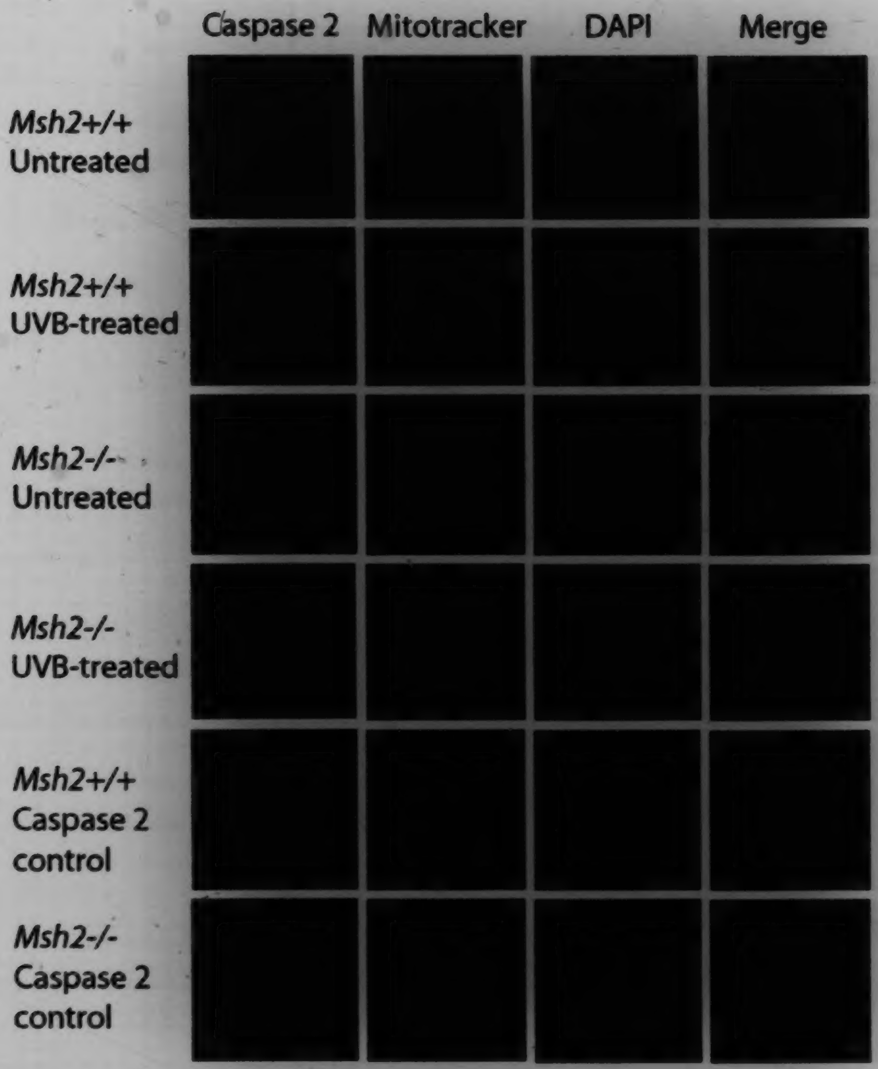
Caspase 2
Mitotracker
DAPI
Merge
Msh2+/+
Untreated
Msh2+/+
UVB-treated
Msh2-/-
Untreated
Msh2-/-
UVB-treated
Msh2+/+
Caspase 2
control
Msh2-/-
Caspase 2
control

Figure 5-11: Caspase 2 may localize to the mitochondria in $Msh2^{+/+}$ and $Msh2^{-/-}$ MEFs

Untreated and UVB-treated $Msh2^{+/+}$ and $Msh2^{-/-}$ MEFs were analysed by confocal microscopy to examine potential caspase 2 localization to the mitochondria. Control slides were stained with fluorescent secondary antibody, Mitotracker red and DAPI. Bar = 10uM.

Caspase 2 localizes to centrosomes in mitotic *Msh6*$^{+/+}$ and *Msh6*$^{-/-}$ murine embryonic fibroblasts

Untreated and UVB-treated *Msh6*$^{+/+}$ and *Msh6*$^{-/-}$ MEFs were probed for caspase 2 using the Chemicon antibody and γ–tubulin, a protein component of the centrosomes. Caspase 2 and γ–tubulin colocalized in cells undergoing cell division. The PCC value was 0.85 in both *Msh6*$^{+/+}$ untreated cells (Fig. 5-12, *Msh6*$^{+/+}$ untreated a, b), indicating a very high signal overlap between caspase 2 and γ–tubulin in mitotic cells. In cells that were not undergoing mitosis, the majority of the PCC values ranged from 0 to 0.30 which indicates that there was no colocalization between caspase 2 and γ–tubulin in these cells. However, some non-mitotic cells (*Msh6*$^{-/-}$ untreated) had PCC values ranging from approximately 0.60 to 0.65, indicating that there was some degree of colocalization in cells that were not dividing (Fig. 5-12). This shows that caspase 2 localizes to the centrosomes of *Msh6*$^{+/+}$ and *Msh6*$^{-/-}$ MEFs that are in the process of undergoing cell division, or have recently undergone cell division, and that this phenomenon is not dependent on Msh6.

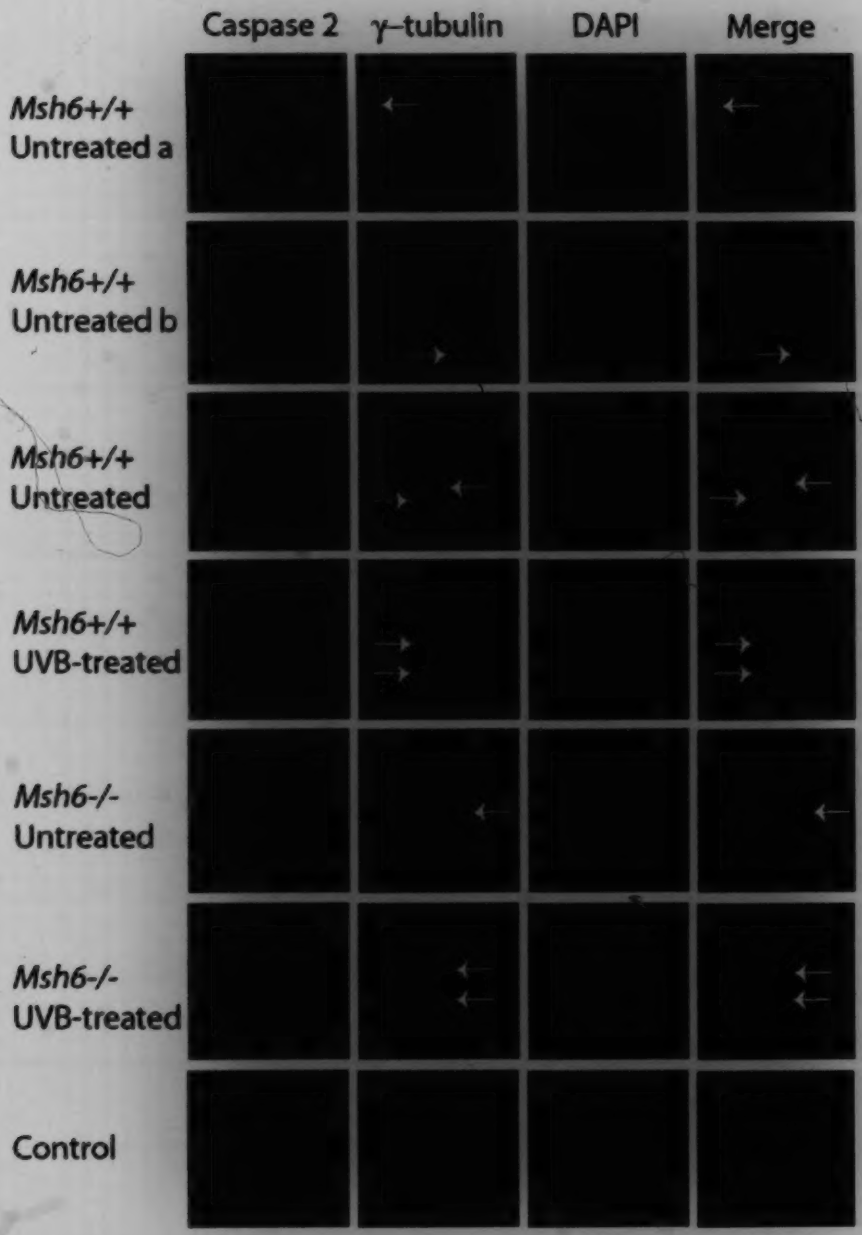
Caspase 2
γ–tubulin
DAPI
Merge
Msh6+/+
Untreated a
Msh6+/+
Untreated b
Msh6+/+
Untreated
Msh6+/+
UVB-treated
Msh6-/-
Untreated
Msh6-/-
UVB-treated
Control

Figure 5-12: Caspase 2 localizes to centrosomes in *Msh6*$^{+/+}$ and *Msh6*$^{-/-}$ MEFs

Untreated and UVB-treated *Msh6*$^{+/+}$ and *Msh6*$^{-/-}$ MEFs were analysed by confocal microscopy to examine caspase 2 colocalization with the centrosomes.
Msh6$^{+/+}$ a) 2 cells showing centrosomal localization of caspase 2 in the upper cell.
Msh6$^{-/-}$ b) the same 2 cells in a) showing centrosomal localization of caspase 2 in the lower cell.Control slide was stained with fluorescent secondary antibodies and DAPI. Bar = 10uM.

Caspase 2 localizes to centrosomes in mitotic *Msh2*$^{+/+}$ and *Msh2*$^{-/-}$ murine embryonic fibroblasts

Untreated and UVB-treated *Msh2*$^{+/+}$ and *Msh2*$^{-/-}$ MEFs were probed for caspase 2 using the Chemicon antibody and γ–tubulin, a protein component of the centrosomes. It can be seen in figure 5-13 that caspase 2 and γ–tubulin colocalized in *Msh2*$^{+/+}$ and *Msh2*$^{-/-}$ MEFs that were undergoing cell division (*Msh2*$^{+/+}$ untreated 1, 2a, 2b and *Msh2*$^{-/-}$ untreated a and b). In these cells, PCC values were above 0.75 and the majority were approximately 0.90, indicating a very high signal overlap between caspase 2 and γ–tubulin in mitotic cells, regardless of genotype. In cells that were not undergoing mitosis *Msh2*$^{+/+}$ UVB-treated and *Msh2*$^{-/-}$ UVB-treated), the PCC values ranged from 0.55 to 0.68 which indicates that there was some degree of colocalization, but not as marked as that in dividing cells (Fig. 5-13). This shows that caspase 2 localizes to the centrosomes of *Msh2*$^{+/+}$ and *Msh2*$^{-/-}$ MEFs that are in the process of undergoing cell division, or have recently undergone cell division, irrespective of Msh2 status.

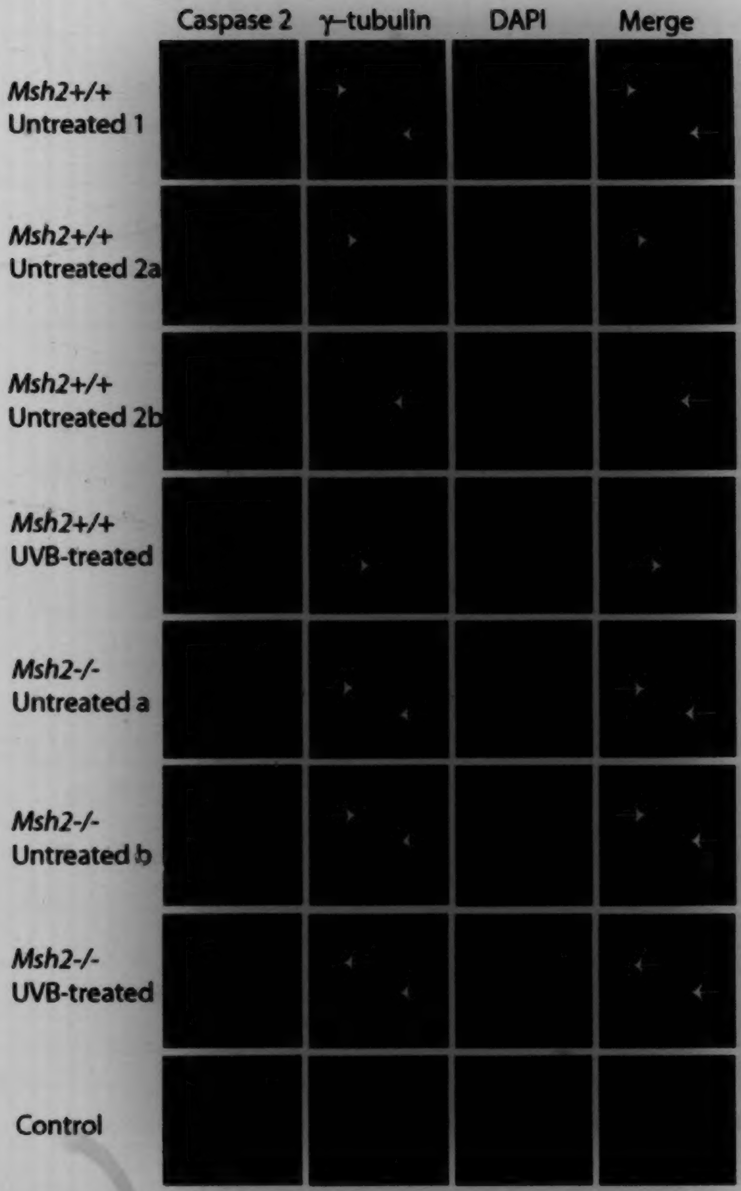
Caspase 2
γ-tubulin
DAPI
Merge
Msh2+/+ Untreated 1
Msh2+/+ Untreated 2a
Msh2+/+ Untreated 2b
Msh2+/+ UVB-treated
Msh2-/- Untreated a
Msh2-/- Untreated b
Msh2-/- UVB-treated
Control

Figure 5-13: Caspase 2 localizes to centrosomes in *Msh2*$^{+/+}$ and *Msh2*$^{-/-}$ MEFs
Untreated and UVB-treated *Msh2*$^{+/+}$ and *Msh2*$^{-/-}$ MEFs were analysed by confocal microscopy to examine caspase 2 colocalization with the centrosomes.
Msh2$^{+/+}$ 1) cell division showing centrosomal localization of caspase 2.
Msh2$^{+/+}$ 2a) cell division showing centrosomal localization of caspase 2 at one pole.
Msh2$^{+/+}$2b) same cell division in a) showing centrosomal localization of caspase 2 at other pole.
Msh2$^{-/-}$ a) cell division showing centrosomal localization of caspase 2 in one cell.
Msh2$^{-/-}$ b) same cell division in a) showing centrosomal localization of caspase 2 in both cells.
Control slide was stained with fluorescent secondary antibodies and DAPI. Bar = 10uM.

Caspase 2 levels in centrosomal fractions of *Msh6*$^{+/+}$ and *Msh6*$^{-/-}$ murine embryonic fibroblasts

To confirm localization of caspase 2 in the centrosome (Fig. 5-12, 5-13), centrosomal fractions were isolated from untreated *Msh6*$^{+/+}$ and *Msh6*$^{-/-}$ MEFs. For analysis, seven different centrosomal fractions were isolated from each genotype of MEFs and protein lysates were harvested. When probed on western blot for γ-tubulin, a centrosome marker, only the last 3 fractions of both *Msh6*$^{+/+}$ and *Msh6*$^{-/-}$ MEFs showed γ-tubulin protein (data not shown). These 3 fractions were used for the following experiment. **Note: densitometry was performed and the values obtained were normalized to the loading control only.** In fraction I there were equal amounts of pro-caspase 2 (Chemicon antibody) in both *Msh6*$^{+/+}$ and *Msh6*$^{-/-}$ MEFs. Compared to wildtype MEFs, there was 2 times and 1.5 times the amount of pro-caspase 2 in *Msh6*$^{-/-}$ MEFs MEFs in fractions II and III, respectively (Fig. 5-14 A). *Msh6*$^{+/+}$ and *Msh6*$^{-/-}$ MEFs had equal amounts of cleaved caspase 2 (Biovision antibody) in fractions I and III, while there was 12 times the amount of cleaved caspase 2 in *Msh6*$^{-/-}$ MEFs compared to *Msh6*$^{+/+}$ MEFs in fraction II (Fig. 5-14 B). This data confirms that caspase 2 localizes to the centrosomes, irrespective of Msh6 status.

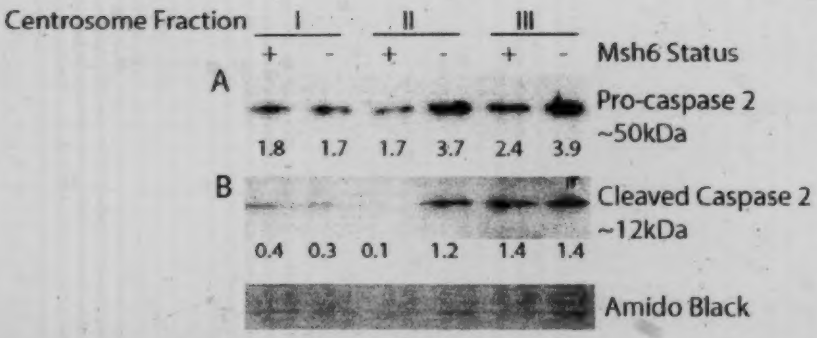

Figure 5-14: A) pro-caspase 2 and B) cleaved caspase 2 levels in *Msh6*$^{+/+}$ and *Msh6*$^{-/-}$ MEF centrosomal fractions

Protein extracts from untreated *Msh6*$^{+/+}$ and *Msh6*$^{-/-}$ MEFs fractionated into centrosomal fractions were analyzed by western blot. Amido black was used as a loading control. Densitometry was used to quantify the protein levels which were normalized to the loading control to obtain the protein levels in each lane.

Caspase 2 does not localize to PML nuclear bodies in *Msh6*$^{+/+}$ and *Msh6*$^{-/-}$ and *Msh2*$^{+/+}$ and *Msh2*$^{-/-}$ murine embryonic fibroblasts

Untreated and UVB-treated *Msh6*$^{+/+}$ and *Msh6*$^{-/-}$ MEFs and *Msh2*$^{+/+}$ and *Msh2*$^{-/-}$ MEFs were probed for caspase 2 using the Biovision antibody and PML, a protein that localizes to PML nuclear bodies. As PML nuclear bodies are associated with transcriptional regulation, apoptosis and maintenance of genome stability, I hypothesized that this could be an appropriate location for caspase 2. However, caspase 2 did not localize to PML nuclear bodies in *Msh6*$^{+/+}$ and *Msh6*$^{-/-}$ MEFs (PCC values below 0.39; Fig. 5-15) nor in *Msh2*$^{+/+}$ and *Msh2*$^{-/-}$ MEFs (PCC values below 0.28; Fig. 5-16). MMR status did not affect the localization pattern of caspase 2, in untreated cells or 24 hours after UVB. Caspase 2 protein did exhibit a more punctate pattern in the nucleus of UVB-irradiated MEFs compared to untreated MEFs.

Caspase 2
PML
DAPI
Merge
Msh6+/+ Untreated
Msh6+/+ UVB-treated
Msh6-/- Untreated
Msh6-/- UVB-treated
Msh6+/+ control
Msh6-/- control

Figure 5-15: Caspase 2 does not localize to PML nuclear bodies in *Msh6*$^{+/+}$ and *Msh6*$^{-/-}$ MEFs

Untreated and UVB-treated *Msh6*$^{+/+}$ and *Msh6*$^{-/-}$ MEFs were analysed by confocal microscopy to examine potential caspase 2 localization to the PML nuclear bodies. Control slides were stained with fluorescent secondary antibodies and DAPI. Bar = 10uM.

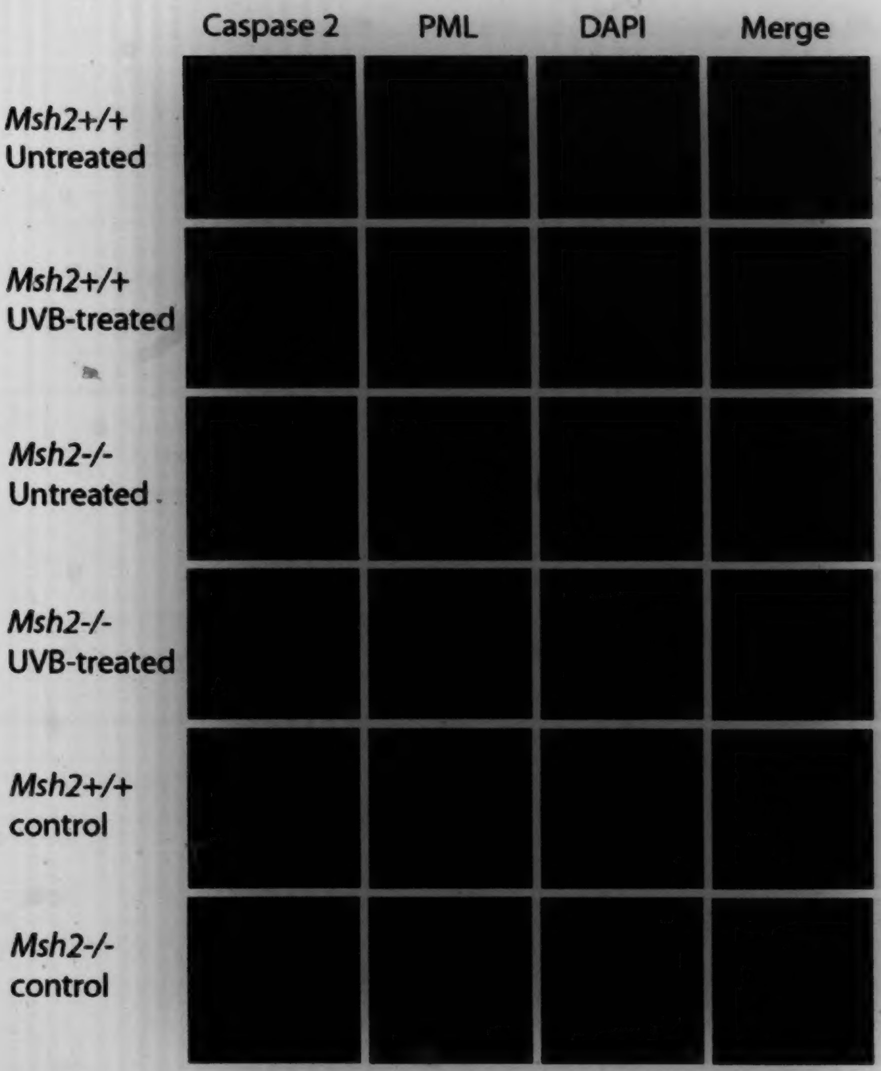
Caspase 2
PML
DAPI
Merge
Msh2+/+ Untreated
Msh2+/+ UVB-treated
Msh2-/- Untreated
Msh2-/- UVB-treated
Msh2+/+ control
Msh2-/- control

Figure 5-16: Caspase 2 does not localize to PML nuclear bodies in *Msh2*$^{+/+}$ and *Msh2*$^{-/-}$ MEFs

Untreated and UVB-treated *Msh2*$^{+/+}$ and *Msh2*$^{-/-}$ MEFs were analysed by confocal microscopy to examine potential caspase 2 localization to the PML nuclear bodies. Control slides were stained with fluorescent secondary antibodies and DAPI.
Bar = 10uM.

Caspase 2 levels in cytosolic, nuclear and membrane/particulate fractions of *Msh6*$^{+/+}$ and *Msh6*$^{-/-}$ murine embryonic fibroblasts

In order to examine the translocation of caspase 2 protein after UVB-induced DNA damage, cell pellets were harvested from untreated *Msh6*$^{+/+}$ and *Msh6*$^{-/-}$ MEFs and at 24 hours after treatment with 300J/m^2 UVB. These pellets were then fractionated into cytosolic, nuclear and membrane/particulate fractions. The Biovision antibody was used in this assay. **Note: densitometry was performed and the values obtained were normalized to the loading control only.** In the cytoplasm there was more pro-caspase 2 protein in untreated *Msh6*$^{-/-}$ MEFs than in untreated *Msh6*$^{+/+}$ MEFs. 24 hours after UVB irradiation, the levels of pro-caspase 2 decreased in the cytoplasm of both *Msh6*$^{+/+}$ and *Msh6*$^{-/-}$ MEFs and there were equal amounts in *Msh6*$^{+/+}$ and *Msh6*$^{-/-}$ MEFs. In the nuclear fraction, untreated *Msh6*$^{+/+}$ and *Msh6*$^{-/-}$ MEFs had equal amounts of pro-caspase 2 and after UVB there was no substantial difference in pro-caspase 2 levels between *Msh6*$^{+/+}$ and *Msh6*$^{-/-}$ MEFs. In the membrane/particulate fraction *Msh6*$^{+/+}$ and *Msh6*$^{-/-}$ MEFs had equal amounts of pro-caspase 2 in untreated cells and after UVB, in which caspase 2 levels increased slightly in both *Msh6*$^{+/+}$ and *Msh6*$^{-/-}$ MEFs. Overall, it can be seen that the majority of pro-caspase 2 resides in the cytoplasm of untreated cells and 24 hours after treatment with UVB, the majority of pro-caspase 2 moves to the membrane/particulate cellular fraction (Fig. 5-17 A). This experiment also shows that the translocation of pro-caspase 2 protein after UVB treatment is not dependent on Msh6.

Note: densitometry was performed and the values obtained were normalized to the loading control only. For cleaved caspase 2, there was no substantial difference in protein levels in the cytosolic fraction of untreated *Msh6*$^{+/+}$ and *Msh6*$^{-/-}$ MEFs. After treatment with UVB, there were equal amounts of cytosolic cleaved caspase 2 in *Msh6*$^{+/+}$ and *Msh6*$^{-/-}$ MEFs. In the nucleus there was virtually no cleaved caspase 2 in untreated fractions of both *Msh6*$^{+/+}$ and *Msh6*$^{-/-}$ MEFs. However, after treatment with UVB, there was a 5-fold and 3-fold increase in the amount of cleaved protein in *Msh6*$^{+/+}$ and *Msh6*$^{-/-}$ MEFs, respectively. In the membrane/particulate fraction, there were equal amounts of cleaved caspase 2 protein in untreated *Msh6*$^{+/+}$ and *Msh6*$^{-/-}$ MEFs and after treatment with UVB, there was no substantial difference in the levels of cleaved caspase 2 in either *Msh6*$^{+/+}$ or *Msh6*$^{-/-}$ MEFs. Overall, it can be seen that the majority of cleaved caspase 2 resides in the cytoplasm of untreated and UVB-treated *Msh6*$^{+/+}$ and *Msh6*$^{-/-}$ MEFs. However, the largest increase in the amount of cleaved caspase 2 occurs in the nucleus after treatment with UVB (Fig. 5-17 B). This shows translocation of cleaved caspase 2 protein after UVB treatment into the nucleus, however this translocation is not dependent on Msh6.

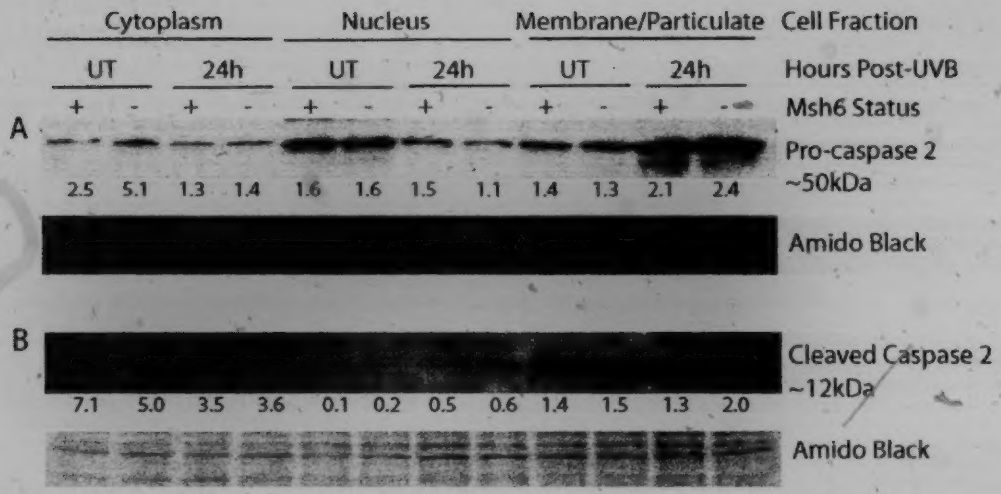
Cytoplasm
Nucleus
Membrane/Particulate
Cell Fraction
UT
24h
UT
24h
UT
24h
Hours Post-UVB
+ - + - + - + - + - + -
Msh6 Status
A
Pro-caspase 2
~50kDa
2.5 5.1 1.3 1.4 1.6 1.6 1.5 1.1 1.4 1.3 2.1 2.4
Amido Black
B
Cleaved Caspase 2
~12kDa
7.1 5.0 3.5 3.6 0.1 0.2 0.5 0.6 1.4 1.5 1.3 2.0
Amido Black

Figure 5-17: A) pro-caspase 2 and B) cleaved caspase 2 levels in *Msh6*$^{+/+}$ and *Msh6*$^{-/-}$ MEF cellular fractions

Protein extracts from *Msh6*$^{+/+}$ and *Msh6*$^{-/-}$ MEFs irradiated with 300J/m^2 UVB and fractionated into cytoplasmic, nuclear and membrane/particulate fractions 24 hours post-UVB were analyzed by western blot. Amido black was used as a loading control. Densitometry was used to quantify the protein levels which were normalized to the loading control to obtain the protein levels in each lane.

Apoptosis levels after caspase 2 inhibitor in *Msh6*$^{+/+}$ and *Msh6*$^{-/-}$ murine embryonic fibroblasts

Z-VDVAD-FMK, a specific and irreversible inhibitor of caspase 2 was used to study the effect of caspase 2 on levels of apoptosis in *Msh6*$^{+/+}$ and *Msh6*$^{-/-}$ MEFs after UVB. Figure 5-18 shows the relative levels of apoptosis 24 hours after treatment with UVB and Z-VDVAD-FMK. Apoptosis levels in *Msh6*$^{+/+}$ and *Msh6*$^{-/-}$ MEFs treated with 300J/m^2 UVB alone were set to 100%.Cells treated with UVB and caspase 2 inhibitor were normalized to their corresponding genotype treated with UVB alone. Figure 5-18 shows that apoptosis in *Msh6*$^{+/+}$ MEFs decreased to an average of approximately 80%, while apoptosis in *Msh6*$^{-/-}$ MEFs decreased to an average of just 95% after treatment with UVB and Z-VDVAD-FMK ($p<0.01$). This illustrates *Msh6*$^{-/-}$ MEFs are less affected by inhibition of caspase 2 than *Msh6*$^{+/+}$ MEFs after UVB. The apoptosis levels remained relatively high in both cell lines after treatment with UVB in the presence of Z-VDVAD-FMK (Fig. 5-18).

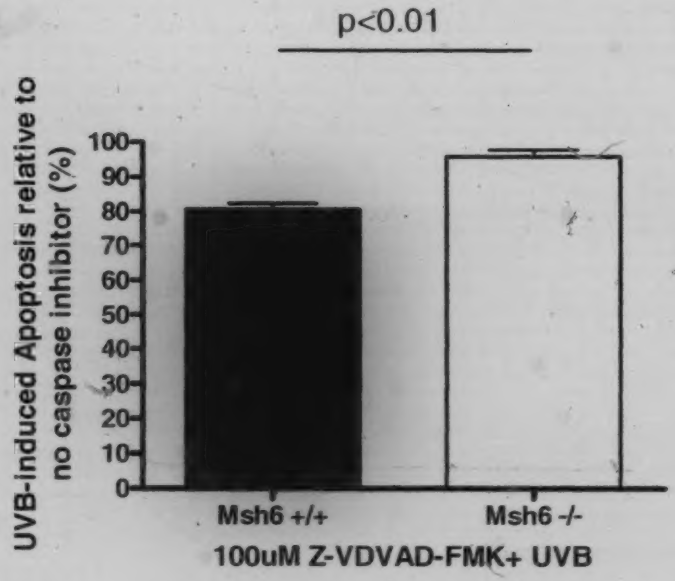

Figure 5-18: Relative decrease in apoptosis levels 24 hours after treatment with Z-VDVAD-FMK, a specific inhibitor of caspase 2

Msh6$^{+/+}$ and *Msh6*$^{-/-}$ MEFs treated with 300J/m^2 UVB alone or in combination with Z-VDVAD-FMK were analyzed by flow cytometry after Annexin V-PI staining. Apoptosis levels of cells treated with UVB alone are set to 100 and apoptosis levels of cells cells treated with Z-VDVAD-FMK in combination with UVB are represented as a percentage of this value. The difference between the relative apoptosis of *Msh6*$^{+/+}$ and *Msh6*$^{-/-}$ MEFs is significant ($p<0.01$, n=3).

Cleaved caspase 3 levels after caspase 2 inhibitor in *Msh6*$^{+/+}$ and *Msh6*$^{-/-}$ murine embryonic fibroblasts

Z-VDVAD-FMK, a specific and irreversible inhibitor of caspase 2 was used to study the effect of caspase 2 on levels of cell death in *Msh6*$^{+/+}$ and *Msh6*$^{-/-}$ MEFs after UVB. Cleavage of caspase 3 was used as a measure of cell death on the protein level. In untreated cells there was no cleavage of caspase 3 in either *Msh6*$^{+/+}$ or *Msh6*$^{-/-}$ MEFs. 24 hours after treatment with 300J/m^2 UVB cleaved caspase 3 levels were equal in *Msh6*$^{+/+}$ and *Msh6*$^{-/-}$ MEFs, similar to the findings in figure 4-11 at 24 hours post-UVB. After treatment with UVB and Z-VDVAD-FMK, the amount of cleaved caspase 3 protein M*sh6*$^{+/+}$ MEFs increased by approximately 40% compared to the M*sh6*$^{+/+}$ MEFs UVB control. In *Msh6*$^{-/-}$ MEFs there was over 2.5-fold more cleaved caspase 3 after treatment with UVB and Z-VDVAD-FMK compared to the M*sh6*$^{-/-}$ MEFs UVB control. Furthermore, after treatment with UVB and Z-VDVAD-FMK there was almost 2-fold more cleaved caspase 3 in *Msh6*$^{-/-}$ MEFs compared to M*sh6*$^{+/+}$ MEFs, consistent with the results in figure 5-18 where there was more apoptosis in *Msh6*$^{-/-}$ MEFs compared to M*sh6*$^{+/+}$ MEFs after UVB . This confirms that *Msh6* knockout MEFs are less affected by inhibition of caspase 2 after UVB irradiation (Fig. 5-19).

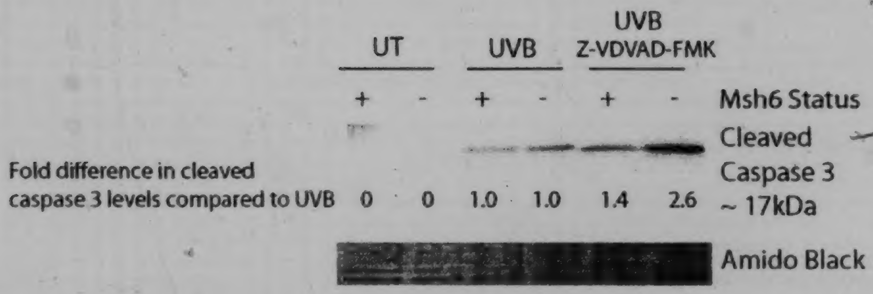

UT
UVB
UVB
Z-VDVAD-FMK
+ - + - + -
Msh6 Status
Cleaved Caspase 3 ~ 17kDa
Fold difference in cleaved caspase 3 levels compared to UVB
0 0 1.0 1.0 1.4 2.6
Amido Black

Figure 5-19: Cleaved caspase 3 protein levels 24 hours after UVB radiation using Z-VDVAD-FMK, a specific inhibitor of caspase 2

Protein extracts from *Msh6*$^{+/+}$ and *Msh6*$^{-/-}$ MEFs treated with 300J/m^2 UVB alone or in combination with Z-VDVAD-FMK were analyzed by western blot. Amido black was used as a loading control. Densitometry was used to quantify the protein levels which were normalized to the loading control and then to the UVB control protein level for each corresponding genotype to obtain the fold difference in protein levels for each lane.

Discussion

MMR proteins play a role in the cellular response to DNA damage, including cell cycle arrest and apoptosis (Hawn et al. 1995; Meyers et al. 2001). These proteins localize to the cytoplasm and to the nucleus, where they form active heterodimers (Wang and Qin 2003). Caspase 2 has also been shown to localize to the nucleus. In fact, it is the only caspase to localize to the nucleus (Colussi et al. 1998; Zhivotovsky et al. 1999; Paroni et al. 2002; Tang et al. 2005). This initiator caspase has been shown to have a physical interaction with cyclin D3, a regulator of the G1 to S transition of the cell cycle (Mendelsohn et al. 2002), providing a link between apoptosis and the cell cycle. Furthermore, caspase 2 is known to be important in activating the intrinsic apoptotic pathway after DNA damage, and is upregulated by UV radiation [(He et al. 2004); (Paroni et al. 2001); reviewed in (Zhivotovsky and Orrenius 2005)]. Based on these characteristics of caspase 2 and MMR proteins, I hypothesized that caspase 2 may be regulated in a Msh6-dependent manner to initiate intrinsic apoptosis after UVB-induced DNA damage.

Caspase 2 protein levels were analyzed by western blot using 2 different antibodies (Chemicon and Biovision antibodies). Both antibodies showed that there were no appreciable differences in pro-caspase 2 protein levels after UVB between *Msh6*$^{+/+}$ and *Msh6*$^{-/-}$ MEFs (Fig. 5-2, 5-3 A). Although cleaved caspase 2 levels (Biovision antibody) increased in both *Msh6*$^{+/+}$ and *Msh6*$^{-/-}$ MEFs after UVB-induced DNA damage there were also no substantial differences in cleaved caspase 2 levels between Msh6-proficient and –deficient MEFs after UVB treatment (Fig. 5-3 B). This suggests that caspase 2 protein levels appear to be regulated in an Msh6-independent manner after UVB, however, I wanted to examine if the localization of caspase 2 within a cell, particularly after DNA damage, may be misregulated in MMR-deficient cells. Thus, I used 2 different methods to study caspase 2 protein localization in *Msh6*$^{+/+}$ and *Msh6*$^{-/-}$ MEFs after UVB treatment to answer this question: via immunofluorescence in *Msh6*$^{+/+}$ and *Msh6*$^{-/-}$ (and *Msh2*$^{+/+}$ and *Msh2*$^{-/-}$*)* MEFs and via western blot of cellular fractions. I also studied the effects of caspase 2 inhibition on global apoptosis levels in *Msh6*$^{+/+}$ and *Msh6*$^{-/-}$ MEFs in order to confirm the role, or lack thereof, of caspase 2 in Msh6-dependent apoptosis after UVB-induced DNA damage.

The immunofluorescence experiments were performed in *Msh6*$^{+/+}$ and *Msh6*$^{-/-}$ MEFs as well as *Msh2*$^{+/+}$ and *Msh2*$^{-/-}$ MEFs in order to determine the involvement of two different MMR proteins, specifically those in the MutSα heterodimer, that recognize and bind to DNA lesions. However, after analysis of immunofluorescence data, it can be seen that *Msh6*$^{+/+}$ and *Msh6*$^{-/-}$ MEFs and *Msh2*$^{+/+}$ and *Msh2*$^{-/-}$ MEFs have very similar protein localization patterns for caspase 2 , and thus the discussion for these cells will be combined, unless the results differ greatly.

Colocalization analysis showed that caspase 2 did not colocalize with either Msh2 or Msh6, in untreated MEFs or 24 hours after UVB-induced DNA damage. The high amount of background staining, particularly in *Msh2*$^{-/-}$ and *Msh6*$^{-/-}$ MEFs, resulted in the apparent colocalization of MMR with caspase 2 in the cytoplasm of the MEFs, however, upon analysis it was seen that this was not the case. 24 hours post-UVB treatment, caspase 2 protein formed discrete foci in the nuclei of *Msh2*$^{-/-}$ and *Msh6*$^{-/-}$ MEFs. These foci did not colocalize with Msh2 or Msh6 in the nuclei of the MEFs, where caspase 2, Msh2 and Msh6 would be active (Fig. 5-4, 5-5).

Reports have shown that caspase 2 localizes to the Golgi complex in HeLa cells (Mancini et al. 2000), to the mitochondria in Jurkat cells (Zhivotovsky et al. 1999) and to PML nuclear bodies in HeLa and HEK293 cells (Tang et al. 2005). I wanted to explore the localization of caspase 2 in MMR-proficient and –deficient primary MEFs. Given that fibroblasts are comprised of a large network of endoplasmic reticulum, I also wanted to test the localization of caspase 2 to the ER. Using antibodies or markers for these organelles, I found that caspase 2 does not localize to the Golgi complex (Fig. 5-6, 5-7), ER (Fig. 5-8, 5-9), or PML nuclear bodies (Fig. 5-15, 5-16) in *Msh6*$^{+/+}$ and *Msh6*$^{-/-}$ MEFs and *Msh2*$^{+/+}$ and *Msh2*$^{-/-}$ MEFs and that determination of caspase 2 localization to the mitochondria was inconclusive via immunofluorescence (Fig. 5-10, 5-11) in *Msh6*$^{+/+}$ and *Msh6*$^{-/-}$ MEFs and *Msh2*$^{+/+}$ and *Msh2*$^{-/-}$ MEFs. This disparity in results compared to published reports may be due to several factors, including: 1) difference in cell lines being utilized. My experiments were done in primary mouse cells, while published reports by various groups have used transformed human cell lines; 2) difference in DNA damaging agent. I used UVB to induce DNA damage, while others have used various agents like etoposide and interferon-γ. Divergent results for mitochondrial localization of caspase 2 may also have been caused by the use of antibodies with different epitopes to caspase 2. Studies using various antibodies raised to different epitopes of caspase 2 were ineffective at showing its presence in the mitochondria (van Loo et al. 2002; Ren et al. 2005).

I found that caspase 2 localized to the centrosomes of MMR-proficient and –deficient MEFs that are actively undergoing cell division, or have just completed cell division. Caspase 2 also localized to the centrosomes of cells that were not undergoing cell division, but to a lesser extent, as seen by colocalization analysis (Fig. 5-12, 5-13). This finding is interesting, as caspase 2 has never before been seen to localize to the centrosomes. That the role of the centrosome goes beyond that of merely an organizer of microtubules is a view that has been explored in the literature (Rieder et al. 2001; Fletcher and Muschel 2006). The idea of centrosomal involvement in the DNA damage-induced cellular response, specifically in the checkpoint response, has also been reviewed (Fletcher and Muschel 2006). In addition, the potential role of the centrosome in apoptosis is not a new idea [reviewed in (Kong 2003)]. Indeed, several proteins involved in the regulation of the DNA damage response localize to the centrosomes, including ATM (Oricchio et al. 2006), ATRIP (Zhang et al. 2007), Chk1 (Kramer et al. 2004; Zhang et al. 2007), Chk2 (Takada et al. 2003; Tsvetkov et al. 2003). We have previously found that the MMR proteins Msh2 and Msh6 also localize to the centrosomes (Campbell et al. manuscript in preparation). That caspase 2 resides in the centrosomes after DNA damage means that the centrosomes may very well have a role in the apoptotic response. The fact that caspase 2 localizes to the centrosomes in mitotic cells may indicate that caspase 2 has a role in regulation of mitosis. In a recent study by Vakifahmetoglu et al. (2008), it was found that caspase 2 was not necessary for "mitotic catastrophe", a mode of cell death that occurs during, or shortly after, misregulated/failed mitosis, although caspase 2 activation occurred after DNA damage-induced mitotic catastrophe. Mitotic catastrophe is thought to be different from apoptosis, but may represent a "pre-stage" of apoptosis (Vakifahmetoglu et al. 2008).

In order to confirm the above immunofluorescence findings, centrosome fractions were isolated from *Msh6*$^{+/+}$ and *Msh6*$^{-/-}$ MEFs and analyzed via western blot for caspase 2 levels. **Note: densitometry was performed and the values obtained were normalized to the loading control only.** Figure 5-14 shows that pro- and cleaved caspase 2 protein is indeed contained in the centrosomes of both *Msh6*$^{+/+}$ and *Msh6*$^{-/-}$ MEFs. Although it appears that caspase 2 levels were increased in *Msh6*$^{-/-}$ MEFs, it has been shown in previous experiments that caspase 2 is Msh6-independent. This increase in caspase 2 protein levels in the centrosome fractions of *Msh6*$^{-/-}$ MEFs may be due to the faster growth rate of these cells compared to their wildtype counterparts which could lead to an upregulation of apoptotic proteins in the cells, despite attempts to reduce this.

Another way that I studied the translocation and response of caspase 2 protein after UVB treatment was by cellular fractionation. *Msh6*$^{+/+}$ and *Msh6*$^{-/-}$ MEFs were fractionated into cytoplasmic, nuclear and membrane/particulate fractions. The membrane/particulate fraction consists of the cell membrane and cellular organelles other than the nucleus. **Note: densitometry was performed and the values obtained were normalized to the loading control only.** It was seen immediately that there is no appreciable difference in pro- or cleaved caspase 2 levels between *Msh6*$^{+/+}$ and *Msh6*$^{-/-}$ MEF fractions, either untreated or 24 hours after UVB treatment. This confirms that caspase 2 translocation within the cell after UVB-induced DNA damage is not regulated in a Msh6-dependent manner. However, the cellular localization pattern of caspase 2 protein expression is illustrated by this data. Pro-caspase 2 protein resides predominantly in the cytoplasm of untreated *Msh6*$^{+/+}$ and *Msh6*$^{-/-}$ MEFs. There is also a large amount of pro-caspase 2 in the membrane/particulate fraction, which increases slightly after treatment with UV radiation. Cleaved caspase 2 protein resides predominantly in the cytoplasm of untreated and UVB-treated *Msh6*$^{+/+}$ and *Msh6*$^{-/-}$ MEFs. However, the largest increase in the amount of cleaved caspase 2 occurs in the nucleus after treatment with UVB, while the largest decrease in both pro- and cleaved caspase 2 occurs in the cytoplasm after UVB treatment (Fig. 5-17). Overall, it can be seen that, 24 hours after treatment with UVB, levels of pro- and cleaved caspase 2 decrease in the cytoplasm, while cleaved caspase 2 levels increase in the nucleus. There is no substantial change in the levels of pro- and cleaved caspase 2 in the other organelles in the cell after UVB-induced DNA damage, although the amount of caspase 2 in these organelles is not unsubstantial. From the immunofluorescence data, it may be surmised that the caspase 2 protein in the membrane/particulate fraction may be contained in the centrosomes and mitochondria and perhaps even the lysosomes and peroxisomes of the cell, a possibility which remains unexplored thus far. The translocation pattern of caspase 2 in *Msh6*$^{+/+}$ and *Msh6*$^{-/-}$ MEFs corroborates that of Zhivotovsky et al. (1999), in which the group found that there was pro-caspase 2 protein in cytosolic, nuclear and mitochondrial cellular fractions, although the majority of pro-caspase 2 resided in the cytosol of untreated Jurkat cells. Upon treatment with etoposide, the greatest increase in cleaved caspase 2 occurred in the nucleus, although there was a large increase in the amount of pro-caspase 2 in the cytosol as well (Zhivotovsky et al. 1999).

Z-VDVAD-FMK, a peptide inhibitor of caspase 2 was also used to test my hypothesis of a role for caspase 2 in Msh6-dependent apoptosis. Figure 5-18 showed that *Msh6*-deficient cells were not affected by inhibition of caspase 2 compared to *Msh6*-proficient cells, that displayed lower levels of apoptosis upon inhibition of caspase 2 (approximately 20% less apoptosis than observed without caspase 2 inhibition). Problems with specificity have been documented in the literature for peptide caspase inhibitors (Berger et al. 2006; Timmer and Salvesen 2007). A recent study by McStay et al. (2007) explored the specificities of peptide substrates and inhibitors for a range of caspases and found that several peptide inhibitors lack specificity to their target caspase. They cautioned against using these reagents alone to draw conclusions (McStay et al. 2007). Thus, my experiments utilized caspase inhibitors as one of several methods to study caspase involvement in Msh6-dependent apoptosis after UVB-induced DNA damage. In the case of Z-VDVAD-FMK, the finding of slight Msh6-dependent changes in apoptosis levels after UVB is in contrast to other data presented in chapter 5 that suggest that caspase 2 is not involved in Msh6-dependent apoptosis after UVB. Further to the above assay on global levels of apoptosis after inhibition of caspase 2, I used the irreversible inhibitor of caspase 2, Z-VDVAD-FMK, in order to assess the contribution of caspase 2 on cell death via cleavage of caspase 3 in *Msh6*$^{+/+}$ and *Msh6*$^{-/}$ MEFs after UVB treatment (Fig. 5-19). 24 hours after treatment with UVB and Z-VDVAD-FMK there was a 2-fold increase in cleaved caspase 3 in *Msh6*$^{-/-}$ MEFs compared to M*sh6*$^{+/+}$ MEFs, confirming the results in figure 5-18 showing more apoptosis in *Msh6*$^{-/-}$ MEFs compared to M*sh6*$^{+/+}$ MEFs after UVB and Z-VDVAD-FMK treatment. If the use of Z-VDVAD-FMK targets the peptide activity of caspase 2 perhaps this assay better illustrates caspase 2 activity on the cellular level compared to western blot or immunofluorescence analysis that relies upon global levels of protein and are limited to the reagents used to visualize this protein.

Based upon immunoblotting and immunofluorescence analysis, caspase 2 does not appear to have a role in Msh6-associated apoptosis after UVB-induced DNA damage. However, more biological assays such as the the caspase 2 inhibitor assays and the immunofluorescence assay showing localization of caspase 2 to the centrosomes of mitotic MEFs, where MMR proteins localize, suggest that caspase 2 may have a role in apoptosis/cellular response regulated by MMR after UVB. Caspase 2 activity, as well as the role of caspase 2 in centrosomes will require further experimentation beyond the scope of this thesis.

References

Baptiste-Okoh, N., A. M. Barsotti and C. Prives (2008). "A role for caspase 2 and PIDD in the process of p53-mediated apoptosis." Proc Natl Acad Sci U S A **105**(6): 1937-42.

Berger, A. B., K. B. Sexton and M. Bogyo (2006). "Commonly used caspase inhibitors designed based on substrate specificity profiles lack selectivity." Cell Res **16**(12): 961-3.

Bergeron, L., G. I. Perez, G. Macdonald, L. Shi, Y. Sun, A. Jurisicova, S. Varmuza, K. E. Latham, J. A. Flaws, J. C. Salter, H. Hara, M. A. Moskowitz, E. Li, A. Greenberg, J. L. Tilly and J. Yuan (1998). "Defects in regulation of apoptosis in caspase-2-deficient mice." Genes Dev **12**(9): 1304-14.

Bolte, S. and F. P. Cordelieres (2006). "A guided tour into subcellular colocalization analysis in light microscopy." J Microsc **224**(Pt 3): 213-32.

Bonzon, C., L. Bouchier-Hayes, L. J. Pagliari, D. R. Green and D. D. Newmeyer (2006). "Caspase-2-induced apoptosis requires bid cleavage: a physiological role for bid in heat shock-induced death." Mol Biol Cell **17**(5): 2150-7.

Cao, X., R. L. Bennett and W. S. May (2008). "c-Myc and caspase-2 are involved in activating Bax during cytotoxic drug-induced apoptosis." J Biol Chem.

Colussi, P. A., N. L. Harvey and S. Kumar (1998). "Prodomain-dependent nuclear localization of the caspase-2 (Nedd2) precursor. A novel function for a caspase prodomain." J Biol Chem **273**(38): 24535-42.

Enoksson, M., J. D. Robertson, V. Gogvadze, P. Bu, A. Kropotov, B. Zhivotovsky and S. Orrenius (2004). "Caspase-2 permeabilizes the outer mitochondrial membrane and disrupts the binding of cytochrome c to anionic phospholipids." J Biol Chem **279**(48): 49575-8.

Fletcher, L. and R. J. Muschel (2006). "The centrosome and the DNA damage induced checkpoint." Cancer Lett **243**(1): 1-8.

Gao, Z., Y. Shao and X. Jiang (2005). "Essential roles of the Bcl-2 family of proteins in caspase-2-induced apoptosis." J Biol Chem **280**(46): 38271-5.

Guo, Y., S. M. Srinivasula, A. Druilhe, T. Fernandes-Alnemri and E. S. Alnemri (2002). "Caspase-2 induces apoptosis by releasing proapoptotic proteins from mitochondria." J Biol Chem **277**(16): 13430-7.

Hawn, M. T., A. Umar, J. M. Carethers, G. Marra, T. A. Kunkel, C. R. Boland and M. Koi (1995). "Evidence for a connection between the mismatch repair system and the G2 cell cycle checkpoint." Cancer Res **55**(17): 3721-5.

He, Q., Y. Huang and M. S. Sheikh (2004). "Bax deficiency affects caspase-2 activation during ultraviolet radiation-induced apoptosis." Oncogene **23**(6): 1321-5.

Kong, Q. (2003). "The centrosome-centered cell-brain in apoptosis." Med Hypotheses **61**(1): 126-32.

Kramer, A., N. Mailand, C. Lukas, R. G. Syljuasen, C. J. Wilkinson, E. A. Nigg, J. Bartek and J. Lukas (2004). "Centrosome-associated Chk1 prevents premature activation of cyclin-B-Cdk1 kinase." Nat Cell Biol **6**(9): 884-91.

Lassus, P., X. Opitz-Araya and Y. Lazebnik (2002). "Requirement for caspase-2 in stress-induced apoptosis before mitochondrial permeabilization." Science **297**(5585): 1352-4.

Lavrik, I. N., A. Golks, S. Baumann and P. H. Krammer (2006). "Caspase-2 is activated at the CD95 death-inducing signaling complex in the course of CD95-induced apoptosis." Blood **108**(2): 559-65.

Lin, C. F., C. L. Chen, W. T. Chang, M. S. Jan, L. J. Hsu, R. H. Wu, M. J. Tang, W. C. Chang and Y. S. Lin (2004). "Sequential caspase-2 and caspase-8 activation upstream of mitochondria during ceramideand etoposide-induced apoptosis." J Biol Chem **279**(39): 40755-61.

Mancini, M., C. E. Machamer, S. Roy, D. W. Nicholson, N. A. Thornberry, L. A. Casciola-Rosen and A. Rosen (2000). "Caspase-2 is localized at the Golgi complex and cleaves golgin-160 during apoptosis." J Cell Biol **149**(3): 603-12.

Marsden, V. S., P. G. Ekert, M. Van Delft, D. L. Vaux, J. M. Adams and A. Strasser (2004). "Bcl-2-regulated apoptosis and cytochrome c release can occur independently of both caspase-2 and caspase-9." J Cell Biol **165**(6): 775-80.

McStay, G. P., G. S. Salvesen and D. R. Green (2007). "Overlapping cleavage motif selectivity of caspases: implications for analysis of apoptotic pathways." Cell Death Differ.

Mendelsohn, A. R., J. D. Hamer, Z. B. Wang and R. Brent (2002). "Cyclin D3 activates Caspase 2, connecting cell proliferation with cell death." Proc Natl Acad Sci U S A **99**(10): 6871-6.

Meyers, M., M. W. Wagner, H. S. Hwang, T. J. Kinsella and D. A. Boothman (2001). "Role of the hMLH1 DNA mismatch repair protein in fluoropyrimidine-mediated cell death and cell cycle responses." Cancer Res **61**(13): 5193-201.

O'Reilly, L. A., P. Ekert, N. Harvey, V. Marsden, L. Cullen, D. L. Vaux, G. Hacker, C. Magnusson, M. Pakusch, F. Cecconi, K. Kuida, A. Strasser, D. C. Huang and S. Kumar (2002). "Caspase-2 is not required for thymocyte or neuronal apoptosis even though cleavage of caspase-2 is dependent on both Apaf-1 and caspase-9." Cell Death Differ **9**(8): 832-41.

Oricchio, E., C. Saladino, S. Iacovelli, S. Soddu and E. Cundari (2006). "ATM is activated by default in mitosis, localizes at centrosomes and monitors mitotic spindle integrity." Cell Cycle **5**(1): 88-92.

Paroni, G., C. Henderson, C. Schneider and C. Brancolini (2001). "Caspase-2-induced apoptosis is dependent on caspase-9, but its processing during UV- or tumor necrosis factor-dependent cell death requires caspase-3." J Biol Chem **276**(24): 21907-15.

Paroni, G., C. Henderson, C. Schneider and C. Brancolini (2002). "Caspase-2 can trigger cytochrome C release and apoptosis from the nucleus." J Biol Chem **277**(17): 15147-61.

Ren, J., M. Shi, R. Liu, Q. H. Yang, T. Johnson, W. C. Skarnes and C. Du (2005). "The Birc6 (Bruce) gene regulates p53 and the mitochondrial pathway of apoptosis and is essential for mouse embryonic development." Proc Natl Acad Sci U S A **102**(3): 565-70.

Rieder, C. L., S. Faruki and A. Khodjakov (2001). "The centrosome in vertebrates: more than a microtubule-organizing center." Trends Cell Biol **11**(10): 413-9.

Robertson, J. D., M. Enoksson, M. Suomela, B. Zhivotovsky and S. Orrenius (2002). "Caspase-2 acts upstream of mitochondria to promote cytochrome c release during etoposide-induced apoptosis." J Biol Chem **277**(33): 29803-9.

Robertson, J. D., V. Gogvadze, A. Kropotov, H. Vakifahmetoglu, B. Zhivotovsky and S. Orrenius (2004). "Processed caspase-2 can induce mitochondria-mediated apoptosis independently of its enzymatic activity." EMBO Rep **5**(6): 643-8.

Ruiz-Vela, A., J. T. Opferman, E. H. Cheng and S. J. Korsmeyer (2005). "Proapoptotic BAX and BAK control multiple initiator caspases." EMBO Rep **6**(4): 379-85.

Samraj, A. K., D. Sohn, K. Schulze-Osthoff and I. Schmitz (2007). "Loss of caspase-9 reveals its essential role for caspase-2 activation and mitochondrial membrane depolarization." Mol Biol Cell **18**(1): 84-93.

Seth, R., C. Yang, V. Kaushal, S. V. Shah and G. P. Kaushal (2005). "p53-dependent caspase-2 activation in mitochondrial release of apoptosis-inducing factor and its role in renal tubular epithelial cell injury." J Biol Chem **280**(35): 31230-9.

Shin, S., Y. Lee, W. Kim, H. Ko, H. Choi and K. Kim (2005). "Caspase-2 primes cancer cells for TRAIL-mediated apoptosis by processing procaspase-8." Embo J **24**(20): 3532-42.

Takada, S., A. Kelkar and W. E. Theurkauf (2003). "Drosophila checkpoint kinase 2 couples centrosome function and spindle assembly to genomic integrity." Cell **113**(1): 87-99.

Tang, J., W. Xie and X. Yang (2005). "Association of caspase-2 with the promyelocytic leukemia protein nuclear bodies." Cancer Biol Ther **4**(6): 645-9.

Timmer, J. C. and G. S. Salvesen (2007). "Caspase substrates." Cell Death Differ **14**(1): 66-72.

Tinel, A. and J. Tschopp (2004). "The PIDDosome, a protein complex implicated in activation of caspase-2 in response to genotoxic stress." Science **304**(5672): 843-6.

Tsvetkov, L., X. Xu, J. Li and D. F. Stern (2003). "Polo-like kinase 1 and Chk2 interact and co-localize to centrosomes and the midbody." J Biol Chem **278**(10): 8468-75.

Tyagi, A., R. P. Singh, C. Agarwal and R. Agarwal (2006). "Silibinin activates p53-caspase 2 pathway and causes caspase-mediated cleavage of Cip1/p21 in apoptosis induction in bladder transitional-cell papilloma RT4 cells: evidence for a regulatory loop between p53 and caspase 2." Carcinogenesis **27**(11): 2269-80.

Vakifahmetoglu, H., M. Olsson, S. Orrenius and B. Zhivotovsky (2006). "Functional connection between p53 and caspase-2 is essential for apoptosis induced by DNA damage." Oncogene **25**(41): 5683-92.

Vakifahmetoglu, H., M. Olsson, C. Tamm, N. Heidari, S. Orrenius and B. Zhivotovsky (2008). "DNA damage induces two distinct modes of cell death in ovarian carcinomas." Cell Death Differ **15**(3): 555-66.

van Loo, G., X. Saelens, F. Matthijssens, P. Schotte, R. Beyaert, W. Declercq and P. Vandenabeele (2002). "Caspases are not localized in mitochondria during life or death." Cell Death Differ **9**(11): 1207-11.

Wagner, K. W., I. H. Engels and Q. L. Deveraux (2004). "Caspase-2 can function upstream of bid cleavage in the TRAIL apoptosis pathway." J Biol Chem **279**(33): 35047-52.

Wang, Y. and J. Qin (2003). "MSH2 and ATR form a signaling module and regulate two branches of the damage response to DNA methylation." Proc Natl Acad Sci U S A **100**(26): 15387-92.

Yuan, H., M. Mutomba, I. Prinz and R. A. Gottlieb (2001). "Differential processing of cytosolic and mitochondrial caspases." Mitochondrion **1**(1): 61-9.

Zhang, S., P. Hemmerich and F. Grosse (2007). "Centrosomal localization of DNA damage checkpoint proteins." J Cell Biochem **101**(2): 451-65.

Zhivotovsky, B. and S. Orrenius (2005). "Caspase-2 function in response to DNA damage." Biochem Biophys Res Commun **331**(3): 859-67.

Zhivotovsky, B., A. Samali, A. Gahm and S. Orrenius (1999). "Caspases: their intracellular localization and translocation during apoptosis." Cell Death Differ **6**(7): 644-51.

~ Chapter 6 ~

Characterization of the death receptor/extrinsic apoptotic response to UVB-induced DNA damage in mismatch repair-proficient and -deficient murine embryonic fibroblasts

The data presented in this chapter are being prepared for submission to Carcinogenesis.

All experimental design and data analysis were performed by Kelly Narine. Experimentation was performed by Kelly Narine with the assistance of Cindy Lentz.

Introduction

Apoptosis can be triggered via 2 major pathways: an intrinsic pathway caused by internal stress, or an extrinsic apoptotic pathway, initiated by ligands binding to membrane-bound death receptors. The main apoptotic ligand-receptor pairs in the tumor necrosis factor (TNF) superfamily include 1) TNFα-TNF receptor 1 (TNFR1), 2) Fas ligand (FasL)-Fas/CD95, and 3) TNF-related apoptosis inducing ligand (TRAIL)-TRAIL receptor 1 or 2 (TRAIL-R1/R2) [reviewed in (Jin and El-Deiry 2005)]. The ligands are type II transmembrane proteins that bind to receptors in order to activate their downstream effects. The receptors in the TNF receptor (TNFR) superfamily are characterized by their death domains and the ability to initiate apoptosis (Baud and Karin 2001). My experiments involve the first 2 pathways of extrinsic apoptosis.

1) TNFα-TNFR1

TNFα is a cytokine primarily produced by macrophages and has a role in the inflammatory response. TNFα can bind to 2 receptors: TNFR1 and TNFR2. TNFR1 is expressed in a wide variety of tissues, while TNFR2 is expressed mainly in the tissues of the immune system [reviewed in (Wajant et al. 2003)]. TNFα can activate the NF-kB pathway and the JNK pathway, but I focused on the TNFα apoptotic pathway through TNFR1 and TNFR1-associated protein with death domain (TRADD). TRADD is bound to TNFR1 via their death domains (DD). Subsequently, receptor-interacting protein (RIP) is recruited to the complex via its DD interaction with TRADD (Devin et al. 2003). TNF receptor-associated factor 2 (TRAF2) also binds to the TNFR1-TRADD complex via the TRADD DD. TRADD and RIP associate with Fas-associated death domain protein

(FADD) and caspase 8 to undergo apoptosis [(Kim et al. 2000); reviewed in (Jin and El-Deiry 2005)]. Alternatively, TNFR1 may initiate apoptosis through another pathway. TNFR1 recruits RIP-associated ICH-1/CED-3 homologous protein with death domain (RAIDD), an accessory protein that associates with RIP through their DDs. This complex recruits caspase 2, leading to induction of apoptosis (Duan and Dixit 1997) (Fig. 6-1 A).

2) FasL-Fas/CD95

These proteins are constitutively expressed in many tissues (Guzman et al. 2003). The FasL-Fas/CD95 apoptotic pathway is initiated by FasL binding to Fas, promoting Fas trimerization. Fas associates with FADD via their DDs. This accessory protein allows binding of pro-caspase 8 to the complex via their death effector domains (DED). Together, the Fas-FADD-Caspase 8 complex is known as the DISC, or death-inducing signaling complex. The DISC enables autocatalytic processing of pro-caspase 8 in to 2 active subunits (18 kDa and 10 kDa) that are released from the DISC, leading to induction of apoptosis (Kischkel et al. 1995). In Fas-mediated apoptosis, there are 2 signaling pathways identified into which cells can be divided. In type I cells, the apoptotic pathway is initiated through the binding of the death receptor with its ligand. This activates caspase 8, which is sufficient to activate downstream caspases and leads to execution of apoptosis. In type II cells, activation of effector caspases by Fas depends on amplification of death receptor signals through the mitochondria via a feedback loop. Active caspase 8 cleaves Bid and leads to release of pro-apoptotic mitochondrial proteins such as cytochrome c and Smac/DIABLO which drive the formation of the apoptosome, thus activating caspase 9. Active caspase 9 activates the executioner caspase 3, which activates caspase 8, completing the feedback loop [(Wang and El-Deiry 2003) reviewed in (Jin and El-Deiry 2005)] (Fig. 6-1 B).

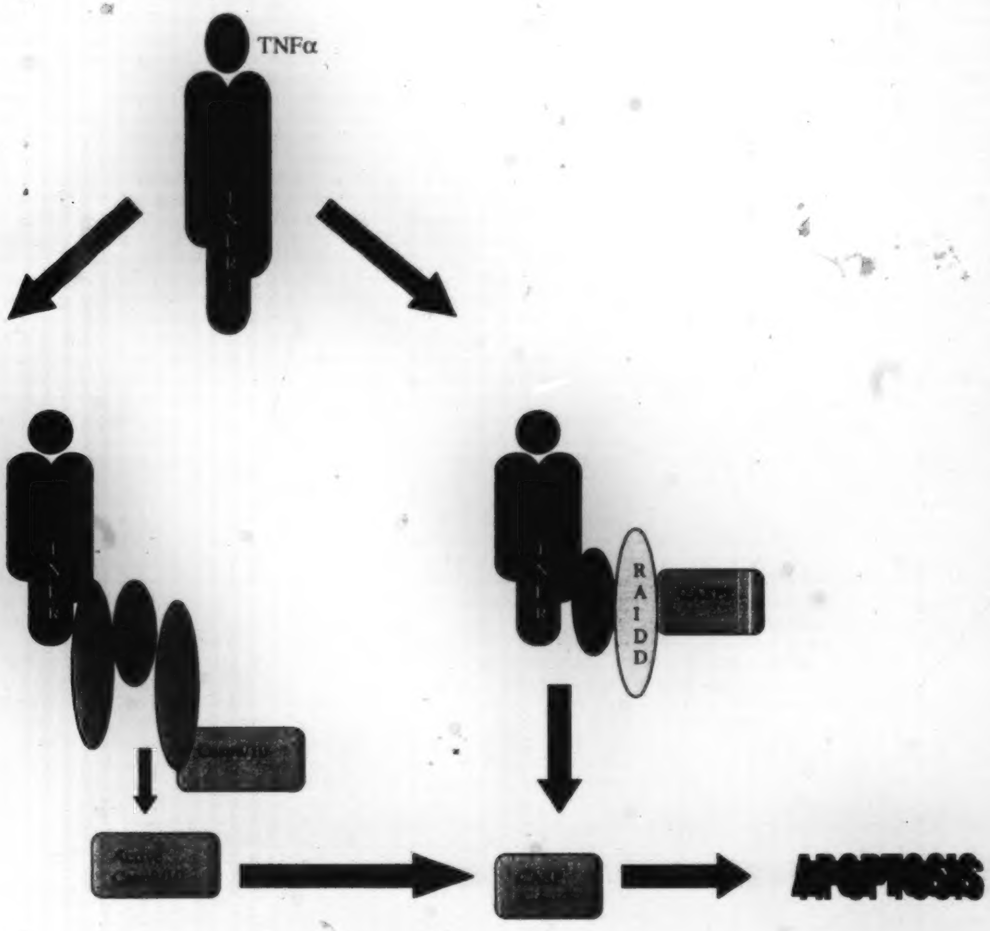

Figure 6-1 A: Death receptor apoptosis- TNFα-TNFR1 pathway
TNFα binding to TNFR1 induces the oligomerization of:
1) TNFR1-TRADD-RIP-FADD-Caspase 8/10 which leads to activation of caspase 8/10 which in turn cleaves effector caspases 3, 6, 7, leading to apoptosis, or
2) TNFR1-RIP-RAIDD-Caspase 2 which cleaves effector caspases 3, 6, 7, leading to apoptosis.

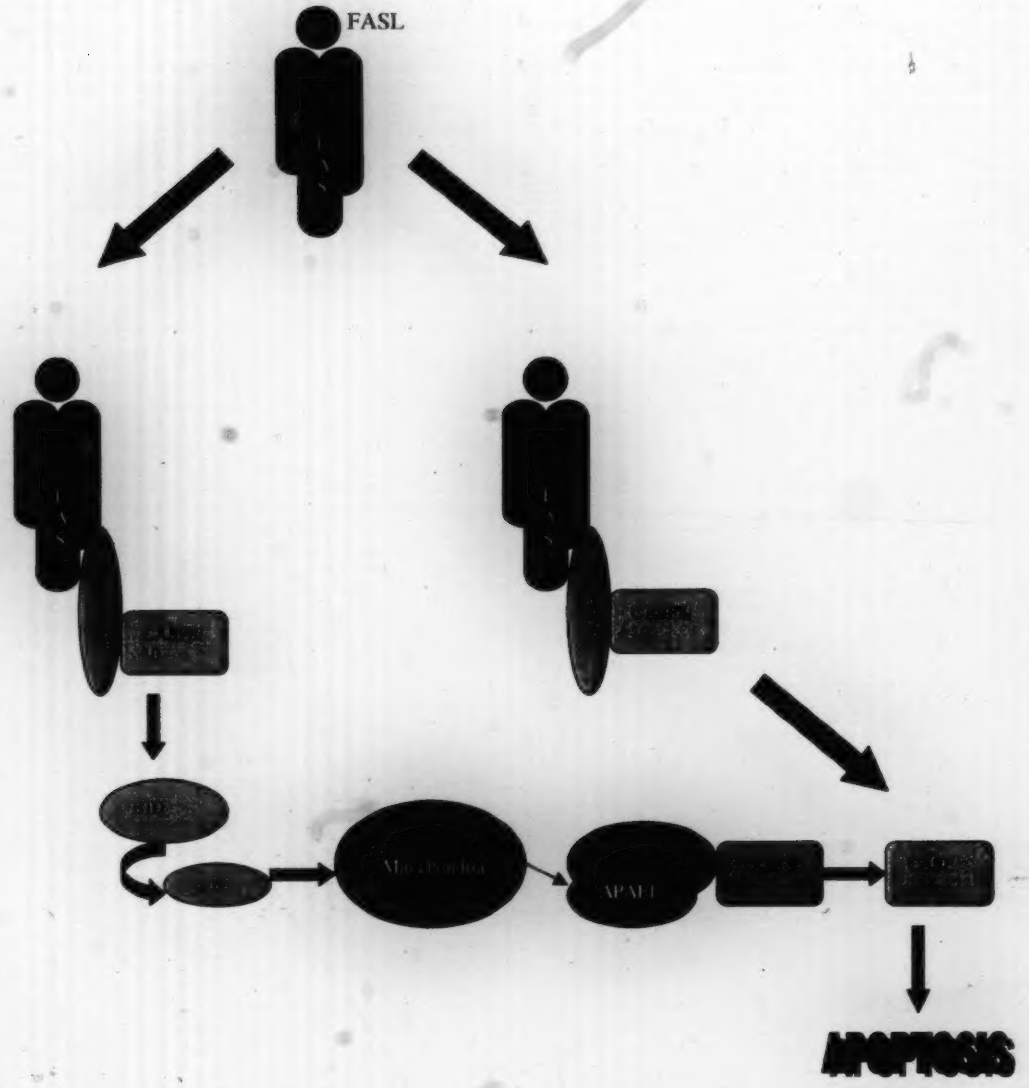

Figure 6-1 B: Death receptor apoptosis- FasL-Fas pathway

FasL binding to Fas induces the oligomerization of Fas-FADD-Caspase 8/10 (death-inducing signaling complex, or DISC) which leads to cleavage of effector caspases 3, 6, 7 and apoptosis. DISC formation also leads to Bid cleavage. Truncated Bid translocates to the mitochondria, leading to cytochrome c release and apoptosome formation. Effector caspases 3, 6, 7 are cleaved, leading to apoptosis, thus amplifying death receptor signals.

UV Radiation and Death Receptor Apoptosis

Many studies have shown a link between the recruitment of the extrinsic apoptotic pathway and UV exposure. Kibitel et al. (1998) showed that TNFα is upregulated by UV in mouse and human cells (Kibitel et al. 1998). Zhuang et al. (1999) and Kock et al. (1990) demonstrated that irradiation of keratinocyes by UVB caused upregulation of TNFα and TNFR1 which led to apoptosis (Kock et al. 1990; Zhuang et al. 1999).

Studies have shown that Fas and FasL are upregulated after exposure to UV. Cells that have been DNA-damaged after UV radiation are eliminated through keratinocyte apoptosis, known as sunburn cell formation. This phenomenon is thought to be an integral step in the removal of precancerous skin cells. The formation of sunburn cells has been shown to be dependent on FasL (Hill et al. 1999). Human keratinocytes constitutively express both FasL and Fas. Leverkus et al. (1997) showed that UV radiation induced FasL and Fas mRNA expression. Furthermore, treatment with a FasL-neutralizing antibody reduced the amount of UV-induced apoptosis of keratinocytes (Leverkus et al. 1997).

DNA Mismatch Repair and Death Receptor Apoptosis

It has been shown that nuclear FADD protein interacts with methyl-CpG binding domain protein 4 (MBD4), a genome surveillance/DNA repair protein. MLH1, which interacts with MBD4 was found in a complex with FADD in the nucleus (Screaton et al. 2003). These findings forge a link between genome surveillance and apoptosis and demonstrate a putative relationship between the death receptor pathway of apoptosis and MMR.

Phosphorylation of FADD at Serine 194 (FADD-pSer194) is associated with cellular arrest at the G2/M phase of the cell cycle after nocodazole treatment (Scaffidi et al. 2000). Studies by us and others have previously shown an involvement of MMR in G2/M arrest after DNA damage, including UVB (Koi et al. 1994; Hawn et al. 1995; Duckett et al. 1996; Reitmair et al. 1997; Umar et al. 1997; Davis et al. 1998; Meyers et al. 2001; Yan et al. 2001; Franchitto et al. 2003; Yan et al. 2003; Narine et al. 2007).

The role of MMR in the DNA damage response after UV radiation [reviewed in (Young et al. 2003)], the role of the death receptor proteins in UV-induced apoptosis, the association of FADD with MLH1 and the role for FADD-pSer194 and the MMR proteins in G2/M cell cycle arrest has led me to hypothesize that the extrinsic apoptotic proteins TNFα-TNFR1 and FasL-Fas may play a role in the Msh6-dependent UVB-induced apoptotic response. Specifically, Msh6 may have a role in the TNFα-TNFR1 pathway of apoptosis through the TNFR1-TRADD-RIP-FADD-caspase 8 complex or through the TNFR1-RIP-RAIDD-caspase 2 complex. Alternatively, Msh6-dependent apoptosis may proceed through the FasL-Fas pathway via the Fas-FADD-Caspase 8 complex, known as the DISC. The following experiments tested the role of the death receptor proteins in Msh6-dependent apoptosis after UVB.

Results

TNF-α has no role in UVB-induced apoptosis in *Msh6*$^{+/+}$ and *Msh6*$^{-/-}$ murine embryonic fibroblasts

TNF-α is a protein ligand in the death receptor apoptotic pathway. The membrane-bound form of TNF-α is cleaved to generate a secreted 17 kDa mature protein and binding of either the soluble TNF-α protein or the membrane-bound protein results in trimerization of the receptor, TNF-R. In order to elucidate the role of TNF-α in Msh6-dependent apoptosis after UVB-induced DNA damage, western blot analysis was performed. Levels of TNF-α precursor were equivalent in *Msh6*$^{+/+}$ and *Msh6*$^{-/-}$ MEFs, both untreated and after UVB. This data indicates that the TNF-α precursor protein does not play a role in Msh6-dependent apoptosis after UVB (Fig. 6-2 A).

Note: densitometry was performed and the values obtained were normalized to the loading control only. Levels of the mature TNF-α protein were similar between untreated and treated *Msh6*$^{+/+}$ and *Msh6*$^{-/-}$ MEFs. Overall, there were very low levels of the mature TNF-α protein in untreated *Msh6*$^{+/+}$ and *Msh6*$^{-/-}$ MEFs and after UVB treatment. At 4 hours post-UVB mature TNF-α peaked and were increased 7-fold over untreated levels in both *Msh6*$^{+/+}$ and *Msh6*$^{-/-}$ MEFs, although the levels were still quite low. Analysis shows that there were no appreciable differences in mature TNF-α levels after UVB treatment between *Msh6*$^{+/+}$ and *Msh6*$^{-/-}$ MEFs (Fig. 6-2 B).

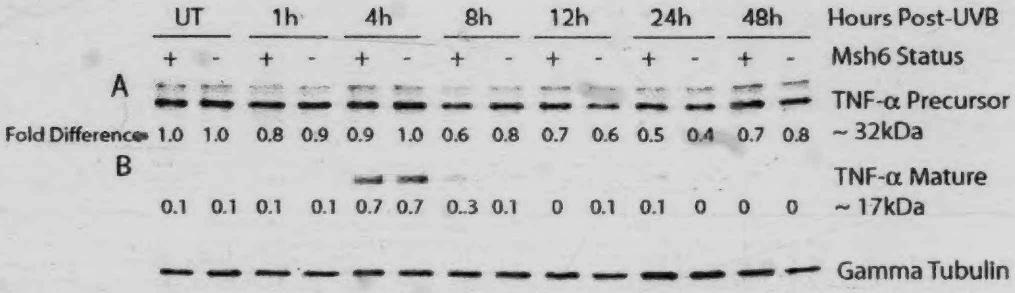
UT
1h
4h
8h
12h
24h
48h
Hours Post-UVB
+ - + - + - + - + - + - + -
Msh6 Status
A
TNF-α Precursor
~ 32kDa
Fold Difference
1.0 1.0 0.8 0.9 0.9 1.0 0.6 0.8 0.7 0.6 0.5 0.4 0.7 0.8
B
TNF-α Mature
~ 17kDa
0.1 0.1 0.1 0.1 0.7 0.7 0.3 0.1 0 0.1 0.1 0 0 0
Gamma Tubulin

Figure 6-2: A) TNF-α precursor and B) TNF-α mature protein levels after UVB radiation

Protein extracts from $\mathit{Msh6}^{+/+}$ and $\mathit{Msh6}^{-/-}$ MEFs irradiated with 300J/m^2 UVB were analyzed by western blot. Gamma tubulin was used as a loading control. Densitometry was used to quantify the protein levels which were normalized to the loading control and then to the $\mathit{Msh6}^{+/+}$ untreated protein level to obtain the fold difference in protein levels for each lane for TNF-α precursor. **Protein levels were normalized to the loading control only for mature TNF-α.**

TNF-R1 has no role in UVB-induced apoptosis in *Msh6*$^{+/+}$ and *Msh6*$^{-/-}$ murine embryonic fibroblasts

TNF-R1 is the prototypical member of the TNF receptor family and binds the ligand TNFα. In order to confirm the lack of Msh6-dependent differences seen in the response to UVB in TNFα levels, TNF-R1 levels were also checked by immunoblotting. Analysis shows that there were no appreciable differences in TNF-R1 levels in untreated cells and over time after UVB treatment in *Msh6*$^{+/+}$ and *Msh6*$^{-/-}$ MEFs (Fig. 6-3). There is no support for a role for TNF-R1 in Msh6-dependent apoptosis after treatment with UVB.

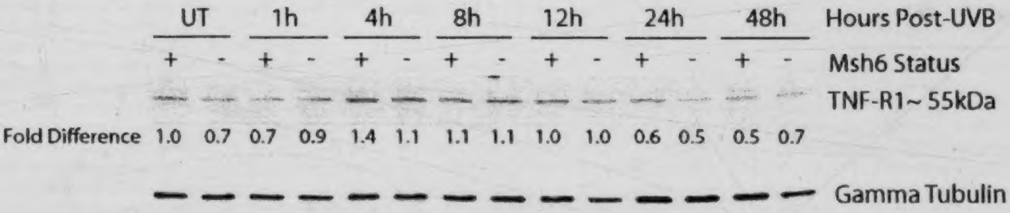
UT 1h 4h 8h 12h 24h 48h
Hours Post-UVB
+ - + - + - + - + - + - + -
Msh6 Status
TNF-R1~ 55kDa
Fold Difference 1.0 0.7 0.7 0.9 1.4 1.1 1.1 1.1 1.0 1.0 0.6 0.5 0.5 0.7
Gamma Tubulin

Figure 6-3: TNF-R1 protein levels after UVB radiation

Protein extracts from *Msh6*$^{+/+}$ and *Msh6*$^{-/-}$ MEFs irradiated with 300J/m^2 UVB were analyzed by western blot. Gamma tubulin was used as a loading control. Densitometry was used to quantify the protein levels which were normalized to the loading control and then to the *Msh6*$^{+/+}$ untreated protein level to obtain the fold difference in protein levels for each lane.

TRADD has no role in UVB-induced apoptosis in *Msh6*$^{+/+}$ and *Msh6*$^{-/-}$ murine embryonic fibroblasts

TRADD is an accessory protein with a death domain that functions to recruit RIP and FADD to the TNF-R1 death-inducing complex. To determine whether TRADD has a role in Msh6-dependent apoptosis in response to UVB, western blot analysis was performed and shows that there were no appreciable differences in TRADD protein levels in untreated cells and over time after UVB treatment in *Msh6*$^{+/+}$ and *Msh6*$^{-/-}$ MEFs, thus indicating that TRADD has no role in UVB-induced apoptosis dependent on Msh6 (Fig. 6-4).

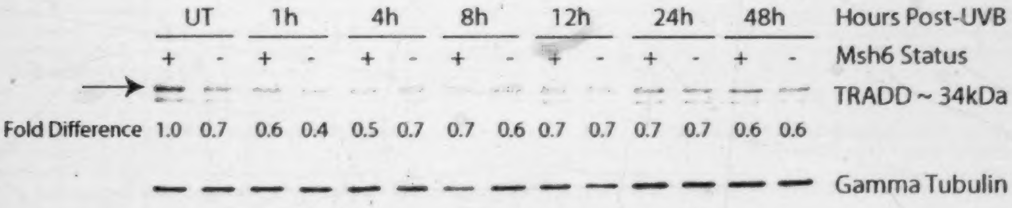
UT 1h 4h 8h 12h 24h 48h
Hours Post-UVB
+ - + - + - + - + - + - + -
Msh6 Status
TRADD ~ 34kDa
Fold Difference 1.0 0.7 0.6 0.4 0.5 0.7 0.7 0.6 0.7 0.7 0.7 0.7 0.6 0.6
Gamma Tubulin

Figure 6-4: TRADD protein levels after UVB radiation

Protein extracts from *Msh6*$^{+/+}$ and *Msh6*$^{-/-}$ MEFs irradiated with 300J/m^2 UVB were analyzed by western blot. Gamma tubulin was used as a loading control. Densitometry was used to quantify the protein levels which were normalized to the loading control and then to the *Msh6*$^{+/+}$ untreated protein level to obtain the fold difference in protein levels for each lane.

RIP has no role in UVB-induced apoptosis in *Msh6*$^{+/+}$ and *Msh6*$^{-/-}$ murine embryonic fibroblasts

RIP is an accessory protein that can form a complex with TNF-R1 and TRADD or with Fas and RAIDD to induce the caspase cascade through caspase 2. I undertook western blot procedures to elucidate if there is a role for RIP in Msh6-dependent apoptosis after UVB treatment of MEFs. Protein analysis shows that there were no substantial differences in RIP levels in *Msh6*$^{+/+}$ and *Msh6*$^{-/-}$ MEFs, both untreated and over time after UVB treatment (Fig. 6-5). This shows that RIP has no involvement in Msh6-dependent apoptosis after UVB.

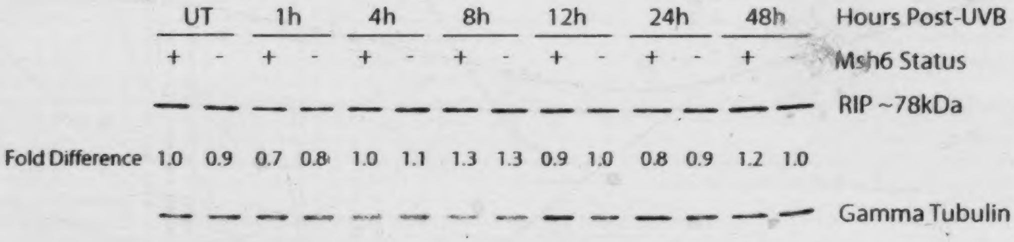
UT
1h
4h
8h
12h
24h
48h
Hours Post-UVB
+ - + - + - + - + - + - + -
Msh6 Status
RIP ~78kDa
Fold Difference 1.0 0.9 0.7 0.8 1.0 1.1 1.3 1.3 0.9 1.0 0.8 0.9 1.2 1.0
Gamma Tubulin

Figure 6-5: RIP protein levels after UVB radiation

Protein extracts from *Msh6*$^{+/+}$ and *Msh6*$^{-/-}$ MEFs irradiated with 300J/m^2 UVB were analyzed by western blot. Gamma tubulin was used as a loading control. Densitometry was used to quantify the protein levels which were normalized to the loading control and then to the *Msh6*$^{+/+}$ untreated protein level to obtain the fold difference in protein levels for each lane.

Fas has no role in UVB-induced apoptosis in *Msh6*$^{+/+}$ and *Msh6*$^{-/-}$ murine embryonic fibroblasts

Fas or CD95 is a membrane-bound receptor protein belonging to the TNF-receptor family. Western blots were utilized to study the role of Fas protein in Msh6-dependent apoptosis after UVB. Protein analysis shows that there was no substantial difference in the levels of Fas in untreated *Msh6*$^{+/+}$ and *Msh6*$^{-/-}$ MEFs. After UVB treatment, Fas protein levels decreased by half in *Msh6*$^{+/+}$ and *Msh6*$^{-/-}$ MEFs compared to the untreated level and remained equal in both cell lines over time (Fig. 6-6). This illustrates that Fas has no role in UVB-induced Msh6-dependent apoptosis.

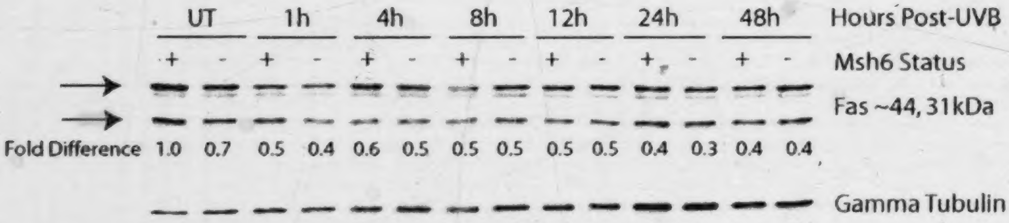
UT
1h
4h
8h
12h
24h
48h
Hours Post-UVB
+ - + - + - + - + - + - + -
Msh6 Status
Fas ~44, 31kDa
Fold Difference 1.0 0.7 0.5 0.4 0.6 0.5 0.5 0.5 0.5 0.5 0.4 0.3 0.4 0.4
Gamma Tubulin

Figure 6-6: Fas protein levels after UVB radiation

Protein extracts from *Msh6*$^{+/+}$ and *Msh6*$^{-/-}$ MEFs irradiated with 300J/m^2 UVB were analyzed by western blot. Gamma tubulin was used as a loading control. Densitometry was used to quantify the protein levels which were normalized to the loading control and then to the *Msh6*$^{+/+}$ untreated protein level to obtain the fold difference in protein levels for each lane.

FADD has no role in UVB-induced apoptosis in *Msh6*$^{+/+}$ and *Msh6*$^{-/-}$ murine embryonic fibroblasts

FADD is an accessory protein with a death domain that is critical for TNFR1- and Fas-induced apoptosis. FADD binds caspase 8 to the receptor complexes, thus causing autocatalytic cleavage of procaspase 8 into cleaved caspase 8. FADD is phosphorylated at serine 194 in humans (serine 191 in mouse) at the G_2/M transition of the cell cycle and FADD phosphorylated at serine 194 is associated with chemosensitivity of prostate cancer cells (Shimada et al. 2004). Protein analysis was used to study the role of FADD phosphorylated at serine 191 (FADD-pSer191) in Msh6-dependent apoptosis after UVB. Data shows that there was no substantial difference in the levels of FADD-pSer191 protein in untreated *Msh6*$^{-/-}$ MEFs compared to untreated wildtype MEFs. After treatment with UVB, levels of FADD-pSer191 remained equivalent in *Msh6*$^{+/+}$ and *Msh6*$^{-/-}$ MEFs and there was no substantial change in the levels of FADD-pSer191 over time in either genotype (Fig. 6-7). This shows that FADD-pSer191 does not play a part in UVB-induced Msh6-dependent apoptosis.

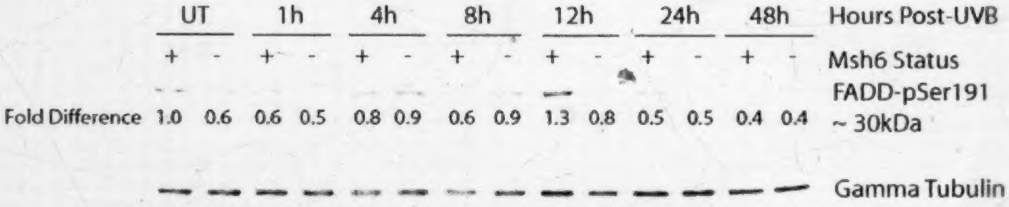

Figure 6-7: FADD-pSer191 protein levels after UVB radiation

Protein extracts from *Msh6*$^{+/+}$ and *Msh6*$^{-/-}$ MEFs irradiated with 300J/m^2 UVB were analyzed by western blot. Gamma tubulin was used as a loading control. Densitometry was used to quantify the protein levels which were normalized to the loading control and then to the *Msh6*$^{+/+}$ untreated protein level to obtain the fold difference in protein levels for each lane.

Caspase 10 has no role in UVB-induced apoptosis in *Msh6*$^{+/+}$ and *Msh6*$^{-/-}$ murine embryonic fibroblasts

Caspase 10 is a protein in the extrinsic pathway of apoptosis that has either a redundant function, or an independent function to that of caspase 8, depending on cell type. In order to elucidate the role of caspase 10 in the Msh6-dependent apoptotic response, protein analysis was performed and shows that untreated *Msh6*$^{-/-}$ MEFs consistently had 40% less pro-caspase 10 protein than did untreated *Msh6*$^{+/+}$ MEFs. After treatment with UVB, there was no appreciable change in the levels of pro-caspase 10 over time in either genotype of MEFs and the levels of pro-caspase 10 were equal between *Msh6*$^{+/+}$ and *Msh6*$^{-/-}$ MEFs over time (Fig. 6-8 A).

The level of cleaved caspase 10 protein in untreated *Msh6*$^{-/-}$ MEFs was consistently almost 2-fold greater than in untreated *Msh6*$^{+/+}$ MEFs. Cleaved caspase 10 levels increased in both *Msh6*$^{+/+}$ and *Msh6*$^{-/-}$ MEFs at 1 hour after UVB treatment. In *Msh6*$^{+/+}$ MEFs the level of cleaved caspase 10 was highest at 4 hours post-UVB and remained higher than baseline levels throughout the timecourse. Cleaved caspase 10 levels were approximately 2-fold less in *Msh6*$^{-/-}$ MEFs at 4 hours after UVB. There was no appreciable difference in the levels of cleaved caspase 10 between Msh6$^{+/+}$ and *Msh6*$^{-/-}$ MEFs at 1 hour and from 8 to 48 hours post-UVB (Fig. 6-8 B). Thus, it does not appear likely that caspase 10 has a role in UVB-induced Msh6-dependent apoptosis.

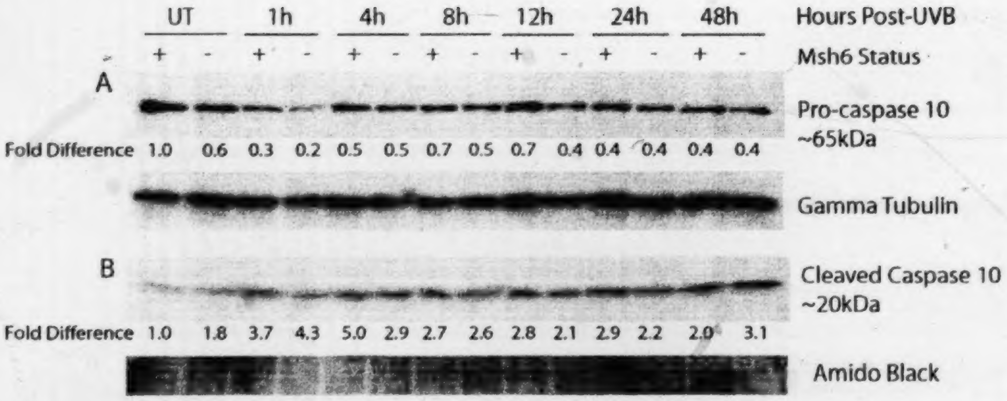
UT
1h
4h
8h
12h
24h
48h
Hours Post-UVB
+ - + - + - + - + - + - + -
Msh6 Status
A
Pro-caspase 10
~65kDa
Fold Difference 1.0 0.6 0.3 0.2 0.5 0.5 0.7 0.5 0.7 0.4 0.4 0.4 0.4 0.4
Gamma Tubulin
B
Cleaved Caspase 10
~20kDa
Fold Difference 1.0 1.8 3.7 4.3 5.0 2.9 2.7 2.6 2.8 2.1 2.9 2.2 2.0 3.1
Amido Black

Figure 6-8: A) pro-caspase 10 and B) cleaved caspase 10 protein levels after UVB radiation

Protein extracts from *Msh6*$^{+/+}$ and *Msh6*$^{-/-}$ MEFs irradiated with 300J/m^2 UVB were analyzed by western blot. Gamma tubulin and amido black were used as loading controls. Densitometry was used to quantify the protein levels which were normalized to the loading control and then to the *Msh6*$^{+/+}$ untreated protein level to obtain the fold difference in protein levels for each lane.

Caspase 8 has no role in UVB-induced apoptosis in *Msh6*$^{+/+}$ and *Msh6*$^{-/-}$ murine embryonic fibroblasts

Caspase 8 is activated by the TNFR1 or the Fas pathways of apoptosis. Upon binding in a complex with the receptors and accessory proteins in these pathways, pro-caspase 8 is converted to its active form and induces apoptosis by triggering the caspase cascade or strengthens the apoptotic signal by causing cleavage of pro-apoptotic Bid. I wanted to investigate the role of caspase 8 in the Msh6-dependent apoptotic cascade after UVB-induced DNA damage. Western blot analysis shows that untreated *Msh6*$^{-/-}$ MEFs consistently had almost 2-fold more pro-caspase 8 protein than did untreated *Msh6*$^{+/+}$ MEFs. After UVB irradiation, levels of pro-caspase 8 increased slightly until 8 hours post-UVB and then decreased back to control levels for the remainder of the timecourse in *Msh6*$^{+/+}$ MEFs. In *Msh6*$^{-/-}$ MEFs there is no appreciable change in pro-caspase 8 levels until 8 hours post-UVB, when protein levels decreased to near wildtype control levels (1.2-fold) and decline gradually to 0.7-fold of wildtype control. Over time after UVB treatment there is no substantial difference in the levels of pro-caspase 8 protein in *Msh6*$^{+/+}$ MEFs versus *Msh6*$^{-/-}$ MEFs (Fig. 6-9 A).

Similar to pro-caspase 8, untreated *Msh6*$^{-/-}$ MEFs consistently had almost 2-fold more cleaved caspase 8 protein than did untreated *Msh6*$^{+/+}$ MEFs. In *Msh6*$^{+/+}$ MEFs, the levels of cleaved caspase 8 increased at 1 hour post-UVB and gradually declined over the timecourse. However, even at 48 hours post-UVB the level of cleaved caspase 8 was still 1.6-fold higher than the control level in *Msh6*$^{+/+}$ MEFs. In *Msh6*$^{-/-}$ MEFs, cleaved caspase 8 levels increased at 4 hours post-UVB and slowly declined over time to control levels.

There were no appreciable differences in the levels of cleaved caspase 8 between *Msh6*$^{+/+}$ and *Msh6*$^{-/-}$ MEFs and cleaved caspase 8 levels did not fluctuate substantially (Fig. 6-9 B).

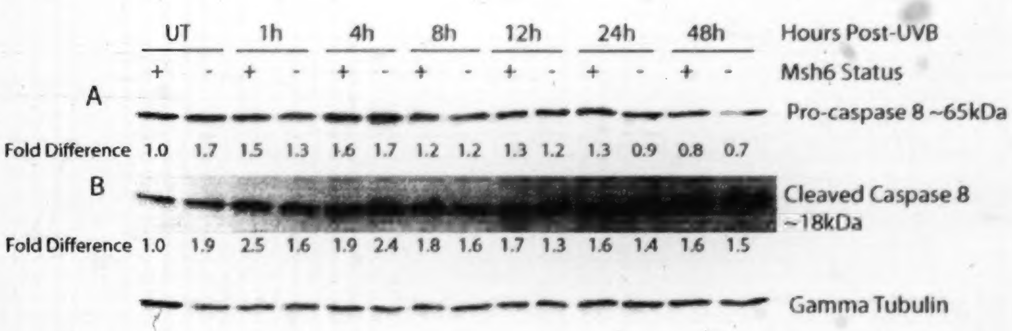
UT
1h
4h
8h
12h
24h
48h
Hours Post-UVB
+ - + - + - + - + - + - + -
Msh6 Status
A
Pro-caspase 8 ~65kDa
Fold Difference 1.0 1.7 1.5 1.3 1.6 1.7 1.2 1.2 1.3 1.2 1.3 0.9 0.8 0.7
B
Cleaved Caspase 8 ~18kDa
Fold Difference 1.0 1.9 2.5 1.6 1.9 2.4 1.8 1.6 1.7 1.3 1.6 1.4 1.6 1.5
Gamma Tubulin

Figure 6-9: A) pro-caspase 8 and B) cleaved caspase 8 protein levels after UVB radiation

Protein extracts from *Msh6*$^{+/+}$ and *Msh6*$^{-/-}$ MEFs irradiated with 300J/m^2 UVB were analyzed by western blot. Gamma tubulin was used as a loading control. Densitometry was used to quantify the protein levels which were normalized to the loading control and then to the *Msh6*$^{+/+}$ untreated protein level to obtain the fold difference in protein levels for each lane.

Apoptosis levels after caspase 8 inhibitor in Msh6$^{+/+}$ and $^{-/-}$ murine embryonic fibroblasts

Z-IETD-FMK, a specific and irreversible inhibitor of caspase 8 was used to study the effect of caspase 8 on levels of apoptosis in *Msh6*$^{+/+}$ and *Msh6*$^{-/-}$ MEFs after UVB treatment. In Figure 6-10, the relative levels of apoptosis 24 hours after treatment with UVB and Z-IETD-FMK are shown. Apoptosis levels in *Msh6*$^{+/+}$ and *Msh6*$^{-/-}$ MEFs treated with 300J/m^2 UVB alone were set to 100%.Cells treated with UVB and caspase 8 inhibitor were normalized to their corresponding genotype treated with UVB alone. Figure 6-10 shows that apoptosis in *Msh6*$^{+/+}$ MEFs decreased to an average of approximately 55%, while apoptosis in *Msh6*$^{-/-}$ MEFs decreased to an average of just 80% after treatment with UVB and Z-IETD-FMK ($p<0.05$). This illustrates that inhibition of caspase 8 caused significantly lower levels of apoptosis in *Msh6*$^{+/+}$ MEFs compared to *Msh6*$^{-/-}$ MEFs after UVB and shows that *Msh6* knockout MEFs are less affected by inhibition of caspase 8 after UVB (Fig. 6-10).

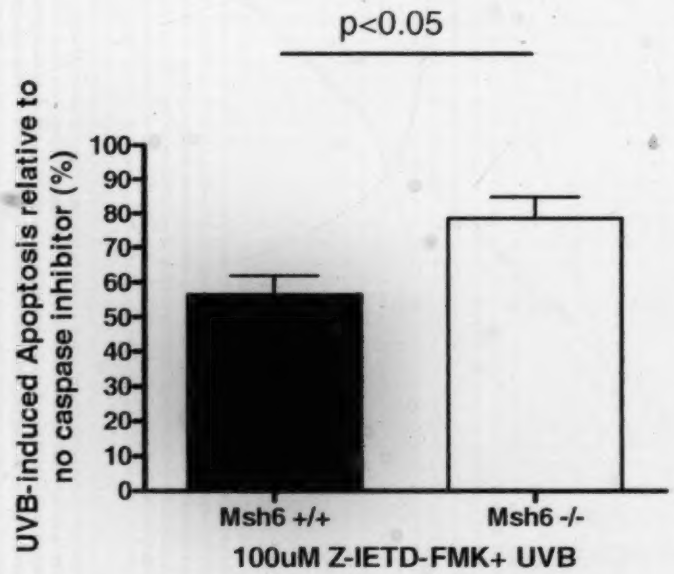

Figure 6-10: Relative decrease in apoptosis levels 24 hours after treatment with Z-IETD-FMK, a specific inhibitor of caspase 8

Msh6$^{+/+}$ and *Msh6*$^{-/-}$ MEFs treated with 300J/m^2 UVB alone or in combination with Z-IETD-FMK were analyzed by flow cytometry after Annexin V-PI staining. Apoptosis levels of cells treated with UVB alone are set to 100 and apoptosis levels of cells treated with Z-IETD-FMK in combination with UVB are represented as a percentage of this value. The difference between the relative apoptosis of *Msh6*$^{+/+}$ and *Msh6*$^{-/-}$ MEFs is significant ($p<0.05$, n=4).

Caspase 3 levels after caspase 8 inhibitor in *Msh6*$^{+/+}$ and *Msh6*$^{-/-}$ murine embryonic fibroblasts

Z-IETD-FMK, a specific and irreversible inhibitor of caspase 8 was used to study the contribution of caspase 8 on cell death in *Msh6*$^{+/+}$ and *Msh6*$^{-/-}$ MEFs 24 hours after UVB treatment. Cleavage of caspase 3 was used as a measure of cell death on the protein level. In untreated cells there was no cleavage of caspase 3 in either *Msh6*$^{+/+}$ or *Msh6*$^{-/-}$ MEFs. 24 hours after treatment with 300J/m^2 UVB cleaved caspase 3 levels were equal in *Msh6*$^{+/+}$ and *Msh6*$^{-/-}$ MEFs, similar to the findings in figure 4-11 at 24 hours post-UVB. After treatment with UVB and Z-IETD-FMK, there was no appreciable difference in the amount of cleaved caspase 3 protein M*sh6*$^{+/+}$ MEFs compared to the M*sh6*$^{+/+}$ MEFs UVB control. In *Msh6*$^{-/-}$ MEFs there was 2-fold more cleaved caspase 3 after treatment with UVB and Z-IETD-FMK compared to the M*sh6*$^{-/-}$MEFs UVB control. After treatment with UVB and Z-IETD-FMK there was also 2-fold more cleaved caspase 3 in *Msh6*$^{-/-}$ MEFs compared to M*sh6*$^{+/+}$ MEFs (Fig. 6-11), consistent with the results in figure 6-10 where there was more apoptosis in *Msh6*$^{-/-}$ MEFs compared to M*sh6*$^{+/+}$ MEFs after UVB . This confirms that *Msh6* knockout MEFs are less affected by inhibition of caspase 8 after UVB.

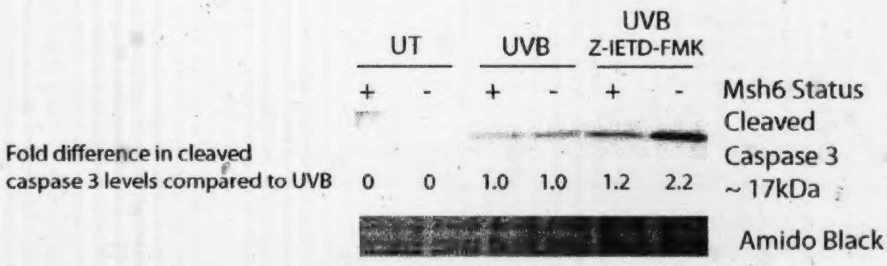
UVB
UT
UVB
Z-IETD-FMK
+
-
+
-
+
-
Msh6 Status
Cleaved
Caspase 3
~ 17kDa
Fold difference in cleaved
caspase 3 levels compared to UVB
0
0
1.0
1.0
1.2
2.2
Amido Black

Figure 6-11: Cleaved caspase 3 protein levels 24 hours after UVB radiation using Z-IETD-FMK, a specific inhibitor of caspase 8

Protein extracts from $Msh6^{+/+}$ and $Msh6^{-/-}$ MEFs treated with $300 J/m^2$ UVB alone or in combination with Z-IETD-FMK were analyzed by western blot. Amido black was used as a loading control. Densitometry was used to quantify the protein levels which were normalized to the loading control and then to the UVB control protein level for each corresponding genotype to obtain the fold difference in protein levels for each lane.

Discussion

Previous work in our laboratory and by other groups has shown evidence for a role for MMR in the response to UVB-induced DNA damage. It is hypothesized that MMR does not remove UVB-induced lesions in DNA (cyclobutane pyrimidine dimers and 6-4 photoproducts) but the precise role of MMR in the damage response after UV radiation is currently unknown [reviewed in (Young et al. 2003)]. After UVB-induced DNA damage, loss of MMR leads to decreased G2/M cell cycle arrest and apoptosis *in vitro* and earlier onset of tumorigenesis *in vivo* (Meira et al. 2002; Yoshino et al. 2002; Peters et al. 2003; Young et al. 2003; Young et al. 2004; Narine et al. 2007; Young et al. 2007).

I hypothesized that Msh6-dependent apoptosis may be acting through the TNFR1 or Fas death receptors post-UVB. Specifically, Msh6 may play a role in transducing the apoptotic signal after cellular insult by UVB through the TNFR1 death receptor-mediated apoptotic pathway via TNFR1-RIP-RAIDD-caspase 2 complex. Alternatively, apoptosis may occur via FADD, which has been found in a complex with MMR protein MLH1, thus inducing the Fas death receptor pathway of apoptosis through caspase 8, or another TNFR1 death receptor pathway of apoptosis through caspase 8.

There is an established role for members of the TNF superfamily in UV-induced apoptosis, including TNFα-TNFR1 and FasL-Fas/CD95 (Kibitel et al. 1998; Hill et al. 1999; Zhuang et al. 1999). TNFR1 is constitutively expressed in most tissue types. It is responsible for mediating the majority of the TNFα signal and is involved in UV-induced apoptosis [reviewed in (Guzman et al. 2003; Chow and Tron 2005)]. Trefzer et al. (1993)

showed that UVB-irradiation of human keratinocytes led to release of TNFα (Trefzer et al. 1993). It has also been demonstrated that TNFα upregulation results from UV and leads to keratinocyte apoptosis after TNFα activates its receptor, TNFR1 (Kock et al. 1990; Kibitel et al. 1998; Zhuang et al. 1999).

Given the role of TNFα-TNFR1 in the UV-induced apoptotic response and the role of MMR in UV-induced apoptosis, I investigated the potential involvement of the TNFα-TNFR1 pathway in Msh6-dependent apoptosis after UVB-induced DNA damage. Protein analysis showed that although there were no appreciable differences in TNFα precursor protein between *Msh6*$^{+/+}$ and *Msh6*$^{-/-}$ MEFs after UVB (Fig. 6-2 A), there was a UVB-induced upregulation of the mature TNFα protein in these cells (Fig. 6-2 B). There were very low levels of mature TNFα in untreated cells and at all timepoints after treatment with UVB, except at 4 hours post-UVB. At this timepoint mature or soluble TNFα protein levels spiked in both *Msh6*-proficient and –deficient MEFs, suggesting that both cell lines underwent a UVB-induced increase in mature TNFα. After this increase at 4 hours after treatment, mature TNFα levels returned to basal levels, indicating that there is no role for TNFα in Msh6-dependent apoptosis after UVB radiation (Fig. 6-2 B).

Protein analysis of TNFR1, the receptor to TNFα, showed that there were no substantial differences between *Msh6*$^{+/+}$ and *Msh6*$^{-/-}$ MEFs with respect to the amount of this protein in untreated MEFs or after UVB treatment. Furthermore, the levels of TNFR1 did not change appreciably from basal levels after treatment (Fig. 6-3). Thus, although there was a spike in mature TNFα in both *Msh6*$^{+/+}$ and *Msh6*$^{-/-}$ MEFs after UVB, there was no similar pattern in the levels of the receptor protein TNFR1 to transduce the apoptotic signal.

TRADD specifically binds to TNFR1 and its putative function is to recruit RIP to TNFR1. FADD may also be recruited to the complex. This TNFR1-TRADD-RIP-FADD complex induces the caspase cascade via activation of caspase 8. Alternatively, TNFR1 may initiate apoptosis through complex formation with RIP and RAIDD to activate caspase 2 and induce apoptosis (Guzman et al. 2003). Western blot analysis shows that the proteins TRADD and RIP have no role in Msh6-dependent UVB-induced apoptosis (Fig. 6-4 and 6-5). This is consistent with a lack of involvement of caspase 2 (see chapter 5) and the lack of differences in caspase 8 protein levels between *Msh6*$^{+/+}$ and *Msh6*$^{-/-}$ MEFs (Fig. 6-8) in Msh6-dependent UVB-induced apoptosis.

Another main death receptor pathway of apoptosis triggered by UVB is the FasL-Fas pathway. Fas is ubiquitously expressed, while FasL expression is more restricted. Expression of both ligand and receptor is upregulated by exposure to UV (Muller et al. 1998; Hill et al. 1999). Western blots probing for FasL were undertaken, but were unsuccessful. Protein analysis performed for the receptor Fas showed that there were no Msh6-dependent changes in Fas levels after UVB, indicating that there is no role for Fas in Msh6-dependent apoptosis after UVB irradiation (Fig. 6-6).

FADD is an adaptor protein that associates with Fas in order to bind pro-caspase 8 to the Fas-FADD complex (Chinnaiyan et al. 1995). FADD localizes to the nucleus in several cell lines and its export to the cytoplasm depends on phosphorylation at serine 194. Within the nucleus FADD was shown to interact with MBD4, a genome surveillance/DNA repair protein which excises thymine from GT mismatches in methylated chromatin. Also found in a complex with FADD was the MMR protein MLH1, an interacting partner of MBD4 (Screaton et al. 2003). This data and the role of FADD as an accessory protein in the extrinsic Fas pathway of apoptosis led me to investigate if FADD has a role in Msh6-induced apoptosis after UVB. Results show that FADD phosphorylation at serine 191 in mouse (the amino acid equivalent to serine 194 of human FADD) had no role in Msh6-induced apoptosis after UVB treatment, as there were no appreciable differences in the levels of this protein between *Msh6*$^{+/+}$ and *Msh6*$^{-/-}$ MEFs after treatment (Fig. 6-7).

As mentioned above, the role of FADD in the Fas pathway is to bind pro-caspase 8 to the Fas-FADD complex via the death domains on each molecule. This complex of Fas-FADD-caspase 8 is known as the DISC (death-inducing signaling complex), first described in this pathway (Kischkel et al. 1995). Caspase 10 is also recruited to the DISC (Wang 2001). Caspase 8 and 10 are initiator caspases with DEDs (Fernandes-Alnemri et al. 1996; Vincenz and Dixit 1997). Despite these similarities it remains controversial whether caspase 10 can functionally substitute for caspase 8 in the DISC to trigger apoptosis (Vincenz and Dixit 1997; Kischkel et al. 2001; Wang et al. 2001; Sprick et al. 2002; Milhas et al. 2005). The pro-apoptotic protein Bid has distinct cleavage sites for both caspases, suggestive of distinct roles for these two caspases (Fischer et al. 2005). Because of the similarities and the differences to caspase 8, I wanted to explore the role of caspase 10 in UVB-induced apoptosis in *Msh6*$^{+/+}$ and *Msh6*$^{-/-}$ MEFs. Cleaved caspase 10 is upregulated in both cell lines after UVB. However, I found that there were no appreciable differences in the levels of pro- and cleaved caspase 10 between *Msh6*$^{+/+}$ and *Msh6*$^{-/-}$ MEFs after UVB treatment (Fig. 6-8).

The recruitment of pro-caspase 8 within the DISC leads to autocatalytic processing of pro-caspase 8 into active caspase 8, which directly activates downstream effector caspases -3, -6 and -7, thus executing apoptosis (Muller et al. 1998). Caspase 8 protein levels were analyzed in UVB-treated and untreated *Msh6*$^{+/+}$ and *Msh6*$^{-/-}$ MEFs. Untreated *Msh6*$^{-/-}$ MEFs have approximately 2-fold more pro-caspase 8 and cleaved caspase 8 protein compared to untreated *Msh6*$^{+/+}$ MEFs. This may be attributed to the fact that *Msh6*-deficient MEFs grew much more quickly than Msh6-proficient MEFs. Perhaps the apoptotic proteins in *Msh6*$^{-/-}$ MEFs were upregulated because of cellular stress despite attempts to reduce this. Over time after UVB treatment there was no substantial difference in the levels of pro-caspase 8 protein in *Msh6*$^{+/+}$ versus *Msh6*$^{-/-}$ MEFs (Fig. 6-9 A), indicating that pro-caspase 8 is not likely involved in Msh6-dependent apoptosis after UVB irradiation. Cleaved caspase 8 levels increased early in both *Msh6*$^{+/+}$ and *Msh6*$^{-/-}$ MEFs after UVB treatment. There were no appreciable differences in the levels of cleaved caspase 8 between *Msh6*$^{+/+}$ and *Msh6*$^{-/-}$ MEFs and cleaved caspase 8 protein levels did not fluctuate substantially, suggesting that cleaved caspase 8 has no role in Msh6-dependent apoptosis after UVB radiation (Fig. 6-9 B).

The significant difference in the levels of UVB-induced apoptosis between *Msh6*-proficient and –deficient MEFs in the presence of Z-IETD-FMK, a peptide inhibitor of caspase 8 was a surprising result. In figure 6-10, the levels of apoptosis in the presence of Z-IETD-FMK decreased to 55% in *Msh6*-proficient cells and to just 80% observed in *Msh6*-deficient cells, suggestive of a role for caspase 8 in Msh6-dependent apoptosis after UVB. Problems with specificity of peptide caspase inhibitors have been documented in the literature (Berger et al. 2006; Timmer and Salvesen 2007). A recent study by McStay et al. (2007) explored the specificities of peptide substrates and inhibitors for a range of caspases and found that several peptide inhibitors lack specificity to their target caspase. Using Jurkat cells, they found that overall Z-IETD-FMK was one of the most effective caspase inhibitors after UV radiation via its specific inhibition of caspase 8. Based on their findings, the authors cautioned against using these reagents alone to draw conclusions regarding the roles of the individual caspases (McStay et al. 2007). My experiments utilized caspase inhibitors as one of several methods to assess caspase involvement in Msh6-dependent apoptosis after UVB-induced DNA damage. The significant difference in apoptosis levels between *Msh6*-proficient and –deficient MEFs indicates an ability of Z-IETD-FMK to be more protective of apoptosis in cells with intact Msh6, not cells lacking Msh6 (Fig. 6-10). If the use of Z-IETD-FMK targets the peptide activity of caspase 8 perhaps this assay better illustrates caspase 8 activity on the cellular level compared to western blot analysis that relies upon global levels of protein and are limited to the reagents used to visualize this protein. Based on this assay, it appears that caspase 8 may have a role in Msh6-dependent apoptosis after UVB radiation. However, further studies must be completed to draw any conclusions.

Further to the above assay on global levels of apoptosis after inhibition of caspase 8, I used the irreversible inhibitor of caspase 8, Z-IETD-FMK, in order to assess the contribution of caspase 8 on cell death via cleavage of caspase 3 in *Msh6*$^{+/+}$ and *Msh6*$^{-/-}$ MEFs after UVB treatment (Fig. 6-11). 24 hours after treatment with UVB and Z-IETD-FMK there was a 2-fold increase in cleaved caspase 3 in *Msh6*$^{-/-}$ MEFs compared to M*sh6*$^{+/+}$ MEFs, corroborating the results in figure 6-10 showing more apoptosis in *Msh6*$^{-/-}$ MEFs compared to M*sh6*$^{+/+}$ MEFs after UVB and Z-IETD-FMK treatment . This is additional evidence that caspase 8 may have a role in Msh6-dependent apoptosis after UVB-induced apoptosis. This may occur through the mitochondrial pathway of apoptosis. A recent study by Guerrero et al. (2007) showed that caspase 9 activation after γ-irradiation led to activation of caspase 8, consistent with a previous study indicating that caspase 8 can be processed downstream of caspase 9 (Slee et al. 1999; Guerrero et al. 2007). Based upon their findings, Sitailo et al. described a proposed signaling pathway after UV radiation; UV activates the mitochondrial pathway of apoptosis, resulting in activation of caspase 9 which in turn activates caspase 3. Caspase 3 may directly or indirectly activate caspase 8 (Sitailo et al. 2002). However, as stated above, further studies are necessary to draw conclusions.

Overall, it appears that there is no role for TNFα-TNFR or FasL-Fas death receptor pathways in Msh6-dependent apoptosis after UVB-induced DNA damage in primary mouse embryonic fibroblasts on the protein level. However, further exploration into the role of caspase 8 in Msh6-dependent apoptosis after UVB radiation is important.

References

Baud, V. and M. Karin (2001). "Signal transduction by tumor necrosis factor and its relatives." Trends Cell Biol **11**(9): 372-7.

Berger, A. B., K. B. Sexton and M. Bogyo (2006). "Commonly used caspase inhibitors designed based on substrate specificity profiles lack selectivity." Cell Res **16**(12): 961-3.

Chinnaiyan, A. M., K. O'Rourke, M. Tewari and V. M. Dixit (1995). "FADD, a novel death domain-containing protein, interacts with the death domain of Fas and initiates apoptosis." Cell **81**(4): 505-12.

Chow, J. and V. A. Tron (2005). "Molecular aspects of ultraviolet radiation-induced apoptosis in the skin." J Cutan Med Surg **9**(6): 289-95.

Davis, T. W., C. Wilson-Van Patten, M. Meyers, K. A. Kunugi, S. Cuthill, C. Reznikoff, C. Garces, C. R. Boland, T. J. Kinsella, R. Fishel and D. A. Boothman (1998). "Defective expression of the DNA mismatch repair protein, MLH1, alters G2-M cell cycle checkpoint arrest following ionizing radiation." Cancer Res **58**(4): 767-78.

Devin, A., Y. Lin and Z. G. Liu (2003). "The role of the death-domain kinase RIP in tumour-necrosis-factor-induced activation of mitogen-activated protein kinases." EMBO Rep **4**(6): 623-7.

Duan, H. and V. M. Dixit (1997). "RAIDD is a new 'death' adaptor molecule." Nature **385**(6611): 86-9.

Duckett, D. R., J. T. Drummond, A. I. Murchie, J. T. Reardon, A. Sancar, D. M. Lilley and P. Modrich (1996). "Human MutSalpha recognizes damaged DNA base pairs containing O6-methylguanine, O4-methylthymine, or the cisplatin-d(GpG) adduct." Proc Natl Acad Sci U S A **93**(13): 6443-7.

Fernandes-Alnemri, T., R. C. Armstrong, J. Krebs, S. M. Srinivasula, L. Wang, F. Bullrich, L. C. Fritz, J. A. Trapani, K. J. Tomaselli, G. Litwack and E. S. Alnemri (1996). "In vitro activation of CPP32 and Mch3 by Mch4, a novel human apoptotic cysteine protease containing two FADD-like domains." Proc Natl Acad Sci U S A **93**(15): 7464-9.

Fischer, U., S. Steffens, S. Frank, N. G. Rainov, K. Schulze-Osthoff and C. M. Kramm (2005). "Mechanisms of thymidine kinase/ganciclovir and cytosine deaminase/ 5-fluorocytosine suicide gene therapy-induced cell death in glioma cells." Oncogene **24**(7): 1231-43.

Franchitto, A., P. Pichierri, R. Piergentili, M. Crescenzi, M. Bignami and F. Palitti (2003). "The mammalian mismatch repair protein MSH2 is required for correct MRE11 and RAD51 relocalization and for efficient cell cycle arrest induced by ionizing radiation in G2 phase." Oncogene **22**(14): 2110-20.

Guerrero, A. D., M. Chen and J. Wang (2007). "Delineation of the caspase-9 signaling cascade." Apoptosis.

Guzman, E., J. L. Langowski and L. Owen-Schaub (2003). "Mad dogs, Englishmen and apoptosis: the role of cell death in UV-induced skin cancer." Apoptosis **8**(4): 315-25.

Hawn, M. T., A. Umar, J. M. Carethers, G. Marra, T. A. Kunkel, C. R. Boland and M. Koi (1995). "Evidence for a connection between the mismatch repair system and the G2 cell cycle checkpoint." Cancer Res **55**(17): 3721-5.

Hill, L. L., A. Ouhtit, S. M. Loughlin, M. L. Kripke, H. N. Ananthaswamy and L. B. Owen-Schaub (1999). "Fas ligand: a sensor for DNA damage critical in skin cancer etiology." Science **285**(5429): 898-900.

Jin, Z. and W. S. El-Deiry (2005). "Overview of cell death signaling pathways." Cancer Biol Ther **4**(2): 139-63.

Kibitel, J., V. Hejmadi, L. Alas, A. O'Connor, B. M. Sutherland and D. Yarosh (1998). "UV-DNA damage in mouse and human cells induces the expression of tumor necrosis factor alpha." Photochem Photobiol **67**(5): 541-6.

Kim, J. W., E. J. Choi and C. O. Joe (2000). "Activation of death-inducing signaling complex (DISC) by pro-apoptotic C-terminal fragment of RIP." Oncogene **19**(39): 4491-9.

Kischkel, F. C., S. Hellbardt, I. Behrmann, M. Germer, M. Pawlita, P. H. Krammer and M. E. Peter (1995). "Cytotoxicity-dependent APO-1 (Fas/CD95)-associated proteins form a death-inducing signaling complex (DISC) with the receptor." Embo J **14**(22): 5579-88.

Kischkel, F. C., D. A. Lawrence, A. Tinel, H. LeBlanc, A. Virmani, P. Schow, A. Gazdar, J. Blenis, D. Arnott and A. Ashkenazi (2001). "Death receptor recruitment of endogenous caspase-10 and apoptosis initiation in the absence of caspase-8." J Biol Chem **276**(49): 46639-46.

Kock, A., T. Schwarz, R. Kirnbauer, A. Urbanski, P. Perry, J. C. Ansel and T. A. Luger (1990). "Human keratinocytes are a source for tumor necrosis factor alpha: evidence for synthesis and release upon stimulation with endotoxin or ultraviolet light." J Exp Med **172**(6): 1609-14.

Koi, M., A. Umar, D. P. Chauhan, S. P. Cherian, J. M. Carethers, T. A. Kunkel and C. R. Boland (1994). "Human chromosome 3 corrects mismatch repair deficiency and microsatellite instability and reduces N-methyl-N'-nitro-N-nitrosoguanidine tolerance in colon tumor cells with homozygous hMLH1 mutation." Cancer Res **54**(16): 4308-12.

Leverkus, M., M. Yaar and B. A. Gilchrest (1997). "Fas/Fas ligand interaction contributes to UV-induced apoptosis in human keratinocytes." Exp Cell Res **232**(2): 255-62.

McStay, G. P., G. S. Salvesen and D. R. Green (2007). "Overlapping cleavage motif selectivity of caspases: implications for analysis of apoptotic pathways." Cell Death Differ.

Meira, L. B., D. L. Cheo, A. M. Reis, N. Claij, D. K. Burns, H. te Riele and E. C. Friedberg (2002). "Mice defective in the mismatch repair gene Msh2 show increased predisposition to UVB radiation-induced skin cancer." DNA Repair (Amst) **1**(11): 929-34.

Meyers, M., M. W. Wagner, H. S. Hwang, T. J. Kinsella and D. A. Boothman (2001). "Role of the hMLH1 DNA mismatch repair protein in fluoropyrimidine-mediated cell death and cell cycle responses." Cancer Res **61**(13): 5193-201.

Milhas, D., O. Cuvillier, N. Therville, P. Clave, M. Thomsen, T. Levade, H. Benoist and B. Segui (2005). "Caspase-10 triggers Bid cleavage and caspase cascade activation in FasL-induced apoptosis." J Biol Chem **280**(20): 19836-42.

Muller, M., S. Wilder, D. Bannasch, D. Israeli, K. Lehlbach, M. Li-Weber, S. L. Friedman, P. R. Galle, W. Stremmel, M. Oren and P. H. Krammer (1998). "p53 activates the CD95 (APO-1/Fas) gene in response to DNA damage by anticancer drugs." J Exp Med **188**(11): 2033-45.

Narine, K. A., K. E. Felton, A. A. Parker, V. A. Tron and S. E. Andrew (2007). "Non-tumor cells from an MSH2-null individual show altered cell cycle effects post-UVB." Oncol Rep **18**(6): 1403-11.

Peters, A. C., L. C. Young, T. Maeda, V. A. Tron and S. E. Andrew (2003). "Mammalian DNA mismatch repair protects cells from UVB-induced DNA damage by facilitating apoptosis and p53 activation." DNA Repair (Amst) **2**(4): 427-35.

Reitmair, A. H., R. Risley, R. G. Bristow, T. Wilson, A. Ganesh, A. Jang, J. Peacock, S. Benchimol, R. P. Hill, T. W. Mak, R. Fishel and M. Meuth (1997). "Mutator phenotype in Msh2-deficient murine embryonic fibroblasts." Cancer Res **57**(17): 3765-71.

Scaffidi, C., J. Volkland, I. Blomberg, I. Hoffmann, P. H. Krammer and M. E. Peter (2000). "Phosphorylation of FADD/ MORT1 at serine 194 and association with a 70-kDa cell cycle-regulated protein kinase." J Immunol **164**(3): 1236-42.

Screaton, R. A., S. Kiessling, O. J. Sansom, C. B. Millar, K. Maddison, A. Bird, A. R. Clarke and S. M. Frisch (2003). "Fas-associated death domain protein interacts with methyl-CpG binding domain protein 4: a potential link between genome surveillance and apoptosis." Proc Natl Acad Sci U S A **100**(9): 5211-6.

Shimada, K., S. Matsuyoshi, M. Nakamura, E. Ishida, M. Kishi and N. Konishi (2004). "Phosphorylation of FADD is critical for sensitivity to anticancer drug-induced apoptosis." Carcinogenesis **25**(7): 1089-97.

Sitailo, L. A., S. S. Tibudan and M. F. Denning (2002). "Activation of caspase-9 is required for UV-induced apoptosis of human keratinocytes." J Biol Chem **277**(22): 19346-52.

Slee, E. A., M. T. Harte, R. M. Kluck, B. B. Wolf, C. A. Casiano, D. D. Newmeyer, H. G. Wang, J. C. Reed, D. W. Nicholson, E. S. Alnemri, D. R. Green and S. J. Martin (1999). "Ordering the cytochrome c-initiated caspase cascade: hierarchical activation of caspases-2, -3, -6, -7, -8, and -10 in a caspase-9-dependent manner." J Cell Biol **144**(2): 281-92.

Sprick, M. R., E. Rieser, H. Stahl, A. Grosse-Wilde, M. A. Weigand and H. Walczak (2002). "Caspase-10 is recruited to and activated at the native TRAIL and CD95 death-inducing signalling complexes in a FADD-dependent manner but can not functionally substitute caspase-8." Embo J **21**(17): 4520-30.

Timmer, J. C. and G. S. Salvesen (2007). "Caspase substrates." Cell Death Differ **14**(1): 66-72.

Trefzer, U., M. Brockhaus, H. Lotscher, F. Parlow, A. Budnik, M. Grewe, H. Christoph, A. Kapp, E. Schopf, T. A. Luger and et al. (1993). "The 55-kD tumor necrosis factor receptor on human keratinocytes is regulated by tumor necrosis factor-alpha and by ultraviolet B radiation." J Clin Invest **92**(1): 462-70.

Umar, A., M. Koi, J. I. Risinger, W. E. Glaab, K. R. Tindall, R. D. Kolodner, C. R. Boland, J. C. Barrett and T. A. Kunkel (1997). "Correction of hypermutability, N-methyl-N'-nitro-N-nitrosoguanidine resistance, and defective DNA mismatch repair by introducing chromosome 2 into human tumor cells with mutations in MSH2 and MSH6." Cancer Res **57**(18): 3949-55.

Vincenz, C. and V. M. Dixit (1997). "Fas-associated death domain protein interleukin-1beta-converting enzyme 2 (FLICE2), an ICE/Ced-3 homologue, is proximally involved in CD95- and p55-mediated death signaling." J Biol Chem **272**(10): 6578-83.

Wajant, H., K. Pfizenmaier and P. Scheurich (2003). "Tumor necrosis factor signaling." Cell Death Differ **10**(1): 45-65.

Wang, J., H. J. Chun, W. Wong, D. M. Spencer and M. J. Lenardo (2001). "Caspase-10 is an initiator caspase in death receptor signaling." Proc Natl Acad Sci U S A **98**(24): 13884-8.

Wang, S. and W. S. El-Deiry (2003). "Requirement of p53 targets in chemosensitization of colonic carcinoma to death ligand therapy." Proc Natl Acad Sci U S A **100**(25): 15095-100.

Wang, X. (2001). "The expanding role of mitochondria in apoptosis." Genes Dev **15**(22): 2922-33.

Yan, T., S. E. Berry, A. B. Desai and T. J. Kinsella (2003). "DNA Mismatch Repair (MMR) Mediates 6-Thioguanine Genotoxicity by Introducing Single-strand Breaks to Signal a G(2)-M Arrest in MMR-proficient RKO Cells." Clin Cancer Res **9**(6): 2327-34.

Yan, T., J. E. Schupp, H. S. Hwang, M. W. Wagner, S. E. Berry, S. Strickfaden, M. L. Veigl, W. D. Sedwick, D. A. Boothman and T. J. Kinsella (2001). "Loss of DNA mismatch repair imparts defective cdc2 signaling and G(2) arrest responses without altering survival after ionizing radiation." Cancer Res **61**(22): 8290-7.

Yoshino, M., Y. Nakatsu, H. te Riele, S. Hirota, Y. Kitamura and K. Tanaka (2002). "Additive roles of XPA and MSH2 genes in UVB-induced skin tumorigenesis in mice." DNA Repair (Amst) **1**(11): 935-40.

Young, L. C., J. B. Hays, V. A. Tron and S. E. Andrew (2003). "DNA mismatch repair proteins: potential guardians against genomic instability and tumorigenesis induced by ultraviolet photoproducts." J Invest Dermatol **121**(3): 435-40.

Young, L. C., J. Listgarten, M. J. Trotter, S. E. Andrew and V. A. Tron (2007). "Evidence that dysregulated DNA mismatch repair characterizes human nonmelanoma skin cancer." Br J Dermatol.

Young, L. C., A. C. Peters, T. Maeda, W. Edelmann, R. Kucherlapati, S. E. Andrew and V. A. Tron (2003). "DNA mismatch repair protein Msh6 is required for optimal levels of ultraviolet-B-induced apoptosis in primary mouse fibroblasts." J Invest Dermatol **121**(4): 876-80.

Young, L. C., K. J. Thulien, M. R. Campbell, V. A. Tron and S. E. Andrew (2004). "DNA mismatch repair proteins promote apoptosis and suppress tumorigenesis in response to UVB irradiation: an in vivo study." Carcinogenesis **25**(10): 1821-7.

Zhuang, L., B. Wang, G. A. Shinder, G. M. Shivji, T. W. Mak and D. N. Sauder (1999). "TNF receptor p55 plays a pivotal role in murine keratinocyte apoptosis induced by ultraviolet B irradiation." J Immunol **162**(3): 1440-7.

~ Chapter 7 ~

General Discussion

In this dissertation I have examined the role of MMR proteins Msh6 and MSH2/Msh2 in the DNA damage response, specifically in the regulation of the cell cycle and apoptosis after UVB-induced DNA damage. I have focused on Msh6, which forms a heterodimer with Msh2, as less is known about the function of this protein than Msh2 or Mlh1. Many studies have shown that MMR has a role outside of repair in response to several types of DNA damage, including UV, IR, 6-TG, cisplatin and MNNG (Duckett et al. 1996; Yan et al. 2001; Meira et al. 2002; Cejka et al. 2003; Peters et al. 2003; Yan et al. 2003; Young et al. 2003; Meyers et al. 2004; Adamson et al. 2005; Clodfelter et al. 2005; Narine et al. 2007). Using *Msh2*- and *Msh6*-proficient and –deficient MEFs from an isogenic background and a human lymphoblastoid cell line deficient in *MSH2* and a MMR-proficient control cell line I tested the hypothesis that the absence of MMR leads to misregulated cell cycle and apoptotic responses after UVB radiation. My work showed that G2/M cell cycle arrest is diminished in *Msh6*-deficient MEFs and *MSH2*-deficient human cells after UVB irradiation. Furthermore, levels of key cell cycle proteins are reduced after UVB in the absence of *MSH2*. I have also demonstrated that Msh6-dependent UVB-induced apoptosis occurs via mitochondrial membrane depolarization. MEFs deficient in *Msh6* have reduced levels of mitochondrial membrane depolarization, misregulated release of cytochrome c into the cytosol and reduced levels of caspase 9 after UVB irradiation. I also demonstrated that *Msh6*-deficient MEFs have misregulated translocation of Bax after UVB irradiation that is associated with the abnormal apoptotic response in the absence of Msh6. Thus, MMR is important in maintaining proper cellular responses such as cell cycle arrest and apoptosis to UVB-induced DNA damage that act to maintain genomic integrity.

Characterization of the cell cycle response to UVB-induced DNA damage in mismatch repair-proficient and –deficient cells

In order to understand the role of MMR in the cell cycle response after UVB-induced DNA damage, cell cycle phase analysis was completed using flow cytometry and protein analysis of several key cell cycle proteins was undertaken. I undertook these studies in *Msh6*$^{+/+}$ and *Msh6*$^{-/-}$ primary mouse cell lines from an isogenic background, however, I encountered great difficulties in obtaining results using available reagents for protein analysis. In order to understand and appreciate the role of MMR in normal cell cycle responses after UVB, I included cell cycle data from human lymphoblastoid cell lines: a *MSH2*-proficient cell line and a *MSH2*-deficient cell line from an individual with bi-allelic MSH2 mutations. When these studies were initiated, there were no published reports on the MMR-dependent, UVB-induced effects on cell cycle. More recent studies have shown that a Msh2-deficiency significantly reduced the percentage of arrested cells *in vivo* and *in vitro* after UVB, using *Xpc*$^{-/-}$*Msh2*$^{-/-}$ mice and derived keratinocytes. This delayed arrest occurred in late S phase rather than in G_2-phase (van Oosten et al. 2005). A very recent study demonstrated that *Msh2*$^{-/-}$ transformed MEFs show reduced S-phase accumulation post-UVB (Seifert et al. 2008). Cell cycle arrest is an important event occurring after UVB-induced DNA damage. It allows for repair of the damage prior to cell replication, and as such, is an integral event in the maintenance of genomic stability. I hypothesized that the absence of MMR would reduce G2/M cell cycle arrest after DNA damage, which could contribute in part to UVB-induced tumorigenesis. Indeed this was the case, as seen by flow cytometric analysis of the cell cycle. G2/M phase was significantly reduced at 24 hours post-UVB treatment in unsynchronized *Msh6*-deficient MEFs compared to unsynchronized *Msh6*-proficient MEFs (chapter 3). As well, G2/M phase was significantly reduced at 48 and 72 hours post-UVB treatment in unsynchronized *MSH2*-deficient cells compared to unsynchronized *MSH2*-proficient cells (chapter 3). The differences seen in the time to G2/M arrest in *Msh6*-proficient MEFs versus *MSH2*-proficient human cells are most likely due to the inherent differences between primary mouse fibroblasts and transformed human lymphoblastoid cells. The findings of reduced G2/M arrest in *MSH2*-deficient and *Msh6*-deficient cells led to more in-depth analysis of the proteins controlling the G2/M phase of the cell cycle. These studies could only be carried out in human cells due to available reagents not being sufficient for detection of murine protein at the time of experimentation. It was shown that CHK1 phosphorylated at Serine 345 and CDC25C phosphorylated at Serine 216 are reduced in *MSH2*-deficient cells compared to *MSH2*-proficient cells over time after UVB irradiation (chapter 3). These proteins are important in the promotion of G2/M cell cycle arrest after DNA damage. These studies are further evidence that MMR proteins play a role in the promotion of G2/M arrest after UVB-induced DNA damage. Because of the effect of *MSH2*-deficiency on CHK1-pSer345, it seems that MMR acts early on in the G2/M cell cycle protein cascade (Fig. 3-1), perhaps as a transducer of the G2/M arrest signal. However, further studies into the precise mechanism of how MMR can affect the phosphorylation status of cell cycle proteins and the activation of cell cycle arrest remain to be explored.

Future Directions

1) Examination of the effect of MMR on other upstream proteins in the G2/M phase of the cell cycle after UVB-induced DNA damage, such as H2AX and ATR. One of the earliest steps in the cellular response to DNA damage, including double-strand breaks, is the phosphorylation of serine 139 of H2AX, a subclass of eukaryotic histone proteins that are part of chromatin (Fernandez-Capetillo et al. 2004). Interestingly, a recent study showed that induction of γ-H2AX (the phosphorylated form of H2AX) in response to greater doses of UVB was decreased in *MSH2*-deficient cells compared with *MSH2*-proficient cells (Seifert et al. 2008) The potential effect of MMR on ATR after UVB is particularly interesting, as ATR has been shown to exist in a complex with the MMR proteins (Wang et al. 2000) and this could shed light on the exact position of MMR in the G2/M cell cycle cascade and the potential mechanism for how MMR activates cell cycle arrest.

Characterization of the mitochondrial/intrinsic apoptotic response to UVB-induced DNA damage in mismatch repair-proficient and -deficient murine embryonic fibroblasts

Previous work in our laboratory has identified a role for MMR in post-UVB-induced apoptosis (Peters et al. 2003; Young et al. 2003). This was identified as an important pathway in the DNA damage-induced pathway to tumorigenesis as mice lacking functional MMR develop skin tumors at a lower cumulative dose of UVB compared to wildtype mice (Young et al. 2004) and has been demonstrated by others (Meira et al. 2001; Meira et al. 2002; Yoshino et al. 2002). However, the mechanism of MMR-associated apoptosis is currently unknown. The mechanism underlying this phenomenon is integral to our understanding of DNA damage recognition and the cell's ability to determine whether DNA repair or apoptosis will be initiated. I hypothesized that the mitochondrial/intrinsic apoptotic proteins were involved in MMR-dependent apoptosis after UVB-induced DNA damage. In order to test this hypothesis, I used isogenic MEFs proficient and deficient for *Msh6*. I tested the hypothesis that Msh6-induced apoptosis after UVB occurs through the mitochondria by quantifying the mitochondrial outer membrane depolarization in Msh6 proficient and deficient cells. I showed that there was a significant reduction in mitochondrial membrane depolarization in *Msh6*-deficient MEFs compared to *Msh6*-proficient MEFs after UVB irradiation. This confirms that *Msh6*-dependent apoptosis is occurring through the mitochondria. *Msh6*-deficient MEFs still undergo apoptosis post-UVB (15% on average compared to 25% on average in *Msh6*-proficient MEFs) and mitochondrial membrane depolarization also still occurs (22% on average compared to 30% on average in *Msh6*-proficient MEFs), indicating that mitochondrial membrane depolarization contributes to *Msh6*-dependent apoptosis. This finding also indicates that mitochondrial membrane depolarization is only partially dependent on Msh6, but Msh6-associated apoptosis is mitochondrially activated.

Since mitochondrial membrane depolarization is associated with mitochondrial membrane permeability and the release of proteins from the mitochondrial intermembrane space, such as cytochrome c and Smac/DIABLO, I examined the levels of these proteins in *Msh6*-proficient and deficient cells after UVB irradiation. I found that cytochrome c release is misregulated in *Msh6*-deficient MEFs. There is an increase in cytosolic cytochrome c in *Msh6*-proficient MEFs after UVB compared to the untreated level, while in *Msh6*-deficient MEFs, the level of cytochrome c in the cytosol remains unchanged from the untreated level, confirming mitochondrial-dependent regulation. Analysis of Smac/DIABLO protein levels after UVB radiation showed that there was no involvement of this protein in the Msh6-dependent apoptotic pathway. Since Smac/DIABLO inhibits the IAPs (inhibitors of apoptosis), this finding suggests that the Smac/DIABLO-IAP pathway is not involved in Msh6-dependent apoptosis. However, further examination of the levels of Smac/DIABLO in mitochondrial and cytosolic cell fractions may yield different results and should be explored. I also examined caspase 9 levels after UVB radiation. Along with cytochrome c and Apaf-1, pro-caspase 9 forms the apoptosome which activates caspase 9 which in turn activates effector caspases in the apoptotic cascade. I showed that activated caspase 9 levels were decreased in *Msh6*-deficient MEFs after UVB compared to *Msh6*-proficient MEFs. Taken together, these data are evidence that Msh6 is required for cells to undergo proper mitochondrial apoptosis following UVB-induced DNA damage.

Pro-apoptotic Bax translocation from the cytosol to the mitochondria is known to cause mitochondrial membrane depolarization, thus I wanted to examine the role of this protein in *Msh6*-mediated apoptosis. My studies showed that Bax translocation is misregulated in *Msh6*-deficient MEFs. After UVB irradiation, *Msh6*-proficient MEFs show an increase in mitochondrial Bax and a decrease in cytosolic Bax, compared to untreated cells. The opposite is true of *Msh6*-deficient cells. There is an increase in cytosolic Bax while the level of mitochondrial Bax remains unchanged. A proportion of human tumors with defective MMR are characterized by mutations in a microsatellite in the coding region of

Bax, resulting in inactivation of the *Bax* gene (Rampino et al. 1997; Percesepe et al. 1998). This inactivation of *Bax* is thought to contribute to tumorigenesis through disruption of apoptosis (de la Chapelle 2003). I observed a Bax misregulation in *Msh6*$^{-/-}$ MEFs compared to *Msh6*$^{+/+}$ MEFs following UVB irradiation. Previous studies by us have shown that spontaneous tumors from *Msh6*$^{-/-}$ mice do not display MSI. Furthermore, our *in vivo* studies of UVB-induced tumorigenesis in *Msh2*$^{-/-}$ and *Msh6*$^{-/-}$ mice do not support the idea that MSI contributes to UVB-induced, MMR-dependent apoptosis (Young et al. 2004). The lack of MMR imparted by *Msh6*-deficiency in primary, non-tumor MEFs may be sufficient to impair the activity of Bax in apoptosis after UVB-induced DNA damage through a MSI-independent pathway(s). The misregulation of Bax in *Msh6*$^{-/-}$ MEFs provides support for the idea that *Bax* inactivation in humans contributes to misregulated apoptosis and contributes to tumorigenesis.

I have shown that p53 levels are not dependent on Msh6 after UVB radiation (chapter 4). Furthermore, the Msh6-dependent and the p53-dependent UVB-induced apoptotic pathways are non-overlapping (chapter 4), indicating that Msh6-associated apoptosis after UVB radiation is p53-independent.

These data show that Msh6 is upstream of the mitochondria in the DNA damage-induced intrinsic apoptotic response. The MMR proteins Msh2, Msh6 and MLH1 are part of the BRCA1-associated genome surveillance complex (BASC) (Wang et al. 2000). MMR proteins themselves are genome surveillance molecules that scan and bind to DNA. MMR proteins also interact with signaling proteins. Thus, MMR proteins are perfectly poised to act as DNA damage sensors and mediators of DNA damage response signals, including those which trigger apoptosis. Indeed, MutSα has been shown to bind to UV-induced DNA adducts [reviewed in (Young et al. 2003)]. I propose that Msh6 is required as a sensor of UVB-induced DNA damage and acts thusly to mediate/transduce downstream intrinsic apoptotic events, including Bax translocation to the mitochondria, mitochondrial outer membrane depolarization, cytochrome c release from the mitochondrial intermembrane space and caspase 9 activation, independent of p53.

Future Directions

1) Examination of Smac/DIABLO levels in mitochondrial and cytosolic Msh6 MEF fractions in order to determine if there is altered translocation of this protein.

2) Based upon the misregulation of Bax in *Msh6*$^{-/-}$ cells, determine if Msh6 can directly interact with Bax in the cytosol and/or nucleus post-UVB.

3) Examination of translocation of pro-apoptotic Bak and truncated Bid (tBid) to the mitochondria following UVB radiation to understand the roles of these proteins in Msh6-dependent apoptosis, as Bak and tBid translocation to the mitochondria are associated with mitochondrial membrane depolarization.

4) Examination of the levels of anti-apoptotic proteins such as Mcl-1, Bcl-2 and Bcl-xl to understand their role in Msh6-dependent apoptosis after UVB radiation, as these proteins bind to and inhibit pro-apoptotic proteins Bax and Bak.

5) Examination of the levels of pro-apoptotic proteins Bim and Puma that promote Bax translocation to the mitochondria, as well as Bad and Noxa that inhibit the anti-apoptotic proteins.

6) Examination of the temporal sequence of Msh6-dependent apoptotic events after UVB radiation in live cells.

Characterization of the role of caspase 2 after UVB-induced DNA damage in mismatch repair-proficient and -deficient murine embryonic fibroblasts

Caspase 2 is a nuclear protein, upstream in the apoptotic cascade. It also links cell cycle to apoptosis by its interaction with cyclin D3 (Mendelsohn et al. 2002). I have shown in chapter 4 that there are Msh6-dependent differences in cleaved caspase 9 protein after UVB, and that Bax levels and translocation are misregulated in *Msh6*-deficient cells after UVB. Activation of caspase 2 has been shown to occur downstream of caspase 9 (Slee et al. 1999; O'Reilly et al. 2002; Samraj et al. 2007). There is also evidence that caspase 2 promotes Bax translocation to the mitochondria (Lassus et al. 2002) and that caspase 2 activation occurs downstream of Bax (He et al. 2004; Ruiz-Vela et al. 2005). In light of these findings, I sought to test the hypothesis that caspase 2 is activated in an Msh6-dependent manner after UVB. In order to elucidate the role of caspase 2 in Msh6-dependent apoptosis after UVB-induced DNA damage, I took several different approaches. After UVB radiation, I studied the levels of caspase 2 protein, the subcellular localization and translocation of caspase 2, as well as global apoptosis levels after inhibition of caspase 2. For these studies, MEFs proficient and deficient in *Msh6* were utilized. In addition, MEFs proficient and deficient in *Msh2* were utilized for immunofluorescene studies in order to expand and confirm results obtained in *Msh6* proficient and deficient MEFs.

Protein analysis showed that there was no Msh6-dependent cleavage of caspase 2 after UVB (Fig. 5-3). Immunofluorescence and subcellular fractionation studies after UVB radiation also showed no Msh6-dependent differences in caspase 2 subcellular localization or translocation 24 hours after treatment with UVB. I expanded localization studies to include *Msh2*-proficient and -deficient MEFs and found that caspase 2 localizes to the centrosomes of dividing cells in a MMR-independent manner. This finding has not been previously reported in the literature. But why would an apoptotic protein such as caspase 2 localize to the centrosomes of mitotic cells? Perhaps the centrosomes have a role in apoptosis. This idea has been explored in the literature and it has been found that several proteins that are involved in the DNA damage response, like p53 and PARP, localize to the centrosomes (Kanai et al. 2000; Morris et al. 2000). Caspase 2 may have a role in the regulation of DNA damage-induced mitotic catastrophe, a type of cell death that occurs in close temporal proximity to misregulated or failed mitosis that may be a "pre-stage" of apoptosis. This is a viable idea, as there are continuously emerging roles for other proteins in the DNA damage response, for example p53 and PARP, which also localize to the centrosomes, whose main goal is to protect the cell from the acquisition and/or propagation of mutations caused by DNA damage.

In contrast to the above immunoblot results, there was a significant difference in the levels of UVB-induced apoptosis between *Msh6*-proficient and –deficient MEFs in the presence of Z-VDVAD-FMK, a peptide inhibitor of caspase 2. *Msh6*-proficient MEFs had lower levels of apoptosis after UVB upon caspase 2 inhibition than did *Msh6*-deficient MEFs, indicating that *Msh6* knockout MEFs were less affected by caspase 2 inhibition than were *Msh6* wildtype MEFs. This finding in combination with the localization of caspase 2 to the centrosomes, where MMR proteins also localize, suggest that caspase 2 may have a role in MMR-associated apoptosis/cellular response after UVB, although further experimentation and confirmation by inhibition of caspase 2 by siRNA is required.

Future Directions

1) Further examination of MMR-dependent apoptosis levels after siRNA inhibition of caspase 2 (as discussed above).

2) Examination of MMR-caspase 2 interactions through co-immunoprecipitation studies or mass spectrometry to determine if caspase 2 can interact with Msh6 and/or Msh2 in the centrosomes, based upon the localization of caspase 2, Msh6 and Msh2 to the centrosomes (as discussed in chapter 4).

Characterization of the death receptor/extrinsic apoptotic response to UVB-induced DNA damage in mismatch repair-proficient and -deficient murine embryonic fibroblasts

Isogenic MEFs proficient and deficient in *Msh6* were utilized to examine the role of the death receptor proteins in Msh6-dependent apoptosis after UVB radiation. Studies have shown that the death receptor/extrinsic apoptotic pathway is recruited after UV exposure, through the TNFR1 pathway and the Fas pathway (Kibitel et al. 1998; Hill et al. 1999; Zhuang et al. 1999)). The MMR protein MLH1 has been found in a complex with FADD in the nucleus (Screaton et al. 2003). In addition, FADD-pSer194 is associated with cell cycle arrest at the G2/M phase, similar to the MMR proteins (Scaffidi et al. 2000). This led to the hypothesis that apoptosis through the death receptor pathway may be Msh6-dependent after UVB-induced DNA damage.

Protein analysis showed that this pathway of apoptosis is not recruited through Msh6 after UVB, either through TNFR1 or Fas. Caspases 8 and 10 have no role in Msh6-dependent apoptosis after UVB, as shown by western blot. However, I found a significant difference in the levels of UVB-induced apoptosis between *Msh6*-proficient and –deficient MEFs in the presence of Z-IETD-FMK, a peptide inhibitor of caspase 8. Inhibition of caspase 8 is protective of apoptosis in cells with intact Msh6, not cells lacking Msh6 which suggests that caspase 8 has a role in Msh6-dependent apoptosis after UVB. This is confirmed by the fact that levels of cleaved caspase 3 are increased in *Msh6*-deficient MEFs compared to *Msh6*-proficient MEFs in response to UVB after inhibition of caspase 8. Although the protein analysis data in chapter 6 appear to rule out the extrinsic pathway in the Msh6-dependent apoptotic response after UVB-induced DNA damage, perhaps these cells are type II cells, in which apoptosis depends on amplification of death receptor signals through the mitochondria via a feedback loop (see chapter 6 introduction). Active caspase 8 cleaves Bid which promotes the release of pro-apoptotic mitochondrial proteins such as Smac/DIABLO and cytochrome c, which drives the formation of the apoptosome, leading to activation of caspase 9. Active caspase 9 cleaves the executioner caspase 3, which activates caspase 8, completing the feedback loop. In chapter 4 I studied the levels and subcellular localization of full-length Bid and found no appreciable difference between *Msh6*-proficient and –deficient MEFs, however, investigation of truncated Bid may yield different results. I was unable to investigate this possibility due to the inability to see the truncated protein in these cells using available reagents. Alternatively, caspase 8 may be activated by caspase 9 (Slee et al. 1999; Guerrero et al. 2007), or directly or indirectly through caspase 3, which is activated through caspase 9 and the mitochondrial pathway of apoptosis [chapter 4; (Sitailo et al. 2002)]. Activation of caspase 8 through caspases 3 and/or 9 seems a more likely possibility, as I have shown that mitochondrial pathway of apoptosis is recruited in an Msh6-dependent manner after UVB-induced DNA damage, because there are Msh6-dependent changes in the levels of cleaved caspases 3 and 9 after UVB-induced DNA damage, and because there was no appreciable induction of the death receptor proteins TNFR1 or Fas. However, further experimentation is required to elucidate this possibility. Figure 7-1 below illustrates a putative model for Msh6-dependent apoptosis after UVB-induced DNA damage.

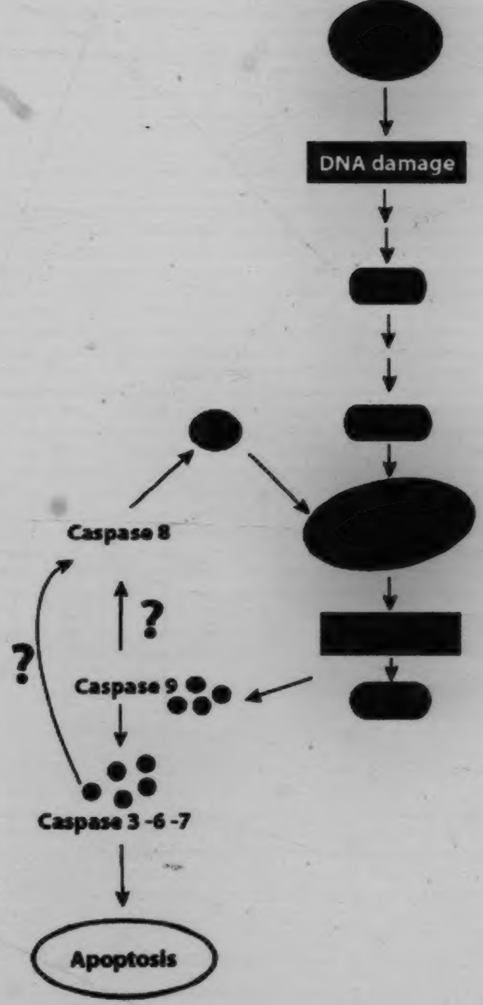

Figure 7-1: Putative model of Msh6-dependent apoptosis induced by UVB radiation

Msh6-dependent apoptosis is induced by DNA damage caused by UVB radiation. Downstream of Msh6, Bax is translocated to the mitochondria which undergo mitochondrial membrane permeability, associated with a reduction in mitochondrial membrane potential. Cytochrome c is released from the mitochondria into the cytosol, and forms the apoptosome with Apaf-1 and caspase 9, which activates downstream effector caspases 3, 6 and 7, effecting apoptosis. Caspases 9 or 3 can activate caspase 8 which in turn cleaves Bid. The truncated Bid can translocate to the mitochondria, thus amplifying the apoptotic signal.

Future Directions

1) Based upon the difference in the levels of UVB-induced apoptosis between *Msh6*-proficient and –deficient MEFs after caspase 8 inhibition using Z-IETD-FMK, examination of the role of caspase 8 in Msh6-dependent apoptosis levels after UVB radiation by siRNA inhibition of caspase 8.

2) Examination of caspase 8 levels after siRNA inhibition of caspase 3 and of caspase 9 to determine if there is a feedback effect on caspase 8 cleavage through the mitochondrial apoptotic pathway after UVB.

3) Examination of truncated Bid levels and translocation to determine if tBid plays a role in Msh6-dependent apoptosis after UVB and determination of possible Bid truncation and mitochondrial translocation through caspase 8, which may be determined via siRNA inhibition of caspase 8.

4) Examination of Msh6-caspase 8 interactions through immunofluorescence and co-immunoprecipitation or mass spectrometry studies.

Conclusions

Based upon the data presented in this dissertation, it can be seen that 1) normal G2/M cell cycle checkpoint induced by UVB radiation is partially dependent on MMR; 2) Msh6-dependent UVB-induced apoptosis occurs through the mitochondria; 3) normal cellular localization and levels of pro-apoptotic Bax is dependent on Msh6; 4) normal cellular localization and levels of pro-apoptotic proteins cytochrome c in response to UVB-induced DNA damage are dependent on Msh6; 5) normal levels of cleaved caspase 9 in UVB-treated cells are dependent on Msh6 and; 6) there is a possibility that Msh6-

associated apoptosis involves feedback loop-dependent activation of caspase 8 via cleaved caspases 9 or 3. These data help elucidate for the first time some of the mechanisms underlying the MMR-dependent UVB-induced DNA damage response and highlight the importance of MMR in the avoidance of UVB-induced tumorigenesis.

References

Adamson, A. W., D. I. Beardsley, W. J. Kim, Y. Gao, R. Baskaran and K. D. Brown (2005). "Methylator-induced, mismatch repair-dependent G2 arrest is activated through Chk1 and Chk2." Mol Biol Cell **16**(3): 1513-26.

Cejka, P., L. Stojic, N. Mojas, A. M. Russell, K. Heinimann, E. Cannavo, M. di Pietro, G. Marra and J. Jiricny (2003). "Methylation-induced G(2)/M arrest requires a full complement of the mismatch repair protein hMLH1." Embo J **22**(9): 2245-54.

Clodfelter, J. E., B. G. M and K. Drotschmann (2005). "MSH2 missense mutations alter cisplatin cytotoxicity and promote cisplatin-induced genome instability." Nucleic Acids Res **33**(10): 3323-30.

de la Chapelle, A. (2003). "Microsatellite instability." N Engl J Med **349**(3): 209-10.

Duckett, D. R., J. T. Drummond, A. I. Murchie, J. T. Reardon, A. Sancar, D. M. Lilley and P. Modrich (1996). "Human MutSalpha recognizes damaged DNA base pairs containing O6-methylguanine, O4-methylthymine, or the cisplatin-d(GpG) adduct." Proc Natl Acad Sci U S A **93**(13): 6443-7.

Fernandez-Capetillo, O., A. Lee, M. Nussenzweig and A. Nussenzweig (2004). "H2AX: the histone guardian of the genome." DNA Repair (Amst) **3**(8-9): 959-67.

Guerrero, A. D., M. Chen and J. Wang (2007). "Delineation of the caspase-9 signaling cascade." Apoptosis.

He, Q., Y. Huang and M. S. Sheikh (2004). "Bax deficiency affects caspase-2 activation during ultraviolet radiation-induced apoptosis." Oncogene **23**(6): 1321-5.

Hill, L. L., A. Ouhtit, S. M. Loughlin, M. L. Kripke, H. N. Ananthaswamy and L. B. Owen-Schaub (1999). "Fas ligand: a sensor for DNA damage critical in skin cancer etiology." Science **285**(5429): 898-900.

Kanai, M., M. Uchida, S. Hanai, N. Uematsu, K. Uchida and M. Miwa (2000). "Poly(ADP-ribose) polymerase localizes to the centrosomes and chromosomes." Biochem Biophys Res Commun **278**(2): 385-9.

Kibitel, J., V. Hejmadi, L. Alas, A. O'Connor, B. M. Sutherland and D. Yarosh (1998). "UV-DNA damage in mouse and human cells induces the expression of tumor necrosis factor alpha." Photochem Photobiol **67**(5): 541-6.

Lassus, P., X. Opitz-Araya and Y. Lazebnik (2002). "Requirement for caspase-2 in stress-induced apoptosis before mitochondrial permeabilization." Science **297**(5585): 1352-4.

Meira, L. B., D. L. Cheo, A. M. Reis, N. Claij, D. K. Burns, H. te Riele and E. C. Friedberg (2002). "Mice defective in the mismatch repair gene Msh2 show increased predisposition to UVB radiation-induced skin cancer." DNA Repair (Amst) **1**(11): 929-34.

Meira, L. B., A. M. Reis, D. L. Cheo, D. Nahari, D. K. Burns and E. C. Friedberg (2001). "Cancer predisposition in mutant mice defective in multiple genetic pathways: uncovering important genetic interactions." Mutat Res **477**(1-2): 51-8.

Mendelsohn, A. R., J. D. Hamer, Z. B. Wang and R. Brent (2002). "Cyclin D3 activates Caspase 2, connecting cell proliferation with cell death." Proc Natl Acad Sci U S A **99**(10): 6871-6.

Meyers, M., A. Hwang, M. W. Wagner and D. A. Boothman (2004). "Role of DNA mismatch repair in apoptotic responses to therapeutic agents." Environ Mol Mutagen **44**(4): 249-64.

Morris, V. B., J. Brammall, J. Noble and R. Reddel (2000). "p53 localizes to the centrosomes and spindles of mitotic cells in the embryonic chick epiblast, human cell lines, and a human primary culture: An immunofluorescence study." Exp Cell Res **256**(1): 122-30.

Narine, K. A., K. E. Felton, A. A. Parker, V. A. Tron and S. E. Andrew (2007). "Non-tumor cells from an MSH2-null individual show altered cell cycle effects post-UVB." Oncol Rep **18**(6): 1403-11.

O'Reilly, L. A., P. Ekert, N. Harvey, V. Marsden, L. Cullen, D. L. Vaux, G. Hacker, C. Magnusson, M. Pakusch, F. Cecconi, K. Kuida, A. Strasser, D. C. Huang and S. Kumar (2002). "Caspase-2 is not required for thymocyte or neuronal apoptosis even though cleavage of caspase-2 is dependent on both Apaf-1 and caspase-9." Cell Death Differ **9**(8): 832-41.

Percesepe, A., P. Kristo, L. A. Aaltonen, M. Ponz de Leon, A. de la Chapelle and P. Peltomaki (1998). "Mismatch repair genes and mononucleotide tracts as mutation targets in colorectal tumors with different degrees of microsatellite instability." Oncogene **17**(2): 157-63.

Peters, A. C., L. C. Young, T. Maeda, V. A. Tron and S. E. Andrew (2003). "Mammalian DNA mismatch repair protects cells from UVB-induced DNA damage by facilitating apoptosis and p53 activation." DNA Repair (Amst) **2**(4): 427-35.

Rampino, N., H. Yamamoto, Y. Ionov, Y. Li, H. Sawai, J. C. Reed and M. Perucho (1997). "Somatic frameshift mutations in the BAX gene in colon cancers of the microsatellite mutator phenotype." Science **275**(5302): 967-9.

Ruiz-Vela, A., J. T. Opferman, E. H. Cheng and S. J. Korsmeyer (2005). "Proapoptotic BAX and BAK control multiple initiator caspases." EMBO Rep **6**(4): 379-85.

Samraj, A. K., D. Sohn, K. Schulze-Osthoff and I. Schmitz (2007). "Loss of caspase-9 reveals its essential role for caspase-2 activation and mitochondrial membrane depolarization." Mol Biol Cell **18**(1): 84-93.

Scaffidi, C., J. Volkland, I. Blomberg, I. Hoffmann, P. H. Krammer and M. E. Peter (2000). "Phosphorylation of FADD/ MORT1 at serine 194 and association with a 70-kDa cell cycle-regulated protein kinase." J Immunol **164**(3): 1236-42.

Screaton, R. A., S. Kiessling, O. J. Sansom, C. B. Millar, K. Maddison, A. Bird, A. R. Clarke and S. M. Frisch (2003). "Fas-associated death domain protein interacts with methyl-CpG binding domain protein 4: a potential link between genome surveillance and apoptosis." Proc Natl Acad Sci U S A **100**(9): 5211-6.

Seifert, M., S. J. Scherer, W. Edelmann, M. Bohm, V. Meineke, M. Lobrich, W. Tilgen and J. Reichrath (2008). "The DNA-mismatch repair enzyme hMSH2 modulates UV-B-induced cell cycle arrest and apoptosis in melanoma cells." J Invest Dermatol **128**(1): 203-13.

Sitailo, L. A., S. S. Tibudan and M. F. Denning (2002). "Activation of caspase-9 is required for UV-induced apoptosis of human keratinocytes." J Biol Chem **277**(22): 19346-52.

Slee, E. A., M. T. Harte, R. M. Kluck, B. B. Wolf, C. A. Casiano, D. D. Newmeyer, H. G. Wang, J. C. Reed, D. W. Nicholson, E. S. Alnemri, D. R. Green and S. J. Martin (1999). "Ordering the cytochrome c-initiated caspase cascade: hierarchical activation of caspases-2, -3, -6, -7, -8, and -10 in a caspase-9-dependent manner." J Cell Biol **144**(2): 281-92.

van Oosten, M., G. J. Stout, C. Backendorf, H. Rebel, N. de Wind, F. Darroudi, H. J. van Kranen, F. R. de Gruijl and L. H. Mullenders (2005). "Mismatch repair protein Msh2 contributes to UVB-induced cell cycle arrest in epidermal and cultured mouse keratinocytes." DNA Repair (Amst) **4**(1): 81-9.

Wang, Y., D. Cortez, P. Yazdi, N. Neff, S. J. Elledge and J. Qin (2000). "BASC, a super complex of BRCA1-associated proteins involved in the recognition and repair of aberrant DNA structures." Genes Dev **14**(8): 927-39.

Yan, T., S. E. Berry, A. B. Desai and T. J. Kinsella (2003). "DNA Mismatch Repair (MMR) Mediates 6-Thioguanine Genotoxicity by Introducing Single-strand Breaks to Signal a G(2)-M Arrest in MMR-proficient RKO Cells." Clin Cancer Res **9**(6): 2327-34.

Yan, T., J. E. Schupp, H. S. Hwang, M. W. Wagner, S. E. Berry, S. Strickfaden, M. L. Veigl, W. D. Sedwick, D. A. Boothman and T. J. Kinsella (2001). "Loss of DNA mismatch repair imparts defective cdc2 signaling and G(2) arrest responses without altering survival after ionizing radiation." Cancer Res **61**(22): 8290-7.

Yoshino, M., Y. Nakatsu, H. te Riele, S. Hirota, Y. Kitamura and K. Tanaka (2002). "Additive roles of XPA and MSH2 genes in UVB-induced skin tumorigenesis in mice." DNA Repair (Amst) **1**(11): 935-40.

Young, L. C., J. B. Hays, V. A. Tron and S. E. Andrew (2003). "DNA mismatch repair proteins: potential guardians against genomic instability and tumorigenesis induced by ultraviolet photoproducts." J Invest Dermatol **121**(3): 435-40.

Young, L. C., A. C. Peters, T. Maeda, W. Edelmann, R. Kucherlapati, S. E. Andrew and V. A. Tron (2003). "DNA mismatch repair protein Msh6 is required for optimal levels of ultraviolet-B-induced apoptosis in primary mouse fibroblasts." J Invest Dermatol **121**(4): 876-80.

Young, L. C., K. J. Thulien, M. R. Campbell, V. A. Tron and S. E. Andrew (2004). "DNA mismatch repair proteins promote apoptosis and suppress tumorigenesis in response to UVB irradiation: an in vivo study." Carcinogenesis **25**(10): 1821-7.

Zhuang, L., B. Wang, G. A. Shinder, G. M. Shivji, T. W. Mak and D. N. Sauder (1999). "TNF receptor p55 plays a pivotal role in murine keratinocyte apoptosis induced by ultraviolet B irradiation." J Immunol **162**(3): 1440-7.